Author:
Williamson, Cara

Title:
Bio-inspired path planning for unmanned air vehicles in urban environments

Bio-inspired Path Planning for Unmanned Air Vehicles in Urban Environments

By

CARA JANE WILLIAMSON

Department of Aerospace Engineering
UNIVERSITY OF BRISTOL

A dissertation submitted to the University of Bristol in accordance with the requirements of the degree of DOCTOR OF PHILOSOPHY in the Faculty of Engineering.

JULY 17, 2020

Word count: forty two thousand six hundred and sixty six

Abstract

Small Unmanned Air Vehicles (SUAVs) are quick launching and fly at low altitudes offering a range of uses within urban environments. Complex urban wind flows present control issues for small platforms and current battery technology does not provide the required endurance for such missions. However, birds of a comparable size are able to manage these flows and reduce energy costs by exploiting the wind environment.

This thesis initially explores the flight paths of urban gulls measured with an ornithodolite while performing orographic soaring along a row of buildings. The air flow was generated using Computational Fluid Dynamics (CFD) and it was found that gulls modulated their flight paths with changing wind conditions and only used part of the potential flow field which could offer the advantage of robust control in gusts.

Further flight strategies were studied by fitting 11 urban gulls with Global Positioning System (GPS) backpacks. The gulls were found to significantly reduce the energetic cost of commuting flights by exploiting a combination of thermal and orographic updraughts generated by urban environments. Gulls adjusted their flight speeds in response to headwinds and updraughts minimising their cost of transport and by closely matching their flapping and soaring velocities the gulls reduced energy costs by up to a third.

Finally, the velocity optimisation strategy used by the gulls was implemented in a path planner. Global and local solution trajectories were found for the same wind conditions as 27 gull flights. The path planner was found to outperform the gulls implementing a higher percentage of soaring and selecting shorter routes. The simulated trajectories highlighted that static and dynamic soaring strategies could be used in complex flow conditions to save energy. Cost ratios for powered and soaring flight were varied to a typical SUAV platform, the result indicated that energy costs could be halved in range based missions for urban SUAVs.

Dedication and acknowledgements

Thank you to all my friends, family and all the people who listened to me talk about gulls for hours, I hope my stories provided enough entertainment to make it worth your time. Thank you to Peter Rock, without your knowledge and expertise in urban gull this research would never have been possible. Thank you to the UvA-BiTS team, for your help, support and patience throughout the fieldwork seasons. To Dr Emily Shepard and the University of Swansea, thank you for your part in initiating my research career, all of your efforts collecting gull tracks on windy days, and formulating a compelling story. Also to Nick and Amir, who also spent too much time with me on the beach in Winter. To the various building managers and estates people who provided access to weird places, with a special thanks to the dBs Music college who gave us access to their resident gulls.

Thank you to all the young engineers that attended the *From Gulls to Drones* workshop, your engagement and enthusiasm for the Urban Gull Project research was an inspiration, I hope that you will continue in your engineering careers with the same passion you demonstrated during those session.

To Anouk, your friendship and never ending positivity made this an enjoyable and, dare I say *fun* experience. Thank you for your part in this journey, I couldn't have done it without you in more ways than one, may there be many more shared belays in the future!

To the rest of the Flight Lab - all the BIF Lab, UAV-Group and fringe members, thank you for making the office a friendly and inviting place to work.

To my supervisors Dr Shane Windsor and Dr Arthur Richards, thank you for your support - financial, academic and otherwise. Thank you Arthur for your hard work leading the FARSCOPE CDT (I don't know how you find the time), the CDT kept doctoral research from becoming a lonely endeavour. Thank you Shane for your patience and trust, without it, this thesis could never have been completed. Thank you for the opportunity to work on this project, your ideas, knowledge and dedication were, and will continue to be, a massive inspiration. I'm sure that I will continue to learn from the advice you've given me over the last 5 years, thank you.

To my Mum and Dad, just like you always encouraged my independence and curiosity, you too both continue to learn and grow, even now, you are my heros.

Most importantly, to Matt, I couldn't ask for a more patient and supporting partner. Thank you for putting up with my long stints at work, for always being there for me and looking after me when I failed to do so, I love you more than everything.

And a final thank you to all the gulls for doing the hard work...

AUTHOR'S DECLARATION

I declare that the work in this dissertation was carried out in accordance with the requirements of the University's Regulations and Code of Practice for Research Degree Programmes and that it has not been submitted for any other academic award. Except where indicated by specific reference in the text, the work is the candidate's own work. Work done in collaboration with, or with the assistance of, others, is indicated as such. Any views expressed in the dissertation are those of the author.

SIGNED: ..... DATE: .....

Table of Contents

List of Tables

Table **Page**

List of Figures

Figure **Page**

List of Acronyms and Abbreviations

A*	A* (algorithm)	LBB	Lesser Black-Backed (gull)
AGL	Above Ground Level	LES	Large Eddy Simulations
ASL	Above Sea Level	LiDAR	Light Detection and Ranging
BNG	British National Grid	MAV	Micro Air Vehicle
BMR	Basal Metabolic Rate	LiDAR	Light Detection and Ranging
CD	Chart Datum	ODN	Ordnance Datum Newlyn
CFD	Computational Fluid Dynamics	OS	Ordnance Survey
CoT	Cost of Transport	QUIC	Quick Urban & Industrial Complex
DEM	Digital Elevation Model	RANS	Reynolds-averaged Navier-Stokes
DSM	Digital Surface Model	RWD	Relative Wind Direction
DTM	Digital Terrain Model	StF	Speed to Fly
EAS	Equivalent Air Speed	(S)UAV	(Small) Unmanned Air Vehicle
(G)DFS	(Greedy) Depth First Search	TAS	True Air Speed
GPS	Global Positioning System	UAS	Unmanned Air Systems
HAS	Height Above Structure	UTM	Universal Transverse Mercator
HG	Herring Gull	WGS	World Geodetic System

List of Nomenclature

A_0	Disk area of flapping wing (m^2)
b	Wing span (m)
$B_{flap,soar}$	Percentage of time in a flight spent flapping or soaring
$\beta_{a,i}$	Angle between velocity and wind vectors in the air or inertial frame (°)
$\bar{c}$	Mean aerodynamic chord (m)
$c_{D_{w,b}}$	Coefficient of drag on the body or wing
$c_{L_{max}}$	Maximum lift coefficient, occurring just before stall
c_{pro}	Profile power coefficient
C	Cost of path (J)
D	Aerodynamic drag force (N)
E	Energetic cost (J)
e	Velocity tracking error (m s^{-1})
f	Flap frequency (Hz)
F	Estimated total path cost
$\gamma_{a,i}$	Climb angle in the inertial or air frame (°)
g	Acceleration due to gravity (m s^{-2})
G	Cost of path so far
$h_{AGL,HAS}$	Altitude above ground level, height above structure (m)
H	Heuristic cost from current node to goal
$\mathbf{J_w}$	Wind Jacobian
$k_{f,s}$	Induced drag factor in flapping or soaring flight
k_p	Power factor increase above minimum power
m	Body mass (kg)
μ	Dynamic viscosity (kg m^{-1} s^{-1})
$\dot{\mathbf{P}}$	Positional displacement vector (m s^{-1})
$\phi_{a,i}$	Heading in the air or inertial frame (°)
r	Flight range (m)
R_e	Reynolds number
ρ	Air density (kg m^3)
$S_{b,w}$	Surface areas of body or wing (m^2)
T	Thrust (N)
$\tau_{flap,soar}$	Time spent in flap or soar behaviour (s)
$\theta_{amp,pnl}$	Wing flap amplitude and planar angles (°)
θ_w	Wind direction (°)
U	Velocity in the air frame (m s^{-1})
$U_{bg,mp,mr,ms}$	Best glide, minimum power, maximum range, minimum sink velocities (ms^{-1})
$U_{stall,a,c,d,ne}$	Key structural load velocities calculated using FAR 23.333 regulations (m s^{-1})
V	Velocity in the inertial frame (m s^{-1})
V_z	Sink speed in the inertial frame (m s^{-1})
W	Wind speed (m s^{-1})
$W_{a_{h,s}}$	Head- or side-wind component in the air frame (m s^{-1})
$W_{i_{h,c}}$	Head- or cross-wind component in the inertial frame (m s^{-1})
W_z	Vertical wind component (m s^{-1})

CHAPTER 1

INTRODUCTION

Unmanned Air Vehicles (UAVs) have the potential to allow operation in many situations that would be infeasible for manned aircraft. Small UAVs (SUAVs) in particular have potential to fly low altitudes in complex terrain such as in a city landscape. However, the small nature of SUAVs creates a number of limitations. Firstly, it limits in onboard energy capacity resulting in low flight endurance which reduces their operational usefulness. Secondly, due to their small size and flight speeds these vehicles are more susceptible to turbulent or unpredicted air flow, common in urban environments, which results in high energy costs and the potential for catastrophic failure.

Many areas of robotics and engineering are turning to nature for inspiration. From insect inspired algorithms [1] to control drone agents, to hairlike sensory arrays to sense airflow [2], and even to bio-mimetic flapping flight [3–5]. Many birds navigate complex urban wind flows successfully and can even harvest the energy within environment to reduce flight costs. This research will investigate the flight strategies that two gull species, the lesser black-backed, *Larus argentatus*, and herring, *Larus fuscus*, employ to take advantage of urban wind flows and how these strategies inspire improvements for SUAVS operating in these same environments.

Mission planning methods for UAVs typically look for the cheapest energetic path between way points without considering wind conditions, which is normally the shortest path. While this reduces the distance travelled and so energy expended it does not take into account how the complexity of the wind field changes the energy landscape

traversed. Some progress has been made in utilising the energy within the environment in order to increase UAV endurance for example, through the use of thermal and dynamic soaring [6–8]. However, these works have made little progress in the way of combining these energy sources with more complex wind flow fields such as found within an urban environment.

Studies of birds have shown that they reduce their Cost of Transport (CoT) by adapting their flight paths to utilise the energy landscape created by complex topography [9]. This project will investigate the potential for developing path planning algorithms for SUAVs based on the analysis of bird flight data within an urban environment with the aim of demonstrating how considering the complex urban wind fields can reduce the energetic cost of flight and provide robustness for SUAVs working in the same environment. This research aims to provide inspiration and guidance for developing a SUAV control system which can optimise flight in complex urban wind flows.

1.1 Contributions

This thesis has three main areas of academic contribution, firstly, demonstrating the value of investigating free-flying birds in urban environments as a means for improving SUAV technology. By combining the flight trajectories of gulls performing orographic soaring with detailed wind models of their environment it was discovered that the gulls flew in a narrow band of their available airspeed and employed a previously unknown strategy for velocity control based on spatial positioning in varying wind conditions. It is proposed that this strategy would not only reduce energy costs through soaring but could also reduce control demand in gusty conditions [10]. This was later supported by simulation studies of UAV flight control in gusty conditions [11].

The second contribution is the compilation of operation and design considerations for urban SUAV platforms. These are based on the first in-depth analysis of free-flying gulls in urban wind conditions. One of the main discoveries being that combined design optimisation of the power curve and the glide polar could be key in development of platforms with powered and gliding flight modes which could lead to significant energy savings. In addition, it was show that by applying cost of transport optimization large energy savings are possible in urban wind fields.

Finally, this thesis contributes by considering the differences in energetic savings of global and local navigation strategies. Large complex wind models and topography maps were used to explore the energy savings which could be made using path planning

algorithms that implement a velocity optimisation strategy discovered in urban gulls. During the analysis it was discovered that wind gradient soaring could be implemented in complex wind fields with a greedy heuristic to provide significant energy reductions with a fast solve time suitable for real-world application. The reductions in flight costs were found to be dependant on the ratio of powered and unpowered flight modes but plateaued at a 48% reduction providing an upper bound for the potential energy saving possible through soaring in urban wind fields.

Overall this work contributes by demonstrating that there are large potential energy savings possible through soaring in urban wind flows and that the strategies used by gulls could potentially be used by SUAVs to greatly reduce flight costs.

1.2 Document Structure

Chapter 2 starts with a brief history of flight research and key moments in which bird flight inspired engineering design. Following this, gliding and soaring flight strategies are introduced with a summary of the techniques used by birds, gliders and UAVs. A further section will discuss the current technology used for tracking free-flying birds and the findings that these technologies have facilitated. A final section will summarise the literature and highlight the position of this research.

Chapter 3 provides a proof of concept case study which set out to determine whether gulls implement energy saving soaring strategies in urbanized environments and whether these strategies could provide new insight into the development of flight control schemes for SUAV technology. Furthermore, some of the software and methodology proposed will be tested for application to a second, wider study. This investigation used an ornithodolite to track gull flight trajectories and combined these paths with CFD wind models of the conditions. The wind flows in this case study were comparatively simple which to later parts of this research which provided an ideal means of testing the benefits and limitations of the techniques used.

Chapter 4 describes a study where 11 lesser-black backed gulls were fitted with GPS sensors that recorded spatial and behaviour data. Commuting flights which occurred during the breeding season were filtered and classified by soaring strategy. The soaring strategies were tested with velocity optimisation schemes based on CoT theory and flight mechanics in order to determine the suitability of these strategies in complex urban wind environments. The velocity optimisation models outlined in this Chapter go on to form the basis of the bio-inspired path planning in the subsequent Chapter.

In Chapter 5, a subset of the commuting flight from the GPS tagged gulls were selected, the commutes demonstrated environmental harvesting behaviour and occurred on windy, overcast days. Wind models for each of the flights were generated using QUIC software and the weather conditions at the time of the flight. Global and local path planning algorithms were tested flying between the same commute locations and in the same modelled conditions as the gulls. The simulation trajectories produced were compared to the gull flights with performance measures based on the range, endurance, percentage of soaring implemented and the energy savings compared to a shortest path flight. Furthermore, Chapter 5 explored the benefit of using global vs. local optimisation and considered how complex flow fields may facilitate certain soaring strategies.

Chapter 6 discusses interesting features of the results and makes recommendations

for future work.

1.3 Aims and Objectives

This research aims to discover the flight strategies that gulls flying in urban environments implement in order to reduce flight costs and considers how these strategies can be applied to SUAVs flying in the same conditions. The objectives of this work were to:

1. Develop large, fine-scale wind models of urbanised parts of Swansea and Bristol, UK.
2. Track urban dwelling gulls using techniques which do not inhibit free-flying behaviours.
3. Develop a method for quantifying the flight strategies of free-flying gulls.
4. Determine whether gulls commuting in urban environments optimise for energetic cost of transport.
5. Develop path planning algorithms for SUAVs in a urban environment using the flight strategies identified in gulls.

CHAPTER 2

BACKGROUND AND LITERATURE

Bio-inspired technology and design is becoming ever more popular in the field of robotics however, the flight of man has long been the result of nature's inspiration. Myth and legend has often been full of man's desire to fly in the air amongst the birds [12]; kites developed in China were shaped as birds from as early as 221 B.C.; Leonardo Da Vinci's flying machines were based on the wings of vertebrate [13]; and the Wright brothers extensively studied the wings of gulls before the first successful powered flight [14].

A pivotal moment in flight history was the realisation by Lord Cayley that aerodynamics and propulsion could be treated as separate systems, noting that birds did not continually flap but also glided using their own weight to provide forward motion [15]. Not long after, in 1903, the first successful heavier-than-air powered flight was performed by the Wright brothers' famous 1903 Flyer after first developing the necessary aerodynamics on their lesser known 1902 Glider [13, 14].

As aircraft technology advanced, moving away from the flow conditions equivocal to those found in nature, it became less common for aviation engineers to study bird flight. However, it had already been determined that some birds must be harvesting energy from the environment through soaring and so the study of bird flight remained popular among ornithologists and later glider pilots, both looking to understand the soaring strategies which allowed birds to remain in flight for extended periods of time.

It had long been established that knowledge of air flow was vital in fully understanding the mechanics of flight and while biologists continued to make observational

studies of bird flight it had already been recognised that there were limitations to the science through a lack of wind measurements and theory to describe the principals being observed [13]. The idea of mass continuity had existed for some time and had already been implemented in the form of wind tunnels used before the first powered-flight [13], but it wasn't until much later, with the determination of Pennycuick a young, ex-RAF pilot and biologist that aeronautical principals were first applied to birds [16]. At the University of Bristol Pennycuick developed a tilting wind tunnel in which birds were studied for the first time in a controlled flow environment [16, 17].

By this time, wind tunnel technology had found its way into a range of applications outside of aviation including the automotive and civil engineering industries [18, 19] and at the same time as Pennycuick was training the first pigeon for flight in the tilted wind tunnel, civil engineers had also adapted wind tunnels, this time to replicate the wind pressures and shears present at low altitudes in the atmospheric boundary layer [18, 20]. Soon after modelling accurate urban flow fields were a possibility and today, with the high processing power of modern computers, the flow interactions around buildings can be modelled to a high level of accuracy [21–23]. UAVs were recorded in use as early as 1849 [13, 24], however, the technology was exclusively military, as a means to delivery explosive payloads. The technology was largely ineffective and even with the Radio-Controlled (RC) advancements of the 1930s these RC aircraft were not able to fly outside of the pilots Line of Sight (LoS) until Sorensen developed a ground terminal system where the pilot was able to keep track of the platform state. Several areas of industry continued to push the development of UAVs, of course the military, but another big influence was MacCready, who founded AeroVironment in 1971 pioneering development in human- and solar-powered platforms before moving on to specialise in High Altitude Long Endurance (HALE) UAVs. However, it was development of the smart phone industry that really pushed forward UAV technology, with major advancements in two of the three key areas of technology; the inventions of the Lithium Polymer (LiPo) battery, the miniaturization of stabilisation and GPS technologies, and the development of the brushless motor. Small (SUAV) and micro (MAV) UAVs quickly became readily available. There small platforms offered potential for a range of industries due to their low-cost, fast launch, and low altitude capabilities. Typically robotic agents have been designed for industries with working conditions described by the three D's; dull, dirty and dangerous, but as UAVs have become cheaper, smaller and more readily available their potential in a range urban roles including infrastructure monitoring, surveillance, emergency response and small payload delivery [25–29].

With engineers once again interested in flight in low Reynold's number conditions, and battery technology not able to offer the range and endurances required by urban missions, there has been a re-popularisation in the study of bird flight particularly in the soaring strategies they employ to harvest environmental energy for transport. The advancements in small stabilisation and GPS sensors has not only improved UAV technology, it has also facilitated the tracking of birds remotely. The development of GPS backpacks [30–32] and advancements in wind modelling means that for the first time detailed flight trajectories of free-flying birds can be analysed flying through the same conditions faced by urban SUAVs.

2.1 Gliding and Soaring

Gliding is considered a likely precursor for many forms of powered flight in vertebrates and has often been considered to have evolved in arboreal dwelling creatures as a method to generate lift, to extend the range of leaps between tree branches, and as a method of creating drag, to reduce the rate of descent in falls [16, 33]. The definition of a glide is unpowered flight, such that no work is done by the bird (or engine), instead, the work must come from transference of potential and kinetic energies. The potential and kinetic energies come from the body's height and speed relative to the surrounding air. A body can sacrifice kinetic energy through a reduction in speed in order to reduce expenditure of potential energy, and so height. Similarly, by using a diving manoeuvre a reduction of height can be used to increase forward speed. As a wing travels through the oncoming air, pressure is built up on the underside creating a lifting force. This resolves the force due to gravity into a forward speed and negative sink. In a glide with a constant velocity the forces acting on the body; weight, lift and drag, are in equilibrium. Changing the angle that the wing greets the airflow, angle of attack, will change the ratio of the resolved aerodynamics forces, lift and drag, see Fig 2.1. The relationship between these forces is best understood through the examination of the sink rate, U_z, as a function of the forward velocity, U_a; this is called the glide polar. As the angle of attack (AoA) of a wing increases the forward velocity and sink rate reduce, this has a natural minimum where the greatest lift is produced before boundary layer separation and stall occurs [16].

Bird flight has been scientifically analysed for many years and arguably it began with Sir George Cayley. Cayley was not only the first to describe the forces required for flight in detail, but also to realise that some birds were flying with considerably less flapping than required [15]. This observation was particularly prevalent in larger birds

able to capture energy from the air around them, and became known as soaring. There are two types of soaring; static and dynamic, this refers to control required in order to perform the soar. In static soaring the pitch or bank angle is held constant to take advantage temporally large-scale vertically rising air such as in a thermal (thermalling) or generated by a ridge feature in the topography (orographic soaring). In dynamic soaring control is adjusted according for a changing wind gradient, whether the changing gradient is due to the motion of the bird or platform through a deterministic spatial gradient (gradient soaring), or through a stochastic spatial or temporally gradient (gust soaring).

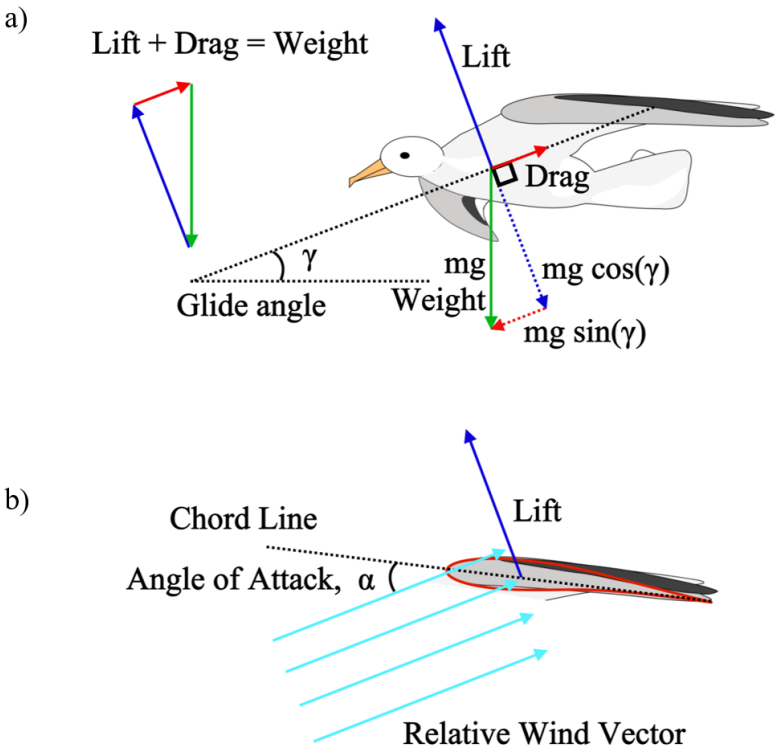

Figure 2.1: Forces in a constant velocity glide and a diagram for the angle of attack

2.1.1 Static Soaring

Static soaring uses vertically rising air with a temporal scale which is long compared to the flight dynamics to offset some or all of the sink in gliding flight. There are two main static soaring types, thermalling and orographic soaring. In thermalling, the exploitable

environmental energy source is pockets or columns of warm air in a convection cycle. Whereas in orographic soaring, the energy source is upwardly deflected wind, such as from a cliff or building.

2.1.1.1 Thermalling

Thermals occur when the air just above the planetary surface has been heated at a faster rate than the surroundings. This tends to occur with a change in substrate, such as over a ploughed area surrounded by vegetation. The thermals are strongest at the centre and are surrounded by a cooler, sink air on the outside. Thermal columns tend to extend from just above the surface to the height of Convection Boundary Layer (CBL) within the larger Planetary Boundary Layer (PBL), marked by a cumulus cloud from the cooled water vapour. The altitude of the CBL varies diurnally, being thinnest at night (at approximately 500 meters) and highest in the three hours either-side of midday in warm and sunny conditions where they can reach heights of 1800 meters [34–36]. Thermals, even in low winds drift and in some cases, pockets or bubbles, can detach, see Fig 2.2.

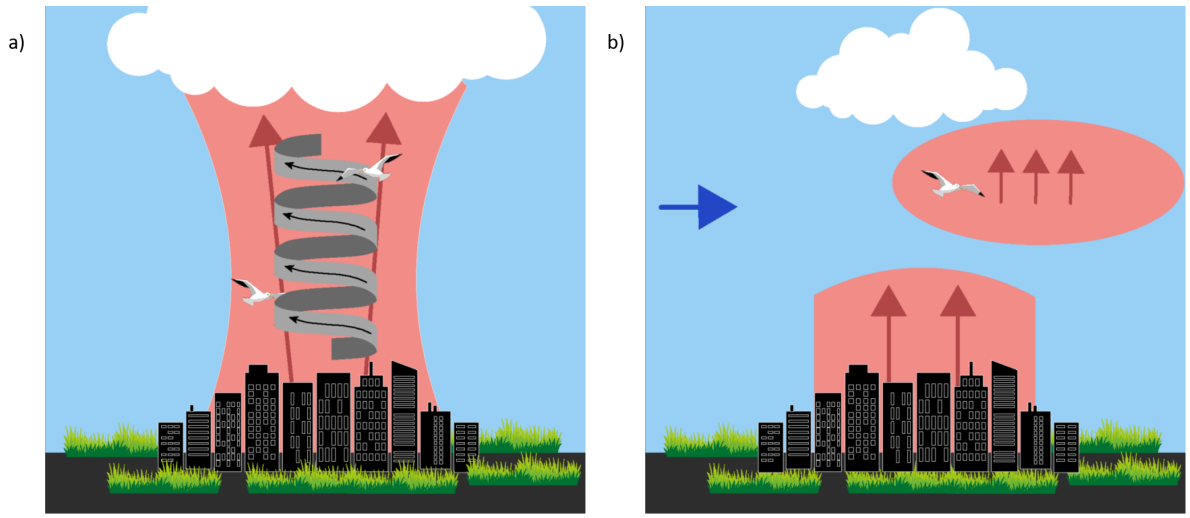

Figure 2.2: a) A thermal column forming over an urbanised area marked by the signature cumulus cloud and a gull thermalling b) A thermal bubble has detached from a thermal column and is drifting with the wind, the gull is "riding" the thermal bubble.

In thermal soaring, altitude is gained by circling within the column of rising air by remaining banked at a suitable angle. Airspeed is kept as low as possible while maintaining control in order maximise altitude gain by offsetting the lowest sink required. The thermal properties of air mean that it is possible to estimated the diameter of the

column, and hence circling radius, based on the speed of the strongest point combined with other climate variables and this property has often been used for autonomous control schemes [37–39], where knowledge of the climb rate at various points in the turn must be known in order to stay within the thermal.

As the thermals are marked with cumulus clouds, glider pilots are able to locate thermals relatively easily, and it is likely that birds use the same methods. Many large birds, such as storks [40], *Ciconia ciconia*, frigates [41], *Fregata magnificens*, and vultures [6], *Gyps africanus*, use thermals and it is not uncommon for manned gliders and birds to share the same thermal [42]. This is relatively unsurprising given that the thermalling strategy of birds was studied long before the first successful glider. The popularisation of glider competitions in the 1940s and '50s meant the technique of thermalling was studied in great detail and MacCready outlined the theory of optimum inter-thermal flight speed used to maximise range while minimising flight time [43]. This strategy is still implemented by pilots today and has been found to match the strategy of many larger birds [6, 42].

Thermals have received attention for soaring UAVs, from the identification of thermal features [44], to implementing autonomous soaring [37–39]. Several approaches have been used to detect the centre of thermals including a range of sensors and trajectory optimisation. With use of thermals Allen was able to extend the endurance of a glider from 2 hours to over 14 hours (over several flights) [37], the control strategy was based on relatively simple control laws equivalent to those learnt by human pilots. With recent advancements in machine learning UAVs were able to learn through reward based control schemes while on-the-fly demonstrating progress in autonomous thermalling [45].

2.1.1.2 Orographic Soaring

Orographic lift is produced as traversing winds are deflected vertically by rising terrain; the phenomenon is known to play an important part in the hydrological cycle and cloud formation [46, 47]. A strong oncoming wind and a steep terrain feature such as a sea cliff can generate enough lift for birds, para-gliders, hang-gliders and even sail-planes, to stay airborne for extended periods of time, see Fig 2.3. In the gliding community, this is known as ridge or orographic lift and some of the gliding techniques are known as slope soaring, slope gliding, sloping or orographic soaring. Many birds have been seen to traverse ridge features using the area of lift in front of the windward side by maintain a flight path parallel to the ridge feature [9, 35, 48, 49] but it is also possible to take

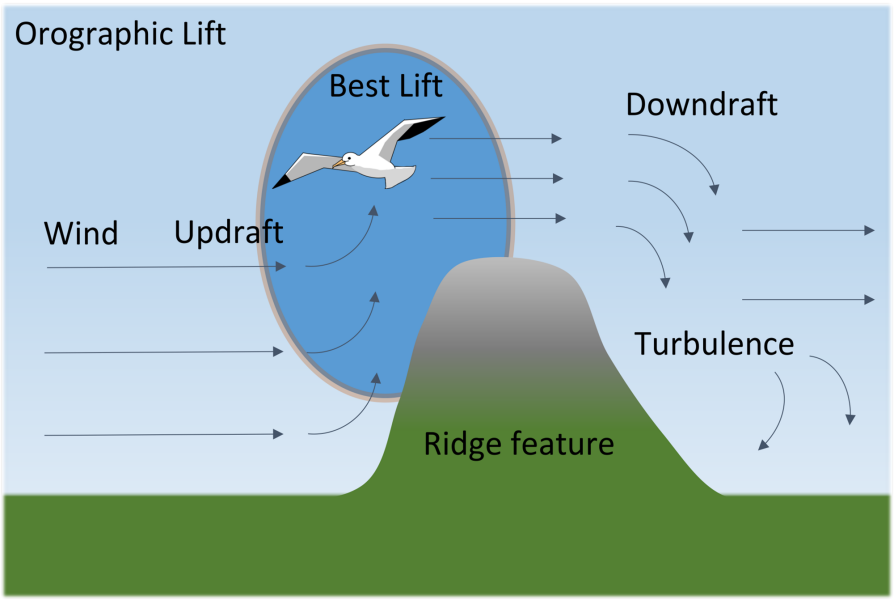

Figure 2.3: Depiction of ridge lift with the area of best lift highlighted

advantage of this flow perpendicularly in order to maintain hovering flight, such as is well documented for kestrals, *Falco tinnunculus*, [50–52] and other raptors (and has been observed in ravens, *Corvus corax*, and lesser-black backed gulls by the Author).

Glider pilots also use orographic lift with reports that for perpendicular winds at 15 knots (7.72 m s^{-1}) will provide enough lift to support a glider [53] and that the maximum lift occurs at a 45° angle upward from the leading edge of the ridge [54]. Often glider pilots will exploit the lift in the mountain wave effect on the leeward side which has the added benefit of being out of the wind with a lower risk factor due to being some distance from the ridge feature [55]. The orographic lift available in mountain regions can be so strong and reliable that in a glider endurance challenge, which see pilots positions themselves into the wind in front of ridge features, recorded a flight time of over 71 hours [56].

Orographic soaring in UAVs was first outlined by Langelaan as increasing flight ranges [57] where it was found that energy costs could be reduced with increased flight times. Langelaan simulated flight trajectories for an orographic soaring UAV using parallel orographic lift features, a point-mass vehicle model and *a priori* wind field were implemented with a tree-based path planning algorithm [34]. This was the basis for research produced by Chakrabarty in which a temporally static energy map was used as part of a cost function explored with a wave-expansion path planning algorithm, A* [58]. The energy map featured was used in place of a heuristic but largely acted to the

same effect, estimating the cost to goal. In both cases significant energy savings were found however, the simulations were restricted to a set altitude and used a limited number of nodes. However, the flight dynamics did accounted for altitude within the cost calculations. From the same research group, Al-Sabban, went on to include time varying uncertainty in the wind fields using a Gaussian distribution in a 3 degree-of-freedom lateral model. A Markov Decision Process algorithm with a most visit cell technique was used to determine the optimum solution, again assuming a constant altitude through the wind field [59]. Real-world implementation has also been achieved where an MAV soaring the updraught in front of a large building to gain substantial altitude [60, 61]. They concluded that with a head wind of over 3 m s^{-1} the updraught in front of the building could sustain UAV flight in the perpendicular or parallel directions. There has been an effort reduce flight costs in a rotary-vehicle using CFD generated urban wind fields. In this case, a small urban area was modelled and a fixed altitude assumed by real-world testing found a reduction in energetic cost [62].

2.1.2 Dynamic Soaring

Dynamic soaring was thought to have first been recorded scientifically by Lord Rayleigh [63] proposing wind gradients as the source of energy for the soaring birds as far back as 1883. Recent work however, now attributes that to Da Vinci documenting soaring birds several centuries earlier [64]. Dynamic soaring is typically described by a series of arcs where the bird or platform exploits the directionality of the wind to manipulated its velocity relative to the wind resulting in a gain of kinetic energy which can then be transferred into potential energy. The dynamic soaring strategy is most famously associated with the albatross, *Diomedea exulans*, these birds are able to soar for weeks if not months at a time [16, 65], but there are documented observations of other large sea birds such as pelicans [64], *Pelecanus onocrotalus*, giant petrels [66], *Macronectes giganteus*, and even great black-backed gulls [64], *Larus marinus*, performing dynamic soaring to cover great distances at very little energetic cost. Over the years understanding of dynamic soaring has developed, initially the process was considered solely through the use of wind gradients but more recently it has been proposed that it is a combination of gusts and gradients which facilitate the soaring of the albatross. The two methods will be described below but it should be noted that there can be some cross-over with the terminology especially in literature regarding the dynamic soaring of albatross where both concepts are used simultaneously.

2.1.2.1 Gradient soaring

Gradient soaring typically relies on a variation of wind speed with altitude. By varying both altitude and direction it is possible to use the wind to propulsive effect, the next description assumes travels is in a crosswind direction but it is also possible to perform up- and down-wind travel through the inclusion of loops. Starting at the bottom of a cycle, the bird climbs into the wind, the birds is able to maintain airspeed and gain altitude due to the increasing wind. At the top of the cycle the bird performs a banked turn to face downwind, now with a tailwind it dives, converting the potential energy back into kinetic energy to overcome drag and to increase airspeed against the decreasing tailwind. By the end of the cycle the bird has made no net energetic gain but travelled some distance, see Fig 2.4.

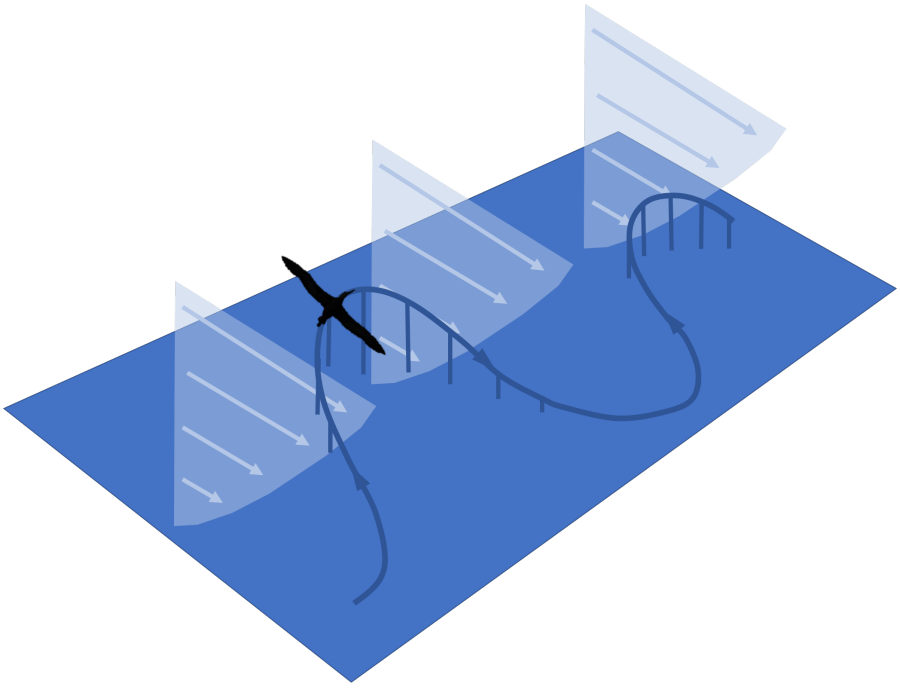

Figure 2.4: The wind profile is slower at the surface than at height facilitating gradient soaring and cross-wind travel.

Another form of gradient soaring uses a closed loop variation in the shear winds on the leeward side of ridge features. Radio-control gliding hobbyists have perfected a technique using cyclical flight paths which maintain mean position but increase in kinetic energy in each cycle. Current records exceeding speeds of 877 km h^{-1} in 2018 [67]. Additionally, some birds have been observed performing dynamic soaring in this way, using the shear to gain velocity before a climb or to keep flight costs low while foraging.

Initially it was thought that albatross were solely using wind gradients to achieve long distances but more recently, with GPS tracking and improved meteorological modelling it has been discovered that the wind gradients alone may provide insufficient energy to explain dynamic soaring. Pennycuick proposed that in addition to the wind gradient, the separated flow pockets between waves provide the additional kinetic energy, in a form of gust soaring [66]. However, this is still under contention [68].

Wind gradients continue to receive a large number of studies looking at optimal trajectory for energy transference in dynamic soaring cycles [68–70]. Most optimisations on dynamic soaring are based in simple gradient fields with little or no variation and are often over flat ground. Theoretically, UAV gliders should be able to soar over flat ground as they have a better glide angle than albatross and can make use of only the wind gradient, however, this has not yet been implemented. Nevertheless, a power-assisted dynamic soaring strategy was proposed by Zhao [71] and in simulation was found to effectively reduce propulsive requirement in gradient only wind fields. Work from Lawrance integrated both static and gradient soaring in to a path planning framework and used modelling techniques to develop methods for predicting thermals and gradient wind fields in one of the more complete works so far [8].

2.1.2.2 Gust Soaring

Gust soaring refers to the manoeuvres that can be made through stochastic pockets of varying wind in order to gain energy. For example, in an upward gust there is an initial increase in updraught followed by a decrease. In an increasing updraught it is possible to gain energy by initiating a climb and it is possible to continue gaining while diving through the decrease. Similarly, it is possible to gain a small amount of lift if diving through a downward gust, as the gust finishes the wing sees a relative upward change and gains lift. Horizontal gusts can also be exploited by changing that bank angle of the platform, by banking into the wind it is possible to convert the gust into lift, albeit with a horizontal propulsive component [72, 73] see Fig 2.5. These manoeuvres have been outlined several times but most thoroughly explained by Lawrance [8]. The same manoeuvres are applicable in gust and gradient soaring but the temporal scale can be somewhat shorter in gust soaring. Even manned gliders perform a variation of gust soaring, called dolphin soaring, through unused thermals, such as those that are too narrow [74].

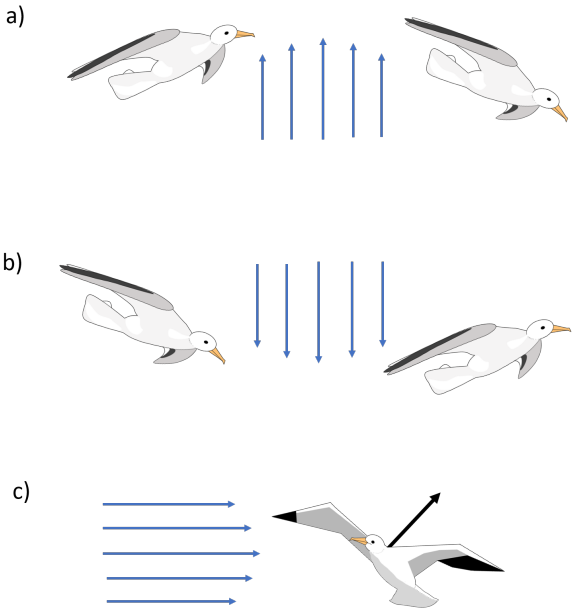

Figure 2.5: a) The gull climbs into the increasing updraught and dives with the decreasing updraught such as in dolphin soaring b) The gull dives with a downward gust and it returns to still air feels and increase in lift c) Banking away from a horizontal gust to receive a side ways lift

Gusts are stochastic and have a short temporal scale meaning that they are an unreliable source of environmental energy. Furthermore, it is vital to have acute gust sensing capabilities which until recently has meant gust soaring for as a means of facilitating soaring in UAVs was an unrealistic goal [75]. However, with recent improvements in wind sensing capabilities, gust soaring offers new potential to SUAVs, not only is it a source of harvestable energy but it also offers a means of improving stability [76, 77].

Langelaan has presented recent work looking at predicting stochastic shear layers for autonomous dynamic soaring using point measurements [34] using only existing on-board sensors measuring position, orientation, static and dynamic pressures, but found that the predictions were insufficient, flying too fast in favourable and too slow in unfavourable winds. Recently, lightweight differential wind probes have been developed by Watkins and which offer potential in wind field sensing, successfully implementing turbulence stability control and more recently demonstrating potential in both gradients and gusts for soaring and stability [76, 77]. These probes extended approximately a chords length in front of the platform and collect differential dynamic pressure readings through 5 holes at a pointed end. This system is reminiscent of the nasal features of

an albatross, acting like pitot tubes work to detect pressure differences in the air flow. Pennycuick proposed that the were able to implement gust soaring because their tubular nasal cavities, which act like pitot tubes, are sensitive enough to detect gusting [16].

2.2 Bird Tracking Methods

There are many animal tracking technologies available that specialise in long term tracking for migration studies [30], basic techniques such as ringing with observation reports, tags with radar, and more recently, GPS tags [32, 78, 79]. While these methods are able to record data over many years the data resolution is low and the research focused on large scale movement. Pennycuick and others have tracked migrating birds by flying alongside them in migration [80, 81], ultimately this helped him to validate the flight models proposed from data collected in wind tunnel experiments [16]. Pennycuick later went on to develop the ornithodolite, a laser range finding binoculars equipped with angular encoders [82] however, requires the user to remain in a stationary location and wait for birds in range. The University of Amsterdam have developed a Bird Tracking System (UvA-BiTS) which is able to record a GPS position every three seconds and has been recently used to predicted meteorological conditions [83]. The UvA-BiTS team have also used tri-axial accelerometers to classify behaviours [32]. While using GPS, accelerometers (bi- and tri- axial) and predicted wind fields has been undertaken before [84–86] and provided great insight into the flight performance of birds [35, 52, 87], these studies have not been focused on the same fine-scale urban flight and aerodynamic analysis. Accelerometers have been used to record body motions and with direct proportionality to exertion in terrain based motion this has been used to estimate the energetic costs in animals [88] and to classify behaviours [35].

Research by Shepard used energy landscapes to model the metabolic cost of animal's daily motion through different terrain types [9]. The cost functions generated have shown that energy expensive terrains are circumnavigated in order to conserve energy. Animals with larger metabolic resting rates will be limited on the extra distance they are able to travel around these. Often over looked is that rewards can be found along some paths which give these paths a greater weighting. For example, a bird may travel a much greater distance along a ridge with updraught at a much lower energy cost than travelling to the same destination directly. The cost function for transport is typically found using the shortest path through the energy landscape however this requires prior

knowledge of energy cost of each layer and distribution of resources. In addition, a single animal is unable to experiment with an individual route however, they may use some kind of discovery algorithm if it is a repeated journey. As such the optimum paths through the energy landscape is best seen through the analysis of multiple individuals over a multitude of journeys. Research in which Shepard tracked condors in the Andes demonstrated that birds favour the windward slopes, the popularity of certain routes between foraging and nesting areas is such that the term *wind-highways* becomes suitable.

2.3 Conclusion

The study of bird flight was key in development of manned flight, with the increased interested in UAV technology the study of bird flight could again be a key in producing platforms effective at operating in complex urban flow. SUAVs have a limited battery capacity so the implementation of soaring capabilities could facilitate their use in urban environments. Previous research has focused on a variety of soaring strategies but many of these cases at a broad-scale with little or no obstacles and do not represent the urban environment. There has been little work focused on urban environments which consider the effect of wind conditions in the context of path following or performance [62, 89, 90], these offer some solutions for wind correction guidance in trajectory following. However these often lack complexity in other ways, for example in simplified models, lack of a 3D environment or low spatial resolution between nodes. With new technology in GPS tracking for birds, combined with the development of complex wind modelling it could now be possible to gain an understanding of the energy landscape in which birds fly [9]. Considering the environment as an energy landscape for movement has been directly applied in path planning methods for UAVs in simple topography [7, 57], this research considers applying these methods in more complex cases in order to move toward wind-aware urban SUAVs.

CHAPTER 3

SOARING ON URBAN WIND-WAYS

Birds modulate their flight paths in relation to regional and global airflows in order to reduce their travel costs. It follows that birds should also respond to fine-scale airflows, although the incidence and value of this remains largely unknown. We resolved the three-dimensional trajectories of gulls flying along a built-up coastline, and used Computational Fluid Dynamic (CFD) models to examine how gulls reacted to airflows around buildings. Birds systematically altered their flight trajectories with wind conditions to exploit updraughts over features as small as a row of low-rise buildings. This provides the first evidence that human activities can change patterns of space-use in flying birds by altering the profitability of the air-scape. At finer scales still, gulls varied their position to select a narrow range of updraught values, rather than exploiting the strongest updraughts available, and their precise positions were consistent with a strategy to increase their velocity control in gusty conditions. Overall, airflows around fine-scale features have profound implications for flight control and energy use, ultimately, strategies such as these could help Small Unmanned Air Vehicles (SUAVs) negotiate complex airflows and reduce energy costs.

Author Contributions: Wind and gull models created by Cara Williamson (me) and gull data capture and statistics models performed by Dr Emily Shepard. The work presented in this chapter has been previously published [10]. Dr Shane Windsor contributed major edits to the publication.

3.1 Introduction

Migration studies have shown that birds make navigation choices based on regional and global weather conditions [87, 91–95] and it should follow that birds also use local, fine-scale airflows. Two gull species, herring, *Larus argentatus*, and lesser black-backed, *Larus fuscus*, common to the UK, have been observed soaring in the Swansea Bay. The Swansea Bay is remarkably flat however, there is a row of four-storey, seafront hotels which the gulls appear to be using. The gulls' method of flying in this area is reminiscent of orographic soaring, typically seen in front of sea-cliffs. This study acts as a proof of concept on two fronts. Firstly, that these gull species are able to use man-made features for orographic soaring. Secondly, to determine whether understanding the gulls' flight strategies could prove useful in urban SUAV technology.

This initial investigation is a relatively simple case study, with one type of energy harvesting and a small field-site as pictured in Fig 3.1. During periods of onshore winds (South-Easterly), the air is travelling in from the sea and then over a long, flat beach, uninterrupted by ground clutter until meeting a row of four-storey buildings where it is deflected upwards. Thus being a relatively simple example of orographic lift generation, perfect for determining whether gulls are using the fine-scale airflows available.

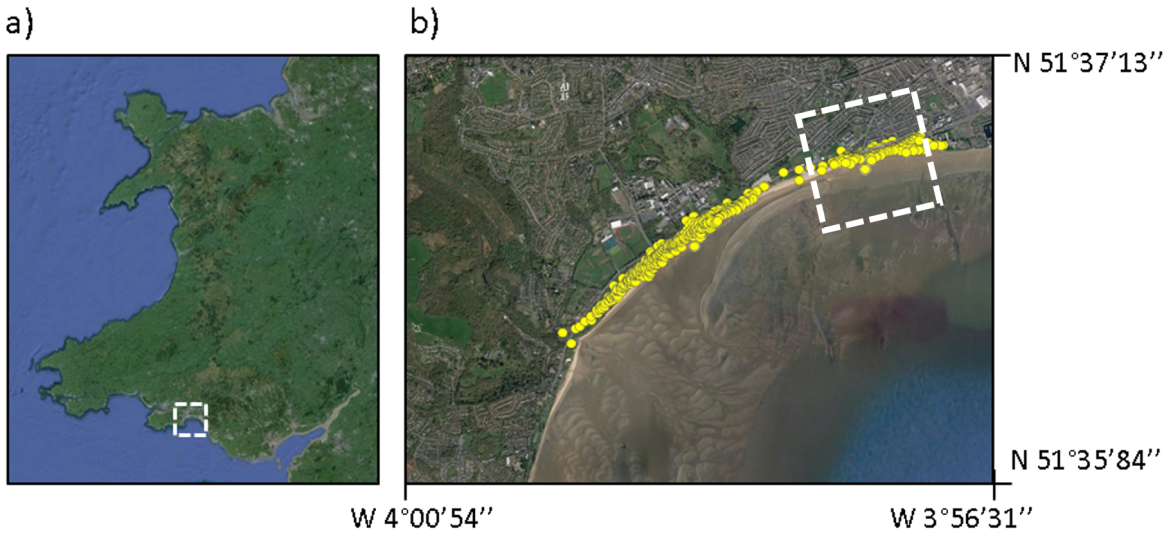

Figure 3.1: a) Location of Swansea Bay marked in white box b) Map of observation area with extent of wind model marked with white box and gull observation data displayed with yellow markers.

3.2 Methods

3.2.1 Data Collection

The flight data was collected from the Swansea Bay area by Dr Shepard using an ornithodolite based on Prof. Pennycuick's design [82], as shown in Fig 3.2. Gull observation data was collected on days with variable wind direction and speeds, the full dataset can be seen on Fig 3.1. Balloon tracking was performed at the beginning of each observation session in order to profile the onshore wind. Recorded information included the location of observer and ornithodolite, the observation fixes in a North-East-Up reference frame centred at the ornithodolite, and an observation index with time delay. The date and time for the start of each observation session is also included and has been used to determine the tide height for each model.

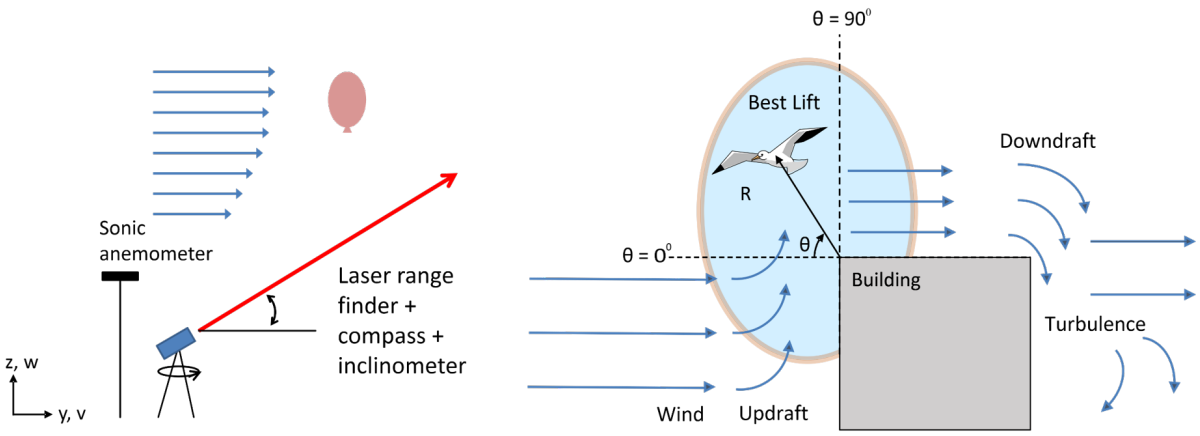

Figure 3.2: Experimental set-up diagram indicating the radial and angular measures used to define trajectory positions relative to the buildings

3.2.2 Wind Models

In order to understand how the gulls are taking advantage of the orographic lift generated in front of the buildings it was necessary to understand the airflow being experienced by the gulls. As such, an accurate model of the observation site was made using publicly available [96, 97] terrain and topography datasets. The wind models was built in the Quick Urban & Industrial Complex (QUIC) software [98] from the Los Alamos National

Laboratory, designed to estimate urban wind fields. The models offer an averaged static estimate of the wind flow in the study area based on the wind profile inputs. The wind profiles were recorded by regular balloon releases. Observation sessions varied in length from thirty minutes to two hours, in order to accurately record the wind conditions a balloon was released at approximately every twenty minutes intervals or after any significant change in wind condition. The captured flight paths were segmented to the nearest temporal balloon track and this time was used to generate the most accurate surface model in accordance with any tidal variation.

3.2.2.1 Digital Elevation Model

The first step in the wind model creation was to generate a map for the experimental area. This process used an elevation map of the location's terrain, typically, elevation data is measured using a laser scan technique (LiDAR) from small fixed-wing or helicopter platform. The UK Elevation dataset is currently managed by Airbus and data can be requested for a small handling fee. The Digital Elevation Models are combined of two models; a Digital Surface Model (DSM) and a Digital Terrain Model (DTM). Data is typically available in four resolutions; 2, 1, 0.5 and 0.25 meter however, at the time of writing the experiment area was only available in at a 2 meter resolution. The DSM model included all surface features present at the time of the laser scan, this includes surface clutter such as vegetation, as well as building infrastructure. DTM model contained only the terrain data, these models are generated by filtering all non-geographical features. Additionally, the DTM contained no water bodies, representing coastal regions at low tide with elevation values recorded in meters above Ordnance Datum Newlyn [99]. The DTM used was formatted as an ASCII grid in British National Grid (BNG), a two-dimensional coordinate system based on the Ordnance Survey OSGB36 geodetic spatial referencing system with a Transverse Mercator projection [100].

ArcGIS software (ArcMap v10.1), was used to convert the DTM from BNG into the Universal Transverse Mercator (UTM) reference system as required by QUIC. The most accurate conversion method required an intermediate projection in to a geodetic system, in this case OSGB36 [100].

3.2.2.2 Tidal Model

The coastal nature of the study site meant that any accurate surface model needed a variable minimum height dependant on the observation time. To apply these adjustments, the tide heights were calculated using a tidal model. Records for the times and heights of

low and high tide over the observation periods were sourced via TideTimes [101] in Chart Datum (CD) and converted to ODN [99]. These records were stored as a lookup table. The tide height is influenced by two frequencies, the Earth's annual rotation and the Moon. These interactions can be considered as two sinusoids with differing amplitudes and frequencies. Interpolation of the records using this sinusoidal model provided the height at time of each balloon released. This method same method is used in tide predictions [102] so was considered an accurate surface estimation. The tide height value was then used as the new minimum for the elevation raster and was applied to the original, no water body, DTM model, such that an elevation model was generated for each of the observation sessions, with the tidal height corrected for the time of each balloon released.

3.2.2.3 QUIC wind modelling

The Quick Urban & Industrial Complex (QUIC) [98] dispersion modelling system was designed as a fast response urban chemical dispersion model that can run with in-the-field with limited processing power such as available on a laptop. Designed as a method for predicting airborne contaminants it can generate a 3D wind field model, is specialised for fast performance and was based wind tunnel measurements of building flow interactions. The software was verified with a real-world experiment in Oklahoma city in 2003 [22, 23]. Several versions have been released, this research used the 2014, 64-bit Windows version with the 2014 MATLAB Compiler, this was the latest version at the time of publication.

The QUIC software contains two wind field solvers, the first, known as the URB model, uses mass conservation and empirical diagnostics to quickly compute the 3D flow field around building complexes. The second solver uses a simplified Reynolds-averaged Navier-Stokes (RANS) CFD model and will be referred to as QUIC-CFD. This model is significantly slower than QUIC-URB, requiring greater processing demand, but produces more accurate wind field solutions. The QUIC-CFD model runs faster than traditional CFD code through the use of a simplified turbulence model with a diagnostic turbulent length scale [98, 103]. Several papers have been published evaluating the accuracy of the the models in comparison to a Large Eddy Simulation (LES) CFD model and real-world measurements from 150 2D and 3D sonic anemometers placed strategically around Oklahoma City [22, 23, 98, 103, 104]. They found that the QUIC-URB and QUIC-CFD models were within 50% of the recorded wind speed 49% and 53% of the time respectively, only 10% lower than a LES CFD alternative (62%). The wind direction in the two models were within 30 degrees of the measured data 43% and 50% of the time, compared to 58%

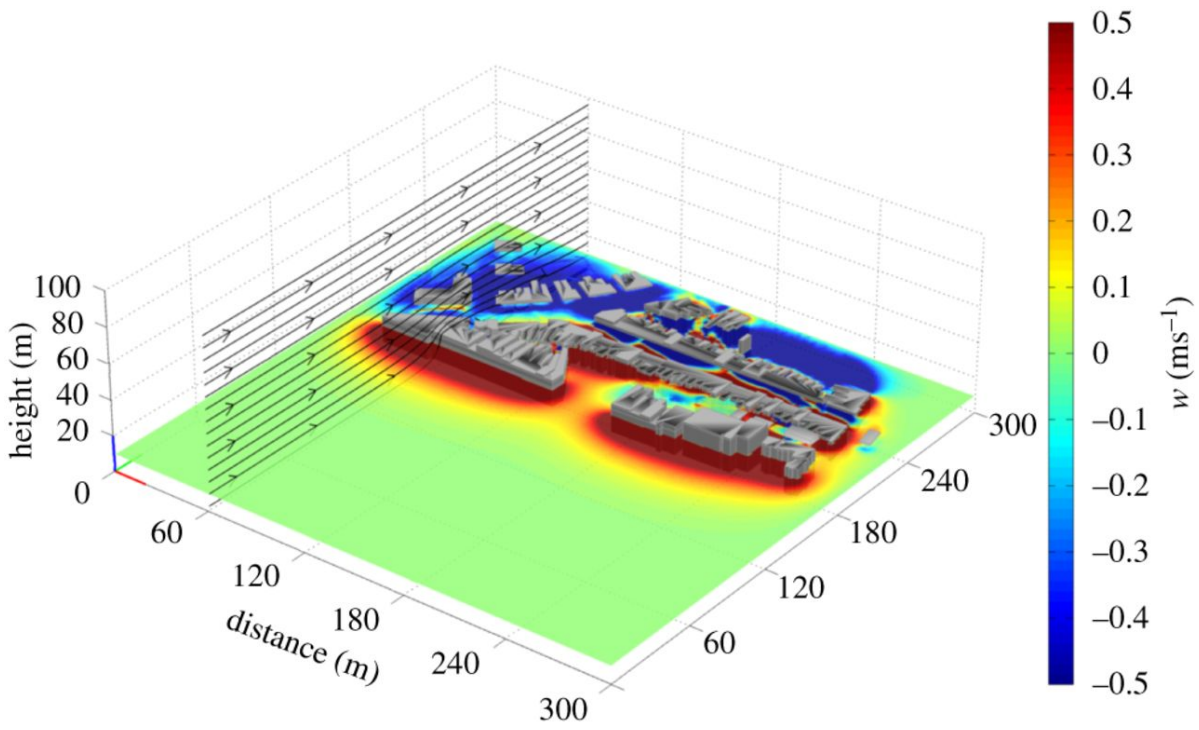

Figure 3.3: The vertical wind vector component (w, indicated with a colour scale) within the study site, at a height of 10 m above ground level and with a wind input of 7 m s^{-1} and a direction of 141° from North. This illustrates the variability of the flow field and the volume of the downdraughts in relation to the updraughts. The colour scale has been limited to ±0.5 m s^{-1} (just above the minimum sink rate).

for the LES CFD model.

QUIC uses elevation and topography inputs to build an environmental model however, it should be noted that while the elevation model is used build a 3D landscape the terrain does not contribute to the orographic updraught generated. For example, a steep hillside does not produce an orographic updraught in the QUIC model where it would in the real world. This does not pose an issue when considered over relatively flat terrain as orographic updraughts generated by building are likely much greater than small terrain features.

3.2.2.4 The Urban Features

A section of the observation area 300 x 300 x 100 meters with a grid size of 1 square meter provides the base for the model. This size was a trade-off between the full size of the observation area and the processing ability of QUIC at high resolution. Typically, the

program has been run and tested over grid sizes of 2,000,000 cells[1]. The building features were taken from the Digimaps on-line database [97] where the Ordnance Survey (OS) topography areas and building height datasets for the United Kingdom are available. Joining the building height attributes table with the topography area in ArcGIS software (v10.1) it was possible to create a two-dimensional shape file suitable for use in QUIC. The algorithms used by the QUIC software are most accurate when the buildings are in alignment with grid cells [103], as such the area was rotated 13° clockwise from North, such as in Figs 3.3 and 3.4.

3.2.3 CFD and URB models

The QUIC CFD and URB models produced similar results however some differences are seen in the building wakes and size of the lift tunnel in Fig 3.5. A randomly sampled flight trajectory was used to compare the two models, across both models the difference in the sampled wind direction was a maximum of 2.3°. In the case of wind speed, the variation between the CFD and URB models reached maximum of 7%, except in the case of the vertical wind component where the small values meant differences of up to 40%. As this component will be heavily used in this research and the CFD models are considered more accurate wind flow representations the CFD models will be used.

3.2.4 The Wind Profiles

The collected flight observations were categorised such that a balloon track occurred at the temporal mid-point. A balloon was released by the observer and tracked with an ornithodolite; laser range finding binoculars used in conjunction with a 2-axis sonic anemometer from Gill Instruments, as seen in Fig 3.2 to record the magnitude and direction of the wind at a height up to 5 meters. Atmospheric conditions such as the air density, temperature and pressure were also recorded and used in the QUIC set-up. The East-North-Up (ENU) coordinates of the balloon were recorded alongside the observation index and time delay. Ornithodolite Analysis, software created at the University of Swansea, was used to calculate the magnitude and direction of the wind at each observation fix. The balloon release took place at the observers location and was used to capture the relatively stable onshore wind profile. The wind profile was used as the boundary layer input data for the wind flow modelling.

[1] E-mail communication

(a) 3D Google map image of the Oystermouth Road hotel area in Swansea Bay

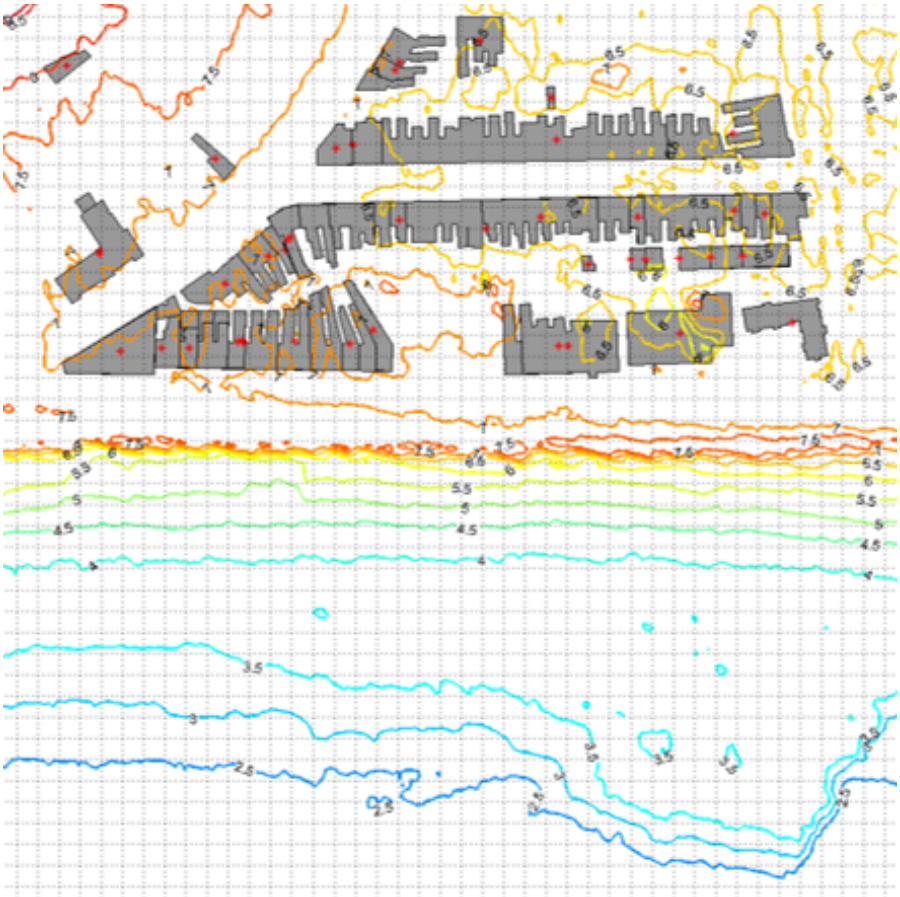

(b) Close-up of run 9 using QUIC's CFD model

Figure 3.4: QUIC model of the Oystermouth Road hotel area with buildings shown in grey and a tide height 2.5 m ODN as shown by coloured contour lines in meters

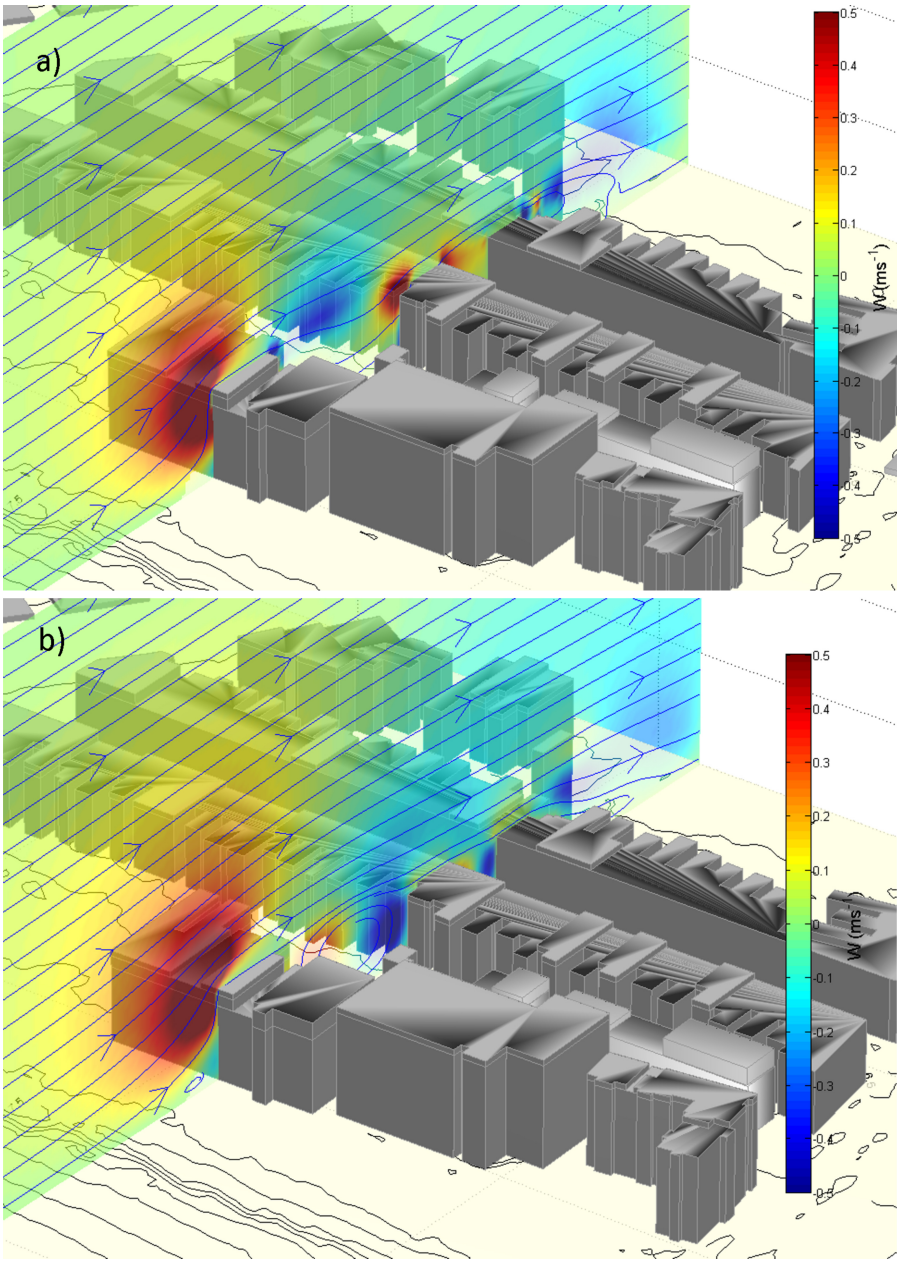

Figure 3.5: Comparison of a) URB and b) CFD models for hotel site with wind direction 140° from North and wind speed 2.3 m s^{-1}. The up- and down-draughts in the YZ plane have been highlighted by introducing colour map limits with stream line overlay of wind in in-flow direction. Notice the differences in the flow between rows of buildings.

A logarithmic profile was fitted to the data and used as an input profile in QUIC. The QUIC software uses the surface roughness, z_0, and Monin-Obukhov reciprocal to better calculate the wind profile. The Monin-Obukhov value is defined as the height at which the buoyant production of turbulence kinetic energy is equal to that produced by the shearing action of the wind [46]. Diurnal values for the Monin-Obukhov reciprocal are typically negative in relation to the unstable stratification of shear layers, the dimensionless value ranges from zero to several tens. The best qualitative match in wind profile was found using a Monin-Obukhov value of -0.001, this value relates to almost neutrally stable layers as could be expected in coastal onshore winds. Individual surface roughness coefficients were chosen to match the inner and outer grids. Surface roughness of an open plane with little or no surface clutter, for the inner grid, and an open water body for the outer grid, corresponding to 0.005 and 0.0002 respectively [105], were selected. The wind direction for the profile was taken as the mean over all the recorded points. Fourteen (Run 2 - 15) wind models were generated, but on closer inspection seven of these were excluded, three due a large number of observation points in flapping flight and four due to missing observer location data. The seven wind models used in this study were generated using the input data summarised in Table 3.1.

Table 3.1: Model conditions where the direction of wind source measured in degrees from North and tide height in meters ODN.

Name	**Date**	**Wind Direction (°)**	**Wind Speed (m s^{-1})**	**Tide Height (m)**
Run 2	2014-06-25	122	7.8	-2.38
Run 3		132	6.7	-3.09
Run 4		140	7.5	-2.10
Run 5	2014-07-07	212	4.8	2.15
Run 6		216	5.6	2.39
Run 14	2015-09-11	137	9.34	2.13
Run 15		144	8.28	3.09

3.2.5 Bird Flight Model

This research investigates how large gulls use orographic lift as an energy resource in their daily motion. The analysis in this research makes two assumptions. Firstly, that the gulls are flying through a temporally static wind field as no turbulence or gusting is taken into account. Secondly, that all the gulls observed can be described by a fixed-wing variation of Pennycuick's glide polar model using averaged biometrics taken from the

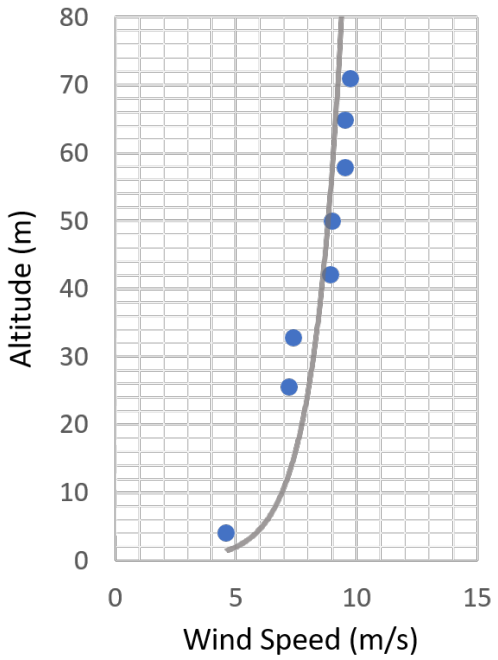

Figure 3.6: Logarithmic wind profile, shown by the grey line, used as input for QUIC model fitted to the balloon observation points, shown as blue markers

Flight database [16]. This investigation will explore how gulls harvest environmental energy from orographic updraughts whilst gliding by considering equilibrium glide.

3.2.5.1 Combining Bird and Wind Data

The bird data was recorded in meters in the East-North-Up reference frame with the observer's position as the origin. The position of the observer was recorded as a WGS latitude and longitude position using a GPS device. The raw bird data was transformed into the wind models reference frame using the site rotation and the observer position vector. The observer's position vector was converted from WGS latitude and longitude into UTM using [106] which converts from units of degrees into meters. The elevation of the observer was found using the DTM elevation raster and the height of the ornithodolite.

The three-axis wind components were interpolated for each observed point using the inner grid wind model output from QUIC using MATLAB interp3 function. Observation points which fell outside the inner grid were discarded. The three-axis ground speeds of the birds at the observed points have been calculated using spatial difference between

observations and the time step. This analysis is interested in the relationship between forward and vertical speeds and as such will consider them separately. The true air speed (TAS) of the birds at the observation fixes are calculated using the two horizontal vector components of ground and wind speed, as shown in Fig 3.7. The vertical air speed is calculated as the difference between the vertical wind speed and the sink speed experienced by the gull. To make fair comparisons between flight trajectories, and from flight trajectories to the glide polar, the TAS was corrected to the Equivalent Air Speed (EAS). The air density at gull altitude was extrapolated using the observed height of the gull, air pressure and temperature were recorded at the observers location.

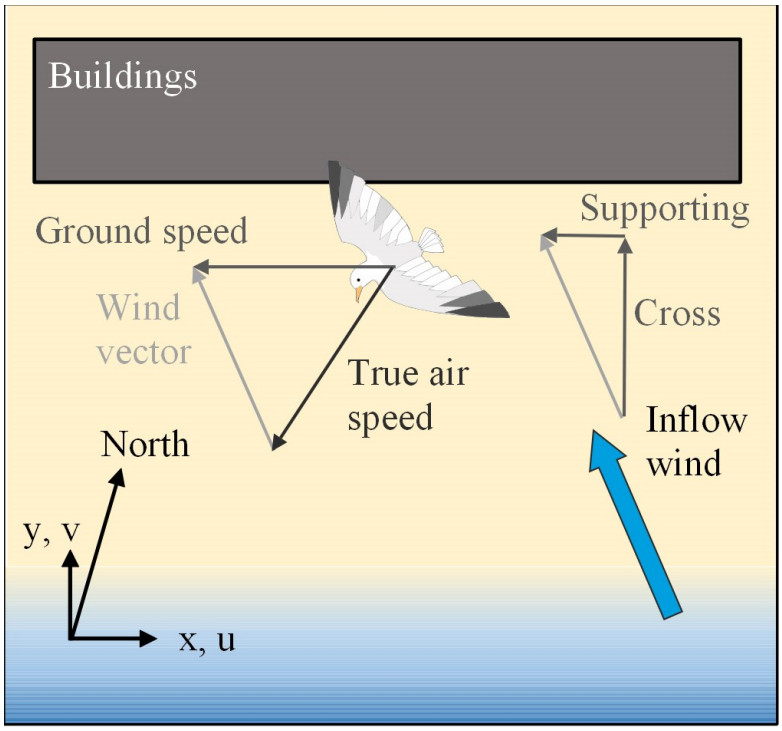

Figure 3.7: A velocity vector diagram demonstrating ground speed and true airspeed of a gull flying in wind conditions consisting of a large cross wind and small supporting wind component

The wind fields generated by the QUIC model were used to analyse data in three ways. Firstly, to estimate the vector components of the airflow aligned to the model grid associated with the 3-dimensional position of the gulls in the observation fixes. In these cases the airspeeds were calculated with the ground speeds measured and the interpolated wind model grid data. Secondly, the vertical component of the airflow (the w component) corresponding to the observation fixes and the maximum available updraught in the model were compared. Finally, the feasible airspeeds that the gulls

could fly at if trading all excess updraught for forward airspeed, found by sampling the glide polar at a sink-rate corresponding to the sampled updraught at the gulls' mean trajectory position.

In case two and three, the trajectories were considered individually rather than as a global dataset. As such, was assumed that the gull was holding velocity and position, including altitude, as such the observed points have been averaged over the entire trajectory. The trajectories were aligned with front of the buildings, and considered as an average along the model's x-axis, effectively reducing the model to a 2D map in the y-z axes. The row of buildings was aligned in the x-axis and the position of the gull in each trajectory path considered as a radial and angular position from the top leading edge corner as shown in Fig 3.2.

3.2.5.2 The Glide Polar

During gliding flight the weight of the flying body is balanced by only lift and drag, D, forces, there is no thrust input. Forward flight is maintained by exchanging potential and, or kinetic energies in order to overcome the drag force such that the bird either has a decreasing altitude or reducing speed. The geometry of a bird's wing and the angle at which it meets the airflow is such that the flow is forced underneath the wing creating a pressure potential vertically over the wing, increasing the pressure on the underside and reducing the pressure on the topside, and consequently generating the lift force. The pressure differential reduces in the direction of the wingtip creating vortices which generate a downwash in the trail of the wing. Induced drag is generated from the downwash effect and is inversely proportional to the squared airspeed, U, and highest at the stall speed and lower, the lowest airspeed which will generate enough lift to overcome weight and where the flow begins to separate from the wing surface becoming unstable. The induced drag is described in the first part of the drag equation, Eq. 3.1, where mg represents the bird's weight, ρ is the air density, b is the wing span, and k_s is the induced drag factor. Bird's vary their wing span, this is represented by β and is a value of one, at full span, or less. The induced drag equation considers that the lift distribution over the wing is elliptical, deduced from Prandtl's lifting-line theory described in [107]. However, Pennycuick proposes that this represents an ideal case only and the drag over a bird's wing would be greater, resulting in an induced drag factor greater than, but close to, one. The value of the induced drag factor has more recently come under scrutiny where alternative models, and even Pennycuick [108], have suggested values of 1 or less, which result from primary feathers acting as winglets and deflecting the wing vortices upwards,

this is particularly relevant in flapping, rather than gliding, flight. Alternative models will be discussed with more detail in the subsequent chapter, see Sec. 4.2.1, and for now, a drag factor of 1.1 will be used, in line with the 2008 Flight model.

$$D = \overbrace{\frac{2k_s m^2 g^2}{\pi \rho b^2 \beta^2 U^2}}^{\text{Induced drag}} + \overbrace{\tfrac{1}{2}\rho U^2 c_{D_b} S_b}^{\text{Parasitic drag}} + \overbrace{\tfrac{1}{2}\rho U^2 c_{D_w} S_w}^{\text{Profile drag}} \tag{3.1}$$

The second and third part of the equation describe further drag forces generated by air resistance and skin friction against the body form and wing surface, these are both considered parasitic drag as they do not form as a result of generating lift. Drag generated by air resistance on the body will be referred to as parasitic drag whereas, drag generated by skin friction over the wing will be referred to as profile drag. Variables C_{D_b} and C_{D_w} are drag coefficients for the body and wings, these have been determined by Pennycuick during wind tunnel experiments over several species. It is a standard practise to record wing surface area during specimen biometrics readings, in the case of a live individual this is achieved by drawing carefully around an outstretched wing and doubling the value. Additionally, the measurement between the wing root and central back is recorded so that the wing area over the back can be added to the total. As surface area of the wing varies with sweep angle, another factor, ϵ, is included in the profile drag equation to account for the sweep factor and is described in equation 3.2 which includes a constant called the planform slope, δ, which is set to one in the Flight database. The body surface area, S_b, is more difficult to measure in live individuals; Pennycuick determined a formula based on the body mass through the examination of many specimens across a number of species, described in equation 3.3.

$$\epsilon = (1 - \delta(1 - \beta)) \tag{3.2}$$

$$S_b = 0.00813 m^{\frac{2}{3}} \tag{3.3}$$

The parasitic and profile drag forces are proportional to the square of the flight velocity, or airspeed, so it follows that at a higher airspeed these drags acting on the bird are greater. However, gulls sweep their wings to control their airspeed, this changes the geometry of the wing, affecting the twist and camber of the aerofoil as well as acting to reduce the surface area of the wing and total drag force. Pennycuick offers two models for drag reduction, an optimised drag reduction and a linear wing sweep model. The optimised drag reduction model reduces wing sweep with increasing airspeed to achieve

the lowest drag force possible, however it has been observed in wind tunnels and free-flying birds that wing sweep reduction tends to be linear [16]. The resulting relationship between the airspeed and drag forces for three models are shown in Fig 3.8.

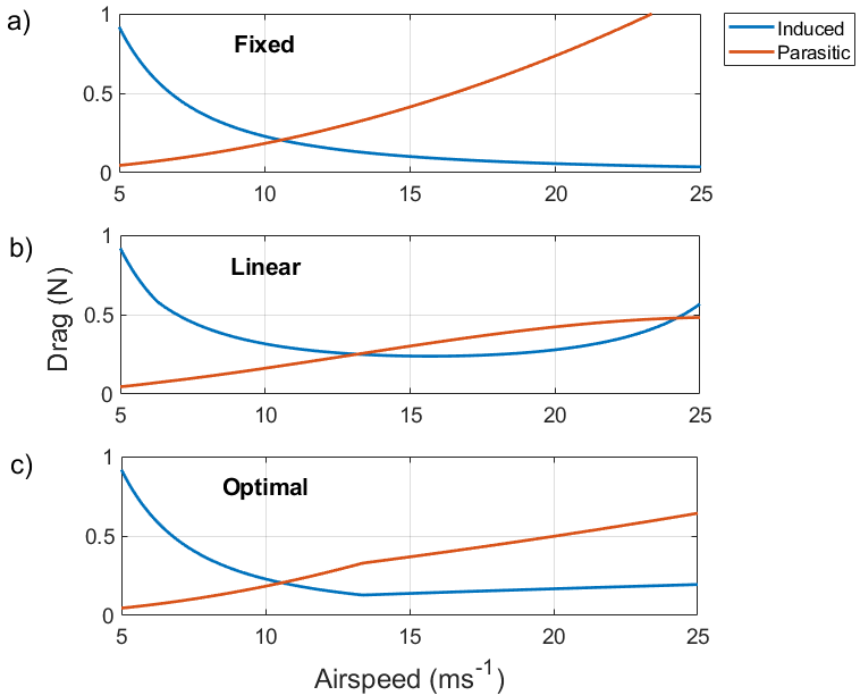

Figure 3.8: Induced and parasite drags for a) linear span reduction, b) optimal drag span reduction and c) fixed wing, at a range of airspeeds, where the parasite drag is the summation of the body and wing friction drags, as described in equation 3.1

Now consider a steady state velocity, such that only potential energy is traded to overcome the total drag force, and lift is held constant to weight. The resulting sink speed, U_z can be calculated as a function of the airspeed, as shown in equation 3.4.

$$U_z = DU/mg \tag{3.4}$$

The resulting curve, demonstrated in Fig 3.9, provides two important airspeeds, firstly the minimum sink speed and secondly, the best glide speed. The minimum sink speed is the airspeed which provides the maximum time spent in flight and the best climb speed. While this speed guarantees the best endurance it does not provide the greatest range. The best airspeed to maximise range is found at the best lift to drag ratio and is indicated by the tangent to the curve at the origin and referred to as the best glide speed, see Fig 3.9.

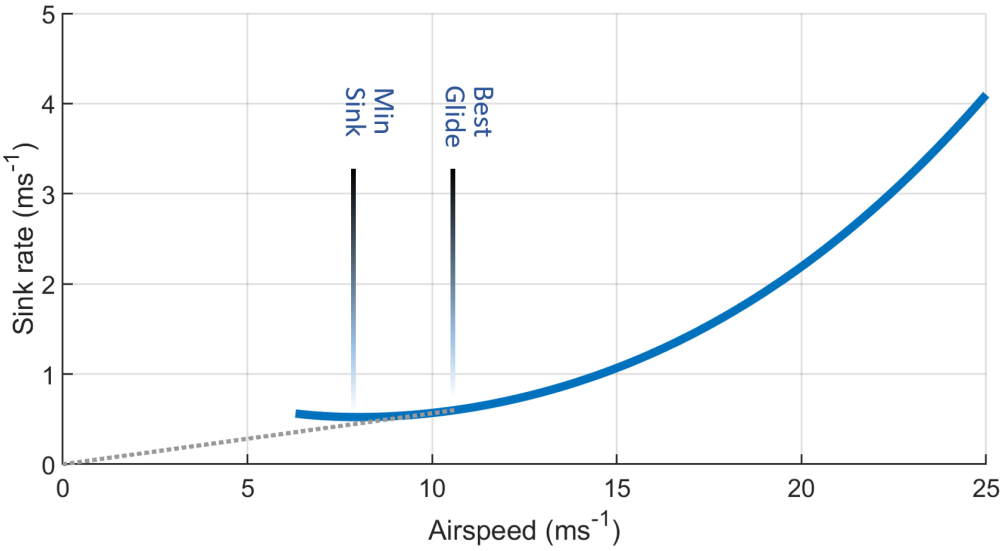

Figure 3.9: Fixed-wing variation of glide polar for average gull, details found in Table 3.2, with optimum endurance velocity (minimum sink) and optimum range velocity (best glide) marked by vertical fade lines.

These three drag models; optimal span reduction, linear span reduction, and fixed-wing span, have been compared using gull biometrics from the Flight database, the results of which, shown in Fig 3.10b, demonstrate that there is very little reduction in sink rate until high levels of wing sweep corresponding to air speeds outside of this study. The three models have been calculated using aerodynamic coefficients for an average gull from characteristics recorded in the Flight database. Given the reliance on measured biometrics to generate the glide polar model extremes in size biomorphics for the two case species were also tested to guarantee minimal effect on the glide polar.

A comparison of four individuals across the two species and using the linear sweep model, as in Fig 3.10a, demonstrated the similar morphology of these birds and validates the data pooling to find an average gull. The comparison of sweep models in Fig 3.10b also demonstrated that there is little variation in the glide polar between drag reduction and fixed-wing models, especially at the airspeed range recorded in this study. As such, the simplest model, the fixed-wing drag model using an average gull biometric model, is used. The average gull biometric is developed from a mean based sampling of available HG and LBB species samples from the Flight software database, it should be noted that some of the samples available have been found dead in dubious and thin condition. Being found in this way is unlikely to effect the wing measurements but could lead to a

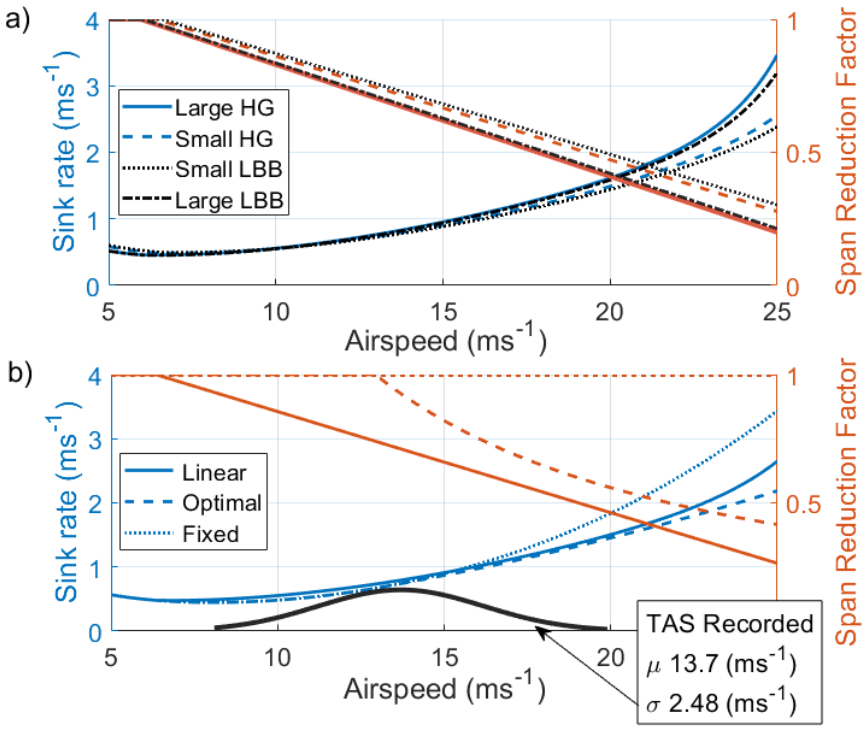

Figure 3.10: a) Comparison of four gulls; large HG (solid), large LBB (dash-dot), small HG (dash), and small LBB (dot) using the linear span reduction drag model, biometrics taken from Flight database and details of which can be found in Table 3.2 b) Comparison of the drag models; linear span reduction (solid), optimal drag span reduction (dash), and fixed wing span (dot), with the distribution of airspeeds recorded from all observation sessions indicated in black.

significant reduction in the body mass measurement, as such, any sample with a body mass outside of a healthy range was discarded from the average.

Table 3.2: Biometrics for the herring and lesser black-backed gulls used in the glide polar models shown in Fig 3.10

Species	**Condition**	**Mass (Kg)**	**Wing Span (m)**	**Wing Area (sqm)**
Herring	Alive	0.86	1.32	0.186
Herring	Dead, thin	0.91	1.45	0.230
Lesser Black-back	Alive	0.72	1.29	0.177
Lesser Black-back	Alive	0.98	1.38	0.201
Average Gull	NA	0.86	1.34	0.197

3.3 Results

Throughout the survey, a total of 3650 observations were collected. There was an average of 118 observations per a 20 minute session. The observation sessions were performed under a variety of wind conditions in order to first ascertain whether the number of gulls gliding in the vicinity increases in favourable conditions. Fig 3.11 demonstrates a clear correlation between the number of gulls gliding and a wind direction providing orographic updraughts. More information on the statistical model and results regarding wind conditions and area use can be found in [10].

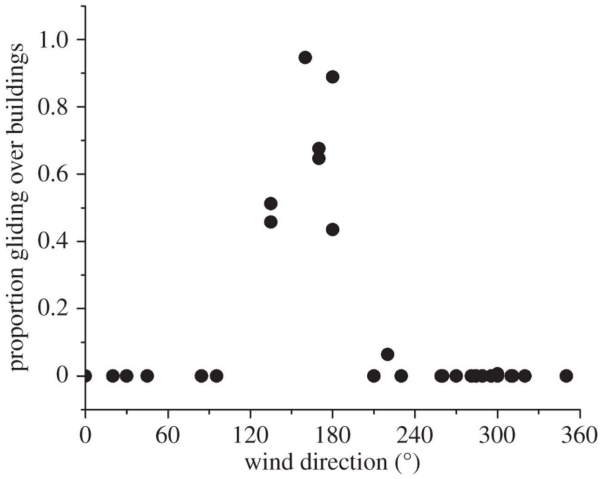

Figure 3.11: The proportion of birds gliding over the hotel site as a function of the total number of birds observed per session is given in relation to the wind direction for that day. There was a clear peak in gull numbers when model predictions indicated maximum availability of orographic updraughts (winds of around 150°).

3.3.1 Airspeed and climb rates in the gliding birds

There were 102 flights recorded in the test area. The flight trajectories analysed had a range of wind speed magnitudes varying from 1.9 to 12.4 m s^{-1}. The mean airspeed for each flight trajectory was calculated and these ranged from 8.1 to 19.9 m s^{-1} (mean $\pm$ s.d. = 13.7 $\pm$ 2.48 m s^{-1}). The strongest predictors of airspeed are the cross-wind component ($t = 6.52$, $p<0.001$, df 794) and the wind support ($t = -7.61$, $p<0.001$, df 794). The gulls increased their airspeed in relation to the crosswind and reduced their airspeed in relation to the supporting wind vector, the same methods as implemented by glider pilots [55] and predicted in [16].

The average climb rate during the flights is slightly above zero, (mean across runs ± sd = 0.12 ±- 0.36 m s^{-1}). Whilst the climb rate is low, it is significantly above zero as shown by a one-tailed Wilcoxon signed rank test (z = 2.05, p = 0.040). The climb rate is also significantly predicted by airspeed (t = -2.24, p = 0.025, df 794).

3.3.2 Fine-scale position and airflow selection

The bird flight paths analysed in conjunction with the QUIC wind models were collected on days where the wind had a largely southerly component and the temperatures and cloud level were such that no thermalling behaviour was captured. The angle of incidence between the buildings and wind direction ranged from 18 - 49° but averaged 34°, the wind speed ranged from 2.2 - 9.3 m s^{-1} with an average of 5.7 m s^{-1}.

The average updraught for each flight trajectory was estimated using the 2D wind model and averaged trajectory path. The mean average updraught speed selected by the gulls was 0.57 m s^{-1} (±0.28 m s^{-1} s.d.) with a range of (1.63 m s^{-1} - 0.05 m s^{-1}). 81% of the gulls flew in a range of 0.4 m s^{-1} (just under the minimum sink in full extension glide) and 0.8 m s^{-1} (which according to Pennycuick's flight model would relate to a 0.7 span reduction). The average w component is particularly interesting when looking at the gull glide polar, as 0.57 m s^{-1} is the sink rate associated with the best glide velocity, see Fig 3.10.

The average updraught speeds selected by the gulls were compared with the maximum updraught available for each model, taken as the updraught at a 2 m radial position from the building edge. Surprisingly, the updraught speed chosen did not correlate with the maximum updraught available (Pearson's correlation n = 96, r = 0.02, p = 0.843), the updraught values chosen are within a limited range as shown by the colour contours populated in Figs 3.12 and 3.13.

Fig 3.13, demonstrates the updraught contours experienced by the gulls in three different wind strengths shown increasing from left to right. Two important observations can be made, firstly, the limited range of updraught dominated by the gulls, and secondly, the angle of the birds over leading edge of the building is changing with wind speed. It was found that both the radial distance increases with wind speed ($y = 0.20$ wind strength $+1.87$, $r^2 = 0.35$, $p < 0.001$) and the angle of the bird above the hotel increases with wind speed ($y = 0.05$ wind strength $+1.49$, $r^2 = 0.17$, $p < 0.001$).

To understand the implications behind these changes, the 2D updraught map is converted into a feasible velocity map using the glide polar as reference, see Fig 3.15. This new map indicates the airspeed at which a gull can travel when using all the

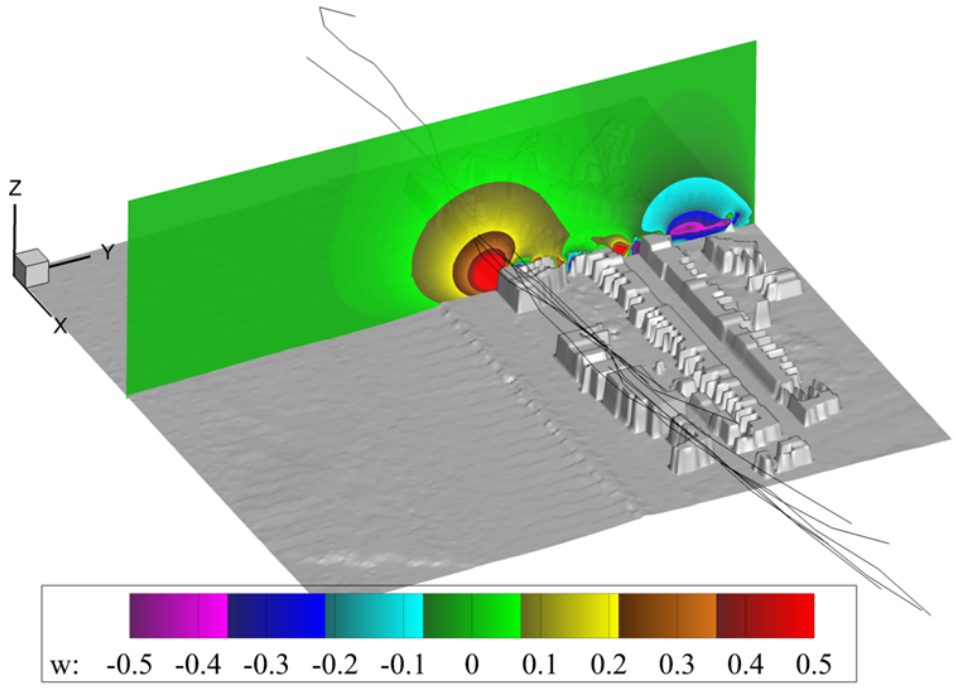

Figure 3.12: The wind model output shown imposed on to the digital profile of the hotel site. The vertical wind component, w, is indicated by the colour contours in meters per seconds. The input conditions are a wind speed of 6.7 m s^{-1}, at 132°from North, with tide height -3.09 m ODN. The bird flight paths for these conditions are indicated by the black lines.

available updraught to overcome the sink experienced in equilibrium glide. The feasible velocity uses the updraughts predicted by the wind model, a glide polar for the fixed-wing equivalent of an average gull based on the Pennycuick measurements in the Flight database, and the average positioning of the gull from the leading edge of the building measure in radial and angular coordinates. These feasible airspeed velocities have been corrected for the supporting wind speed recorded at the time of flight and the flight direction, this created two feasible velocity maps per wind model. These maps were then use to predict the ground speed that a gull would travel at based on it's spatial position in the wind field and direction of travel. The calculated ground speeds were compared to the measured data, with the results shown in Fig 3.14.

The grounds speeds of the gulls recorded were generally faster than predicted by the equilibrium glide model where the black link in Fig 3.14 shows a prefect prediction. Gulls were recorded flying in both directions along the seafront, presumably to- and from-foraging and roosting areas. As behaviour outside of the recorded flights are unknown the directions are considered simply in the x direction. A positive x direction is towards

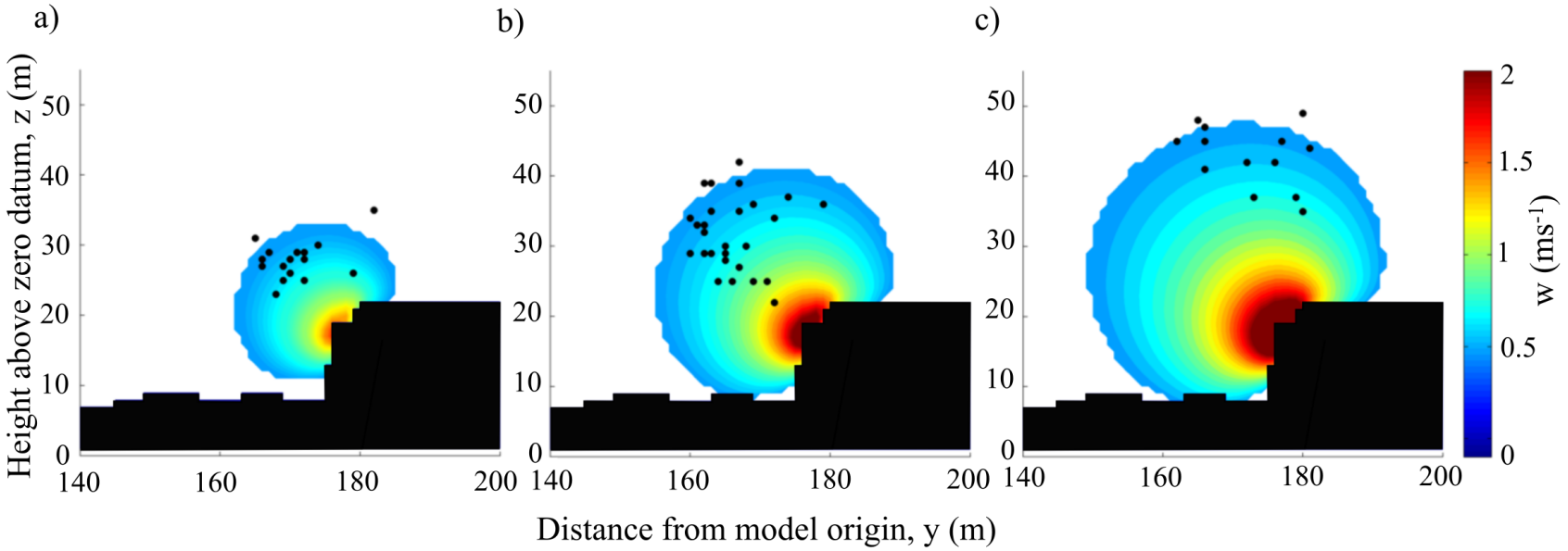

Figure 3.13: Three updraught maps and corresponding gull positions shown with increasing wind speeds a) 3.4 m s^{-1}, b) 5.5 m s^{-1}, and c) 7.6 m s^{-1}. The gull positions increase in radial and angular position with the increased cross-wind component of wind speed.

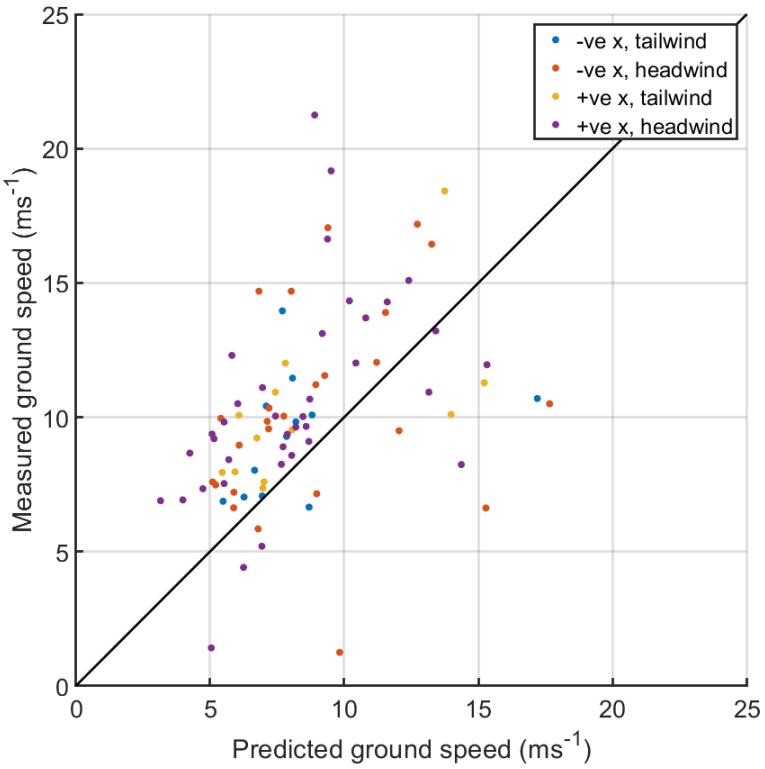

Figure 3.14: The predicted ground speeds using the wind and glide polar models compared to the recorded ground speeds. Results are the average speed for each flight based on the 2D model. Flight direction $\pm x$ and supporting wind vector marked in different colours.

Swansea city centre and potential foraging area, and a negative x is away from the city centre, possibly towards a roosting area. The wind direction at the time of flight is considered in terms of the supporting wind vector and so the data is split into head- and tail- wind however, the supporting wind vector can be considered very small compared to the crosswind perpendicular to the buildings. This results in four direction groups, however, there was no significant variation between the groups, indicating that while the gulls were flying faster than predicted using the modelled wind field and equilibrium glide model this was not influenced by the flight or wind direction.

3.4 Discussion

Birds have been known to make adjustments for weather conditions during migration but this study provides evidence that birds also make adjustments in daily commutes.

Gulls made adjustments not only at the broad-scale by selecting to fly along the bay in winds that facilitate orographic soaring but also at a much finer-scale by adjusting their position in the updraught generated by the buildings depending on the wind speed.

3.4.1 Airspeeds and climb rates

The gulls were found to adjust their airspeed for the wind conditions which is consistent with other findings [87, 91, 92, 94, 95], increasing their airspeed based on both the supporting and crosswind components. Given the gulls were commuting between nesting and feeding grounds it was considered that they would aim to travel as fast as possible whilst maintain equilibrium glide, so as to keep energy costs to a minimum whilst maximising on time spent foraging. However, the gulls were not found to increase their airspeed in line with the available updraughts.

With higher crosswinds and greater updraught availability the gulls had potential to spend less time in flight on the windier days. Requiring only a reduction in sweep and angle of attack in order to move further along the glide polar into a higher airspeed and greater sink rate. The observations indicated that the gulls instead increased their radial distance from the buildings to maintain a fairly constant range of airspeeds. This validates the choice of using a fixed-wing gull model, as commuting flights stay within a comparable drag range. For example, the maximum available updraught has a speed of 2.5 m s^{-1} allowing for a maximum airspeed of 24 m s^{-1} however, the average airspeed for that model was just 13.7 m s^{-1}.

The results showed a small level of altitude gain and this was significantly predicted by a decrease in airspeed. Such that the gulls flying slower gained more altitude than those flying faster as would be expected by an increase in sink rate as dictated by the glide polar. In general, the gulls did not seem to use the orographic updraughts to gain altitude but to facilitate progress. The mean updraught contour which the gulls positioned themselves in indicate the gulls may be aiming to fly at the best glide velocity to maximise range rather than the minimum sink velocity to maximise endurance.

3.4.2 Position based control

The results also indicated the position that the birds use is carefully selected in order to improve their flight control. The distance to the buildings demonstrate a preference for the flight speeds but this is not explained in their angle selection as the contours allow for any angular position whilst maintain chosen airspeed. Instead, the gulls

positioned themselves at the crest of the updraught tunnel on windier days and a possible explanation is a control strategy for gust mitigation.

A horizontal displacement due to a gust at a low angle relative to the wind field would move the bird through a large range of w values, see position A in Fig 3.15. This would required the bird to make a large adjustment of airspeed in order to maintain vertical position. Where as the same displacement in a high angle, see position B, would require no change in velocity.

A vertical displacements at a high angle could even be self-stabilizing. A decreases in height would result moving to a contour with increased updraught which would in turn increase the height of the bird returning it to the initial position. Similarly a increase in height would result in a lower updraught causing the bird to naturally sink back toward the original position. This stable position could massively reduce control costs in gusty conditions. The relative amplitude of gusts is likely to increase with the wind speed which could explain why the gulls favour the crest of the updraught at higher wind speeds.

Using partial spatial velocities of the wind field further demonstrates the robust position at the tunnel crest. In order for position control to be robust to vertical gusts the change in wind field with altitude must be negative. In Fig 3.16a the vertical wind field partial differential demonstrates a circular region above the leading edge of the building that provides the conditions for the self-regulating phenomenon. A negative region, where the strength of the vertical wind field is decreasing with positive altitude, provides a decreasing amount of lift with height gain resulting in a return to the original position due to a vertical gust or the loss or gain of lift due to any change in height. Fig 3.16 demonstrates little to no change in the horizontal wind field with a vertical position change, and so is of little importance. Horizontal position changes are demonstrated in Fig 3.16b & c, similarly in part b there is a circular area above the building leading edge which is particularly robust to changes in horizontal wind field. Interestingly, part c exhibits a zero line acting above the edge of the building which makes the crest of the tunnel, optimal control would be positioned on or close to this line.

The optimal region analogy goes some way to explain why the gulls vary their angular position over the building on windy and potentially, gusty days but does not explain why the gulls use a lower angle at lower wind speeds. Perhaps this result could be due to reasons beyond flight control such as a position which facilitates a better view of the beach for foraging purposes.

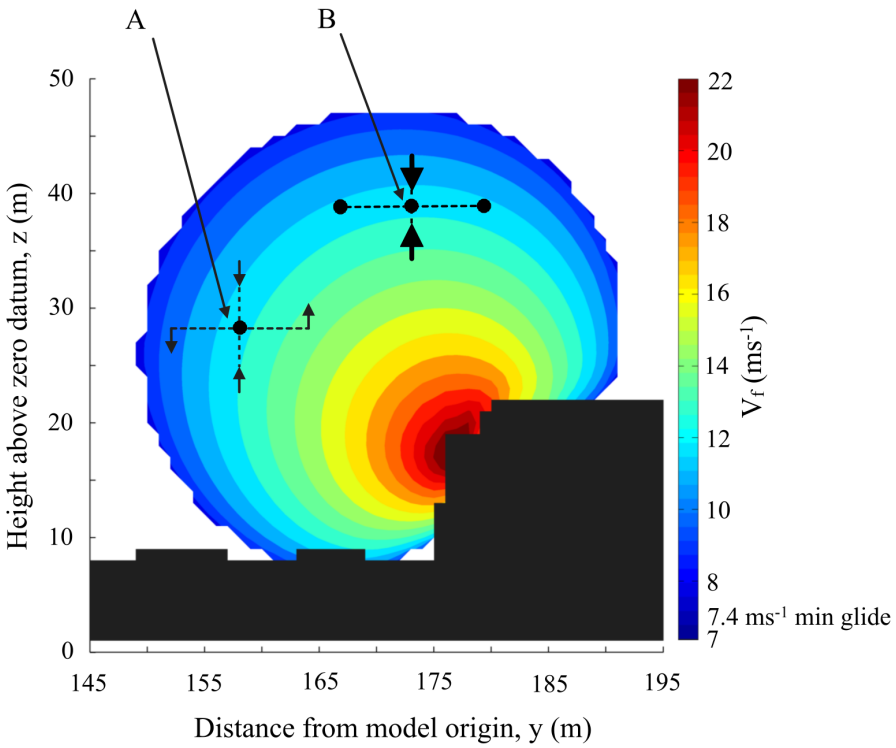

Figure 3.15: A velocity contour map in relation to flight over the hotels. Predicted airspeeds (in meters per seconds) of birds flying parallel to the hotels are indicated in colour. Two possible positions (A and B) are given for flight at 12 m s^{-1}, with dashed lines representing horizontal and vertical displacements from an equilibrium position and black arrows representing the change in lift force produced if the bird does not make any corrective actions. Position A demonstrates the wide velocity range available for a given horizontal displacement for birds flying at relatively low angles. The velocity range available for the same horizontal displacement is much lower at position B, while for vertical displacements the stabilizing forces are stronger at B than A. The input wind conditions are 9.34 m s^{-1} with a direction of 137° from North and a tide height of 1.14 m ODN.

3.4.3 Summary and review of methods

This research demonstrated a clear energy saving strategy implemented by the gulls utilising the airflows generated man-made infrastructure. Additionally, this research has discovered a flight control scheme previously unconsidered. Flight control at low altitude in the complex airflows created by urban infrastructure is a significant challenge for SUAVs. The airspeeds and wind speeds are comparable meaning that gusts can by impossible to recover from. There have been investigations in energy saving methods over greater distances [58, 109] but not at the fine-scales covered here. Understanding the strategies that soaring birds use in these same conditions could provide real flight

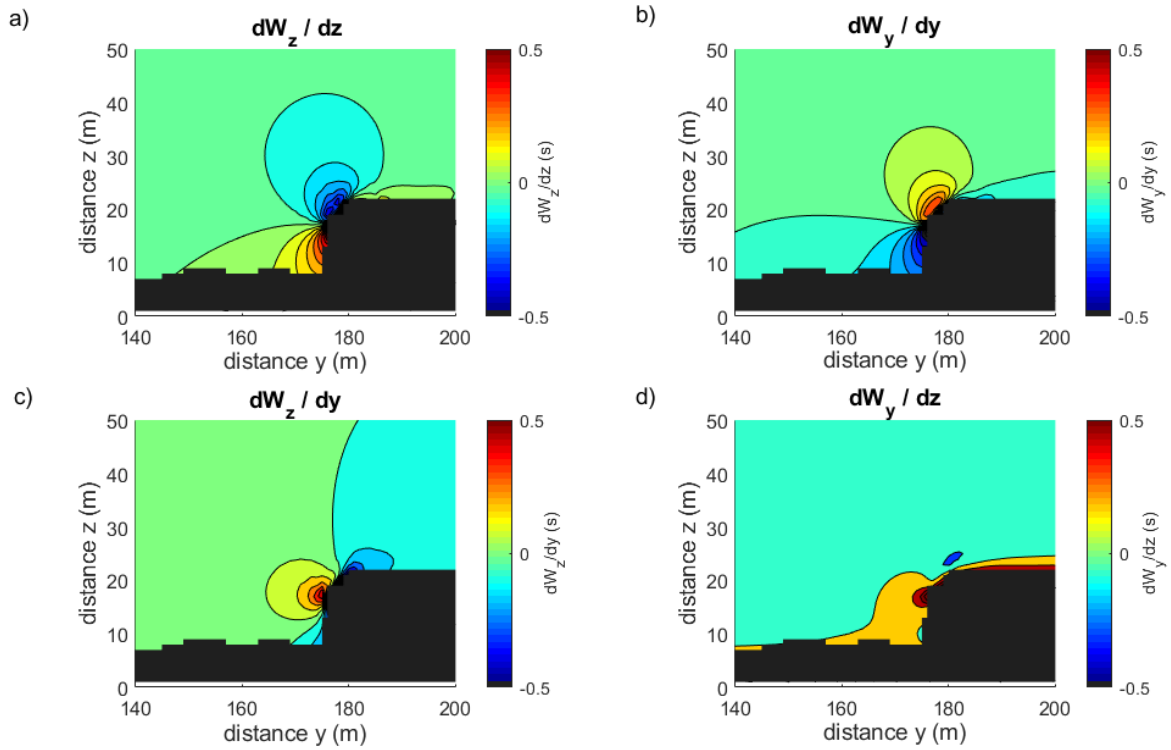

Figure 3.16: The plots show the partial spatial differentials of the wind field in the vertical and horizontal directions where the figure titles label the axes variations. Wind input conditions match that of Fig 3.15, where the wind speed is 9.34 m s^{-1} with a direction of 137° from North and a tide height of 1.14 m ODN.

control advantages in SUAVs.

This Chapter used Pennycuick's ornithodolite to record gull flight trajectories and balloon launches to record the wind conditions. Fitted wind profiles were used as the inputs conditions for a QUIC-CFD modelled environment and every attempt was made to provide as high a level of accuracy to the QUIC models as possible. The terrain was included at a high 2 meter resolution and adjusted for the tidal height at the time of field recordings. The QUIC model uses terrain height when considering boundary layer placement but does not use the terrain in mass flow calculations and as such the this substrate does not contribute to the orographic updraught calculated. A terrain step exists directly proceeding the row of buildings, this is included in the environmental model but does not contribute to the total orographic updraught so, the vertical wind field is underestimated and may account for the small average altitude gain observed in the flight paths. Additionally, the gull glide polar was generated using the Pennycuick

2008 model, this involved using biometrics from a combination of caught birds and found cadavers. While no gulls found in dubious conditions were added there is potential that the body mass is underestimated. Furthermore, Pennycuick's model relies on several aerodynamic characteristics that are estimates calculated through the study of several species, and not necessarily the two species studied here. Despite these factors, the average updraught that the gulls were found to position themselves in fell exactly on the predicted sink rate at a best glide velocity. Furthermore, the velocity control scheme based on spatial positioning is unaffected by an underestimation in updraught as it is the shape of the lift tunnel which provided the basis for the idea.

3.5 Conclusions

- The gulls performed orographic soaring on urban features.
- The gulls made fine-scale navigation choices based on the wind conditions.
- The gulls do not appear to be increasing their flight speed with wind speed to take advantage of the increased updraught strength.
- Fine-scale flow assessment of the gulls performing orographic soaring demonstrated that they flew at speeds close to the best glide velocity and used the updraught generated by the deflected wind to offset the sink rate.
- Airspeed can be controlled by radial distance from the leading edge of the building by positioning within a suitable updraught strength to offset sink.
- Gulls may implement a gust mitigation control scheme by varying their angular position from the leading edge of the building.

CHAPTER 4

ENERGY SAVING VELOCITY STRATEGIES

Small Unmanned Aerial Vehicles (SUAVs) operating in urban environments must deal with complex wind flows and endurance limitations caused by current battery technology. Birds offer inspiration regarding how to fly in these environments and how to exploit complex wind flows as an energy source. On a broad-scale, migrating birds adjust airspeed to minimize cost of transport (CoT) in response to wind conditions, but it is unknown whether birds implement these strategies in fine-scale, complex environments. Global Positioning System (GPS) backpacks were installed on eleven urban gulls in order to track flight through the city, the gulls were found to soar extensively during daily commutes, utilising thermal and orographic updraughts. CoT theory is outlined with a proposed model for optimising airspeed for wind whilst maintaining flight trajectory. Gull flight data is categorised into soaring strategies and then tested for CoT adjustments. It was found that the birds were able to make energy savings of 31% based on having a best glide speed when soaring that was similar to their minimum power speed when flapping. These models calculated optimum airspeeds based on wind speed and direction and could be implemented on SUAV platforms with wind sensing capabilities. This approach could significantly reduce energy requirements for SUAVs flying in urban environments.

Author Contributions: Field experiment set-up and management, GPS tracking data collection, nest and ground truthing observations, and initial data processing (database design and population with bird and geophysics data) was part of a joint effort between PhD students Cara Williamson and Anouk Spelt, and is documented in [110]. The University of Amsterdam provided the Bird Tracking equipment (UvA-BiTS) and access to the gull behavioural model. This work has been previously published as part of the AIAA SciTech 2020 Inproceedings [111] and is currently under review for consideration as an AIAA Journal paper. Dr Shane Windsor contributed with edits to the paper.

4.1 Introduction

Small Unmanned Air Vehicles, SUAVs, have the potential to fly at low altitudes within the urban environment making them suitable for a range of missions such as infrastructure monitoring, surveillance, emergency response and small payload delivery [25–29]. However, current SUAVs have two main technology limitations, firstly, SUAVs have limited capacity to cope with the high levels of turbulence and complex flows created by wind interactions within the urban landscape [112–114]. Secondly, due to the power-weight constraints in battery technology, SUAVs have a limited range and endurance [76, 115]. This research takes a novel approach to finding ways of overcoming these limitations by looking at the ways birds make use of wind flows in the urban environment to reduce their energetic cost of flight.

Birds of comparable size and weight to small SUAVs are able to navigate the complex city wind flows and exploit the environment to reduce the energetic cost of flight. During the breeding season, urban gulls spend up to 40% [110] of their time in flight, flying to and from foraging locations through these complex wind-scapes. Choosing appropriate flight strategies has the potential to substantially reduce their energetic flight costs and could be key for breeding success. Understanding the energy saving strategies urban gulls are using to reduce flight costs could be used to extend the range and endurance of SUAVs flying in a similar environment.

Flight mechanics theory shows that transport costs can be minimized by adjusting airspeed with relation to wind conditions. In unfavourable conditions such as headwinds, airspeed should be increased and in favourable conditions such as tailwinds, airspeed should be reduced. Vertical wind components also effect transport costs, a down draft will increase the cost of transport (CoT) and therefore airspeed should be increased, and an up draft will reduce CoT and so airspeed should be decreased. Gull species studied in migration and in long-range open water commutes have been found to make velocity and even altitude adjustments to headwinds that act to maximize CoT savings [87, 94]. However, these flights tend to experience uniform and predictable flow conditions which are not representative of the urban environment.

A recent study found that urban gulls spend up to 10% more time in flight than those in traditional habitats [110], so it may be that the complex flows generated by our architecture creates more soaring opportunities than are available in more traditional habitats. Certainly studying gulls in this environment can provide new insight into managing these complex flows. Previous work found that gulls exploit the wind-

highways generated by urban terrain [10] and a SUAV flight control strategy based on the gulls' flight behaviour achieved a throttle reduction of 15% whilst minimizing overall control-effort [11]. Additional SUAV studies have found that exploiting urban flow can successfully be used to gain significant altitudes [116] and that choosing the correct airspeed and climb angles for the wind gradient can be used to make savings of 12% in the field [76]. Certainly then, studying birds in urban environments can present strategies which are advantageous to SUAV technology. However, there has been little research in the way free flying birds use wind flows in the urban environment, and whether velocity adaptions for CoT are common for all wind conditions.

This Chapter aims to discern whether CoT velocity adaptions are advantageous when implemented in the complex flow conditions created by urban infrastructure using commuting urban gulls as a case study. Firstly, the relevant flight mechanics theories regarding velocity optimisation are outlined before detailing a velocity optimisation algorithm suitable for use when flying on a fixed heading with knowledge of current wind conditions. Following this, the methods used for capturing and analysing flight data from GPS tagged gulls is described, including how the data was down-selected and categorized into different soaring strategies. The velocity optimisation models are then tested against the different flight strategies employed by the gulls to determine their potential for energy savings in urban environments.

4.2 Flight Models

This section contains the flight mechanics theory behind the velocity optimisation models used throughout this chapter. The glide polar and mechanical power curve models are outlined along with the key velocities involved with optimising flight performance. Following, is an explanation of CoT theory where the relationship between airspeed and the wind conditions is introduced. The CoT relationship is used a the basis for an algorithm calculating the optimum airspeed for a fixed trajectory and known wind conditions. Three potential flight speed selection models for flapping flight are then introduced.

4.2.1 Velocity curves

Avian flight has typically been studied at two very different scales. At one end of the spectrum, the precise mechanics and aerodynamics of flight has been studied in controlled environments such as wind tunnels, which has given rise to detailed models used to predict flapping power requirements [17, 117, 118] and optimum glide ratios [119–122]. While on the broad scale, flight mechanics models have been used to study the energy saving techniques implemented by migratory birds in relation to weather systems [87, 91, 92, 94, 95]. The two methods are complimentary, performance models generated in fine-scale experiments can, in part, be validated with free-flight data, and the flight data can be used to tune performance models. The flight data in this study is not only collected at a high-frequency but also contains classification of behaviours and flight modes facilitating a more detailed analysis of how gulls take advantage of the wind conditions in mid-range, complex environment flights.

In gliding flight, body weight is balanced solely by the aerodynamic forces lift and drag. As there is no thrust input forward moment comes at the expense of trading either potential or kinetic energies. The glide polar, introduced in the previous chapter, section 3.2.5.2, is the graphical representation of gliding while trading potential energy where the sink rate of a body is mapped to airspeed. In flapping flight, the power required to overcome the drag force is provided in the act of flapping. Here the induced drag is considered proportional to the absolute minimum power required to stay in flight and is calculated by modelling the moving wings as an actuated disc [16]. Equation 4.1 defines the power required to maintain steady-level flight.

$$P = \overbrace{\frac{2k_f m^2 g^2}{\pi \rho b^2 \beta^2 U}}^{\text{Induced}} + \overbrace{\tfrac{1}{2}\rho U^2 c_{D_b} S_b}^{\text{Parasitic}} + \overbrace{\frac{1.05 c_{pro} k_f^{\frac{7}{4}} m g^{\frac{3}{2}} S_b c_{D_b}^{\frac{1}{4}}}{\rho^{\frac{1}{4}} b^{\frac{3}{2}} AR}}^{\text{Profile}} \tag{4.1}$$

The drag forces in flight vary with velocity in a manner which results in a minima for both the glide polar and power curve (Fig 4.1e & f). These minima represent the lowest rate of energy exchange, which in flapping flight is the minimum power output and in gliding flight is the minimum sink rate, the velocities at which these occur will be referred to as the minimum power, U_{mp}, and minimum sink, U_{ms}, velocities respectively. Flying at these airspeeds will result in maximum flight endurance but does result in the lowest energy cost for a given distance. The lowest energy cost for transport can be found at the tangential to each of the curves (Fig 4.1e) and referred to as maximum

range velocity, U_{mr} for flapping flight, and best glide velocity, U_{bg}, for gliding flight.

Probably the most widely used glide polar model for birds was developed in 1989 by Pennycuick [123]. The drag functions, described with detail in the previous chapter, in section 3.2.5.2, contain aerodynamic characteristics which, as with all good science, have been updated over the years in response to new research. The previous chapter used values published in the 2008 Flight model and made comparisons between wing span reduction models and gull biometrics. This chapter, however, compares alternative aerodynamic characteristics used in the induced and parasite drag functions. The original (P89) [123] and newer (P08) [16] Pennycuick models will be compared with an alternative model (T16) published in 2016 by Taylor *et al* [52].

The P89 and P08 models differ only in the body drag coefficient factor, C_{D_b}, equal to 0.4 and 0.1 respectively. The Taylor model uses a function of the wing to body surface area fraction, see equation 4.2, as well as having several other differences to the two Pennycuick models.

$$C_{D_b} = 0.01\frac{S_w}{S_b} \tag{4.2}$$

The T16 model also varies to the Pennycuick models in the induced drag function where P89 and P08, use an induced drag factor, k_s, of 1.1 whereas, T16 uses a lower value of 1.0 only. The drag factor originates from Prandtl's lifting-line theory [107] and assumes an elliptical wing. Traditionally, it was assumed that the induced drag factor must be greater than 1.0, as this is reserved only for the ideal wing. However, more recently it was discovered that the addition of winglets deflects the wingtip vortices up and out from the wing, increasing the downwash and effectively performing as though the wing span is increased. This may be somewhat irrelevant for gulls in gliding flight but could effect the drag produced while flapping where the wing tips bend slightly upwards during the down stroke section of the flap cycle.

A further difference between the Taylor and Pennycuick models occurs in the calculations of the parasite drags, where in the Pennycuick models the coefficient is held fixed at 0.014, but in the Taylor model the drag coefficient is considered a function of the Reynolds number, see equation 4.3.

$$C_{D_w} = 2.656R_e^{-\frac{1}{2}} \tag{4.3}$$

Where the Reynolds number, R_e, is defined by equation 4.4, where $\bar{c}$ is the wing mean aerodynamic chord and μ is the dynamic viscosity of the air. All other variables remain as defined in section 3.2.5.2.

$$R_e = \frac{\rho \bar{c} U}{\mu} \tag{4.4}$$

In this chapter, the induced drag factor and drag coefficients used in calculating the glide polar as proposed by both Pennycuick and Taylor were compared using the fixed-wing drag model. Fig 4.2 demonstrates the similarity between the three models, in fact, using the Pennycuick 2008 values provides key performance velocities with less than 1% variation to the Taylor model. For this reason, the 2008 model will continue to be used.

An induced drag factor is also used in the derivation of the power curve used in flapping flight, k_f. In Pennycuick's Flight software the induced drag factor for flapping flight is considered 1.2, higher than during gliding flight. In 2013, Pennycuick captured ornithodolite observations of various species arriving from migration in order to verify characteristics used in the drag curve derivation, such as the drag factor [108]. In theory, as birds arrive from migration they should be travelling at the max range velocity in order to minimise the energetic cost required during migration. In the Flight software, maximum range velocity is calculated considering the chemical power stored in the fat reserves, but here, only the mechanical power is considered. Pennycuick observed that LBB gulls arrived back at an airspeed of 14.4 ± 1.34 m s^{-1}, well within range of the max range velocity shown in Table 4.1 and Fig 4.3. Nevertheless, the 2008 model is compared with an alternative described below.

Additional power curve models which consider the full flap cycle have often been used when studying flapping birds in a wind tunnel in order to determine the mechanical power delivered by the beating wings. In these cases the variations which occur in velocity, height, position as well as the angle, surface and flapping frequency of the wing are all considered. This is made possible during wind tunnel experiments where these factors are visually tracked. Here, a simplified version, which considers steady and level flight only is summarised in equation 4.5.

$$P = \overbrace{\frac{k_f T^3}{(2\rho A_0)^2}}^{\text{Induced}} + \overbrace{\tfrac{1}{2}\rho U^2 c_{D_b} S_b}^{\text{Parasitic}} + \overbrace{2\sum_{i=1}^{25}(\frac{1}{2}\rho U_i S_{w_i} C_{D_w})}^{\text{Profile}} \tag{4.5}$$

Where the velocity over each wing segment is calculated as a function of the airspeed, U, flapping frequency, f, maximum flap amplitude angle, θ_{amp}, and segment span, b_i.

$$U_i = U + f\theta_{amp} b_i \tag{4.6}$$

The thrust, T, is calculated as a function of the airspeed and body mass.

$$T = \frac{mg}{U} \tag{4.7}$$

The rotational area of the wings, A_0, is not calculated as circular but as the area swept by the wing and is dependant on the maximum wing beat angle, θ_{amp}, and planar angle, θ_{pln}.

$$A_0 = \frac{b}{2}^2 \theta_{amp}\theta_{pln} \tag{4.8}$$

Information regarding the average flap frequency (3.5 Hz) and wing surface geometry have been taken from recorded data, angles for the disk wing area have been taken from the literature where θ_{amp} is 25° [124], and θ_{pln} is 5°. The variables are fixed despite these variable being known to vary with airspeed. Fig 4.3 attempts to compare the two models where it should be noted that the alternative model has a mechanical power value that increases at a rate four times that of the Pennycuick model as it moves away from the minima. There are large variations in the proposed key velocities, as the second model uses estimates for several characteristics the Pennycuick power curve is used throughout the chapter. Additionally, the results from Pennycuick's 2013 study of arriving migrating birds further supports that the power curve is more accurate that the alternative, given the closer maximum range velocity, using this model also provides the additional benefits of remaining consistent with the selected glide polar model. Final key velocities for LBB gull model, using the average from 11 LBB used in this study, are summarised in Table 4.1, and biometrics used to generate both curves are found in Table 4.2.

Table 4.1: Performance airspeeds for flapping and gliding flight for average gull

Velocity Name	**Symbol**	**Airspeed, (m s^{-1})**			**Optimisation**
Gliding		P89	P08	T16	
Minimum Sink	U_{ms}	7.1	8.0	7.9	Endurance
Best Glide	U_{mp}	9.3	10.6	10.6	Range
Flapping		M1		M2	
Minimum Power	U_{mp}	11.9 (2.8 W)		11.5 (4.9 W)	Endurance
Maximum Range	U_{mr}	15.4 (3.3 W)		12.9 (5.2 W)	Range

4.2.2 Cost of Transport Theory

When flying through moving air it is important to consider the effect of the wind on relative motion. The energetic cost required to travel a given distance can vary significantly

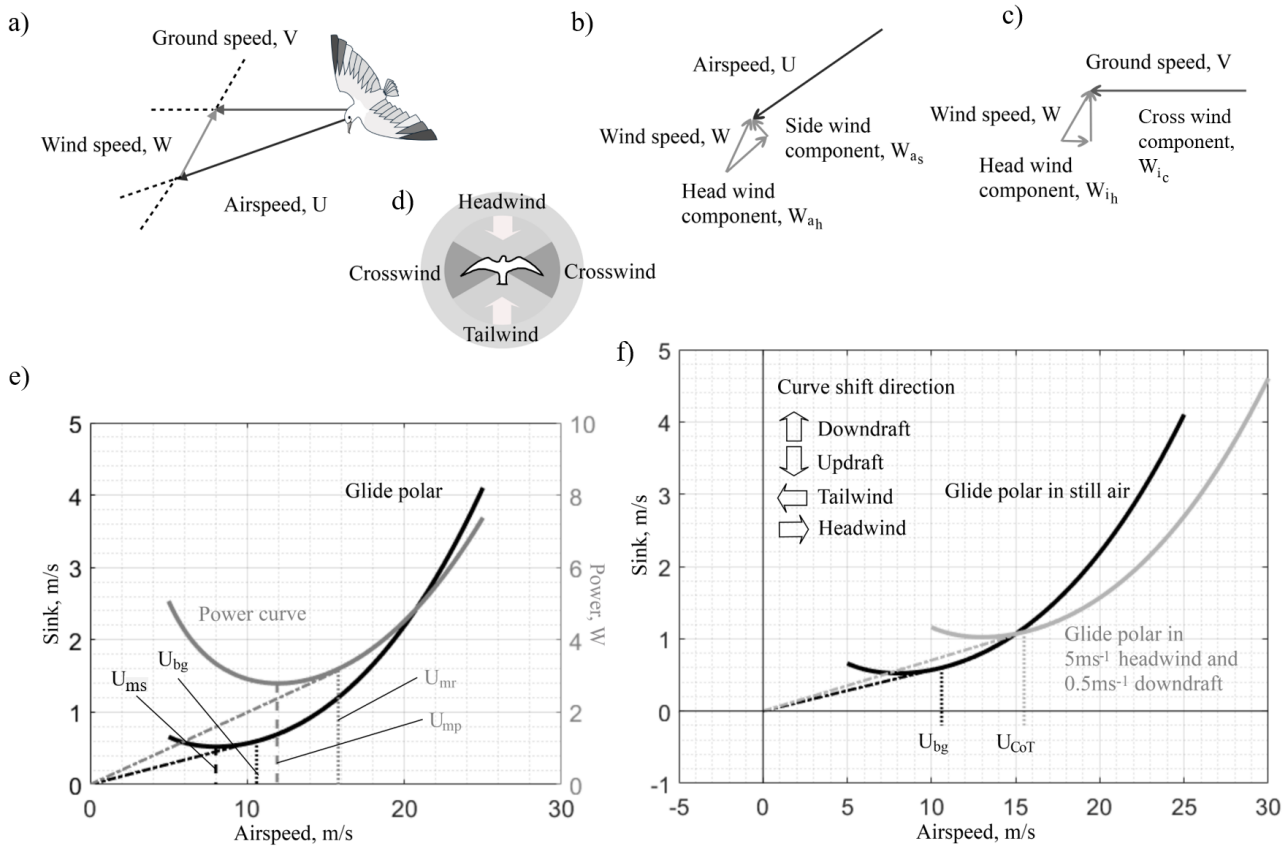

Figure 4.1: a) Vector diagram of inertial, air and wind speed vectors. b-c) The head- and side-winds in the air and ground frames respectively. d) Definition of head-, cross-, and tail-wind angles where headwind is considered $\pm(0° - 60°)$, crosswind is $\pm(60° - 120°)$, and a tailwind is $\pm(120° - 180°)$. e) Glide polar and power curve for the average gull (Table 4.2). f) Curve shifting for head/tailwinds and up/downdraughts where the glide polar in still air is indicated by the black line and shifted curve is shown in grey.

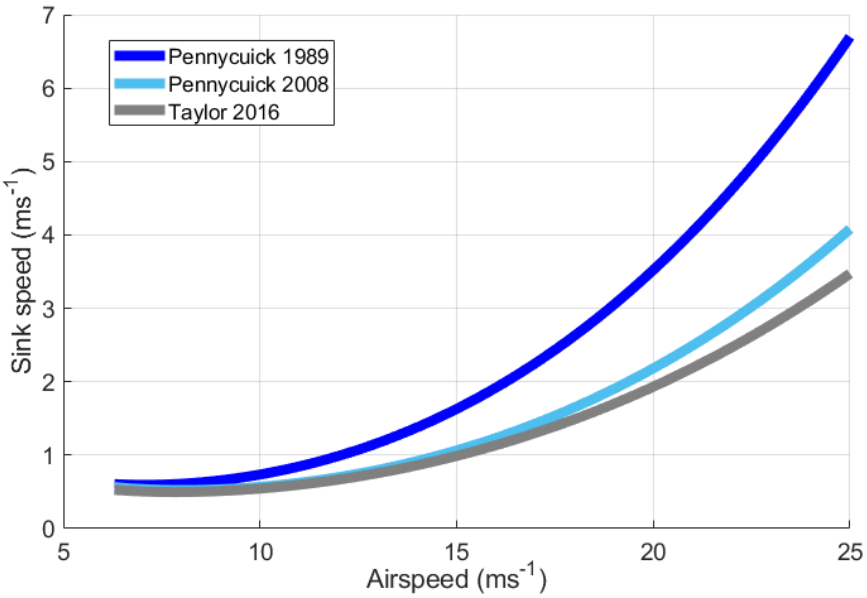

Figure 4.2: Comparison of three glide polar models; Pennycuick 1989 [123] shown in dark blue, Pennycuick 2008 [16] shown in light blue (and used in this study), and Taylor 2016 [52] shown in grey. The best glide and minimum sink velocities are summarised in Table 4.1 .

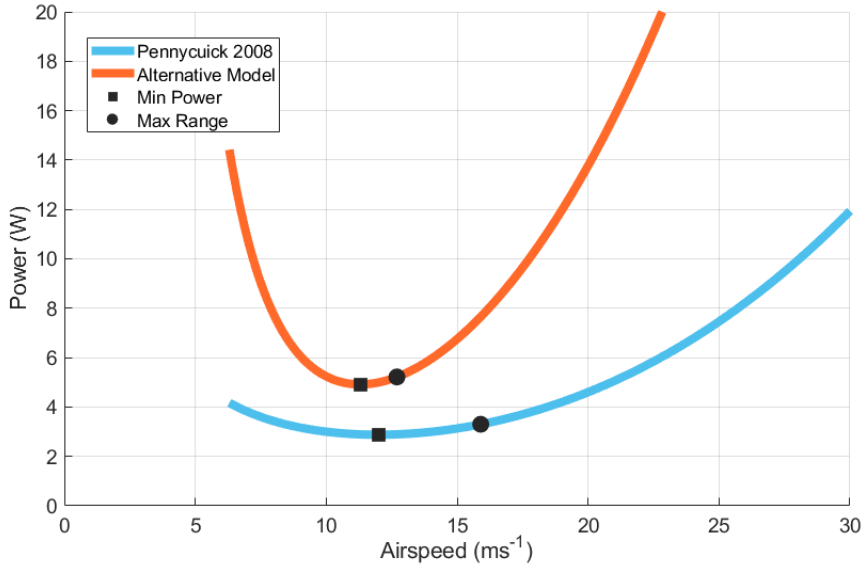

Figure 4.3: Comparison of power curve models; Pennycuick 2008 [16] shown in blue (and used in this study), and alternative thrust based model shown in orange. The minimum power and maximum range velocities are are shown with the markers and summarised in Table 4.1.

depending on the direction and velocity of the wind flow. For example, progress in the inertial frame is impeded when flying at a set airspeed in a headwind compared to still air which increases the duration and cost of flight. The velocity reference frames can be seen in Fig 4.1 and are related by Equation 4.9 where V is the ground speed vector, U is the airspeed vector and W is the wind speed vector. It is worth noting here, that this work uses the wind vector direction in the traditional meteorological measurement format where the direction measures from North the origin of the wind source.

$$U = V - W \tag{4.9}$$

Many studies have derived the necessary velocity changes required in order to minimise flight cost [8, 16, 43, 52]. In a recent study, Taylor [52], derived Equation 4.10 which considered the cost of transport in the air frame of reference, (Fig 4.1b). The cost of transport ($-dE/dr$), or the energy cost E, for a given range r, is considered in terms of the thrust requirements, DU, for a given airspeed, minus the effect of any weight supporting vertical wind. The wind conditions, where W_h and W_s are the head- and side-wind components, are also taken into account. In summary, the equation shows that CoT is reduced by updraughts ($W_z > 0$) or tailwinds ($W_h < 0$) and increased in downdraughts ($W_z < 0$) or headwinds ($W_h > 0$).

$$-\frac{\mathrm{d}E}{\mathrm{d}r} = \frac{DU - mgW_z}{\sqrt{(U - W_{a_h})^2 + W_{a_s}}} \tag{4.10}$$

It should be noted that wind vectors, composed of head and side winds, can be considered in two ways aligning with reference to the air frame (Fig 4.1b) or the inertial frame (Fig 4.1c). CoT is calculated for a given distance so could be considered in the inertial frame [125], however in environmental harvesting strategies it is the airspeed in relation to the wind which should be optimised [52]. This study considers the wind vectors in the air and ground frame as side and cross winds respectively.

In gliding flight if the updraught is greater than the minimum sink rate the CoT optimisation can break down as flying at a faster speed can still decrease the CoT. In this case it is possible to fly at speed which matches the sink rate on the glide polar. For glider pilots, the theory is best known as Speed to Fly (StF), or MacCready's theory [43]. Calculating the new optimum airspeed in both StF and CoT can be achieved by shifting the glide polar for the experienced conditions as depicted in Fig 4.1f. An updraught shifts the curve toward the x-axis, in CoT theory the optimized velocity tends to the minimum sink velocity until the updraught is equal to the minimum sink. In StF theory,

the thermal strength can be much greater than the minimum sink value, and here the optimized velocity increases with thermal strength.

Gulls soaring using orographic lift have been found to position themselves such that sink was offset and altitude maintained rather than to benefit from increasing velocity [10], suggesting that they follow CoT during orographic soaring. However, several soaring species of bird have been found to follow MacCready's StF in inter-thermal glides so this was also tested [6, 41, 126].

4.2.3 Velocity optimisation algorithm

This section details a velocity optimization algorithm that can be used to generate the optimum airspeed for CoT minimization when flying on a fixed heading with knowledge of current wind conditions. An iterative process was used to calculate the optimum airspeed and resultant ground speed. An algorithm is used as it considers the coupled relationship between variation in airspeed and the air relative wind direction. This was especially relevant to a dataset where the measured data is the ground speed, trajectory heading, and wind conditions, but, the hypothesis to be tested is based on variance within the airspeed. Theoretically, as the gulls adjust their airspeed, and hence, air relative heading, there is a compensation for slip in order to maintain inertial heading. It is not possible to consider this compensation with the dataset here. In any case, the gulls are not necessarily adjusting solely their slip angle but also asymmetrically fine-tuning the geometry of their wings with changes in chamber, twist and sweep. As is easily observed when watching gulls soar at a crosswind angle, such as in the case of orographic soaring. For this reason, no slip angle will be considered, only the wind direction in terms of the air and inertial frames of reference.

The trajectory holding assumption follows that daily commuting flight, lasting between 10 - 30 minutes, are long enough for the bird to want to reduce energy costs, but short enough that using wind drift will not provide any total benefit. Additionally, many of these commutes exhibit orographic soaring behaviour in which following a ridge feature is vital to continue energy harvesting. This is also applicable for SUAV technology where holding a fixed trajectory is part of the mission plan. The algorithm process is outlined in Section 4.2.3, where the inputs are the glide polar, GP, a two column matrix where the first column is the airspeed range and the second is corresponding sink; the flight trajectory heading, ϕ_i; and the wind conditions, where W is magnitude and θ_w is direction. Remaining calculated variables are the inertial and air relative wind angles, β_i and β_a, where β_i is the angle between wind and ground speed vectors, β_a is the angle

between wind and airspeed vectors, W_{a_h} is the air relative head wind. The optimised airspeed is represented by U_{opt} and the error margin, e, is the magnitudinal difference between optimised airspeed iterations.

The algorithm starts with the non-adjusted airspeed velocity, U_{bg}, and calculates the angle between the wind and ground speed vector using the trajectory heading and wind conditions. Following on, the relative wind direction in air and inertial frames are calculated and used to find the air relative headwind. The inertial and air frame wind relative angles, $\beta_{a,i}$, are described by vector diagram Fig 4.4.

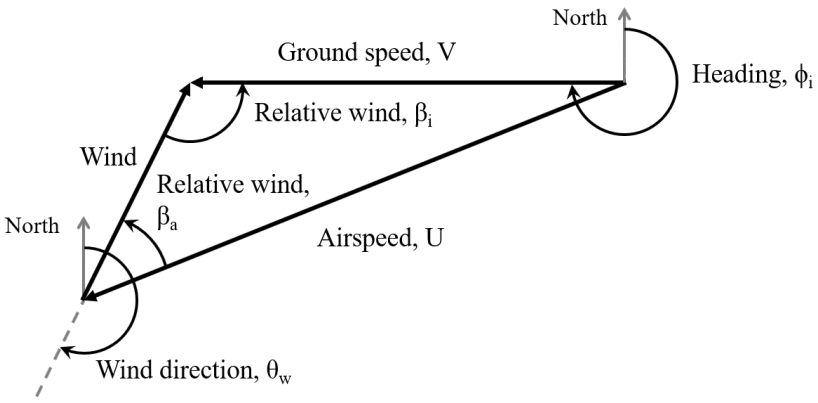

Figure 4.4: Relative wind angles in the inertial and air reference frames shown here with a South-south-westerly wind and a East bound trajectory.

The glide polar is then shifted by the headwind and any vertical wind present. The new optimised airspeed is identified by finding the maximum gradient in the newly shifted glide polar, however, the same result can be achieved using a look-up table as described by [52]. Finally, the new ground speed vector is calculated using the new airspeed and the assumption that the ground trajectory heading is held constant. The process should be repeated with the new ground speed until an error between the current and previously optimised airspeeds is less than 0.1 m s $^{-1}$. Convergence was found in the vast majority of wind condition cases, except for very high wind speeds in the inertial crosswind. While this could prove relevant for orographic soaring cases in this study, the magnitude of the wind speed required is outside of the range explored here. The extent of the non-convergent pocket is explained demonstrated in Fig 4.5.

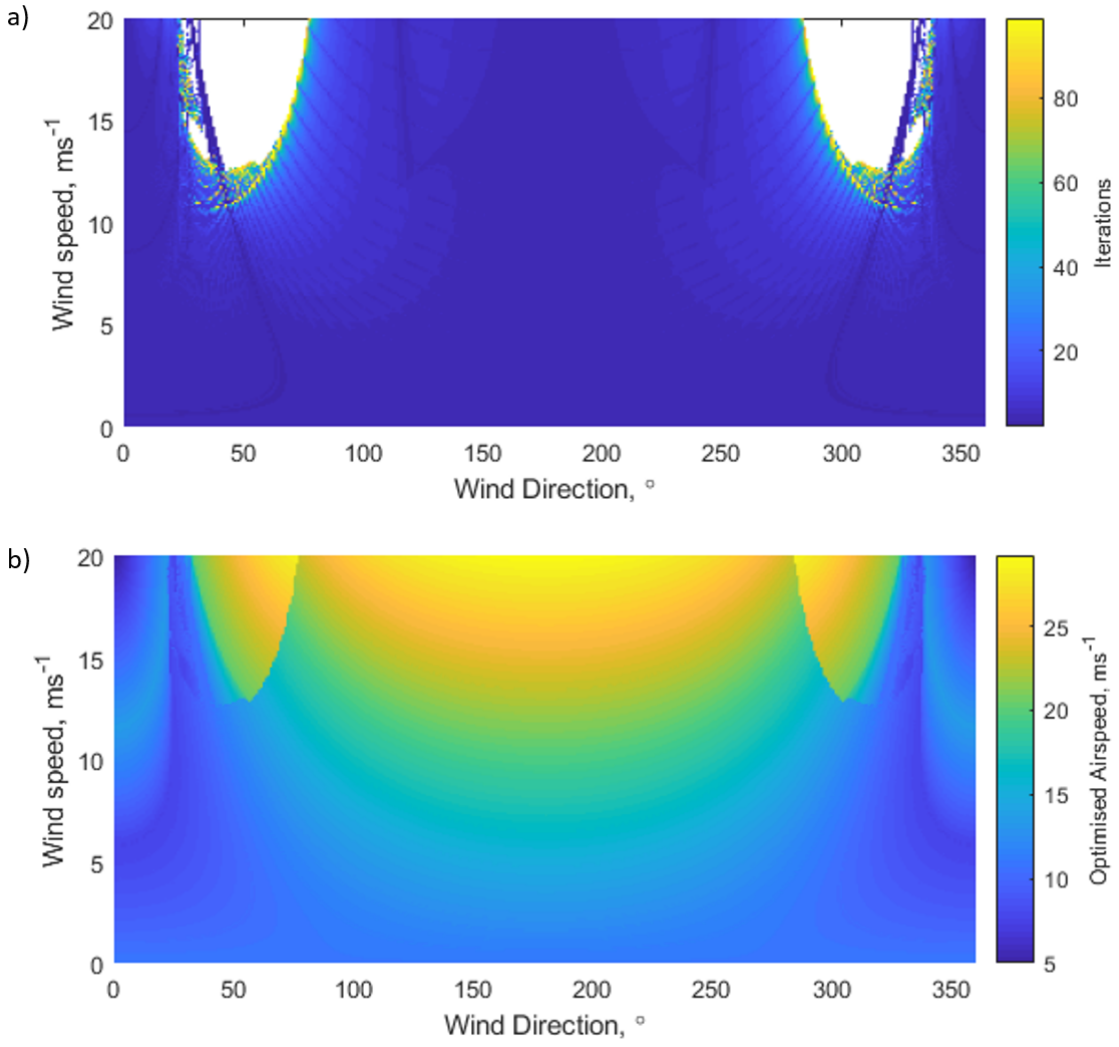

Figure 4.5: a) The number of iterations required for airspeed optimisation convergence where the pockets of white space represent areas of error oscillation above 0.1 m s $^{-1}$ rather than convergence b) The optimised airspeed results from convergence where the non-converged regions where resolved to the lowest error calculated in 100 iterations.

Algorithm 1 Optimise airspeed velocity

function OPTIMISE AIRSPEED VELOCITY($GP, \phi_i, W, \theta_w, U_{bg}$) ▷ Where U_a - opt. airspeed, β_a - opt. relative wind angle. Optimise airspeed based on a fixed trajectory and wind conditions
  $U_{opt}(i) = U_{bg}$ ▷ Start algorithm using best glide velocity
  $V = U_{bg}$ ▷ Set initial ground speed to best glide velocity
  $i = 0$
  while $e > 0.1$ & $i < 100$ **do** ▷ Loop until error margin is met or number of iterations exceeds 100
    $i = i + 1$
    $\beta_i = \arcsin(W/V)\sin(\theta_w - \phi_i)$ ▷ Calculate the inertial relative wind angle
    $\beta_a = 180 - ((\theta_w - \phi_i) + \beta_i)$ ▷ Calculate the air relative wind angle
    $W_{a_h} = W\cos\beta_a$ ▷ Find the air relative headwind
    $GP_s[:,1] = GP[:,1] + W_{a_h}$ ▷ Shift the glide polar using the air relative headwind
    $GP_s[:,2] = GP[:,2] + W_z$ ▷ Shift the glide polar using vertical wind *(optional)*
    $idx = max(GP_s[:,1]/GP_s[:,2])$ ▷ Index location of the new lift to drag maximum
    $U_{opt}(i+1) = GP_s[idx,1]$ ▷ Optimised airspeed
    $e = |U_{opt}(i+1) - U_{opt}(i)|$ ▷ Calculate the error margin
    $V = \sqrt{(U_{opt}(i+1)^2 + W^2 - 2U_{opt}(i+1)W\cos\beta_a)}$ ▷ Calculate new ground speed
  end while
end function

4.2.4 Velocity test models

The velocity optimisation models use the glide polar and power curves generated by the aerodynamic characteristics from Pennycuick's 2008 model [16] and the gulls' biometrics in Table 4.2. A fixed-wing variation of the glide polar model was used due to the sufficient similarity at airspeeds of < 16 m s^{-1} (accounting for 69% of the data) to other methods which include span reduction. Optimised velocity was calculated by shifting the glide polar by the airspeed and/or vertical wind, and a new tangent calculated as described in Fig 4.1e. The power curve model for flapping flight was also generated using sampled gull biometrics and values from Pennycuick's 2008 Flight model with a drag factor, k, of 1.1 being used. The Pennycuick model predicts that gulls fly at minimum power velocity due to power constraints in the pectoral muscles [16] however, some literature suggests that this would mean no airspeed optimisations are then required [87]. To test these theories we selected three models:

- Model 1 - Flying at minimum power speed but maintaining flight time. This model used U_{mp} as the optimum velocity but shifts airspeed only if there is a headwind. There is no adjustment from U_{mp} in tailwinds. The adjusted velocity is the minimum of the headwind shifted curve.

- Model 2 - Flying at minimum power speed with no attempt at airspeed optimization, the only change being the effect of wind on the ground speed.

- Model 3 - Matching flight speed to CoT optimised best glide velocity, U_{bg} during both gliding and flapping flight.

4.3 Methods

This section includes details for the empirical data capture and processing. The gull tracking, details of environmental data sets, flight path filtering and the classification of soaring strategies are presented here.

4.3.1 Bird tagging

This research analysed the flight paths of 11 lesser black-backed gulls, *Larus fuscus*, tracked using GPS backpacks [32] over two breeding seasons in the city of Bristol, UK. All work was approved by the University of Bristol Animal Welfare and Ethical Review Body (UIN: UB /15/069). Bird handling and tagging was conducted under BTO permit A /2831, additional details can be found in [110]. Bio-metrics for the individuals were recorded at the time of capture and used to characterize the morphology of an average individual (Table 4.2).

Table 4.2: Wing and body measurements calculated from measured bio-metrics

	Span (m)	**Mass (kg)**	**Wing area (m^2)**	**Aspect ratio**	**Chord (m)**	**Frontal area (m^2)**
Mean, μ	1.15	0.741	0.168	7.85	0.146	0.0067
Standard Deviation, σ	0.065	0.061	0.018	0.63	0.011	0.00036

4.3.2 Bio-logging data

The Global Positioning System (GPS) loggers collected spatial fixes containing latitude, longitude, altitude and a date-time stamp, with each fix being immediately followed by a one second burst of 20 Hz three-axis accelerometer data. The spatial data were used to reconstruct the flight paths of the gulls and the acceleration data were used to classify flight behaviour at each position. The behavioural model used was developed by Shamoun-Baranes *et al* [35], it uses 14 selected features of the acceleration data and a random forest classifier of 100 trees trained on a large set of annotated acceleration clips based on timed observations. We added a further twenty manually classified acceleration data clips for each of the gulls in this study to the training set. The behavioural classes for

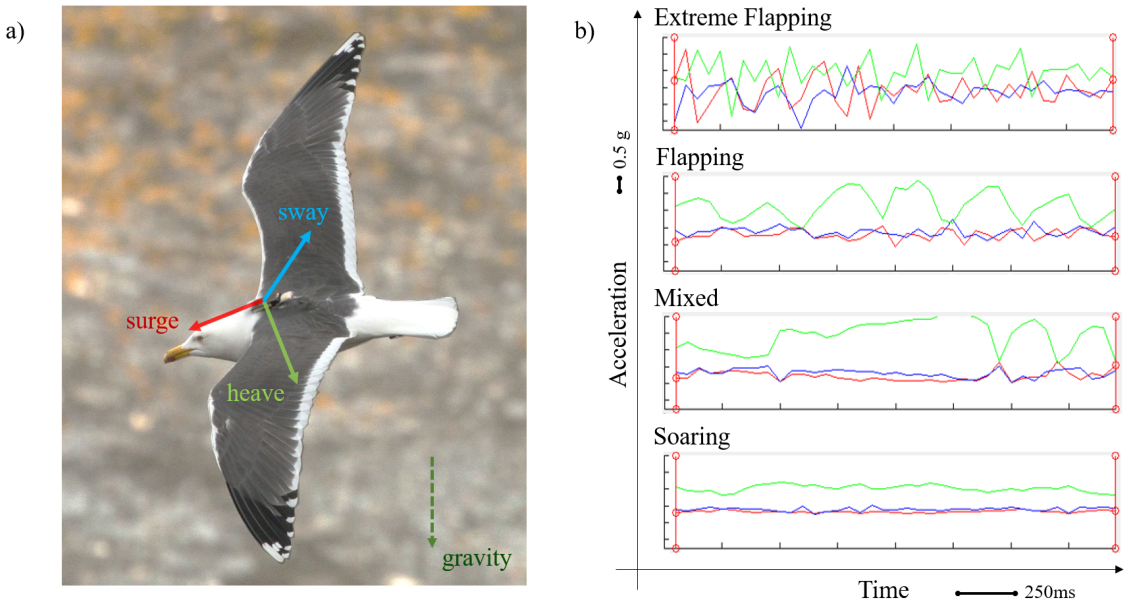

Figure 4.6: a) Lesser black-backed gull with fitted GPS tag. b) The tri-axial accelerometer signals for four flight behaviours; extreme flapping, flapping, mixed and soaring as described in [35, 110]

the full model include: soaring, flapping, extreme flapping, mixed flight, walking, pecking, float, boat, stationary, and other. This study used four of these behaviour classes (Fig 4.6); extreme flapping (such as in take-off and landing), flapping, soaring, mixed flight (a combination of soaring and flapping). Further details of the behaviour classification can be found in [35, 110]. A spatial fence trigger was used to adjust the GPS capture frequency of the tags. When the gulls were on their nest, the capture rate was set to a GPS fix every 10 mins (600 s). The devices were programmed to increase frequency to a minimum of every 5 mins (300 s) after leaving the nest area, defined by a radius of 50 m. As a result the outbound flights recorded were often incomplete. The tags were charged by solar panels and when the tag had a sufficiently high battery voltage the tag switched to a high frequency data capture rate of every 4 s. This study filtered the dataset for commuting flights containing high frequency data, considered as a fix every 4 - 6 s.

4.3.3 State variables

State variables associated with the flights such as velocity, altitude and attitude were calculated as follows. The ground speed of the gulls at the time of data capture was

considered the instantaneous speed as calculated by satellite Doppler shift, as opposed to point-to-point differencing. Vertical and horizontal ground speeds were calculated separately in the case of gliding flight in order to compare forward and sink speeds. The altitude above sea level (ASL) was calculated using the GPS measured altitude. The altitude above ground level (AGL) and altitude above structure (HAS) were calculated using a digital elevation model from 2 meter resolution LIDAR data [96]. Heading and directional change angles were calculated using the latitude and longitude captured by the tags with a Haversine transformation adjusted for latitude at the nest location and accurate to 1%, which was considered accurate enough for the short point to point distances calculated.

4.3.4 Commuting Flights

Commuting flights were defined as non-stop flights between frequently visited locations. These flights were chosen under the assumption that the individuals are not foraging or searching, but travelling between known locations and as such, more likely to be conserving energy. The full data set was filtered to include only flights to and from 72 locations based on repeated visits. The locations were found using a combination of observation and spatial clustering of terrestrial location fixes. The commuting flight were defined using the filter criteria below:

- A series of flight behaviour data points enclosed by two terrestrial fixes at take-off and landing.
- A direct flight between the take-off and landing locations with no additional stops (terrestrial points).
- Start and end locations cannot be the same.
- A flight must have 10 or more fixes per km flown ensuring that trajectory resolution is suitably high.
- A flight must have more than 10 total fixes to ensure that flights are suitably long for evaluation.
- The flight must be repeated on 4 occasions such that there is a comparison set.
- Flights with obvious detours, foraging or loitering were removed.
- Start and end locations are at least 2 km apart.

This resulted in a set of 192 flights ranging between 2 and 20 km, with μ = 6.3 km, σ = 3.5 km.

4.3.5 Weather data

Weather data in this study was sampled from high resolution United Kingdom variable (UKV) forecasting model output data. The forecasting model has a spatial resolution of 2 km and a temporal resolution of 1 hour and has the highest resolution of any available data set over the UK [127]. Each GPS fix was assigned to the nearest 1-hour time prediction and then spatially interpolated. The wind speed and direction were interpolated for altitude and used to calculate airspeed. The forecast data were validated using data from a two week period collected by two locally situated weather stations; one at the nest and a second towards the North-East foraging areas. The Pearson produce-moment correlation coefficients computed for wind speed (R = 0.87, n > 120,000, RMSE = 1.87 m s^{-1}) and wind direction (R = 0.81, n > 120,000, RMSE = 33.6°), as shown in Fig 4.7, showed that forecasting model gave wind estimates in good agreement with those measured directly.

4.3.6 Soar Strategies

Data points were given an additional flight mode classification based on the soaring strategies being utilised. All data points previously classified as soar behaviour mode were further categorised into soaring strategies; gliding (with subsets high and low altitude), thermalling, orographic and other using a decision tree classifier (Fig 4.8). The soar strategy classification algorithm compared state variables against a set of thresholds, as shown in Fig 4.8. Data were averaged through a moving mean with a window size of 3 to account for noise. The threshold for the first branch was the sink rate considered as the satellite measured vertical velocity. The second threshold was based on the altitude, AGL and HAS were both used to consider terrain features. The final threshold determined circling behaviour where the heading change and standard deviation were considered.

- Gliding is unpowered flight where gravitational and kinetic energies are traded. Here, it was defined as soaring behaviour with a sink rate (downward vertical velocity) greater than 0.55 m s^{-1}. This was selected as the minimum sink rate from the glide polar (Fig 4.1e). Classification of gliding was performed on the

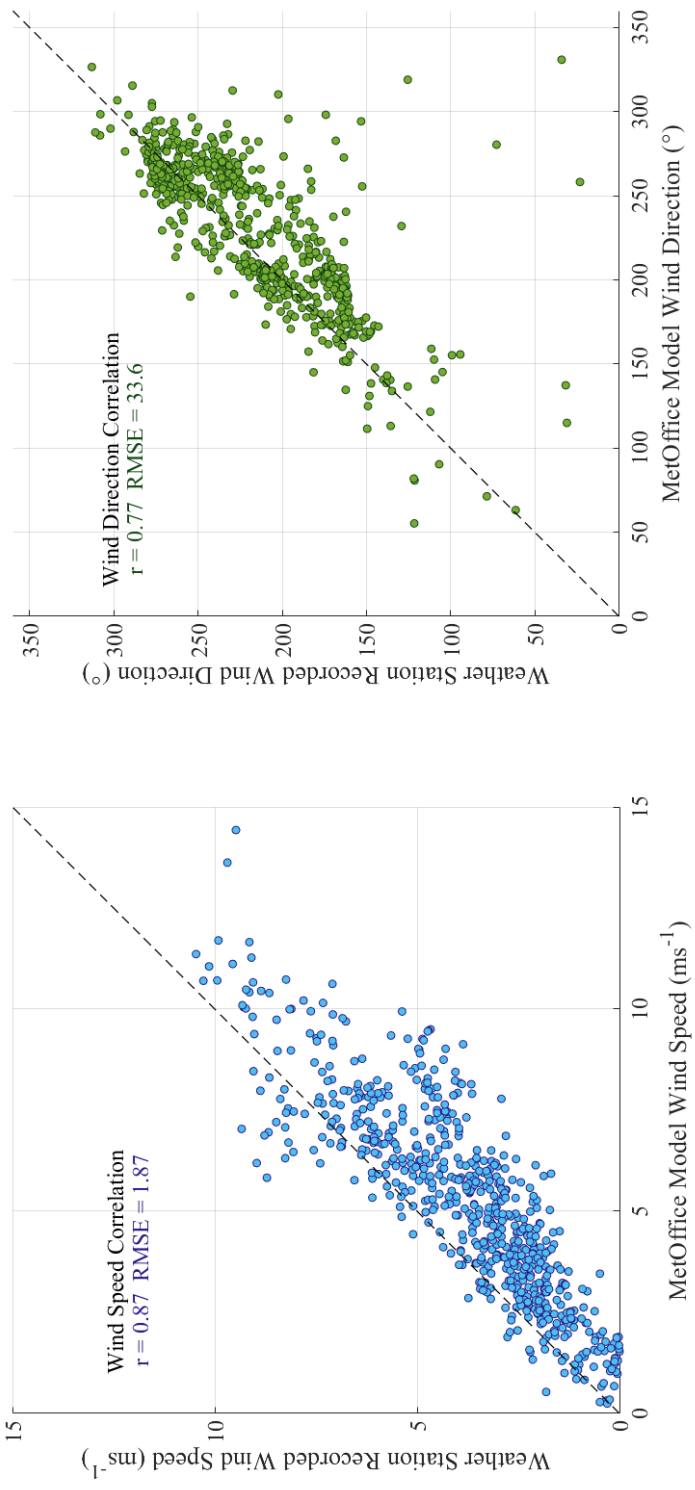

Figure 4.7: MetOffice model output plotted against weather station measurements for weather stations locations at the nest [51.459145°, -2.603555°], and foraging area [51.500583°, -2.548134°] combined, for the dates 1-14/06/2017 inclusive. A strong correlation can be seen in the wind speed (R = 0.87) on the left, and direction (R = 0.81) on the right.

first branch of the decision tree (Fig 4.8). In some analysis gliding was further classified by altitude. High-altitude gliding such as between thermals, (Fig 4a), was classified by the same altitude threshold as the second branch in the decision tree. Low-altitude gliding was defined as below this threshold and occurred between sections of flapping, mixed or orographic soaring modes.

- In thermal soaring altitude is gained by circling in columns of warm rising air, as shown in Fig 4.8a. This was characterized firstly by high altitude flight where both altitude above ground level, h_{AGL} and height above surface structure, h_{HAS}, were considered. Secondly, by a high variance in flight direction, $\sigma(\phi_i)$, and a consistent heading change, $\Delta\phi_i$, of 30°or greater between fixes, shown by the final lower branch of the decision tree (Fig 4.8).

- Orographic soaring uses updraughts generated on the windward side of a terrain feature, such as a cliff, hill or building, to offset sink in gliding flight. It requires a relatively low altitude to be within range of any updraughts. Examples of orographic soaring can be seen in Fig 4b,c. The strategy was classified when the circling and altitude measures were below given thresholds, as seen in the upper final branch of the decision tree (Fig 4.8).

- The "Other" class contains any soaring behaviour which did not fall into the previous categories. This class contained a small fraction of low altitude thermalling, or circling in areas of very strong orographic lift, see examples Fig 4.3.6c, but mostly contains high-altitude soaring with no directional variance. This was most likely travel through unexploited thermals or detached thermal bubbles, an example of which is shown in Fig 4.3.6a.

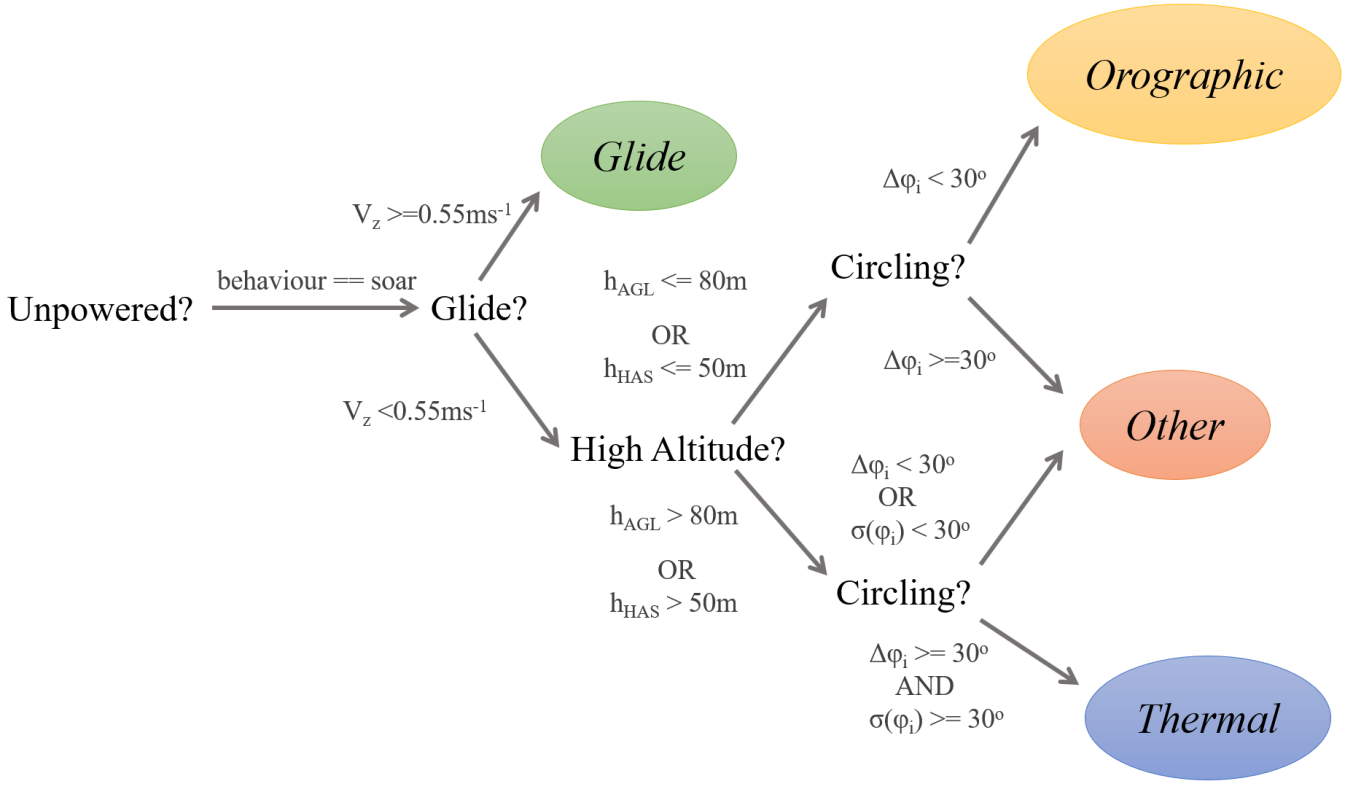

Figure 4.8: Flight strategy decision tree with threshold values. The first branch sorts by flight behaviour. The second branch sorts gliding or soaring. The third branch sorts using two altitude thresholds. The final branch sorts by heading change.

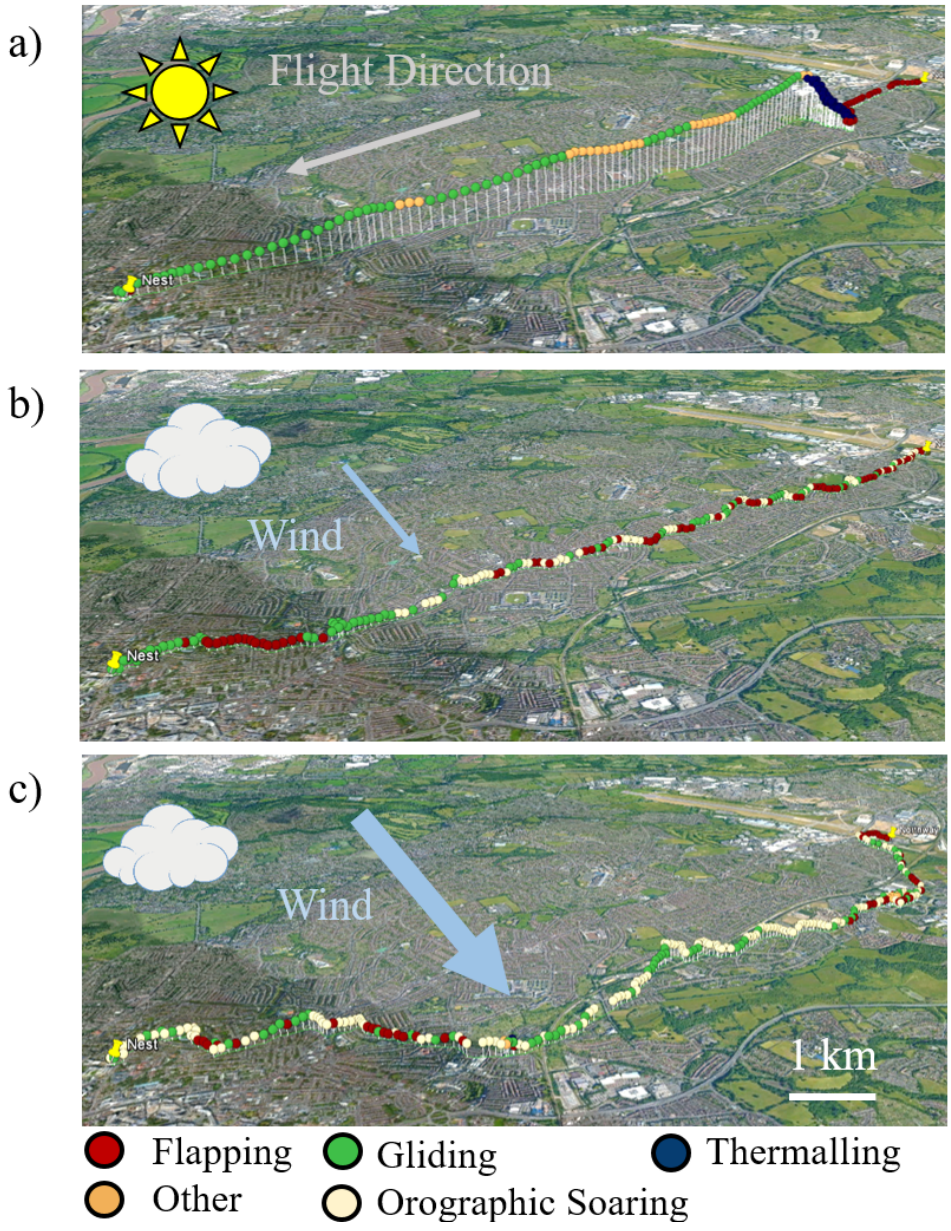

Figure 4.9: Flights from the same individual that occurred with 3 different weather conditions. a) high thermal availability b) overcast day with low westerly wind c) day with a high westerly wind. Background courtesy of GOOGLE EARTH [128].

Soaring strategy classification was validated with three methods. First, by expert comparison with a set of 10 selected flights across the range of soaring strategies. Flights were selected that had examples of all soaring types including samples with values close to the classification thresholds. Second, using a systematic variation of the threshold values to check for classification robustness. In this validation case, varying threshold changes tended to have greatest effect on the amount of data being classified as the Other soaring strategy. The results of the threshold testing can be found in Appendix C. Third, by using a machine learning classification model trained with algorithm classified data and input variables from a geophysical, meteorological and time of day data set as found in [35]. Specifically, thermal and orographic flight strategies were tested as these strategies occurred in different conditions. The Classification Learner toolbox in MATLAB 2018a was used with a medium grain, k-clustering algorithm and a 5-fold test-train ratio. The classification of thermal and orographic points was found to agree with the decision tree algorithm with a 95% accuracy.

4.3.7 Inter-thermal gliding

Inter-thermal samples were generated by finding thermal-glide pairs that fell within three criteria; firstly, there must be 5 or more consecutive thermal points in the initial and subsequent thermals, secondly, the glide section joining the two thermal sections must contain more than 50% gliding strategy data with a low directional variance, and finally, all thermal-glide data must be high frequency data. All commuting flights were searched for thermal-glide pairs giving a total of 19 high-quality thermal-glide pairs. The thermal climb rate was calculated as the average vertical velocity and the inter-thermal velocity was calculated as the average airspeed performed over the entire glide sequence between thermals.

4.4 Results

4.4.1 Time budgets and soaring strategies

When flying in urban areas the gulls were able to make extensive use of environmental energy, soaring 30% of the time (Fig 4.10b). This increased to 44% when just commuting flight was considered (Fig 4.10c). The gulls used a mix of different gliding and soaring strategies (Fig 4.10d), the most common combination being thermal soaring followed by sections of high-altitude gliding and occasional soaring (labelled other) through

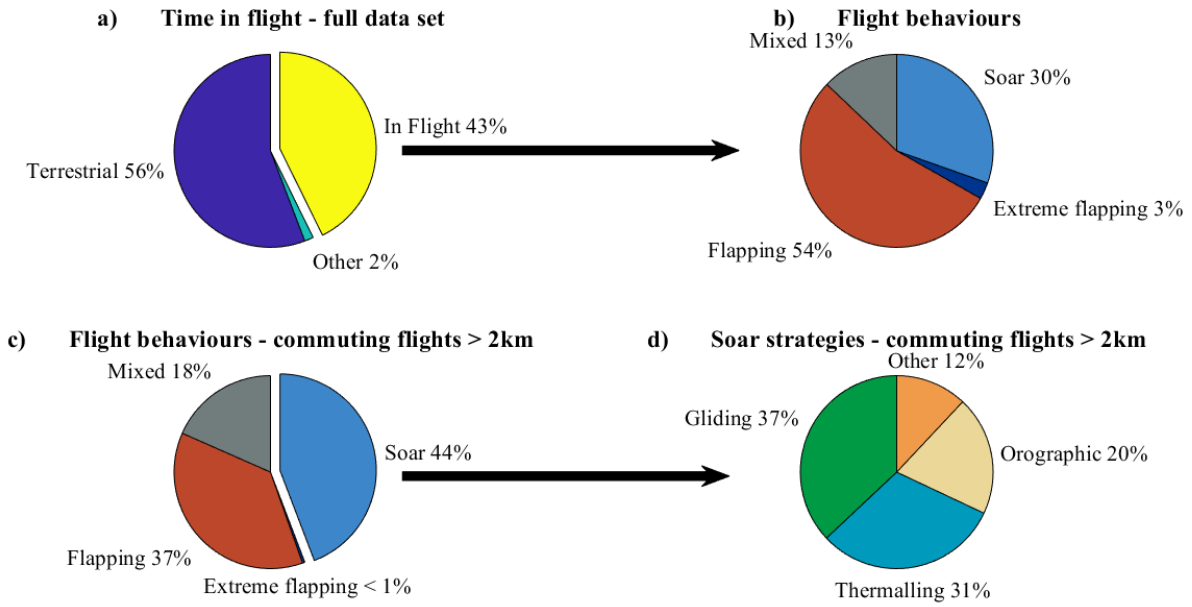

Figure 4.10: a) Time budgets for terrestrial and in-flight behaviour. b) Time budgets for in-flight behaviour c) Commuting flight behaviours d) Soaring strategies used in commuting flights, with low- and high- altitude gliding being grouped.

updraught pockets such as thermal bubbles. On days with low thermal availability but some wind, orographic soaring was used extensively in combination with low-altitude gliding and mixed flight.

The high amount of thermal soaring behaviour measured suggests that the urban environment provides a significant level of thermal availability. Commuting flights that used thermalling were recorded with high percentages of non-flapping flight, with some flights containing as much as 100% soaring flight. These flights also contained soaring consistent with passing through thermals or thermal bubbles without circling to gain altitude and without the need to deviate significantly from the shortest commuting path, suggesting there was a greater number of thermals available than required.

The urban environment offered soaring opportunities when there was little or no thermal availability. These flights contained a mix of orographic soaring, low-altitude gliding and mixed flight and on average contained a higher fraction of flapping flight that thermalling flights. Flights featuring orographic soaring also featured higher levels of mixed behaviour, with some flights featuring as much as 60% soaring flight and 40% mixed, and no flapping flight. It was expected that orographic updraught availability

would be higher on days with stronger winds and as such these conditions would feature a higher percentage of orographic soaring. However, orographic soaring showed only a small increase with wind speed compared to a significant decrease in the proportion of flapping flight and an increase in the proportion of mixed flight. The percentage of orographic soaring increased with relation to the wind speed with a positive Pearson correlation (R = 0.19, n = 2623, p < 0.001), suggesting the gulls were able to make use of orographic updraughts across a range of wind speeds. The percentage of flapping was found to decrease with increasing wind speed with a negative correlation (R = -0.34, n = 11285, p < 0.001). The relatively low correlation could be explained by an absence of flapping flight on days with low wind speeds and high thermal availability. Mixed flight, however, was found to increase with wind speed with a strong positive correlation (R = 0.64, n = 5829, p < 0.001). Overall, these changes in behaviour in relation to wind speed indicates that the gulls were able to make use of the higher environmental energy available on windy days, but may have had higher control demands as represented by the higher level of mixed manoeuvring flight.

4.4.2 Airspeeds of flight behaviours and soar strategies

The gulls were found to have different airspeeds depending on their flight behaviour or soaring strategy, (Table 4.3). In flapping and soaring flight, the gulls flew at velocities slightly below the predicted minimum power, U_{mp} = 11.9 m s^{-1}, and best glide, U_{bg} = 10.6 m s^{-1}, velocities respectively. The mixed flight average airspeed was considerably higher and could be associated with gusts and fast corrective manoeuvres. Unexpectedly, the average velocity in soaring flight was slightly higher than that in flapping flight, however the difference was not significant.

The altitudes flown by the gulls varied from 0 to 923 m (AGL) where the median altitude flown on non thermalling days was 34 m. When thermalling the gulls thermalled to a mean maximum altitude of over 600 m. To make velocities comparable equivalent airspeeds are used, taking into account the increase in velocity at altitude due to lower air density. When soaring strategies were compared using an ANOVA, all the airspeed distributions were found to be statistically different from flapping flight and each other, apart from the low altitude gliding and other soaring strategies, which were significantly different from flapping flight but not from each other. Interestingly, the high altitude gliding, such as between thermals was faster than the low altitude gliding, such as between intermittent flapping or orographic soaring ($f_{high-low}$ = 619, p***).

Thermalling flight, indicated in Fig 4.11 in blue, had the lowest average velocity at

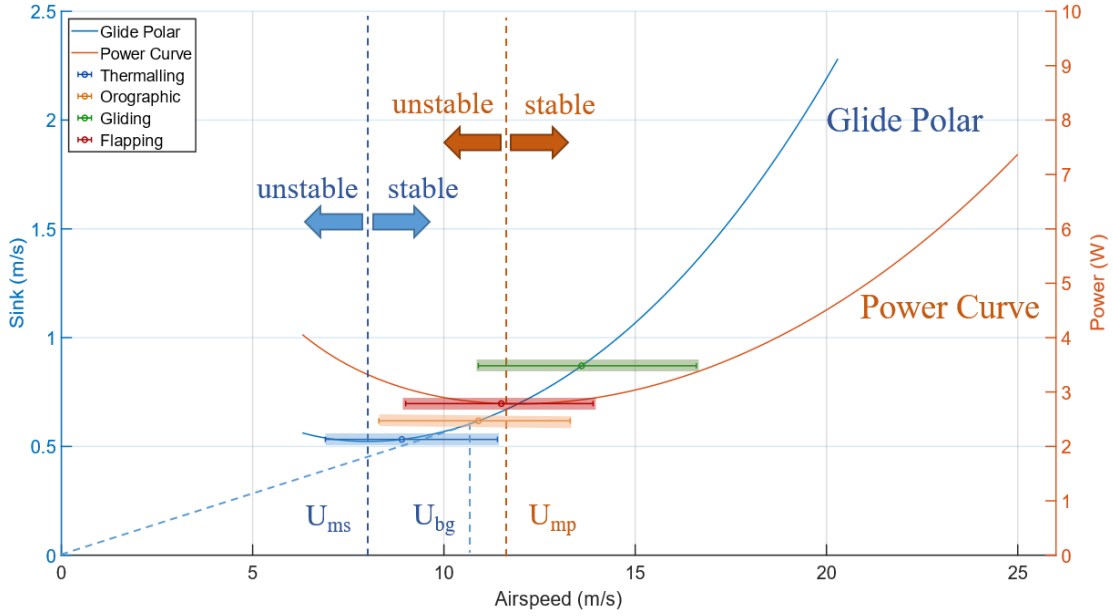

Figure 4.11: Glide polar (blue) and power curve (orange) shown with the airspeeds for soaring strategies thermalling (blue), orographic soaring (yellow) and gliding (green), and flapping flight (red). The mean airspeeds are indicated by a dot and the bar indicates the standard deviation. The stable and unstable regions of each curve are also indicated and labelled. Min power, min sink and best glide velocities are indicated by the dashed lines for reference.

9.6 m s^{-1}, and was close to the minimum sink velocity at 8.2 m s^{-1}, which would provide the best altitude gain but was still fast enough to avoid stall. During orographic soaring the average airspeed was 10.9 m s^{-1}, close to the best glide velocity for soaring flight, at 10.6 ms^{-1}. The average gliding airspeed was much higher at 13.8 m s^{-1} and was significantly higher than the best glide velocity ($p < 0.001$).

4.4.3 Airspeed optimisation in soaring strategies

The gulls used different airspeed adaptions in relation to the relative wind direction depending on the soaring strategy being used. The relationships between airspeed and the air relative wind direction are plotted for four soaring strategies (Fig 4.12), and demonstrate the different airspeed adaptions used in each strategy.

In high altitude gliding the gulls made the expected adjustments for the wind direction but flew slightly faster than expected (Fig 4.12a), as shown by the data following the shape of the curve but with many points higher than the predicted CoT optimum. In thermalling flight the gulls made relatively little adjustment to their airspeed for

Table 4.3: Airspeeds for flight behaviours and soar strategies

Flight type	**Mean** μ (m s^{-1})	**Standard deviation** σ (m s^{-1})	**ANOVA** f-value	p-value
Flight behaviours				
Flap	11.4	3.7	$f_{flap-soar}$ = 0.95	p = 0.33
Soar	11.9	4.4	$f_{soar-mix}$ = 134,	p***
Mixed	12.7	4.6	$f_{flap-mix}$ = 176,	p***
Soar strategies				
Thermal	9.6	3.7	$f_{therm-flap}$ = 1870	p***
			$f_{therm-soar}$ = 1091	p***
Orographic	10.9	3.8	$f_{oro-flap}$ = 75	p***
âŮŸ			$f_{oro-soar}$ = 62	p***
Other	12.3	4.6	$f_{oth-flap}$ = 26	p***
			$f_{oth-soar}$ = 32	p***
Gliding (all)	13.8	4.5	$f_{glide-flap}$ = 20	p***
			$f_{glide-soar}$ = 26	p***
Gliding (low altitude)	11.7	3.2	$f_{low-flap}$ = 2493	p***
			$f_{low-soar}$ = 1786	p***
Gliding (high altitude)	14.8	4.7	$f_{high-flap}$ = 2074	p***
			$f_{high-soar}$ = 992	p***
Where p significance levels are p*<0.05, p<0.01, p***<0.001**				

the relative wind direction (Fig 4.12b), as shown by their consistent airspeed for all relative wind directions. The gulls did make adjustments for the wind direction during low altitude gliding and orographic soaring (Fig 4.12c, d), where it can be seen that the gulls followed the predicted model except around a 50 ° relative wind direction. This angle corresponds to a cross-wind in the inertial frame and would occur when flying along an object facing perpendicular to the wind. Here, the gulls flew slower than predicted by the CoT model.

The soaring strategy velocity responses for wind direction were also generated in the ground speed frame in order to demonstrate that the results were not caused by false correlation from using the wind data set in the measured and modelled data. The ground speed models shown in Fig 4.13 agree with the airspeed results from Section 4.4.3, showing a trend of flying faster in high-altitude inter-thermal flight and slower in strategies which take advantage of updraughts.

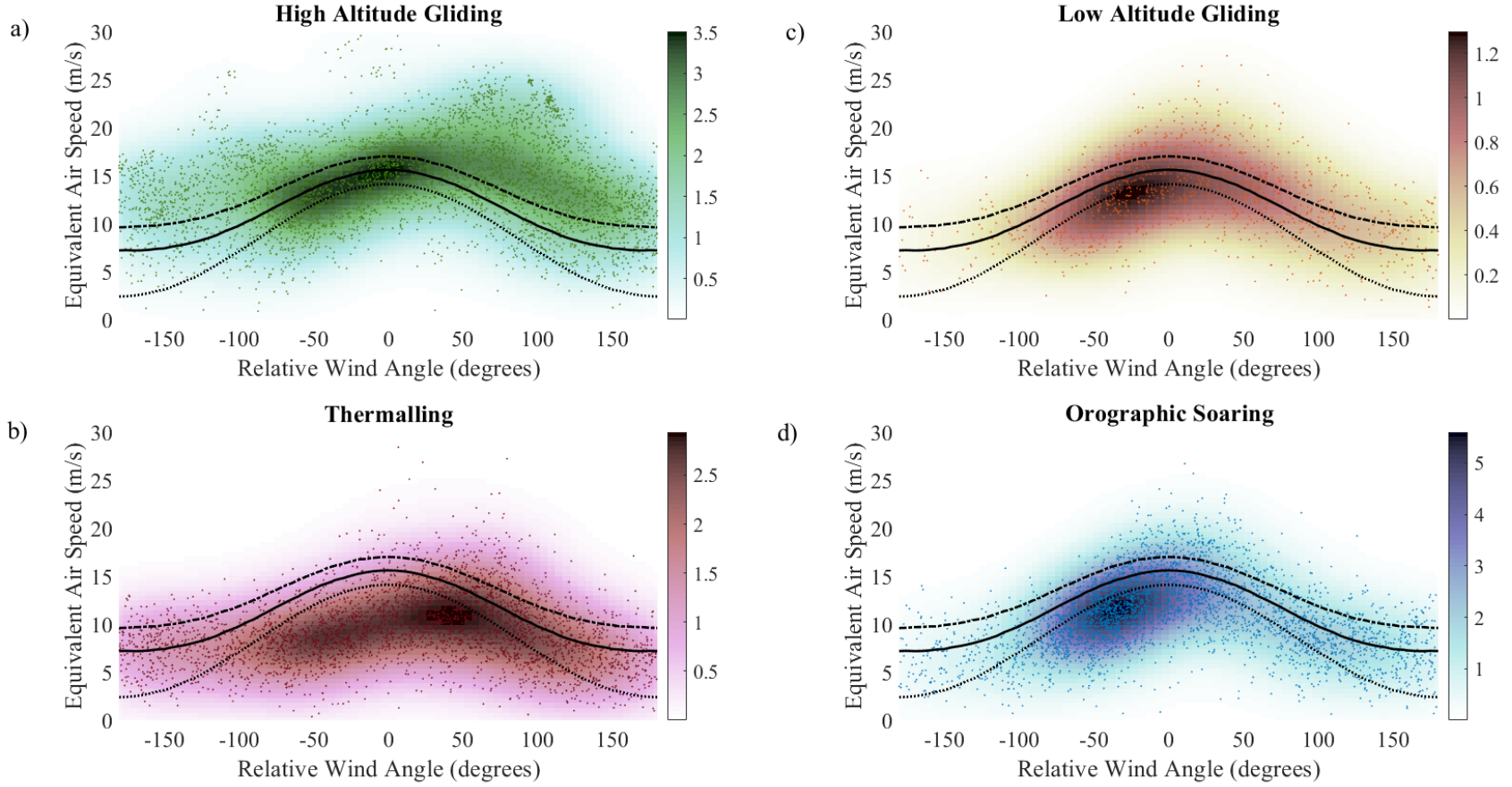

Figure 4.12: Equivalent airspeeds at the relative wind direction compared to CoT model a) High altitude gliding flight b) Thermal soaring c) Low altitude gliding flight c) Orographic soaring. The central line in each plot is the optimum CoT airspeed for a 6 m s^{-1} wind with no updraught, the upper line is the optimum with an added downdraught of -0.5 m s^{-1}, and the lower line is the optimum for an added updraught of 0.5 m s^{-1}. The data points represent the collected gull airspeeds between 4.5 and 7.5 m s^{-1}. A Gaussian filter has also been applied to the gull data to demonstrate the density of the measure data where the colour bar represents the number of data points per 5 ° by 0.5 m s^{-1} spacing.

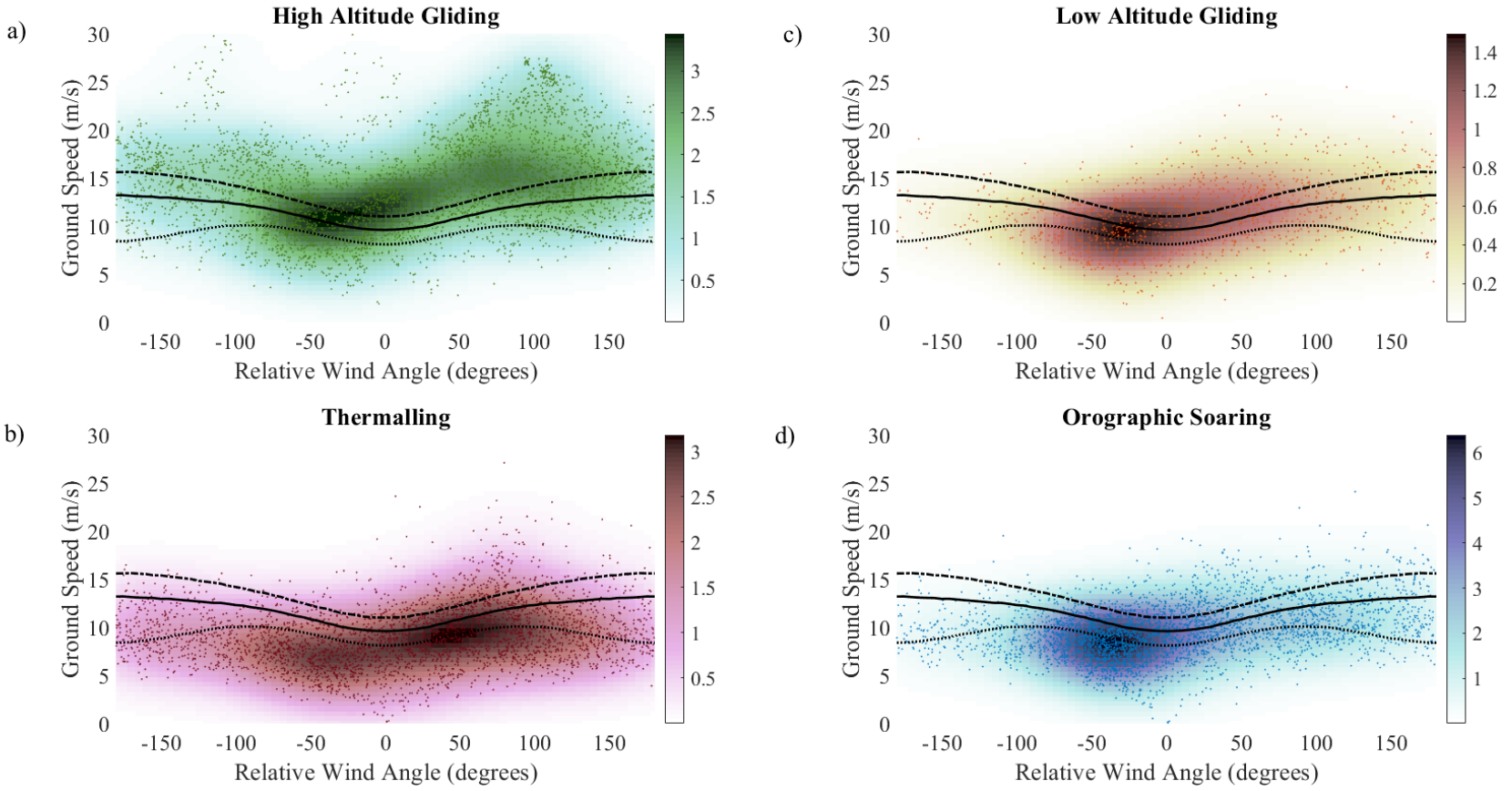

Figure 4.13: Ground speed comparisons at the relative wind direction compared to CoT model a) High altitude gliding flight b) Thermal soaring c) Low altitude gliding flight c) Orographic soaring. The central line in each plot is the optimum CoT ground speed calculated for a 6 m s^{-1} wind with no updraught, the upper line is the optimum with an added downdraught of -0.5 m s^{-1}, and the lower line is the optimum for an added updraught of 0.5 m s^{-1}. The data points represent the measured ground speeds between 4.5 and 7.5 m s^{-1}. A Gaussian filter has also been applied to the gull data to demonstrate the density of the measure data where the colour bar represents the number of data points per 5 ° by 0.5 m s^{-1} spacing.

All plots show resulting ground speed from the optimised airspeed using CoT modelling with the horizontal wind, the central line indicates has no vertical wind. Upper and lower lines shows a down- and up-draught respectively both of 0.5 m s^{-1} strength. A density distribution of the measured data points with a grid size of 5 ° by 0.5 m s^{-1} was used in combination with a Gaussian smoothing filter of 5σ, purely to qualitatively demonstrate the change distribution of the collected data.

Additionally, the Pearson R correlation coefficients were calculated for the measured velocity responses compared to model data generated using a) measured wind data and b) a randomized sample from the same wind data population. The tests were performed for flapping flight, and orographic and low-altitude gliding flight combined. In both cases there was no correlation between the model and the measured data when the model was generated using a random sample, and a relatively high correlation between the model and measured data when the model was generated using measured wind data. Results as follows: flapping flight (R = 0.6, RMSE = 3.12, n > 10000, p < 0.001) flapping flight randomized sample (R = 0.004, RMSE = 4.88, n > 10000, p < 0.001) orographic and low-altitude flight combined (R=0.65, RMSE = 3.41), orographic and low-altitude flight randomized sample (R = -0.01, RMSE = 5.39, n > 10000, p < 0.001).

4.4.4 Inter-thermalling

During high-altitude gliding the gulls flew faster than the best glide velocity so it was expected that the gulls would fly at an airspeed described by MacCready's StF theory, shown as a dashed line in Fig 4.14. However, the results showed that the gulls flew slower than the optimum cross-country speed, as shown by the 19 inter-thermal flights indicated by the filled markers.

A second model using headwind adjustments and thermal strength is shown with square markers and also over predicts the flight speeds. Modelling the airspeed using CoT adjustments for horizontal wind is indicated by the vertical crosses and gave a much closer approximate to the measured gull airspeeds.

4.4.5 Flapping flight and wind direction

During flapping flight the gulls appear to fly at their best glide speed modified for the relative wind direction according to CoT theory, as represented by Model 3 coloured green in Fig 4.15. The mean ground speed predicted by adjusting best glide velocity for the head and cross winds conditions experienced by the gulls was a close match to

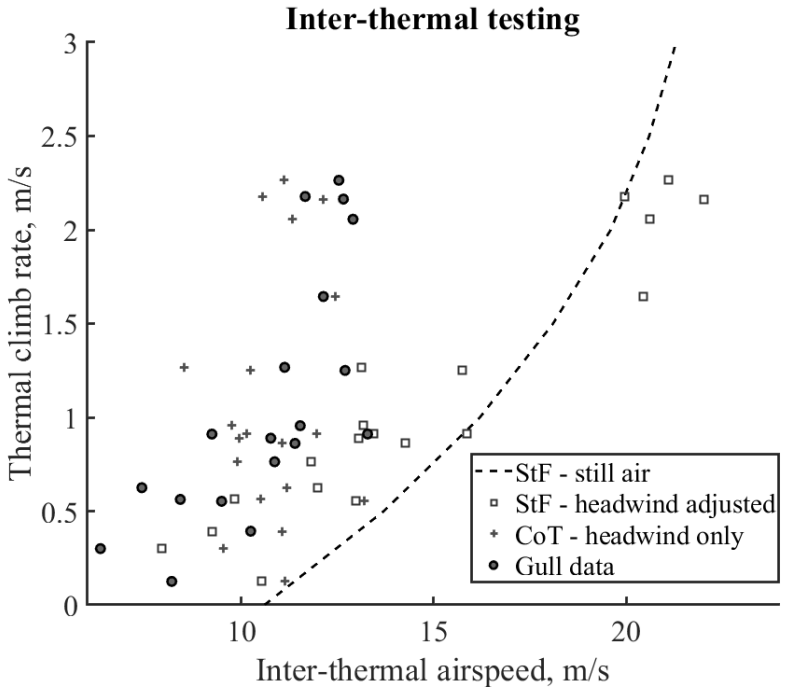

Figure 4.14: StF and CoT models compared with 19 inter-thermalling flights.

the flight speeds recorded, while the model slightly under estimated the ground speeds flown by the gulls during a tailwind. Using a model which adjusted minimum power airspeed to maintain minimum flight duration (Model 1 shown in white) produced an over estimate of ground speeds for head and cross winds and also under estimated the ground speed in tailwinds. Meanwhile maintaining minimum power velocity regardless of the wind conditions (Model 2 shown in pink) produced a good estimate of ground speed in crosswinds but under-estimated in headwinds and over-estimated in tailwinds.

The gulls' minimum power velocity is only slightly above their best glide velocity. This means that transitioning from soaring flight to flapping flight can be done efficiently without requiring a large power output for acceleration. This suggests that flapping at a velocity close to the best glide speed could be advantageous in complex flow environments where updraughts are readily available. This could facilitate energy harvesting where the mechanical power requirements at the mean airspeed for head- and tail-winds, correspond to only a +6% rise from the minimum power requirement, as seen in Table 4.4. The average airspeeds, also shown in Table 4.4, indicate that when orographic soaring the gulls slow down in cross and tailwinds, which both offer favourable CoT conditions. In gliding flight the gulls' airspeeds are higher, indicating either an absence of updraughts or that the birds are not exploiting them.

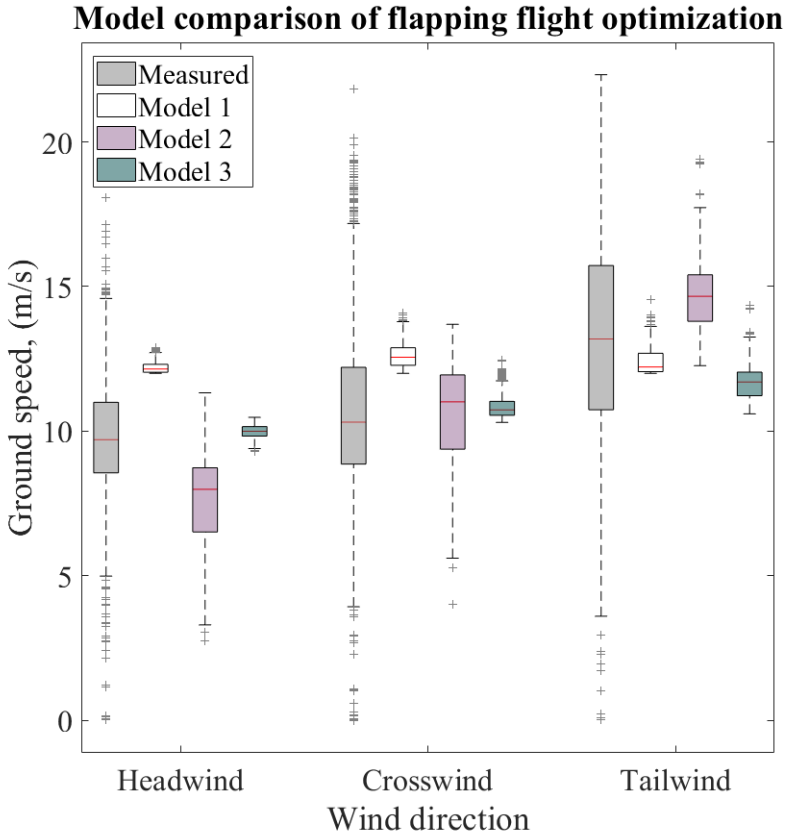

Figure 4.15: Measured ground speeds taken from GPS compared against 3 models, model 1: Optimising for U_{mp} and shifting with headwind, model 2: Maintaining U_{mp} regardless of headwind, model 3: Optimising to match U_{bg} and shifting with headwind.

4.5 Discussion

With the increase in SUAV technology, the fine-scale flight strategies of birds offers inspiration for improved methods of energy harvesting. Implementation of avian soaring strategies on SUAV technology has the potential to greatly increase both endurance and range performance which would otherwise be restricted by the relatively low on-board power capacity. However, studies in this area are often performed via simulation [11, 129–132] or in comparatively simple flow conditions [6, 76]. This study considers that urban nesting gulls could offer valuable insight into the flight strategies suitable for the complex flow environment generated by city landscapes.

The flights of 11 urban nesting gulls were tracked using GPS loggers which allowed the measurement of their position, velocity and behaviour. The gulls were able to extensively harvest environmental energy during their daily commutes using a combination

Table 4.4: Mean airspeeds for wind conditions

	Wind Direction		
	Headwind	*Crosswind*	*Tailwind*
Flap			
Mean airspeed, μ (ms^{-1})	14.8	11.8	9.2
Power at mean airspeed, (W)	3.0, (+6%)	2.8, (U_{mp})	3.0, (+6%)
Standard deviation, σ (ms^{-1})	3.2	2.8	3.1
Sample size, n	3408	5417	2460
ANOVA f-values	$f_{head-cross}$ = 1184	$f_{cross-tail}$ = 1856	$f_{tail-head}$ = 4769
ANOVA p-values	p***	p***	p***
Orographic			
Mean airspeed, μ (ms^{-1})	14.2	11.0	7.4
Standard deviation σ (ms^{-1})	2.9	2.5	2.7
Sample size, n	916	1199	508
ANOVA f-values	$f_{head-cross}$ = 658	$f_{cross-tail}$ = 633	$f_{tail-head}$ = 1935
ANOVA p-values	p***	p***	p***
Gliding (low altitude)			
Mean airspeed, μ (ms^{-1})	15.3	12.5	9.6
Standard deviation σ (ms^{-1})	3.3	3.4	3.8
Sample size, n	584	1058	731
ANOVA f-values	$f_{head-cross}$ = 221	$f_{cross-tail}$ = 314	$f_{tail-head}$ = 901
ANOVA p-values	p***	p***	p***
Where p significance levels are p*<0.05, p<0.01, p***<0.001**			

of different soaring strategies to exploit thermal and orographic updraughts. Building materials, such as concrete and asphalt, cause urban heat island effects [36, 133] so it follows that an abundance of these materials also generates high levels of thermal updraughts that these gulls were seen to exploit. Additionally, gulls have been shown to use man-made infrastructure for orographic soaring in coastal areas where the buildings act as artificial cliffs [10], and this study indicates that this can be extrapolated over cities where the urban canyons create a network of wind-highways for soaring. Clearly, there is a large source of environmental energy within the urban environment available for harvesting in soaring flight. This suggests that SUAVs designed with soaring capabilities could be able to drastically reduce their flight costs during urban missions given the right control schemes.

4.5.1 Soaring strategies

The gulls used different strategies and airspeeds to harvest energy from different environmental sources. We found that the gulls made use of thermal updraughts combined

with high altitude gliding. In thermalling flight their airspeed remained close to their minimum sink velocity regardless of wind direction. Using a low airspeed promotes maximum altitude gains by requiring the lowest sink offset. In gliding flight, the minimum sink and stall speeds are extremely close; the minimum sink speed lies at the boundary of the unstable velocity region where a small decrease in velocity could result in deceleration to the stall speed [16, 134]. Flying with a small safety margin above the minimum sink alleviates risk which is particularly important when flying in crowded thermals [55]. Glider pilots and other bird species have also been found to make this same risk mitigating compromise [6, 126, 135].

When gliding between thermals, the gulls made use of CoT optimisation for horizontal winds and although results indicate that there may be some velocity adjustment for updraught, the gulls did not fly at the high speeds predicted by StF. It is possible that the gulls did not perform StF due to an apparent abundance of thermal availability. The gulls were also seen performing soaring flight between thermals consistent with flying through a thermal or thermal bubble [136] but not circling . Flying at a glide speed slightly above the best glide could mean the gulls are able to make use of the updraughts without overly extending the flight time. This could be particularly relevant during chick rearing period where time away from the nest could impact breeding success. Interestingly, a recent simulation study optimising the velocity of UAVs in inter-thermal flight [137] found evidence which could support this theory. The study found that inter-thermal flight was optimal at a velocity between the best glide and StF velocities. The best glide velocity optimises for the energy cost per distance whereas the MacCready predicted velocity provides the overall best flight time when considering the time required to gain altitude. For the gulls, this suggests that while CoT is an important factor, that time away from the nest could also be an important driver.

The gulls were also able to perform high levels of soaring flight during periods of low thermal availability. In these cases, they performed a combination of flapping, gliding and orographic soaring flight. The orographic soaring analysis showed that the gulls flew slower than expected when making CoT adjustments only for headwinds indicating that the gulls are making use of orographic updraughts available in the cities. Other bird species have also been found to reduce airspeed in orographic soaring when compared to straight gliding [41] further supporting the gulls' exploitation of orographic lift. Surprisingly, the orographic soaring was not limited to wind directions consistent with soaring in parallel to ridge features. Flying with a tailwind over terrain features provides updraughts on the windward side of the feature, followed by a section

of downdraught on the leeward side. Gulls flying perpendicularly over buildings could use the updraught on the windward side to gain altitude for clearance over the building. This could explain the large range of velocities measured in tailwinds and suggests gulls or SUAVs should slow down through the updraught on the windward side of buildings and speed up through the leeward downdraught to harvest as much energy as possible.

4.5.2 Wing morphology and flight envelope

Wing morphology has a profound effect on the gulls' velocity envelope. Gulls have a relatively low wing loading like many soaring birds, but when compared to other marine bird species (such as albatross) they have a lower aspect ratio. The low wing loading results in being able to circle in narrow thermals but means a lower cross-country speed [41]. The gulls have a much lower wing loading (44 N m^{-2}) than that of manned gliders (> 80 N m^{-2}) and some other thermalling bird species [6, 41].

Perhaps the gulls' low wing loading influences the cross-country speeds more than predicted in the StF model. We explored the wing loading constraints on velocity by comparing the flown airspeeds against a velocity envelope generated using FAR 23.333 regulations for light aircraft [138] and found that the maximum airspeed for a gull-sized platform would be 21 m s^{-1}, a speed that would be reserved only for extreme manoeuvre cases shown in Fig 4.16 a.

While the low wing loading of the gull may limit their glide speed, their wing aspect ratio could have, in part, contribute to their success in urban environments. A relatively low aspect ratio results in greater wing-beat power [41] which could be beneficial to the gulls three-fold. Firstly, by facilitating ground based take-offs. Secondly, by assisting in high-powered manoeuvres that could be required when navigating around obstacles. Finally, in the extreme flapping behaviour as seen during foraging [110]. However, the aspect ratio of the gull wing is no doubt a trade-off between having a high aspect ratio wing for good glide performance and a lower aspect ratio wing for lower power requirements in flapping flight. The gulls have a large aspect ratio which provides a relatively high glide ratio of 15 but low enough that the power cost in flapping flight is kept to a minimum.

A flight envelope charts the velocity versus the load factor and shows the performance safety limits of an aircraft. The important velocities in the flight envelope are the stall speed, U_{stall}, manoeuvre speed, U_a, cruise speed, U_c, never exceed or maximum operating speed, U_{ne}, and finally, the maximum dive speed, U_d. Normal flight operation occurs between U_a and U_c. The velocities from the performance curves were also added. These

are labelled as, minimum sink velocity, U_{ms}, best glide velocity, U_{bg}, minimum power velocity, U_{mp}, and maximum range velocity, U_{mr}. Interestingly, the optimal performance velocities are all in the slower region of the flight envelope and contain the majority of the recorded airspeed, as shown in the histogram in Fig 4.16 b.

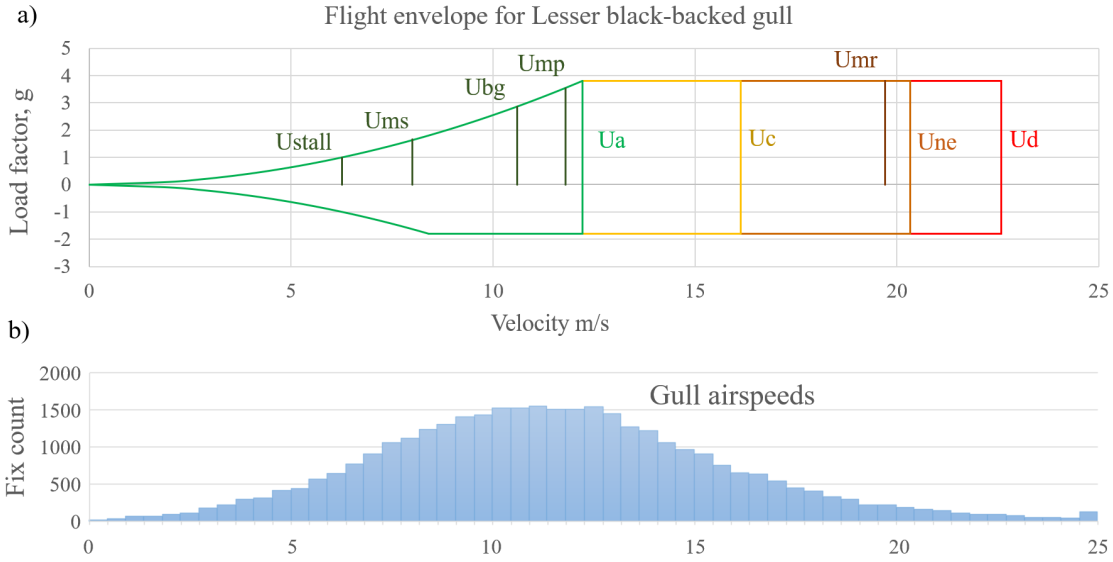

Figure 4.16: a) Flight envelope for the average lesser black-backed gull using FAR regulations [138]. b) Histogram of airspeeds recorded in this study.

4.5.3 Energy savings

The birds' flight speeds measured during orographic soaring, low-altitude gliding and flapping flight are very similar, suggesting that matching flapping speed to the soaring speed could have energy saving benefits. In flapping flight alone, the energetically cheapest speed to fly for a given distance is the maximum range velocity. Using the established Pennycuick power model [16] for an average gull, flying a set distance at maximum range velocity would equate to a 14% saving compared to flying the same distance at the minimum power velocity. This considers only the exerted mechanical power required over the time to complete the distance, and that the distance flown is relatively short such that body fuel storage is not considered. Considering that on average a commuting trip consists of 44% soaring behaviour, there is a 35% energy reduction compared to flying at maximum range velocity, demonstrating an obvious potential

benefit to flying slower than maximum range. Furthermore, the shallow minima of the power curve encompasses the velocity ranges required for all wind directions with only a +6% increase in mechanical power from the minimum power requirement, even with this power increase accounted for the energy savings would be 31%.

SUAVs could benefit from this speed matching strategy by taking into account the best performance velocities during the design phase of the platform. Matching the minimum power and best glide velocities for a platform would result in efficient use of environmental energy while demanding the lowest mechanical power for a motor when environmental energy sources are unavailable. Additionally, the performance curves of the platforms should have wide shallow minima to facilitate velocity matching for a wide range of wind speeds and result in low sink speeds. The FAR regulations for a gull sized platform resulted in relatively low maximum velocities however, as SUAV platforms do not require the same wing beat power demands as gulls, the aspect ratio can be increased, further reducing mechanical power demand.

Applying the optimised airspeed adjustments on SUAVs requires information regarding the heading trajectory and the wind conditions. Current on-board sensors record airspeed and trajectory heading, however the surrounding wind conditions are not normally measured. There have been recent developments regarding flow sensing in flight, where the wind conditions can be calculated using differential airspeed sensors [77], distributed pressure sensors [139], and estimated by tracking the drift of the vehicle when circling [140]. As these techniques continue to improve, airspeed matching that facilitates energy harvesting may become more common place too. Current energy harvesting methods focus on locating updraughts, however platforms in the future, such those designed for smart cities [141, 142], may need to follow strict trajectories. The methods used by the gulls suggests that energy harvesting can often be achieved without having to deviate significantly from a direct flight path and that by being aware of the wind field that there are considerable opportunities for energy savings when flying in urban environments.

4.5.4 Review of Methods

The GPS loggers were installed by a licensed professional, handling time and visiting the nesting sites was kept to an absolute minimum in order to prevent disturbing natural behaviours. Biometrics of the gulls were taken at the time of capture, due to the fluctuations in body mass due to foraging payloads these biometrics were averaged to generate a single gull model. Individual variations were also compared and differences

between individuals were found to have no significant effect on the performance curves and key velocities. Uncertainty in the spatial measurements were considered and found to make a difference of less than 1% on commutes of 3 km, and as such were not included in the modelling. Altitude measurements by GPS devices were known to harbour the greatest inaccuracy and as such all velocity measurements used the speed calculated by the Doppler shift in the movement of the GPS satellites between signal transmission and reception. Classification of soaring strategies was vital to the investigation and so the classification were validated using three methods. The model part with the greatest level of uncertainty lies in the weather data, the MetOffice UK variable Unified Model forecasting output data has the highest spatial and temporal resolution available but was not at the same fine-scale as the flight trajectories. However, the weather data was validated against strategically placed weather stations and given the number of flight paths, it is probable that inaccuracies at the fine-scale were statistically cancelled. Furthermore, the ANOVA statistical testing accounts for random error in the model. A possible systematic error could have been introduced with the velocity models, however, the glide polar model when compared using alternative aerodynamic characteristics and biometrics was found to have an uncertainty of less than 1%. The power curve model used could introduce a greater level of uncertainty but the main findings in this study indicate that the gulls are likely flying below the minimum power velocity due to taking advantage of environmental energy available for harvesting through soaring. This conclusion is found despite the power curve model selected. Overall, the velocity strategies aligned closely with predictions from the flight models which is a reflection of the effort to keep errors with in data collection and flight modelling to an absolute minimum.

4.6 Conclusions

- Urban gulls demonstrated that there is extensive environmental energy available in the urban environment, as shown by the high percentage of soaring flight during their daily commutes.

- Thermalling is a good strategy in the right conditions, with tracks suggesting that thermals are so numerous in the city that it was not necessary for the birds to use every thermal or deviate significantly from the shortest path.

- The gulls thermal slightly faster than the minimum sink speed, in what may be a trade-off between maximum energy gains and stall avoidance.
- The inter-thermalling velocities of the gulls were not full explained by CoT or StF models which suggests that both energy and time could be drivers in velocity selection.
- High levels of non-flapping flight were performed on days with low thermal availability through the combined use of orographic soaring and gliding.
- The gulls flew at their best glide velocity during orographic soaring, making adjustments to fly faster in head winds and slower in updraughts.
- For gulls flight at minimum power speed in flapping flight is close to the best glide velocity in soaring. This means the gulls can switch easily between flapping and soaring as updraughts are discovered promoting maximum energy harvesting potential.
- Adjusting for headwinds in flapping flight while maintaining a speed close to the best glide velocity requires a mechanical power increase of +6% but could result in energy savings of +31%.
- CoT optimisation is suitable for use in the urban environment and should be considered in the platform design of SUAVs in order to improve flight performance.

CHAPTER 5

PATH PLANNING IN AN URBAN ENVIRONMENT

Birds adjust their flight paths and airspeeds in response to the wind they experience but it is not know to what extend they plan their route based on the weather conditions. Within SUAV path planning there are two extremes; global optimisation, where trajectories are planned with consideration with full knowledge of the map environment, or local, where trajectories are derived using a short planning horizon. This section considers both global and local optimisers for route finding through the same urban environment and wind field as tagged commuting gulls. The simulated and gull trajectories are compared for overall flight performance to determine whether local optimisation can provide significant energy savings for SUAVs. The path planner outperformed the gulls with both optimisation methods and highlighted that both static and dynamic soaring types could be key for energy saving in complex flow conditions. Furthermore, the path planner was used to compare possible cost ratios between powered and soaring flight and found that to perform a higher amount of soaring flight the platform must travel greater distance, this results in a cost of transport for a commuting flight that plateaus as the cost of powered flight increases against soaring flight which could suggest a upper bound to the performance of future SUAV platforms. Finally, the wind speed strength was also compared, as the wind speed increases there was a higher availability of environmental energy however, there was also higher costs of powered flight associated which resulted in faster and more direct routes in the gulls and simulations.

Author Contributions: All methods and analysis were performed by PhD candidate Cara Williamson while under the supervision of Dr Shane Windsor and Dr Arthur Richards.

5.1 Introduction

SUAVs, with so many potential urban roles, accelerating advancements in UAS technology, and continued progression in airspace regulation [25–29], will inevitably become common place in urban environments. However, while their small size and low-altitude capabilities make them so desirable for urban missions, these factors mean that even low-winds can be an issue. The complex flow generated from wind-building interactions varies in speed and direction over short spatial proximities and these variations can often be at the same scale as a platform's airspeed [141]. Currently, urban mission planning uses shortest path routes between way points with some obstacle avoidance and trajectory smoothing guidance control but this can produce energetically sub-optimal routes by not considering the potential cost of flying in unfavourable wind conditions or conversely, potential gains of flying in favourable conditions.

There have been a considerable number of studies which account for wind, either implementing full, *a priori*, wind field knowledge [8, 37, 57, 58, 62] or naive wind fields cases replicating on-board sensing [34, 75, 76, 109] but these are often at a broad-scale with little or no obstacles and do not represent the urban environment. Several works which focused on urban environments have considered the effect of wind conditions in the context of path following or performance [89, 90] with some solutions for wind correction guidance in trajectory following. In one recent study, a minimum energy trajectory path planner was implemented for a quad-rotor in a windy urban environment and reported potential savings of 39.4% [62] in a 2D simulation demonstrating the potential of wind-aware urban planning.

In Chapter 4, 11 LBB gulls were tagged with GPS backpacks and it was found that they were able to exploit the updraughts in the urban environment in order to soar on average 44%, and that this level of soaring could be facilitated by their adaption of flight airspeed to the local wind conditions and by closely matching minimum power and best glide velocities in flapping and soaring flight. Furthermore, that these flight adaptions could be reducing their energy expenditure by 31% compared to flapping at the maximum range velocity. In this chapter, a dynamics model based on the aerodynamic characteristics of a gull is implemented in a wind-aware urban path planner with flapping and soaring flight modes. The velocity optimisation from Chapter 4 is included and the performance of the simulated trajectories is compared against 27 of the commuting gull flights. The wind fields are generated in QUIC-URB [103] and represented a static estimation of the conditions at the time of flight.

While velocity optimisation performed by the gulls in Chapter 4 was implemented at a local level their commuting routes varied depending on the weather conditions. This feature could suggest some level of forward planning navigation and is further supported by the results of Chapter 3, where it was seen that on days with the right conditions more gulls commuted along the front of the bay in order to exploit the available updraught. As such, the path planner in this chapter will compare two algorithms, the A* and a Depth First Search (DFS) [143–146]. The DFS will use a 1 node branch (10 meter) horizon expansion whereas the A* will use a frontier expansion. In this way the DFS acts locally, reacting to make the next best move whereas the A* selects a path having explored a much higher percentage of the total map, up to a fully global knowledge of the map, if required. A comparison of these two extremes may offer some insight into the level of navigational strategy employed by the gulls. Both algorithms have potential within SUAV navigation, for example, a global solution is suitable for pre-mission planning or in the development of urban air-way routes, whereas a local optimiser could improve on-board navigation during active flight where the platform may need to react to changing wind conditions. The algorithms will optimise for the minimum cost trajectories and the cost function will be made of two parts. Firstly, an energetic cost to describe the path travelled and secondly, a distance-to-goal heuristic in order to ensure that the trajectories provide a route to the goal. Two heuristic cases will be compared, an ideal cases which supports a quasi-global solution and a greedy case which is often implemented to improve solve time for real-world application [144, 147].

It is expected that the A* algorithm & ideal heuristic combination will generate more efficient and cheaper routes than the gulls. This is due to the path planner having *a priori* static wind field compared to the imperfect wind-sensing and hard to predict temporal-variance associated with real-world navigation. Additionally, other reward drivers which may influence the gulls such as social interactions are unaccounted for. It is expected that the DFS algorithm & greedy heuristic combination will produce comparably efficient routes to the gulls, if a solution can be found. If the simulation is found to perform better it could suggest that gulls optimise using additional drivers such as expanding search range even in commutes, as well as indicating the failures to account for uncertainties that occur in simulation based modelling such as a lack of complex turbulence factors. The two extremes of combinations will be referred to as global and local cases, where the global case is the A* algorithm & ideal heuristic combination and the local is the DFS algorithm & greedy heuristic combination. However, it should be noted that the *"global"* case can only be considered as quasi-global where the global

refers to the map knowledge and cannot be considered the true global solution due to a two stage optimisation procedure. The use of the inner velocity optimisation loop creates a constraint on a optimisable state where the global solution may be to operate outside of the Cost of Transport optimum.

The morphology and aerodynamic characteristics between a gull and a small fixed-wing platform may be quite similar but the cost ratio between power requirements in powered and unpowered flight are quite different. The cost of flapping and soaring flights in birds is often considered as a multiple of the Basal Metabolic Rate, BMR, or rate of energy used at rest. In the same way SUAV platforms have a minimum current that must be continuously drawn in order to maintain any communication links (GPS, video-feed, etc.), this can vary platform to platform based mission requirements. Furthermore, variations in the size, geometry, motor performance, airspeed, etc. of a SUAV will dictate the current drawn while in powered flight. As such, the cost ratio will be varied while maintaining the model dynamics and assumption that powered flight will only occur when it is not possible to soar or glide obeying the velocity optimisation algorithm. The optimum velocity for soaring flight is slower than for powered (or flapping) flight, while soaring has a lower cost the flight time will increase, this could result in a limit to the possible energy savings of implementing soaring flight, although it is unknown if this will be apparent in the results. Due to prevailing wind conditions, the commuting flight groups mainly occurred at the similar wind directions (μ = 222 °, σ = 77 °) over a range of wind speeds (μ = 5.94 m s^{-1}, σ = 2.43 m s^{-1}) meaning that it is possible to consider the effect of wind speed on the cost of flight. The wind speeds could greatly effect the cost of flight, for example, a headwind would result in a higher cost, either through an increase in flight time or due to a increase in airspeed to ensure progress is made. However, higher wind speeds could also facilitate more energy harvesting, although in previous Chapters 3 and 4 the gulls used only a narrow band of their airspeed range and did not utilise the maximum updraughts available.

In summary, this Chapter aims to explore the energy saving potential of a wind-aware path planner for SUAVs with soaring capability flying in urban environments. This is achieved by comparing two path planners with map knowledge extremes modified to incorporate a bio-inspired velocity optimisation algorithm based on CoT theory which was found to match the airspeed selection of urban flying gulls. A cost function directly based on flight dynamics and the BMR ratios of flapping and soaring flight creates the basis of the energy based optimisation within these two algorithms furthering the bio-inspired

element of design. The comparison of the two algorithms aims to highlight the level of on-board computation required during navigation for SUAV technology and also to offer some insight to the extent at which gulls may pre-plan commuting routes. Furthermore, the BMR ratios within the cost function will be varied in order to determine whether energy savings are being made in the gulls' commute and what level of energy savings may be available for SUAV platforms due to their higher comparative powered flight costs. Finally, a range of wind speeds are tested to determine whether there is an effect on the level of environmental energy that can be harvested.

5.2 Methods

This section contains the methods for this Chapter, it will start with a section describing the the flight modelling in Section 5.2.1 summarising the gull inspired velocity optimisation algorithm, the flight dynamics and an energy based cost function. Next the commuting gulls flights will be introduce in Section 5.2.2, followed by the flight performance measures used to compare the gull and simulated trajectories in Section 5.2.3. This is followed by the methods used to map the environment in section 5.2.4 which outlines the wind models with weather validation, description of the 4 Dimension node space and the obstacle integration. Finally, the two path planning algorithms and heuristic costs will be outlined in Section 5.2.5.

5.2.1 Flight modelling

5.2.1.1 Performance Curves

The average LBB gull bird model detailed in Chapter 4 was used again here. It was previously shown that the air speed of urban gulls could be modelled using CoT optimisation theory. The air speed was calculated using minimum power velocity for flapping flight and best glide velocity in low-altitude gliding and orographic soaring flight modes. Performance curves generated for the average tagged LBB gull will be used for the path planner simulations for a fair comparison with the gull flights.

5.2.1.2 Velocity optimization

The optimum airspeed was calculated using CoT optimization algorithm developed by shifting the performance curves with the relative wind direction. In this case, it was assumed that trajectory following occurred and by using a spatially defined node space

the trajectory is also known in this case. Additionally, the wind speed and direction of the nodes is known in the *a priori* wind field case. The algorithm proceeds in the following step sequence and is defined in more detail along with equations in Section 4.2.3:

Algorithm 2 Optimise airspeed velocity

function OPTIMISE AIRSPEED VELOCITY($GP, \phi_i, W, \theta_w, U_{bg}$) ▷ Where U_a - opt. airspeed, β_a - opt. relative wind angle. Optimise airspeed based on a fixed trajectory and wind conditions
  $U_{opt}(i) = U_{bg}$ ▷ Start algorithm using best glide velocity
  $V = U_{bg}$ ▷ Set initial ground speed to best glide velocity
  $i = 0$
  while $e > 0.1$ & $i < 100$ **do** ▷ Loop until error margin is met or number of iterations exceeds 100
    $i = i + 1$
    $\beta_i = \arcsin(W/V)\sin(\theta_w - \phi_i)$ ▷ Calculate the inertial relative wind angle
    $\beta_a = 180 - ((\theta_w - \phi_i) + \beta_i)$ ▷ Calculate the air relative wind angle
    $W_{a_h} = W\cos\beta_a$ ▷ Find the air relative headwind
    $GP_s[:,1] = GP[:,1] + W_{a_h}$ ▷ Shift the glide polar using the air relative headwind
    $GP_s[:,2] = GP[:,2] + W_z$ ▷ Shift the glide polar using vertical wind *(optional)*
    $idx = max(GP_s[:,1]/GP_s[:,2])$ ▷ Index location of the new lift to drag maximum
    $U_{opt}(i+1) = GP_s[idx,1]$ ▷ Optimised airspeed
    $e = |U_{opt}(i+1) - U_{opt}(i)|$ ▷ Calculate the error margin
    $V = \sqrt{(U_{opt}(i+1)^2 + W^2 - 2U_{opt}(i+1)W\cos\beta_a)}$ ▷ Calculate new ground speed
  end while
end function

The ground vector and wind conditions are kept constant and the optimum airspeed, air relative heading, experience headwind/side wind and ground speeds are calculated based on the curve shifting technique described in 4.2.2. The velocity algorithm implements CoT characteristics such that the air speed is adapted as follows:

- Fly faster in unfavourable conditions - (downdraughts/headwinds/crosswinds perpendicular to the ground speed)
- Fly slower in favourable conditions - (updraughts/tailwinds/sidewind perpendicular to the airspeed)

5.2.1.3 Flight envelope

The model is able to make velocity optimisations within the flight envelope range. This range extends from the stall speed through to the never exceed velocity. The stall speed was calculated using the equation 5.1, stall is considered the point at which flow separates over the wing when in gliding flight however, this was also considered the minimum velocity in flapping flight mode, at 6.3 m s^{-1}. The upper velocity range was calculated by considering the equivalent wing loading limits based on the FAR 23.333 regulations

used for determine wing loading and structural limitations for small platforms [138], a 3.8 g load factor and was calculated using equation 5.5 to be 20.3 m s^{-1}. The proposed velocity envelope can be seen in Fig 4.16 from the previous Chapter.

$$U_{stall} = \sqrt{\frac{2mg}{C_{l_{max}} \rho S}} \tag{5.1}$$

Where U_{stall} is the stall speed, m is the body mass, g is the gravitational constant, $C_{l_{max}}$ is the max lift coefficient, ρ is the air density and S is the wing surface area.

$$U_a = U_{stall} \sqrt{3.8} \tag{5.2}$$

Where U_a is the FAR recommended manoeuvre speed. Where turns above this airspeed may generate a force greater than an aircraft's structural limitations.

$$U_c = 4.77 \sqrt{\frac{mg}{S}} \tag{5.3}$$

Where U_c is the FAR recommended maximum cruise speed in order to comply with additional forces associated with gusting.

$$U_d = 1.4 U_c \tag{5.4}$$

Where U_d is the dive speed, rather an unintuitive name, is not held for dive manoeuvres but, is the maximum velocity flown at in an extreme dive during aircraft testing.

$$U_{ne} = 0.9 U_d \tag{5.5}$$

Where U_{ne} is the FAR recommended never exceed speed, which is the upper limit of platform airspeed, held for only the most extreme cases.

The velocity optimisation stage of the algorithm dictates that the airspeed must be higher that the still air range optimum in a head wind and lower in a tail wind but also caps the optimisation by the velocity envelope where the stall speed is the lower limit and the never exceed velocity is the upper limit. These limitations are suggested by the aerodynamics (stall speed) and potential structural limits (never exceed speed) and while the FAR regulations are for an aircraft it stands to reason that a bird will also have an upper velocity limit, from Fig 4.16 it stands to reason that the flight envelope is comparable to the airspeeds at which the birds are flying. The flight envelope may appear to be restrictive of the velocity optimisation but within the simulations presented

here the stall and never exceed airspeeds were selected only 0.21% and 1.06% of the total number of optimisation cycles demonstrating that the velocity envelope rarely limits the CoT optimum.

5.2.1.4 Dynamics equations

There are multiple possible derivations of 6 degrees of freedom flight dynamics equations but this study will use the derivations as described by Lawrance. The main features of this are presented here and further detail can be found in [8]. For simplicity, the flying body has been modelled as a point mass such that no control surface dynamics or any forces generated by side slip are considered. While this is not representative of a real-world SUAV model, it could be considered more representative of a body with morphing wing capability such as the gull.

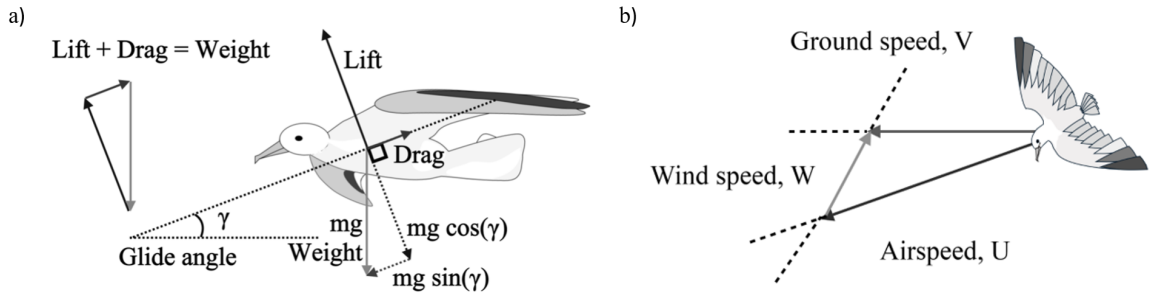

Figure 5.1: a) The lift, drag, and weight forces are shown acting on a bird b) the velocity vector for airspeed, wind speed and ground speed.

The aerodynamic forces, lift, drag and weight, and the velocity vectors, airspeed, ground speed and wind speed, are described in Fig 5.1. The air-relative heading and climb angle are described as the angles between the inertial frame platform heading and climb angle and the air speed vector. The airspeed vector is described by equation 5.6 where the relationship between ground, wind and air vectors is described in equation 5.7. The subscripts a and i denote the air and inertial frames, γ is the climb angle and ϕ is the heading angle.

$$\vec{U} = |U| \begin{bmatrix} cos(\gamma_a)cos(\phi_a) \\ cos(\gamma_a)sin(\phi_a) \\ -sin(\gamma_a) \end{bmatrix} \tag{5.6}$$

$$U = V - W \tag{5.7}$$

Lawrance derives the air relative specific power, $\frac{\dot{E}_a}{m}$, as a combination of three factors describing the power required to overcome the drag force, the power available when soaring in static sources such as updraughts, W_z, and the power available due to motion through the wind gradients, $\mathbf{J_w}$.

$$\frac{\dot{E}_a}{m} = -\overbrace{U\frac{D}{m}}^{\text{Drag}} - \overbrace{gW_z}^{\text{Static}} - \overbrace{U\begin{bmatrix} cos(\gamma_a)cos(\phi_a) \\ cos(\gamma_a)sin(\phi_a) \\ -sin(\gamma_a) \end{bmatrix}^T \mathbf{J_w}\dot{\mathbf{P}}}^{\text{Gradient}} \tag{5.8}$$

Where D is the drag, U is the airspeed, and $\dot{\mathbf{P}}$ is the inertial displacement rate vector.

In this case the drag differs from the Lawrance model, here the drag from the Pennycuick model [16] are used. Where drag in flapping flight is described by equation 5.9 and the drag in soaring flight is described by equation 5.10. Where $D_{flap,soar}$ is the drag force produced in flapping or soaring flight, $k_{f,s}$ is the induced power factor in flapping or soaring flight, m is the body mass, U is the airspeed, g is the gravitation constant, ρ is the air density, b is the wing span, $S_{b,w}$ is the surface area of the body or wing, $c_{D_{b,w}}$ is the drag coefficient of the body or wing, AR is the wing aspect ratio and finally, c_{pro} is the profile power coefficient based which varies per bird species and is closely related to the aspect ratio.

$$D_{flap} = \overbrace{\frac{2k_f m^2 g^2}{\pi\rho b^2 U^2}}^{\text{Induced}} + \overbrace{\tfrac{1}{2}\rho U c_{D_b} S_b}^{\text{Parasitic}} + \overbrace{\frac{1.05 c_{pro} k_f^{\frac{7}{4}} m g^{\frac{3}{2}} S_b c_{D_b}^{\frac{1}{4}}}{U\rho^{\frac{1}{4}} b^{\frac{3}{2}} AR}}^{\text{Profile}} \tag{5.9}$$

$$D_{soar} = \overbrace{\frac{2k_s m^2 g^2}{\pi\rho b^2 U^2}}^{\text{Induced}} + \overbrace{\tfrac{1}{2}\rho U^2 c_{D_b} S_b}^{\text{Parasitic}} + \overbrace{\tfrac{1}{2}\rho U^2 c_{D_w} S_w}^{\text{Profile}} \tag{5.10}$$

This study uses fixed spatial distances and as such considers the possible motion firstly in the inertial frame then generates the corresponding air-relative values. The wind gradient Jacobian describes the change in wind velocity in the corresponding world-frame directions and was calculated using a bespoke function applying one-direction differencing at the model walls such as at obstacle boundaries. The air relative power

is then used to calculate the energetic cost or gain of moving to the corresponding neighbour.

5.2.2 Gull flights

The commuting flight data set from the previous Chapter was filtered further for flights that contained only high resolution data (considered 1 fix per every 6 seconds or better), and on overcast days in order to primarily select flights where little or no thermalling occurred. This was due to the lack of a thermal model in the QUIC software. For this reason, the filtered flights had predominately low mean altitudes in the range of (15 - 86 m AGL) and contained a mixture of flapping, mixed, gliding and orographic soaring flight modes. To make flights comparable, commutes which were repeated several times and were to or from proximal locations were selected. This gave four main commuting groups, show in Table 5.1, over a range of wind speeds, and with some variation in wind direction.

The flights analysed mainly consisted of inbound commutes due to the GPS capture rate trigger set with spatial fencing around the nest (described in Section 4.3.2), it is presumed the return journey is after a successful foraging trip however, there has been no adjustment of the body mass to account for this. Three outbound flights remained in the dataset due to the directness and energy savings consistency with the rest of the data set. The range and duration of all flights were also comparable and will be compared as a full set. Due to the specialized foraging nature of the gulls, it is often not possible to compare the flights of more than one individual, however, each flight group contains repeated commutes from the same individual so it is assumed that differences in the flights are based on the flow conditions of the day.

Table 5.1: Selected gull flights

Flight ID	Gull ID	Wind speed (m s^{-1})	Wind direction (deg)	Time ratio	Distance ratio	Flap (%)	Soar (%)	Mixed (%)	Energy ratio	Flight Direction
A: Northway waste transfer centre										
B: Arts and Social Science Library Nest										
7	5308	7.72	261.03	1.49	1.39	37.2	27.4	35.4	0.82	A → B
6	5309	8.51	252.02	1.43	1.39	28.8	16.3	54.9	0.71	A → B
5	5309	8.34	253.53	1.34	1.34	47.2	15.9	37.0	0.83	A → B
4	5309	8.42	252.64	1.45	1.41	25.5	20.4	53.5	0.68	A → B
3	5309	8.13	258.42	2.04	1.90	20.1	47.3	32.2	0.88	A → B
2	5309	6.16	56.46	2.81	1.89	27.0	28.4	44.3	1.34	B → A
1	5309	2.57	47.97	2.22	1.44	60.3	8.3	31.5	1.59	B → A
A: Abbeywood MOD										
B: Arts and Social Science Library Nest										
27	5308	1.15	42.86	1.60	1.65	16.6	65.8	17.1	0.65	A → B
26	5308	4.79	251.32	1.44	1.49	68.4	22.1	8.9	1.11	A → B
24	5308	3.73	232.32	1.60	1.49	45.3	26.8	27.4	0.97	A → B
23	5308	6.52	263.73	1.57	1.51	35.1	34.4	29.4	0.84	A → B
22	5308	6.83	259.29	1.84	1.69	26.5	48.9	24.6	0.88	A → B
21	5308	7.18	271.23	2.16	1.94	20.0	44.1	35.9	0.92	A → B
25	5308	3.87	253.77	1.68	1.71	37.8	43.3	18.9	0.94	A → B
A: Gainsborough Square										
B: dBs Music College Nest										
15	5481	11.37	267.10	1.55	1.45	28.2	6.1	64.9	0.75	A → B
14	5481	6.97	254.00	2.34	1.47	8.2	52.8	39.0	0.80	A → B
10	5481	5.27	116.01	1.58	1.42	50.3	34.3	15.4	1.01	A → B
9	5481	3.96	191.26	1.77	1.68	57.7	23.4	17.7	1.24	A → B
12	5481	7.83	250.13	1.46	1.52	17.4	19.7	62.9	0.60	A → B
16	5481	3.46	263.89	2.59	2.47	41.4	37.9	20.7	1.51	A → B
11	5481	3.4	215.15	4.49	1.99	12.7	76.6	10.5	1.80	A → B
8	5481	4.15	150.00	2.05	1.42	16.8	78.3	4.9	0.83	A → B
17	5481	2.86	289.94	2.66	1.91	65.3	27.1	7.6	2.00	B → A
13	5481	6.45	261.97	2.86	1.68	6.9	61.3	31.8	0.95	A → B
A: Abbeywood MOD										
B: dBs Music College Nest										
19	5481	9.53	254.93	1.52	1.63	21.2	31.0	47.2	0.67	A → B
20	5481	4.18	290.01	1.41	1.39	68.9	22.6	6.2	1.10	A → B
18	5481	6.85	259.00	2.14	1.37	27.2	20.7	51.6	1.03	A → B

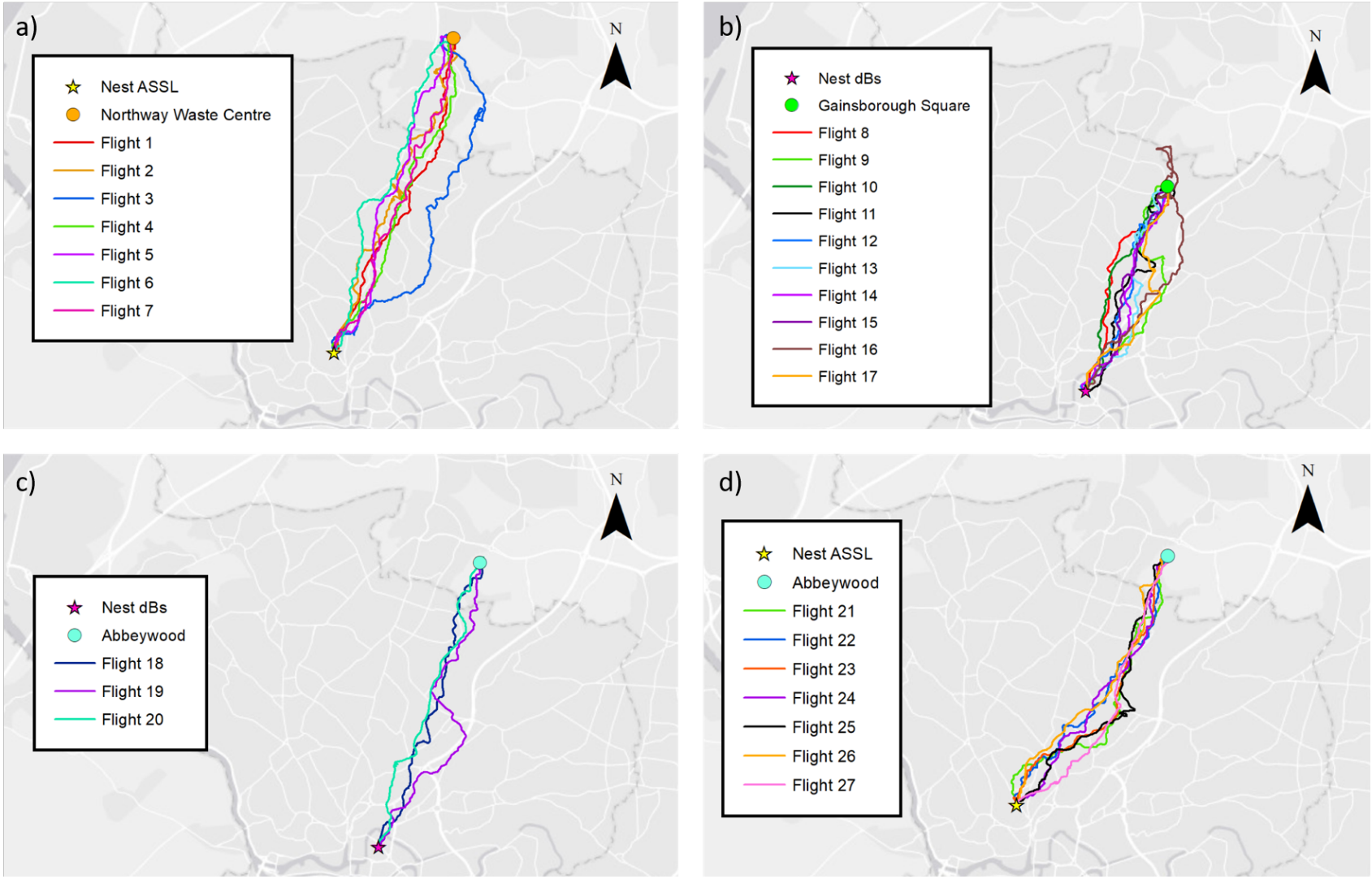

Figure 5.2: The four commute groups as described in Table 5.1 selected for simulation, each GPS fix is shown by the coloured marker and each colour represents a unique flight.

5.2.3 Flight performance measures

The flight performance of the commutes were measured against the equivalent shortest path using only flapping flight with an airspeed that is adjusted for the wind conditions. The performance measures fall into four categories; time, distance, energy and percentage of soaring flight. These measures were also used for the path planner and allow for a direct comparison between the simulations and gull flights. The time and distance measures were calculated using the flight data and normalised by the modelled shortest path data for each unique start and end location. As the wind conditions are a heavy influence on the flight speeds of the gulls, the airspeeds for the shortest path flights were calculated using velocity model 1 from Section 4.2.4. In model 1 the airspeed in flapping flight is adjusted for head- and tail-winds focused around the minimum power velocity.

The distance based measure, referred to as the distance ratio, was generated using equation 5.11:

$$\frac{r_{flight}}{r_{shortestpath}} \tag{5.11}$$

The time based measure, otherwise referred to as the time ratio, was calculated using equation 5.12:

$$\frac{\tau_{flight}}{\tau_{shortestpath}} \tag{5.12}$$

Where,

$$\tau_{shortestpath} = \frac{r_{shortestpath}}{V_{flapoptimsed}} \tag{5.13}$$

Where the amount of flapping or soaring behaviours were calculated using a time based method in both gull and path planner cases and shown as percentages:

$$B_{flap,soar} = (\frac{\tau_{flap,soar}}{\tau_{flight}}) \tag{5.14}$$

As this research is focused on finding flight strategies which have the potential to conserve energy, the flights were tested against flying the most direct line between the start and end locations whilst flying at the minimum power velocity and used the Basal Metabolic Rate (BMR) ratios taken from wind tunnel studies of gliding [148] and flapping [149] comparable species of gull. Gliding flight was found to be twice as expensive as the resting BMR and flapping flight was found to be seven times the resting BMR. In some

studies a summed value of the acceleration data is used as a proxy for the effort of the body and so energetic cost. This is referred to as the Overall Dynamic Body Acceleration (ODBA). An updated version, Vectorial Body Acceleration (VeDBA), also filters out the low frequency signals thought to be associated with the trajectory or motion of the medium, rather than motion due to the effort of the body. The gulls' recorded VeDBA and ODBA measurements were compared across different flight behaviours and airspeeds. There was an obvious difference between flight behaviours but there was no discernable difference discovered across a range of different airspeeds, neither linear nor parabolic centred around a minimum. The ratio between flapping and soaring flight for the ODBA and VeDBA was found to be 3.9 and 3.15 respectively, as these values lie either side of the BMR cost ratios at 3.5, it was decided to use the BMR cost ratio. Mixed flight behaviour was considered to be low cost and re-classed as soaring behaviour when calculating the soaring percentages as the mixed behaviour type contains a range of possible events including but not limited to single flaps, manoeuvres such as banking, and body reactions to gusts in soar. Flights which cost less than flying the most direct path were considered to have made energy savings. The energy savings ratios were calculated using equations 5.15 - 5.20, where the ground speed for each of the shortest path comparisons was calculated using the velocity optimisation algorithm which adjusted for the wind conditions.

The cost of a flight, C_{flight}, was considered a summation of the power cost for each flight behaviour, $P_{flap,soar}$, multiplied by the time spent in that flight behaviour, $\tau_{flap,soar}$.

$$C_{flight} = P_{BMR_{flap}} \tau_{flap} + P_{BMR_{soar}} \tau_{soar} \tag{5.15}$$

The cost of the shortest path flight, $C_{shortestpath}$, is calculated using the power ratio of flapping flight and the time to fly the shortest path flight.

$$C_{shortestpath} = P_{BMR_{flap}} \tau_{shortestpath} \tag{5.16}$$

Where shortest path flight time is,

$$\tau_{shortestpath} = r_{shortestpath} U_{mp} \tag{5.17}$$

And the fraction of soaring and flapping flight always adds to one.

$$B_{soar} + B_{flap} = 1 \tag{5.18}$$

Equations 5.15 - 5.18 and can be combined and rearranged to solve for the axes in 5.3 where percentage of soaring flight is a function of the distance ratio.

$$B_s = \frac{(-P_{BMR_{flap}} U_{mp} - P_{BMR_{flap}} U_{mp} \frac{r_{flight}}{r_{shortestpath}})}{P_{BMR_{flap}} U_{mp} \frac{r_{flight}}{r_{shortestpath}} - P_{BMR_{soar}} U_{bg} \frac{r_{flight}}{r_{shortestpath}}} \tag{5.19}$$

Energy savings can be considered as the ratio of the cost of the flight normalised by the cost of the shortest path flight. Where a flight using more energy than the shortest path has a value greater than 1.

$$\frac{C_{flight}}{C_{shortestpath}} \tag{5.20}$$

The graphical representation for the energy savings region depicted in 5.3 assumes flight in still air. The energy savings region, is the area above the dashed line, while not fully due to the still air assumption it represents a performance measurement which can be used to compare all flights.

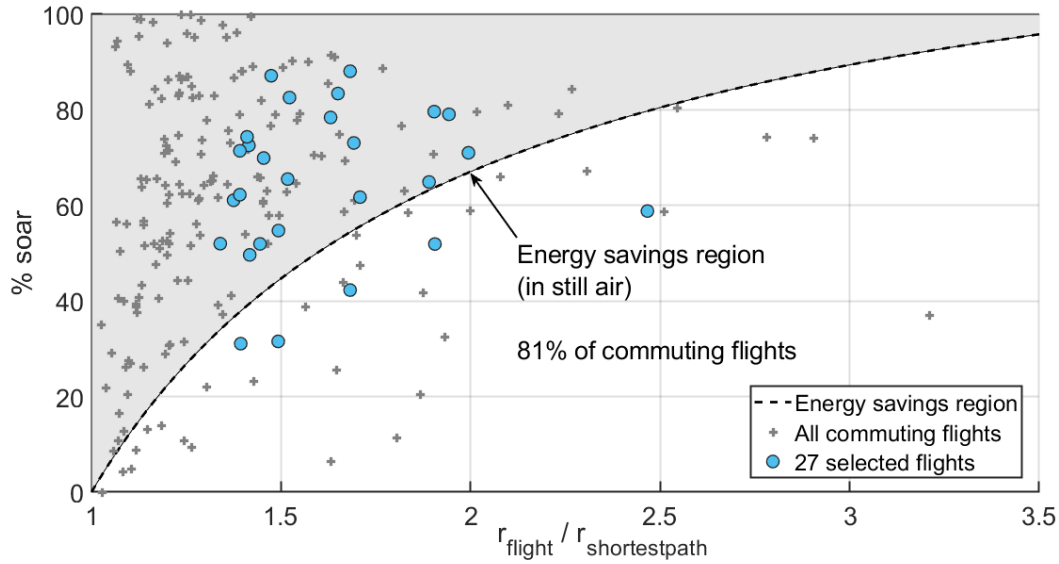

Figure 5.3: The energy savings region demonstrates the percentage of soaring flight required to fly the increased flight distance compared to the shortest path. The commuting flight dataset from the previous chapter (192 flights) is shown with the plus markers and the 27 selected flights for the simulation comparison are shown in blue.

As seen in the previous chapter, the wind conditions effect the airspeed that should be selected. Increasing or decreasing speed away from the minimum power velocity in flapping flight requires an increase in power. To account for the increased power

requirement the power ratio for powered flight was multiplied by a power factor, k_p, such that the power adjusted cost of flight, C_{pp}, is calculated as:

$$C_{pp} = k_p P_{BMR_{flap}} \tau_{flap} + P_{BMR_{soar}} \tau_{soar} \tag{5.21}$$

Where the power factor, k_p, is calculated as the increase away from the minimum power velocity, as shown in Fig 5.4.

$$k_p = \frac{P_{mech_{opt}}}{P_{mech_{mp}}} \tag{5.22}$$

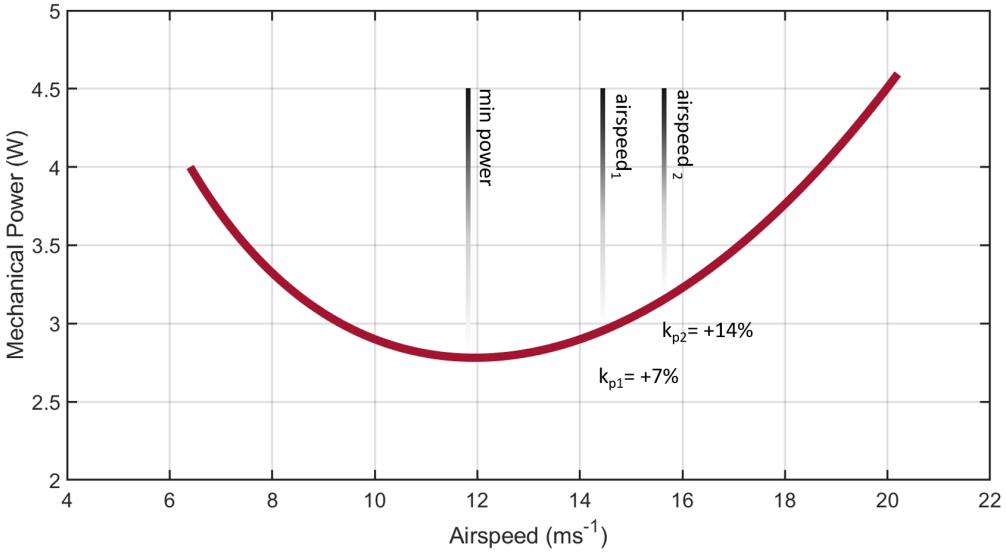

Figure 5.4: Faster airspeeds require more power, this increase in power is considered the power factor and is used to increase the BMR power ratio for flapping flight. The power curve is shown in red with the minimum power velocity and two example airspeeds and power factors.

The energy required to fly to the goal was considered in two ways due to the occasional disparity in flight directness between the gulls and simulations. The total energy was normalised by the shortest path distance to goal to create the cost of transport, CoT_{AB}, or by the total flown distance, CoT_{flown}.

5.2.4 Mapping the environment

The environment mapping used a large section of the Bristol urban landscape, 8.5 (L) x 5 (W) x 0.3 (H) km, which encompassed all of the selected flights and an extended area to

account for boundary layer flow, this area was used to generate the QUIC wind models. A reduced section of the mapped area was used for the path planner simulations, 8.14 x 3.16 x 0.1 km.

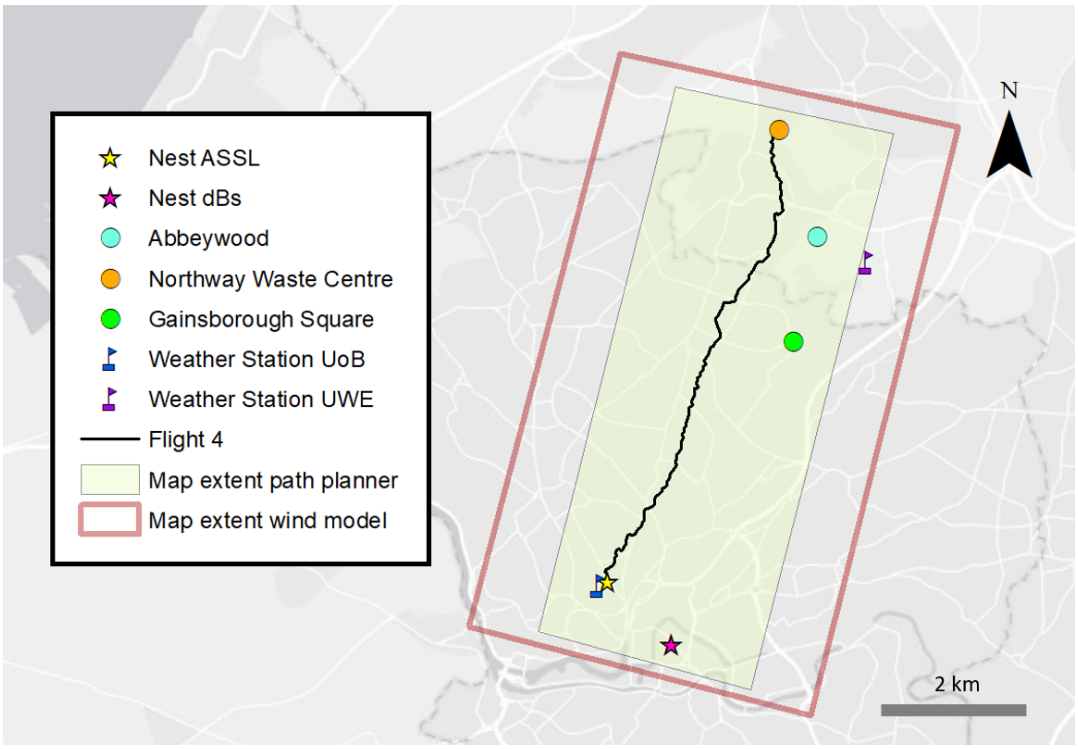

Figure 5.5: Map of wind model (red) and path planner (green fill) extent with nest markers shown by the star markers with ASSL [51.459610°, -2.601616°] in yellow and dBs [51.451567°, -2.588421°] in pink. The foraging locations are shown by the circular markers, where Abbeywood [51.503877°, -2.558377°] is cyan, Northway [51.517490°, -2.566222°] is orange and Gainsborough Square [51.490429°, -2.563377°] is green. The two weather station are marked on the map by the flags where the UoB weather station [51.459145°, -2.603555°] is shown in blue and the UWE weather station [51.500583°, -2.548134°] is shown in purple. Gull flight 4 from Northway to the ASSL nest is marked with the black line.

The environment layers consisted of a 2 metre resolution digital elevation model containing the terrain data [96], DTM, a vector based topography layer taken from [97] containing building footprints, a building height layer was joined to the topography layer using ArcGIS v10.1. The DTM and topography layers were converted into QUIC compatible file formats using the conversion process described in Section 3.2.2.

The experiment area in Bristol has a variable landscape elevation where regions can differ by greater than 100 metre. One of the largest variations and steepest gradients occurs between the two nest sites. The current QUIC model, as described in Section

3.2.2.3, does not calculate the contribution to orographic updraught from terrain based features and as such, it was decided to consider broad-scale flight performance between the gull and simulation flights, over fine-scale details based on the wind models.

5.2.4.1 Wind models

Wind models for the 27 selected commuting flight were generated with QUIC software using a 64 bit desktop computer with a 16 core 3.7 GHz CPU with 64 GB RAM. The high RAM and processing capacity allowed a model size of 25.93 million cells with 22,000 buildings compared to a recommended maximum of 10 million cells, or 1-2 million for quick field-site operations, by the QUIC program creators [1]. The wind models were run in batch production mode with 10 models at a time, where custom wind profile input files were written based on the MetOffice forecasted predications for the conditions at flight start. Wind profiles were generated using the geo-potential heights output by the MetOffice forecasting model. Solve times were extensive, even with the use of the QUIC-URB model, chosen for it's reduced run time compared to the full QUIC-CFD model as used in 3.2.2. The solve times often ran to more than 36-48 hours per model batch [2] due to the high combined number of buildings and cells. The high cell count in the models was well outside of the program design specification but this should of had no effect on the accuracy of the models, and the validation seems to support this notion, see Figs 5.7 and 5.6. The wind models were further sub-sampled to be used in the path planner, the smaller area, marked on Fig 5.5, of size 3.16 x 8.14 km and height of 100 m, with a cell size of 10 x 10 x 1 m, and total node count of 25.98 million using the inbuilt interpolation functions within MATLAB.

5.2.4.2 Wind model validation

The MetOffice forecasting model used for generating the 27 custom wind profile input files for QUIC wind field generator was validated over a two week period [3] by comparing the forecast predictions with the data collected by weather stations in two locations Fig 5.5. Three of the wind models generated by QUIC fall into the same two week period and were used to validate the QUIC wind field outputs. The wind model data were sampled at the locations of both weather stations for comparison, see Figs 5.7 and 5.6.

[1] Discussed via email
[2] Observational, not recorded
[3] See Section 4.3.5

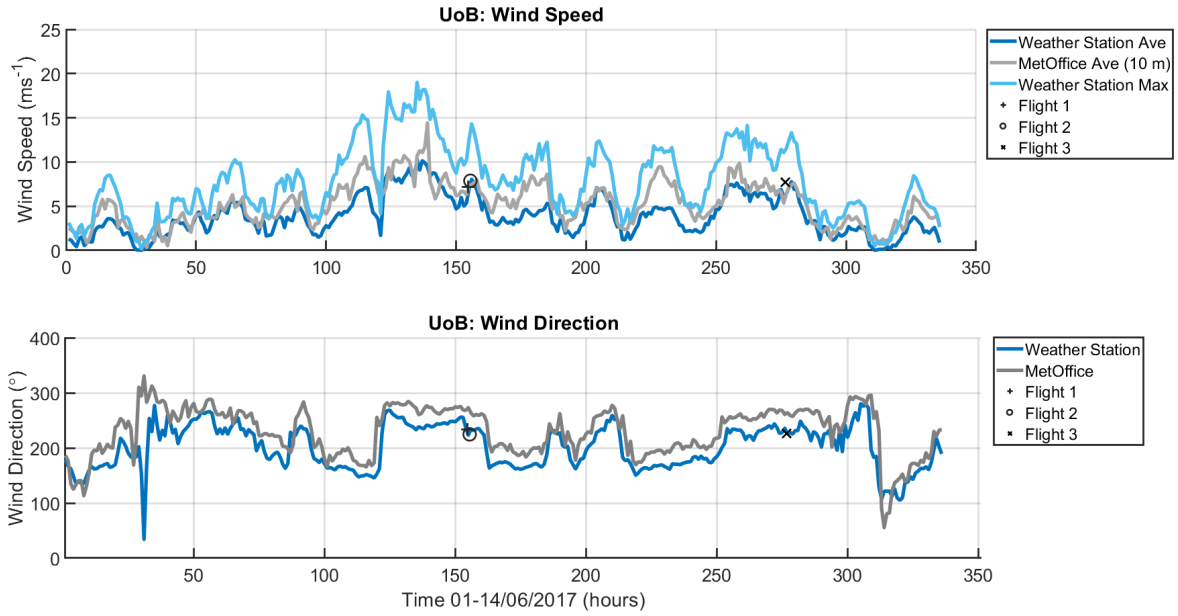

Figure 5.6: Coloured lines represent the data from the Met office forecasting model and the weather station located at [51.459145°, -2.603555°] over the 2 week period 01-14/06/2017. The markers show the QUIC wind field sampled at the same location. There is an extremely close match for both a) wind speed and b) wind direction.

5.2.4.3 4D node space

The node space for the path planner is considered in 4 dimensions. It was decided that the algorithm should be restricted to only move in directions representative of forward flight so in order to allow the algorithm to visit every possible space on the map, without obstacles, a heading dimension was added. This allowed the algorithm to visit every space on the map from eight different directions. The 3 spatial dimensions have equal horizontal directions, where spacing resolution was either dx=dy=10m or dx=dy=20m, and a consistent climb angle of $\gamma_i = 5.7°$ such that $\frac{dz}{dx,y} = 0.1$, equivalent to dz=1m or dz=2m, for the 10 and 20 meter horizontal resolutions respectively. The direction based dimension uses a consistent heading step change of $\phi_i = 45°$ such that there are 8 possible directions with which a space on the map be entered. For the 10 meter resolution map, there are 317 x 815 x 101 x 8 nodes (208.8 million) in total. Each node has 9 neighbours consistent with forward flight and a heading range of ±45° and a climb range of ±5.7°, resulting in a total node-branch combination of 1,897.4 million and 242.9 million at the 10 m and 20 m grid resolutions respectively.

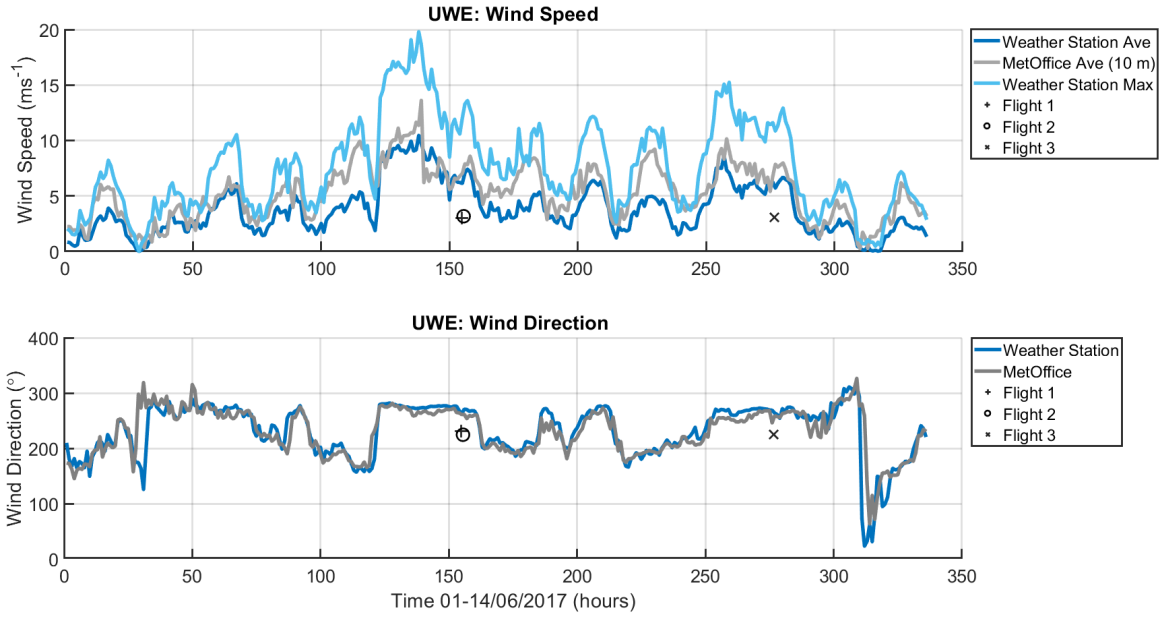

Figure 5.7: Coloured lines represent the data from the Met office forecasting model and the weather station located at [51.500583°, -2.548134°] over the 2 week period 01-14/06/2017. The markers show the QUIC wind field sampled at the same location. The QUIC model underestimates a) wind speed quite significantly but has a close estimation for b) wind direction.

Using a direction dimension has the advantage of allowing a space in the map to be revisited from a different direction. This solves this problem of non-global optimisation while restricting flight direction by allowing all spatial areas of the map to be fully explored and provided the additional benefit of allowing circling behaviour to occur.

5.2.4.4 Adding the buildings

The buildings were considered as inaccessible space on the map and therefore treated as closed nodes. Each node was considered as filling the maximum spatial volume of the node extent, for example, 10 m x 10 m x 1 m, centred at the node location. The building volume was calculated using the topography blue-prints and building height with an additional minimum distance from the building of 2 m. The reduced map building data set contained 13,418 individual buildings, these were converted into nodes using MATLAB's inbuilt volume union function with a tolerance of 50%. Nodes which overlap at greater than 50% or create a barrier between two nodes were added to the closed node list. This results in a slightly reduction in the branch exploration size of just under 1%.

In the cases where flights start and/or end on a building, such as in the case of landing at the nest, these closed nodes (accounting for each available branch direction) were re-opened allowing take-off and landing.

5.2.5 Path planning

This section outlines the algorithm and heuristics used in the simulations. Two cases for both algorithm and heuristic costing are considered to explore the navigational efforts of the gulls and understand the best options for SUAV flight.

5.2.5.1 Algorithms

The A* algorithm is considered the best performing path planner for a full *a priori* environment keeping totals on every visited node and always expanding the nodes with the lowest total cost. This algorithm provides the cheapest global option from start to end location for the given flow conditions. The comparative algorithm, will be a Depth First Search considering only the best performing option in each new child set. This represents a fully reactionary process, with a minimal planning horizon (in this case a step of 1), always choosing the next best move to reach the goal and means that it is possible for the DFS algorithm to perform sub-optimally. Becoming trapped in a local minima is particularly relevant in for motion through a rugged landscape such as is provided by the complex urban wind field being investigated here. While this sub-optimal performance is considered problematic in optimisation theory it could be a satisfactory representation of animal behaviour making it a fitting choice for comparison with commuting gulls.

The algorithms both use a closed list and an open list. The open lists contained all the expansion frontier nodes which are waiting to be expanded. The closed lists contained nodes which cannot be expanded and any node previously searched. The lists were created as logic column vectors, with an additional identifier list containing an index pointer to the node index.

The A* algorithm uses an expanding frontier and requires storing knowledge of pre-visited nodes whereas the DFS algorithm selects the cheapest child of each newly expanded node. Each expansion cycle took a maximum of 0.004 seconds (this included the integrated velocity optimization cycle and frontier sorting), meaning that complete map exploration could take up to 3,040 hours (127 days). The largest portion of the cycle time was taken finding the minimum cost open node during frontier expansion and due to the size of the map it was found to be quicker to use memory expansion and

logic indexing than a priority queue. Memory expansion was used for the open, closed and identifier column vectors, they were initiated at 10% of the node space size and are expanded by a further 10% when full and was found to improve the simulation run-time by a factor of 10 or higher.

The path planner code is based on a traditional A* algorithm where the cost for moving between parent and child nodes is a called function and outlined by the equations in Section 5.2.1. The heuristic cost is described by the equations in Section 5.2.5.3.

Path planner pseudocode with algorithm and heuristic switch options shown in the optimal path algorithm 3.

5.2.5.2 Cost function

The cost function is used to calculated the energetic cost of the simulation path. There are three main parts, the path cost so far, G, moving from the start node S to the parent node P, the cost to move from the current or parent node, P, to child node, N, and finally, the estimated or heuristic cost, H, from the child node, N, to the goal, G. This section will outline the path and cost to move portions of the equation, whereas the heuristic estimation will be covered in Section 5.2.5.3.

$$F(N) = G(N) + H(N) \tag{5.23}$$

Where $G(N)$ is the path cost so far and calculated as the cost from the start node to the parent, $C(S,P)$ plus the cost of the parent to the neighbour or child node, $C(P,N)$.

$$G(N) = C(S,P) + C(P,N) \tag{5.24}$$

The cost, C, was calculated using the step-duration, using the optimized velocity in the ground frame and the step distance, the power cost ratio (such that powered flight is more expensive) for each step in the path. The flight mode used is decided in each step where soar mode is always prioritized over flap mode.

Firstly, air relative energy is calculated (use the power equation and duration), this is compared against the energy required to move state using energy differencing and considers the change in kinetic and potential energy. If there is excess energy, either due to air relative energy harvesting or due to kinetic-potential energies trading, then soar mode is selected, where this value is zero or negative then flap mode must be used. Meaning that in negative air relative power manoeuvres either flap mode must be initiated or there needs to be a power balance through trading altitude or velocity.

Algorithm 3 Optimal Path Algorithm

function OPTIMAL PATH(s, g) ▷ Where s - start, g - goal
Algorithm finds optimal path from start to goal Initialise start conditions
    $openList(s) = true$ ▷ Frontier list
    $closedList(obstacles) = false$ ▷ Closed nodes list
    $parentList := s$ ▷ Parent indices list
    $gCost :=$ map with default value infinity ▷ Cost to node list
    $gCost(s) = 0$
    $fCost :=$map with default value infinity ▷ Estimated total cost list
    $fCost(s) = h(s)$
    $currentNode = s$ ▷ Set currentNode to start
    while $openList\ empty$ & $currentNode = g$ **do**
        $children = neigbours(currentNode)$
        for child children(currentNode) **do** ▷ Loop for each child of current node
            if $closedList(child) == true$ **then**
                continue
            end if
            $gCostTent(child) = gCost(currentNode) + costToMove(child)$ ▷ Calculate cost to move
            if $openList(child) == false$ **then**
                $openList(child) == true$
            end if
            if $gCost(child) > gCostTent(child)$) **then**
                $gCost(child) = gCostTent(child)$
            end if
            switch $Heuristic$ ▷ Calculate heuristic cost from child to goal
            case $Greedy$
            $fCost(child) = gCost(child) + hCost_{Greedy}(child)$
            case $Ideal$
            $fCost(child) = gCost(child) + hCost_{Ideal}(child)$
        end for
        switch $Algorithm$ ▷ Switch between A* and DFS algorithms
        case $A*$
        $[\ minf_idx] = min(fCost)$
        case DFS
        $[\ minf_idx] = min(fCost(children))$
        $parentList(currentNode) = minf_idx$
        $currentNode = minf_idx$
    end while
    $optimalPath := reconstructPath(g, s, parentList)$
end function

Algorithm 4 Reconstruction of Path

function RECONSTRUCT PATH($s, g, parentList$) ▷ Where s - start, g - goal
Reconstruct path uses the parent list to retrace the optimal path from goal to start
    $current = goal$
    while $current = start$ **do**
        $optimalPath := current$
        $current = parentList(current)$
    end while
    $optimaPath = reverse(optimalPath)$
end function

$$\overbrace{\dot{E}_{a_{C,P}}\tau_{soar_{C,P}}}^{\text{Harvested energy}} - \overbrace{\frac{1}{2}m(U_C^2 - U_P^2)}^{\text{Kinetic energy}} + \overbrace{mg(h_C - h_P)}^{\text{Gravitational potential energy}} > 0 \tag{5.25}$$

Flap or soar mode is initiated depending on the sign of the balanced energy equation. Such that every move either has an energy surplus which is presumed to be dissipated by the bird or is balanced. No negatively balanced motions can take place. This will likely still produce over estimated energy saving results despite the assumption of energy dissipation. In reality, the gull could use surplus energy to increase speed or gain additional height however, for the purposes of this study it is assumed that altitude gain or high velocity flight is not prioritized as much as overall cost of transport minimisation.

The final cost which is passed back to the main algorithm is based on the physiological power ratio between flapping and soaring flight.

$$C(P,N) = \tau_{soar_{P,N}} P_{BMR_{soar}} \tag{5.26}$$

$$C(P,N) = \tau_{flap_{P,N}} P_{BMR_{flap}} \tag{5.27}$$

Where $\tau_{soar,flap_{P,N}}$ is the duration required to soar or flap from the parent to child node, and $P_{BMR_{soar,flap}}$ is the physiological power requirement for soaring or flapping flight as a multiple of the BMR (Basal Metabolic Rate). The ratio of the flapping and soaring power requirements, sometime referred to as the BMR ratio, can be considered with the following equation:

$$BMR_{ratio} = \frac{P_{BMR_{flap}}}{P_{BMR_{soar}}} \tag{5.28}$$

5.2.5.3 Heuristic

The heuristic cost acts as an estimate for the remaining, untravelled path, from the current location to the goal. We consider two heuristic cases, an ideal and greedy heuristic. The ideal case is both admissible and consistent such that it is always considered an under-estimation of the cost to goal and is always considered less than in the previous frontier expansion. An ideal heuristic has been found to be key in returning an optimal solution, however, greedy heuristics have application of real-world scenarios where over-estimating the cost to goal can result in faster convergence to a solution for little cost sacrifice [150, 151].

The ideal heuristic was calculated in each expansion cycling using a soar only energy cost estimation. Cost to goal is considered the duration from current location to goal when soaring a direct LoS trajectory at an airspeed optimised for the mean averaged wind field. A small additional cost is added for a negative vertical distance to goal and is also underestimated.

$$H_{ideal}(N,G) = \begin{cases} \tau_{soar_{N,G}} - (z_N - z_G)BMR_{ratio}, & \text{if}(z_N - z_G) < 0 \\ \tau_{soar_{N,G}}, & \text{otherwise} \end{cases} \tag{5.29}$$

Where $z_{G,N}$ are the vertical node step positions of the goal and child node, such that if the goal is 1 position higher than the child node there is an additional cost of one power flapping unit.

This heuristic was found to be both admissible and consistent at BMR ratios of 3.5 and 6 but not at a BMR ratio of 1, where flapping and soaring flight are equal in cost. This was because flapping flight velocity can be faster than the soaring flight velocity which resulted in a lower duration and greater heuristic cost. The results for this are shown in Figs 5.8 - 5.10. For the heuristic to be considered admissible the estimate to goal must always be less than the actual cost to goal, see equation 5.30. This is consistent with the heuristic curve, $H(C,G)$ shown in red, always being below the admissible curve, $G(C,G)$, shown in green which represents the actual cost to goal from that location.

$$H(N,G) \leq G(N,G) \tag{5.30}$$

For consistency to hold, the heuristic cost from the parent to the goal must be equal or greater than the heuristic cost of the child to goal plus the cost to move from the parent to the child. This is represented in Figs 5.8 - 5.10 by the red heuristic, $H(C,G)$, curve always being below the blue curve, where the blue curve represents the heuristic cost of the parent to goal minus the cost to move between parent and child, $H(P,G) - C(P,C)$.

$$C(P,N) + H(N,G) \leq H(P,G) \tag{5.31}$$

The greedy heuristic option uses a combination of distance, altitude and the BMR ratio. The minimum power velocity for flapping flight is 11.9 meters per second and resulting in a duration per node visited between 0.85 and 1.2 seconds, meaning an over-estimation factor of approximately 10. The altitude part of the heuristic, costs nodes which are below the final goal altitude at BMR ratio multiplied by the step numbers and nodes above the final altitude. The greedy heuristic is neither admissible nor consistent

and is intentionally over-estimated in order to speed up the processing and determine suitability on-the-fly application.

$$h_{greedy}(N,G) = \begin{cases} BMR_{ratio}(r_{N,G} - (z_N - z_G)), & \text{if}(z_N - z_G) < 0 \\ BMR_{ratio} r_{N,G}, & \text{otherwise} \end{cases} \tag{5.32}$$

Where $r_{N,G}$ is the 2D distance from the child node to the goal.

5.3 Results

5.3.1 Comparison of algorithms and heuristics

The A* algorithm with the ideal heuristic had the highest performance in terms of the mean percentage of soaring flight (82.6%) and the directness to goal (1.19) but at the cost of solve time performance, see Table 5.2. The DFS algorithm with an ideal heuristic had the next highest mean percentage of soaring flight (77%) but had a lower directness measure (1.31), and also had a high solve time. As expected, when the greedy heuristic was employed the performance reduced in both algorithm cases, slightly unexpectedly, the A* algorithm underperformed in comparison to the DFS in terms of soaring percentage but had a lower total energetic cost due to a higher level of directness, see Fig 5.11 and Table 5.2. It should be noted that only three flights were chosen for each algorithm at a low, medium and high wind speed (3.46, 6.45, 11.37 m s^{-1}) in this comparison due to the very high solve times and that the 20 m node resolution was used here.

The shortest path simulation for the highest wind speed resulted in no solution due to reaching a node location with wind speed greater than the resulting ground speed. Hence, only the low and medium wind speeds are included in the energy and endurance ratios shown in Table 5.2. It could be argued that using a wind-aware and energy-based path planner, in this case, is infinitely better than using the shortest path route combined with the CoT based velocity control.

The GDFS had fast solve times and interestingly, in terms of soaring percentage, the gulls' commutes were equal to the these cases however, the gulls did tend to fly less directly, see Fig 5.12. The solve times for the ideal heuristic cases were extremely high, in some cases taking more than 2 days to solve, whereas the greedy cases solved in sub 10 seconds. For further comparison of the path planner to the gulls' flights, the GDFS combination is used due to the closeness in performance with the gulls and fast solve time. In the next results section the cost ratio between flight modes is increased, this

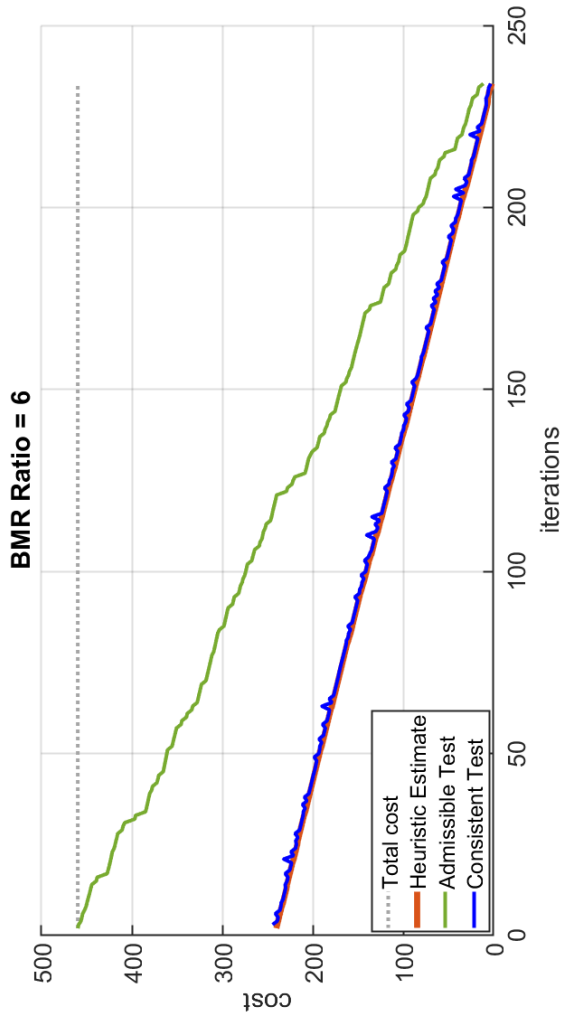

Figure 5.8: The total cost is shown by the grey dashed line, the green curve shows admissibility (as described by equation 5.30, the blue line shows the running consistency test (as described by equation 5.31) and the orange line shows the heuristic estimate. At a BMR ratio = 6 the ideal heuristic is both consistent and admissible, so the solution can be considered globally optimum.

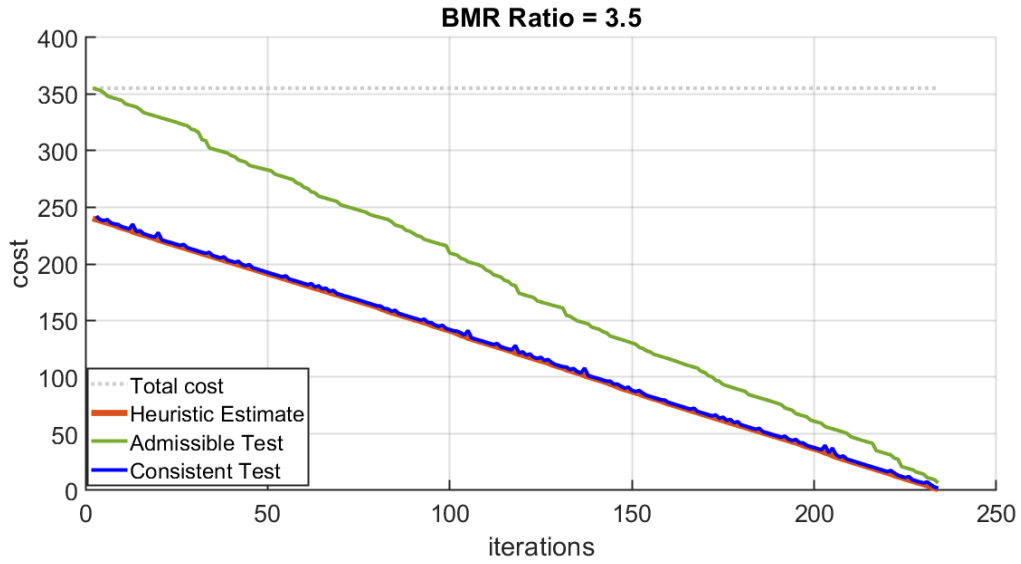

Figure 5.9: The total cost is shown in by the grey dashed line, the green curve shows admissibility (as described by equation 5.30), the blue line shows the running consistency test (as described by equation 5.31) and the orange line shows the heuristic estimate. At a BMR ratio = 3.5 the ideal heuristic is both consistent and admissible, so the solution can be considered globally optimum.

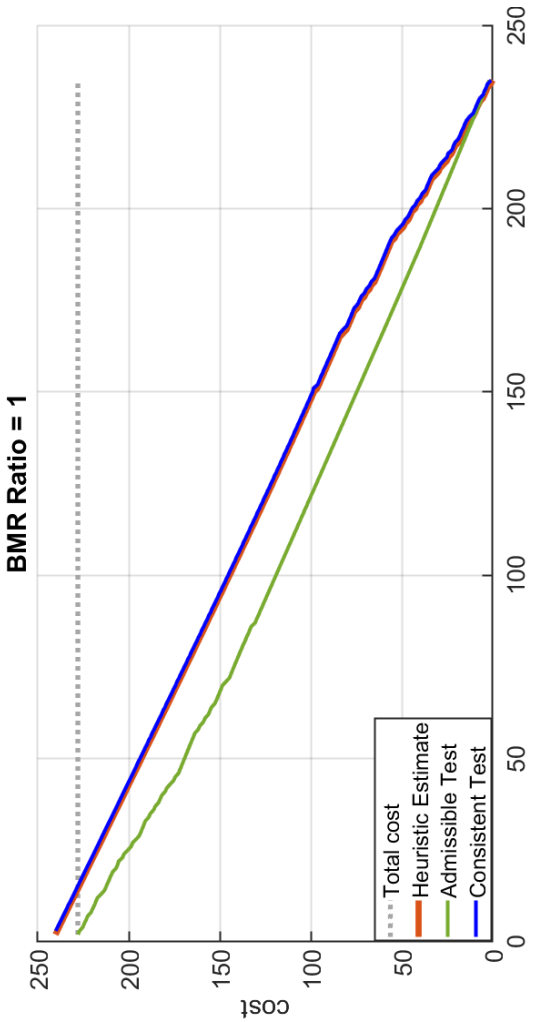

Figure 5.10: The total cost is shown in grey dashed line, the green curve shows admissibility (as described by equation 5.30), the blue line shows the running consistency test (as described by equation 5.31) and the orange line shows the heuristic estimate. At a BMR ratio = 1 the ideal heuristic is neither admissible nor consistent.

Table 5.2: Algorithm and heuristic comparison

	Distance Ratio	**% soar**	**Energy ratio**	**Endurance ratio**	**solve time (s)**
*A**	(n = 3)	(n = 3)	(n = 2)	(n = 2)	(n = 3)
Greedy	1.19 (0.0077)	62.4 (0.0416)	0.62 (0.0133)	0.65 (0.0116)	6.17
Ideal	1.16 (0.0225)	82.6 (0.0162)	0.60 (0.0210)	0.48 (0.0086)	$2.3e^4$
DFS	(n = 3)	(n = 3)	(n = 2)	(n = 2)	(n = 3)
Greedy	1.22 (0.0617)	64.5 (0.0056)	0.63 (0.0140)	0.60 (0.0100)	5.8
Ideal	1.31 (0.0614)	77.0 (0.0400)	0.69 (0.0059)	0.66 (0.0515)	$1.05e^5$
Gulls (n = 27)	*1.62 (0.2610)*	*64.5 (18.44)*	*1.02 (0.3557)*	*1.98 (0.7267)*	
Gulls (n = 3)	*1.86 (0.5286)*	*74.3 (17.23)*	*1.07 (0.3868)*	*2.32 (0.6861)*	

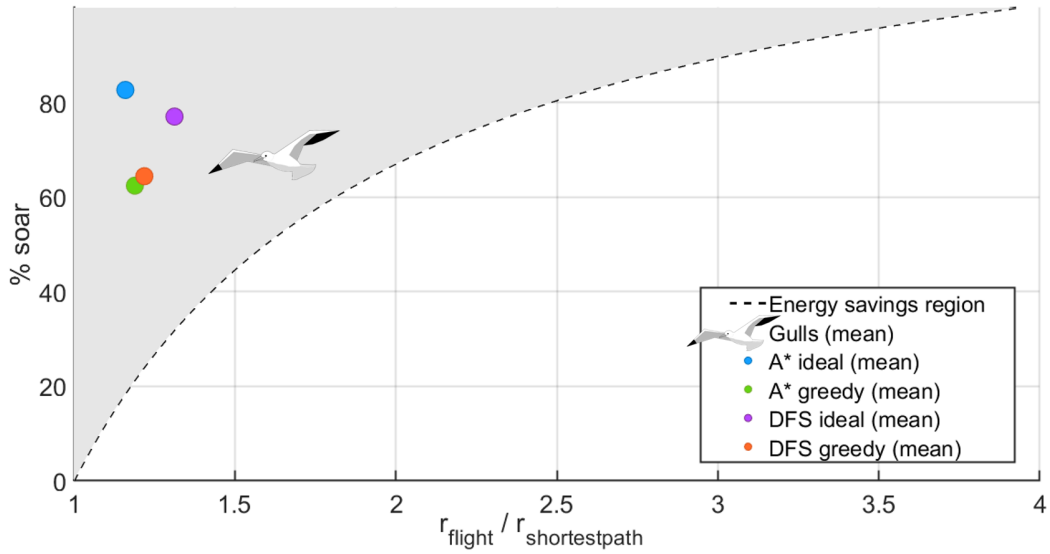

Figure 5.11: Graph to show the ratio of flight distance compared to the shortest path and the percentage of soaring flight in order to reduce cost below flapping the shortest path, this is indicated by the energy savings region to the left of the dotted line. The blue and pink markers indicate the mean result for the greedy heuristic A* and DFS algorithms respectively. The green and orange markers represent the mean result for the idea heuristic cases for A* and DFS respectively. These cases were all run at a 20 m grid resolution. The gull icon shows the mean result for the 27 commuting flights.

massively increased the solve time of an ideal heuristic test case, taking up to 12 days to solve with a BMR ratio of 6.

5.3.2 Increasing the cost of powered flight

As the power cost ratio of powered to unpowered flight increased the algorithm reacted by adapting the path solution to limit the powered flight. This has the interesting effect that both the duration Fig 5.14 and flown distance Fig 5.15 are increased when compared to

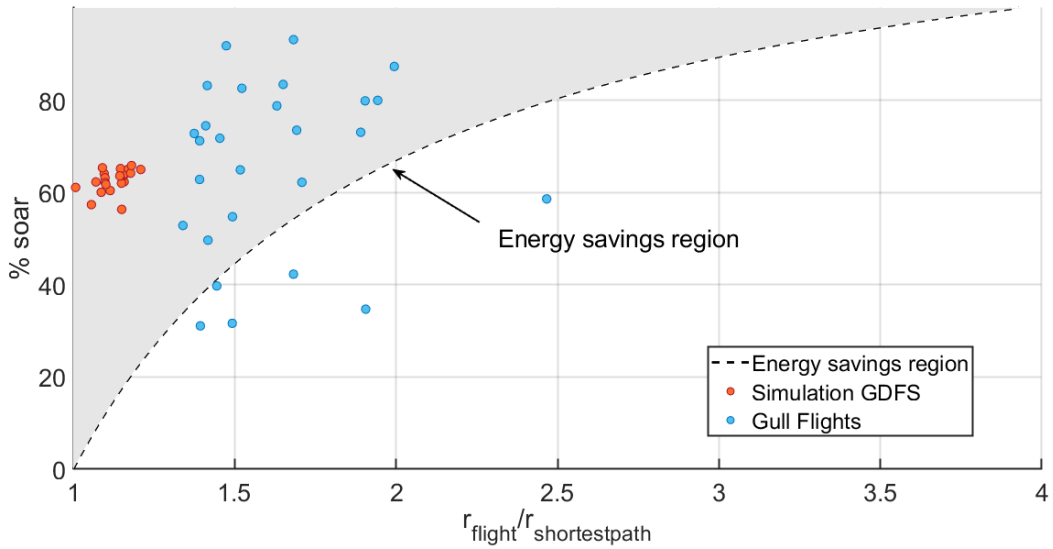

Figure 5.12: The blue markers are the gulls' commuting flights and the orange markers are the greedy heuristic with the best-first search algorithm. These simulation results were run at a 10 m grid resolution.

the shortest path route, while the energetic cost Fig 5.17 of the flight is reduced towards a stable plateau of 48% of the shortest path cost.

Initially, while the cost of flapping and soaring are equal, the energetic cost of the solutions are 10% higher than the shortest path routes. This is due to the slower soaring flight speed which leads to a larger energetic cost due to the increased flight duration, also of 10%, accompanied with no increase in distance.

As the power cost of flapping and soaring diverge the energetic cost of the flight compared to a fully powered shortest path route decreases. At a power ratio of 3.5, suggested as a gull's power ratio in the literature [35], the energy savings average 33% with an increase in flight distance and duration of 13% and 25% respectively. As the power ratio increases the cost of flight compared to the powered shortest path route continues to decrease, culminating in a plateauing effect at 52% (range 39 - 61%) of the shortest path flight cost, an equivalent to a 48% energy reduction. At the same time, simulating an increase in the power ratio demonstrates an increase in flown distance and duration with average increases of 50% (range 8 - 68%) and 71% (range 18 - 90%) respectively. The percentage of soaring flight also demonstrates an increase with power ratio, levelling towards an average of 77% (range 72 - 82%) soaring flight.

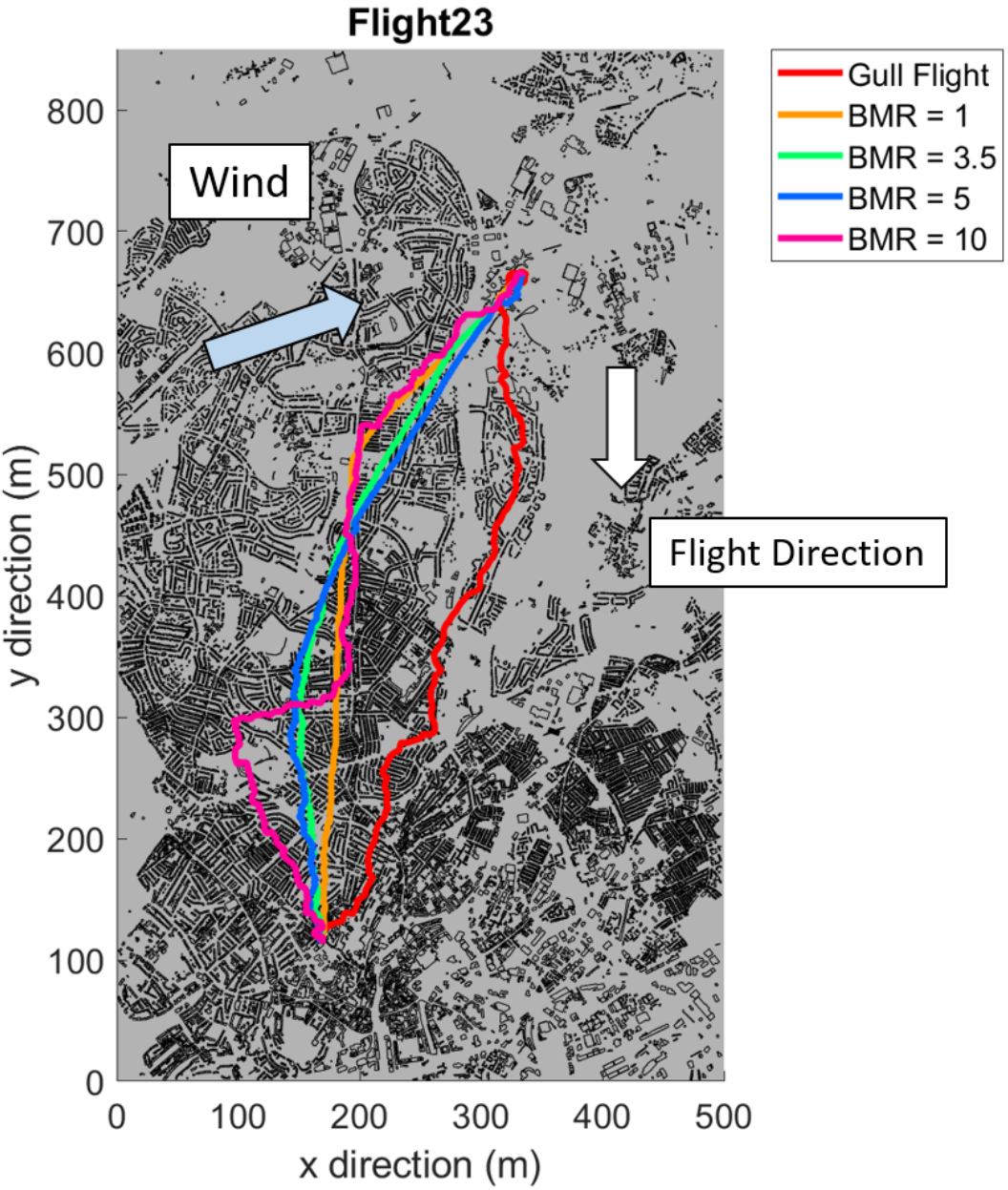

Figure 5.13: The simulation examples for BMR ratios 1 (orange), 3.5 (green), 5 (blue) and 10 (pink) accompanied by the corresponding gull flight (red). Flight direction and wind conditions are indicated by the arrows. Wind speed = 4.8 m s^{-1}, Wind Direction = 263.7° from North. For more example see Appendix D

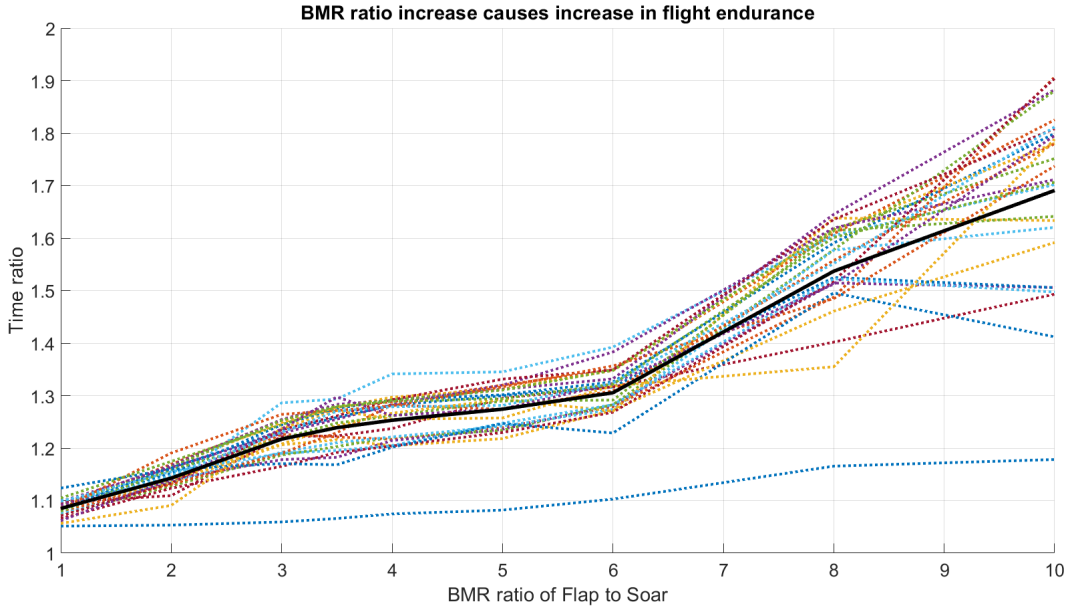

Figure 5.14: The flight duration compared to the shortest path flight increases with increasing powered flight cost. The dashed coloured lines indicate the 27 individual commuting flights, the heavy black line indicates the mean of the 27 flights at each BMR ratio.

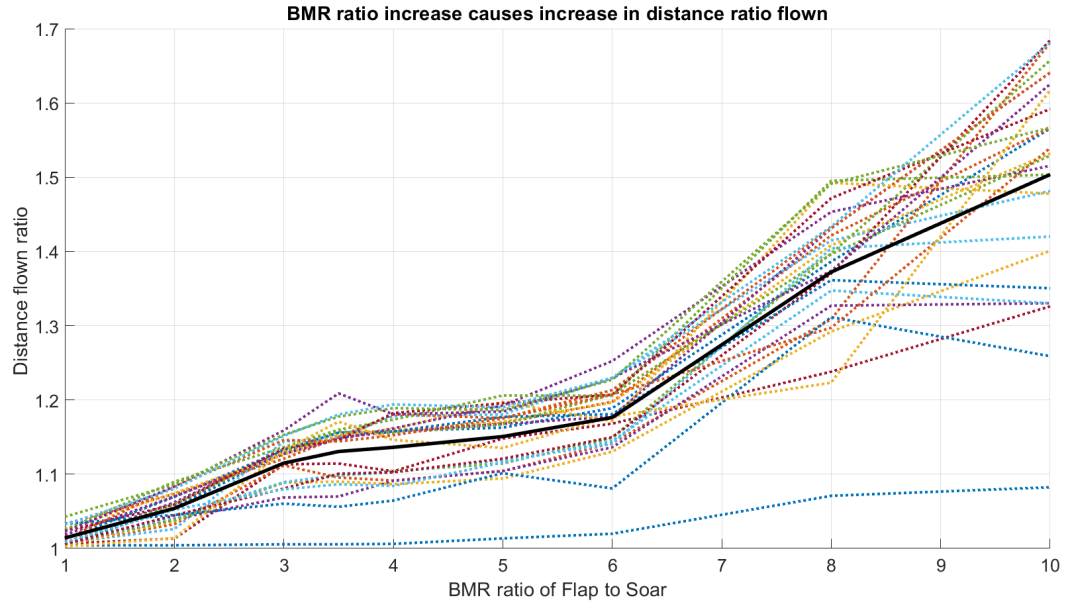

Figure 5.15: The distance flown increases with increasing powered flight cost. The dashed coloured lines indicate the 27 individual commuting flights, the heavy black line indicates the mean of the 27 flights at each BMR ratio.

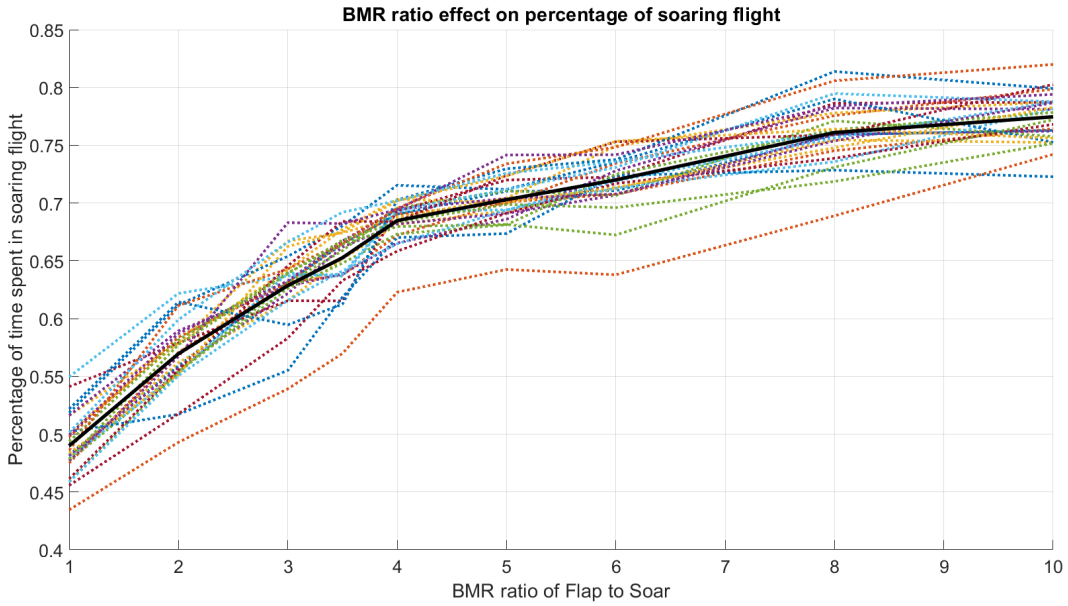

Figure 5.16: The percentage of soaring flight increases with increasing powered flight cost. The dashed coloured lines indicate the 27 individual commuting flights, the heavy black line indicates the mean of the 27 flights at each BMR ratio.

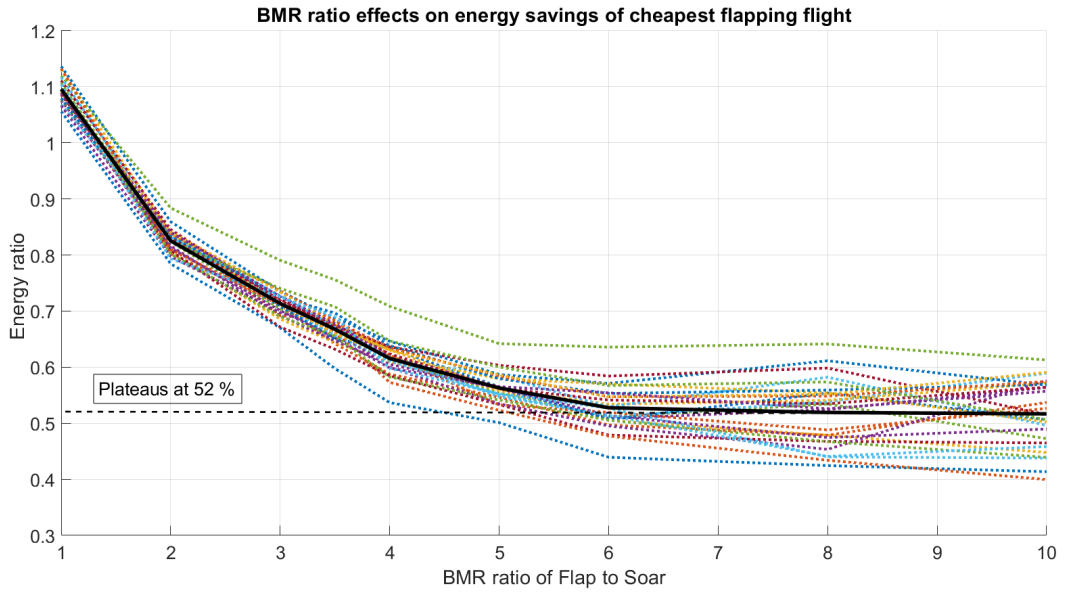

Figure 5.17: The energy savings compared to the shortest path reduce with increasing powered flight cost, plateauing at 52% of the shortest path cost. The dashed coloured lines indicate the 27 individual commuting flights, the heavy black line indicates the mean of the 27 flights at each BMR ratio.

5.3.3 Effect of flight cost with wind-speed

The effect of wind speed on the simulation flight energetics appears to be complex. Mid-strength winds (4 - 6 m s^{-1}) provided the best energy harvesting through static soaring, shown by the pink markers in Fig 5.18. At high wind speeds (> 6 m s^{-1}) the simulations were able to harvest a high amount of energy through wind field gradient exploitation, shown by the green markers in Fig 5.18. The maximum static soaring harvested is a factor of four less than the gradient soaring energy harvested as is reflected in the change in y-axis scales. The static soaring energy harvested at high wind speeds becomes negative at high wind speeds whereas the gradient soaring energy is greatly increased, this is due to exploiting the wind field gradient in downdraughts.

This effected the static soar energy total due to gradient soaring in both up- and down-draughts, see Fig 5.20 and 5.21, reducing the cumulative total. The final axes in Fig 5.18, shows the drag costs increased with increasing wind speed due to the higher average airspeed selected by the optimiser. The increase in drag costs required a higher mechanical power, but in bird flight it is not clear how this directly corresponds to the energetic effort of the bird, as such the costs were calculated in two ways.

Firstly, the CoT was considered where flapping flight has a fixed energy rate, in these cases, for both the gulls and the simulations, the CoT decreased with increasing wind speed, circle markers in Fig 5.19c and d. When the total flown distance was used to normalise the total cost a spike feature appeared, in the gull and path planner results which suggests that this wind speed may be linked to greater flight directness.

Secondly, the CoT was considered where flapping flight increased by the power factor described in Section 5.2.3. This created an interesting feature shown in the crosses in Fig 5.19c and d where a minima appeared at min-strength (4-6 m s^{-1}) winds and an increase in CoT at very high winds (> 8 m s^{-1}). Again, this feature appeared in both the gull and path planner results. Additionally, when the cost of the flight was normalised by the total flown distance the CoT reduced as wind speeds increased which suggests that higher wind speeds may require more deviation from the shortest path. It should be noted that Fig 5.19 uses different scaling for the gull and simulation results for part a and d in order to highlight the similarity in data shape rather than the specific quantities, where the path planner has a CoT for the flown distance up to approximately twice that of the gulls but a comparative CoT for the AB distance to that of the gulls. This results is mainly due to the directness of the path planner results where there is a lower total flown distance.

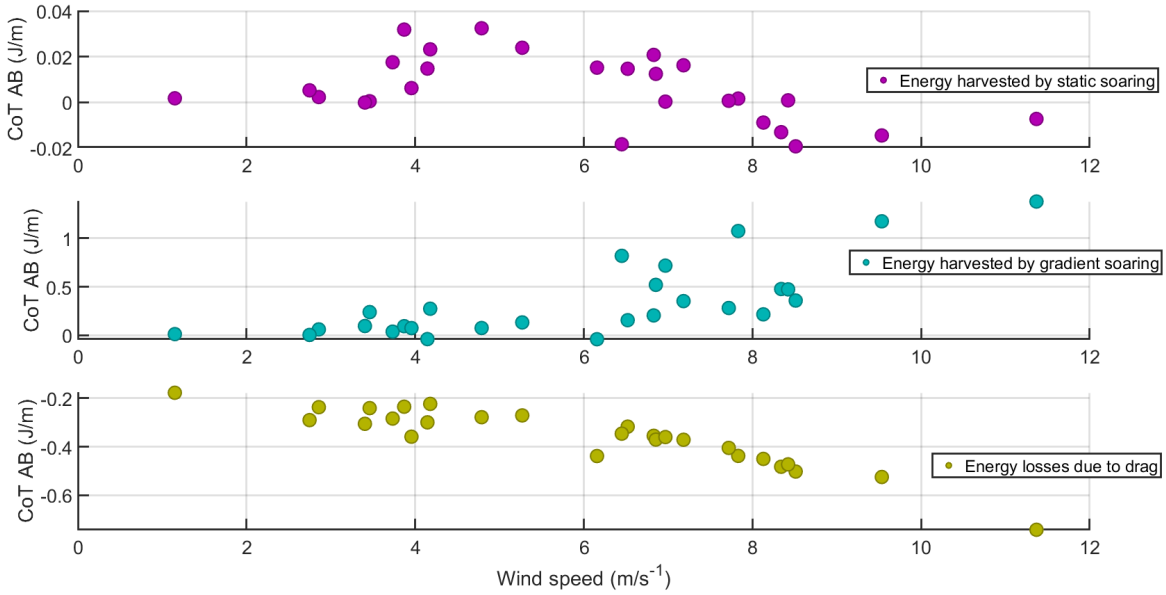

Figure 5.18: The plots show the cumulative energy harvested from static (pink-top) and gradient (teal-middle) wind based energy harvesting while in soaring flight mode compared against the 10 m height wind speed from the input profile. The bottom plot shows the cumulative energy required to overcome drag in flapping flight mode. All 27 commuting flights are shown, generated using the GDFS planner with a ratio of 3.5 for the BMR power costs. The maximum static energy harvested is a factor four less than the gradient energy harvested, as is reflected in the y-axis scale, and at high wind speeds the static energy becomes negative where gradient energy is being harvested while flying through down draughts.

5.4 Discussion

The complex wind fields of the urban environment can present control issues for SUAV platforms due to gusts [141] however, by studying the flight strategies of gulls flying in similar conditions it has become apparent that these conditions could also offer a solution to the range and endurance limitations caused by the low on-board energy storage. It was found that urban gulls were able to employ soaring and non-flapping flight on average 64.5% of the time by exploiting both the updraughts and wind gradients in urban wind fields. Further to this, a path planner programmed with gull characteristics was able to match this performance demonstrating the viability of implementing bio-inspired flight strategies on SUAV technology.

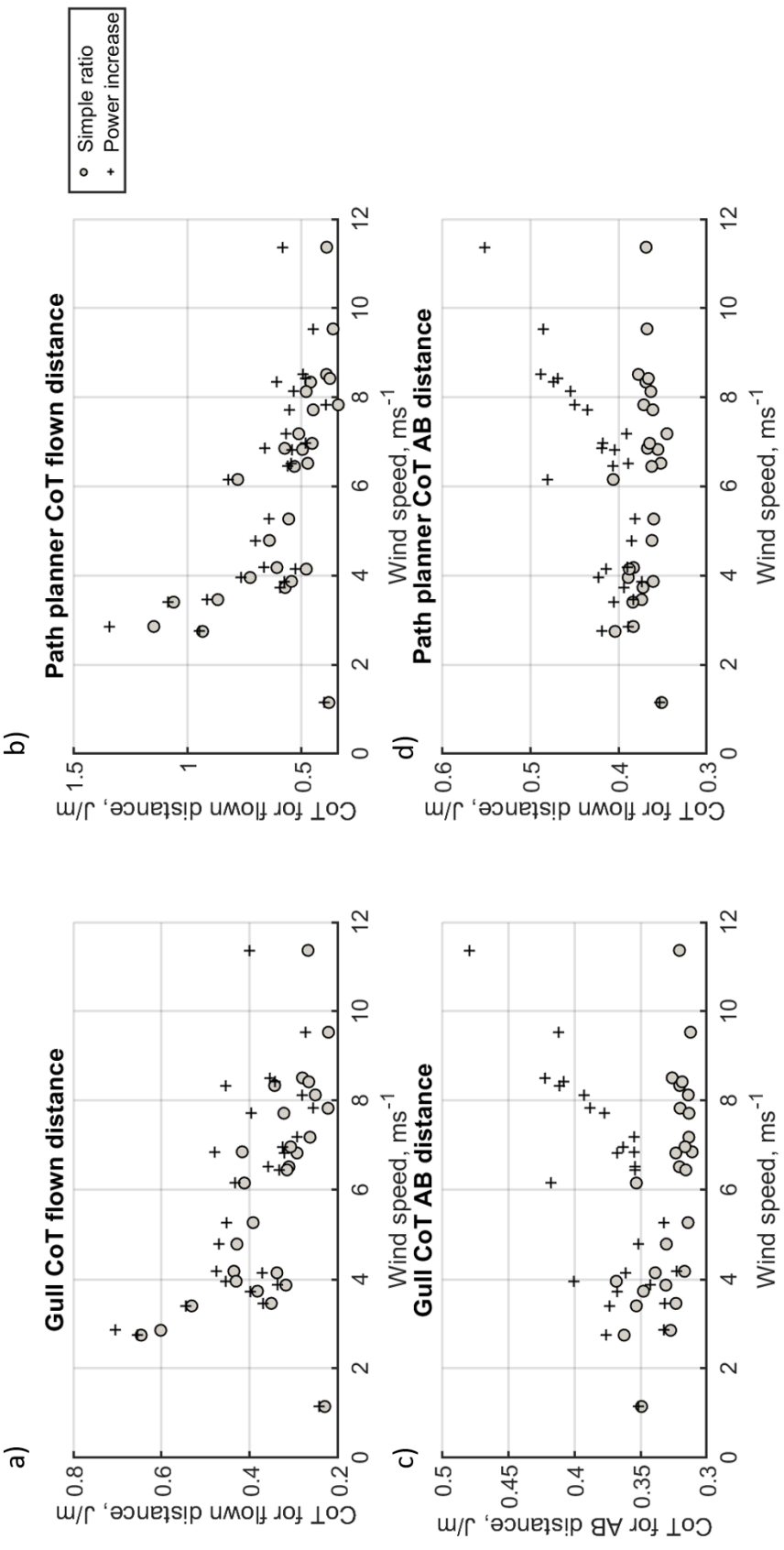

Figure 5.19: The estimated flight costs of the gulls for the 27 commuting flights are shown in a) and c) and the path planner solutions for the corresponding flights in b) and d). The energetic costs have been normalized by the shortest path a) and b), and the total flow distance b) and c). In the flown distance cases for gulls and simulations the flight costs reduce with increasing wind speed. In the minimum distance cases the CoT remains constant with increasing wind speed (grey circles) but when the increased power demand is considered (black crosses) the CoT increases for increasing wind speed.

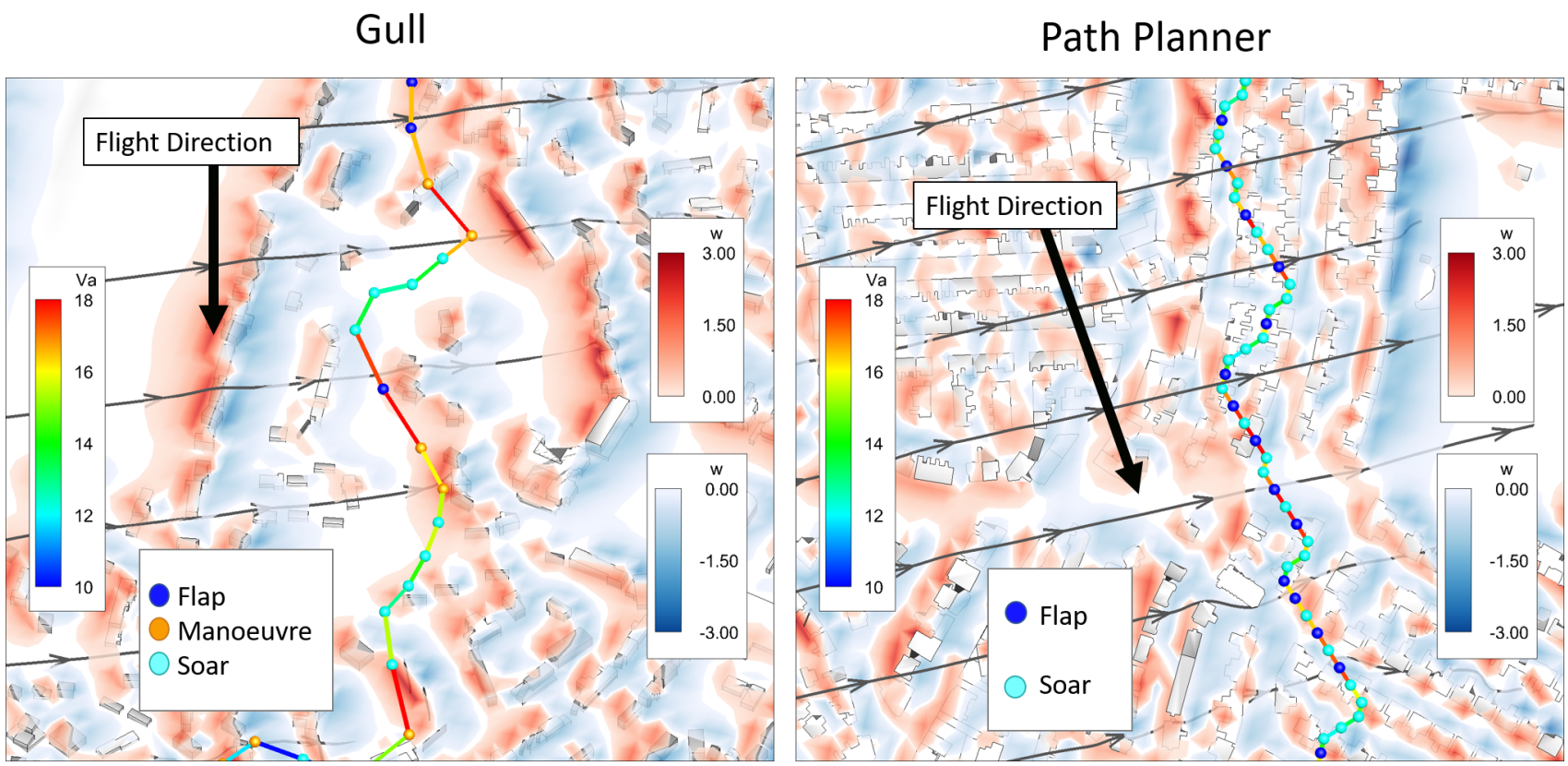

Figure 5.20: Examples of gradient soaring in the gull a) and path planner b) trajectories, the plots show similarities in strategy where in both cases there is a cyclical variation of flight direction, airspeed and flight mode while traversing in a strong horizontal wind gradient. The wind direction is shown by the flow vectors (grey) and the vertical wind, w, demonstrates the up- and down-draughts. The spatial scaling in each figure remains constant but the temporal resolution in the gull (4 s) and simulation (approx. 1 s variable) differs.

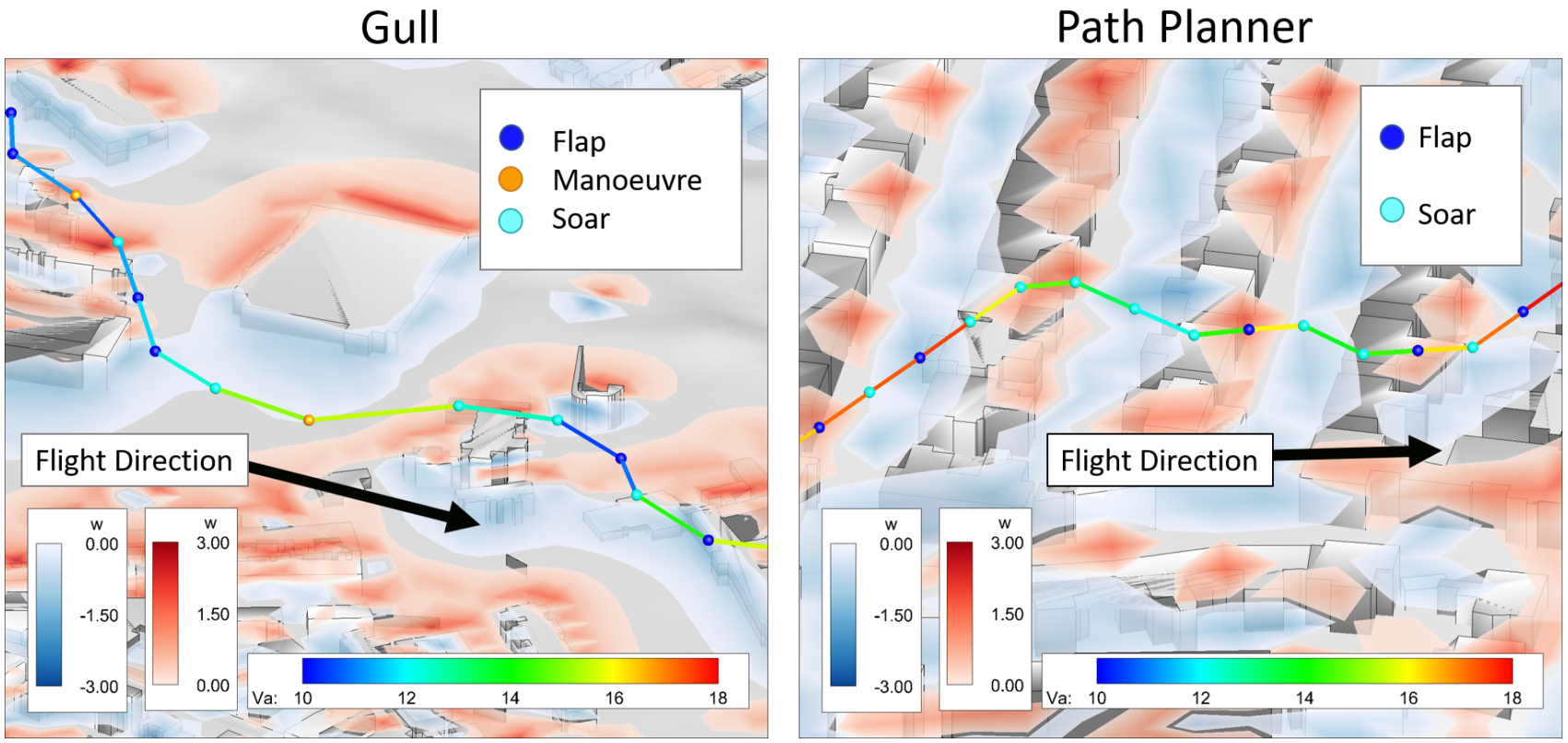

Figure 5.21: Examples of dolphin soaring in the gull a) and path planner b) trajectories, the plots show a similarities in strategy where in both cases soaring occurs in the updraught before diving in the down draught. In dolphin soaring, as the down draught diminishes there is added lift reinitiating climb which could explain the rising trajectories in these cases. The vertical wind, w, demonstrates the up- and down-draughts. The spatial scaling in these figures varies, in order to best view the behaviour through the changing vertical wind field.

5.4.1 Algorithm comparison

Four combinations of path planner algorithm and heuristic cost were tested for overall flight performance of the solutions and solve times. As expected, using an ideal heuristic cost resulted in the lowest energy trajectories but at the expense of computation costs, meaning suitability is limited to offline planning or much lower map complexity, possibly suitable for designing airway networks for a few prevailing wind speeds and directions. In this case, the ideal A* combination provided lower energy trajectories and lower solve times than the ideal DFS alternative tested. The poor solve time performance from the DFS is a result of the algorithm set-up. If DFS algorithm can no longer move but has not reached the goal it will revert back to finding the minimum of the unclosed nodes for one step, restarting at the lowest open but unexplored node so far and resulting in a higher number of iterations and solve time than A*.

Using a greedy heuristic had the expected effect of reduced flight performance but with the benefit of huge solve time improvements suitable for integration within fast operations pre-planning software or even on-the-fly re-routing. The GDFS combination solved slightly faster than the Greedy A* combination and produced trajectory solutions with performance most similar to the gulls and slightly better than the A* on the commutes compared. This demonstrated that optimising for the immediately local wind conditions provides relevant energy savings and improved trajectories. The GDFS combination does not necessarily provide the global optimum but could be further enhanced by introducing *random walks*. Nevertheless the GDFS could provide fast and efficient route planning based on very little input knowledge, the wind field at the child node was sampled however, this value could be estimated based on wind gradients measurements instead.

Recent developments in 3D printing have led to the design of gradient based wind probes these have been successfully implemented on SUAVs in real-world flights to detect and react to turbulence [77] as well as to perform gradient-based soaring that reduced throttle requirements [76, 152] . With wind sensing capabilities such as these the GDFS planner could provide fast and efficient trajectories through an urban environment.

5.4.2 Navigation choices in gulls

Comparison of the gull and GDFS trajectories highlighted some interesting features. While the path planner and gulls performed a similar level of soaring flight, the path

planner choose direct paths in order to make significant energy savings, whereas the gulls often had little or no energy savings but increased range and endurance instead. There are a few possible reasons for this behaviour, relating to localisation and resource awareness strategies.

Firstly, it is known that some bird species use visual cues for navigation in familiar environments, most famously, homing pigeons, *Columba livia domestica*, following distinctive landmarks [153, 154], and recently it has been proposed the gulls may use optic flow in altitude control while commuting over sea [155]. It is probable that the gulls in this study also use familiar landmarks however, the flights in this study varied in route and tended to occur at relatively low altitudes above ground level (μ = 29 m, σ = 16 m) which could limit visual navigation in some parts of the flight due to partially restricted views. Furthermore, at these ranges it is unlikely that the gulls are navigating using magneto-reception. It is now becoming apparent that some birds, particularly seabirds, are reliant on the olfactory system in both foraging and homing. In particular it has been found the shearwaters, *Puffinus*, displaced distances of 800 km from the nest were less able to orientated themselves when influenced with zinc sulphate - a temporary anosmia, but were unaffected by magnetic disruption [156, 157]. Additionally, shearwaters administered the same olfactory inhibitor and released in the dark were unable to find their nests until after dawn [158]. It is therefore possible that the gulls are also navigating through olfactory sensing, this may in partway, explain an interesting difference in chosen flight directions. The first section of the gulls' flights are occasionally headed down wind such that later sections of the flight need to face a headwind (see Appendix D). The path planner however, found that routes were cheaper by starting with a slight headwind component and using a slight tailwind component in later parts of the flight, the flights are generally crosswind to the goal direction. Work by McLaren considers the optimal flight orientation of gulls in wind based on the minimisation of flight energetics where it is proposed that allowing drift in these crosswind flights could have a level of energy conservation with the potential that wind conditions may change with proximity to the destination [87]. However, it could also be possible that the direction choice is influenced by scent plume direction when no visual clues are available, for example obstructed by a building. Following an increasing scent gradient generates a similar trajectory and scent following have been seen in other sea birds [159, 160]. Another alternative, is that the path planner selection has been created by the spatial grid and heading resolution, it could be that the planner prefers to travel diagonally at first to create greatest proximal gains toward the goal and overshoots before turning

back, however, a similar path choice was also found in the ideal A* cases.

Secondly, it is possible that the gulls use energy harvesting to increase the flight range with the benefit that this could improve resource awareness. Gulls are considered social birds [161] that are specialist foragers but also opportunistic [110], as such it has been suggested that they share resource information and use scouting strategies [162]. In one of the commuting flights, see Appendix Fig D.3, a trajectory passes over another of the foraging destinations without visiting it. Perhaps, this could have been scouting for a future foraging trip or an area where other gulls were present.

While the levels of soaring flight which the gulls are able to achieve suggests an energy based driver in their navigation strategies, the extended flight distance suggests there could be additional drivers unaccounted for in the path planner model. Although this limits the conclusions which can be ascertained about the navigational strategies of gulls there is still benefits available for SUAV path planning. Certainly, the aim of the study was to discover a method of improving the potential mission range and endurance for SUAVs, but unless the mission type is surveillance where loitering flight is required it is mostly likely more desirable to make direct flights at a lower energetic cost, such as performed by the path planner.

5.4.3 Cost of flight behaviour

The cost ratios of powered and soaring flight is significantly different across birds and SUAVs. The ratio ascribed to the gulls in this study is based on respiration measurements of trained gulls gliding [148] and flapping [149] in a wind tunnel. The experiments were across two different species of gull, herring and laughing, respectively, but both species are of a similar size to the lesser black-backed used here. In fact, when the BMR ratio based on the literature (3.5) was used, the path planner produced an almost exact match to the level of non-flapping flight seen in the commuting flights. Interestingly, the ratio taken from the literature also closely matched the VeDBA (3.15) and ODBA (3.9) ratios found from averages of the two behaviour types over the gull dataset. Comparisons of heart rate and ODBA readings in free-flying vultures were found to strongly correlate [163] which indicates a certain level of reliability in the ODBA method. However, when initially determining a cost ratio to use, VeDBA and ODBA measurements were examined across a range of airspeeds in an attempt to quantify the effort required at higher speeds. there were very clear differences between the means in behaviour types, however, the standard deviations are large (flapping $\mu = 0.1924, \sigma = 0.2750$, soaring $\mu = 0.0773, \sigma =$

0.1231) and there was no discernable variation across a range of airspeeds, parabolic or otherwise. It is possible that variations in the exertion required in the same behaviour but different airspeeds cannot be captured at the measurement rate of GPS device accelerometers. In studies of cockatiels, *Nymphicus hollandicus*, it was found that the flapping frequency, wing angle and down stroke impulse all had an effect on the airspeed [118, 164] and while the average flap frequency of the gulls, at 3.5 Hz, is well within the Shannon-Nyquist requirements for data sampling [165], the changes in wing-beat impulse are not. For this reason, the BMR ratio was selected from the literature sources and the power variations were considered based on the deviation from minima on the power curve. The benefit of using the BMR method was ability to increase the cost ratio and create a comparison for SUAVs. Colleagues in the University of Bristol Flight Laboratory flying a Skywalker X8 [166, 167], recorded mean climb and cruise current draw at 21 and 19 amps respectively, while in gliding flight (add still transmitting communication including video link) there was a current draw of 0.25 amps, resulting a cost ratio of approximately 80. However, this platforms has an average speed twice, and mass four times, that of the modelled gull. Power required in flight is proportional to the mass and weight such that this the power increases by a factor of 8. Meaning that a similar platform, scaled to the gull model would have a cost ratio of 10, the upper limit of the cost ratio variation in this study. The main finding from the variation was that there is a limit in the possible energy savings. This was a result of higher flown distances and flight times such that energy savings plateaued and flight costs were effectively halved.

Considering the cost ratio in this way could benefit engineers designing SUAV platforms, the size and velocity of a platform will dictate the thrust, and so, power demand required in flight but additionally will constrain the optimum airspeed in glide. Smaller platforms could have a lower cost ratio and may not benefit from implementing soaring behaviour to reduce energy costs. In the same way that some small avian species use gliding and soaring flight sparingly, even in migration [16]. In the same way, many larger platforms, with higher cost ratios, could benefit by implementing a dual flight mode in order to halve flight costs.

5.4.4 Wind speed and soaring

Another factor that should be taken into account when designing urban ready SUAVs is the wind speeds which the platforms will regularly be faced with as this could have a large effect on the CoT. Here, wind field were tested with a range of 10 m s^{-1}, a value

similar to the normal flight speed in still air, and found that while there were higher levels of harvested energy, CoT for the commuting flights increased at high wind speeds due to the high power requirement. While it is uncertain how the airspeed affects the power exerted by the birds[4], it is certainly an issue for SUAVs where the relationship between airspeed and motor demands are well defined [134]. Another potential factor of the wind strength is the gust factor, while this has the potential to increase control costs but with longer temporal or spatial variations there is a source for environmental energy harvesting. The energy harvested through air relative power, or gradient soaring, increased with increasing wind speed. Interestingly, the static energy harvested, reached a maximum at mid-range wind speeds. It could be possible that at very high speeds the orographic updraughts are not sufficient to offset the higher sink rate associated with the much higher airspeeds. However, the results from Chapter 3 would disagrees as gulls were found to perform orographic soaring at even higher wind speeds (up to 9 m s^{-1}). It is possible that at this wind strength gradient soaring becomes more effective. At cross winds that are a similar speed to the optimum glide speed it is possible to perform wind hovering on the updraughts but as the strategy does not optimise CoT it would never be performed by the GDFS path planner. This strategy is also not present in the gulls' commutes, demonstrating that the flights selected are in fact commuting and not performing any foraging. The variation in wind speed and energy harvesting mode could be relevant in designing control schemes with multiple soaring strategies.

Bristol has a Westerly prevailing wind direction and the gulls' commuting flights tended to have a crosswind. Given that the wind speed is often comparable to the airspeed it prevents having to journey in one direction with a strong head-wind. This method also has the potential to increase the number of soaring opportunities, not only is orographic lift available at this angle but it is also possible to exploit the wind gradients. Typically, commuting seabirds have been found to fly outbound with a headwind and inbound with a tailwind and this is thought to reduce the additional flight costs associated with carrying a payload. However, there are many studies which also demonstrate the benefits of exploiting crosswinds, particularly in seabirds such as that are able to perform gradient soaring [168, 169]. Two forms of gradient soaring were found in this study, in both the simulations and the gulls' trajectories. Firstly, a horizontal shallow-arc soaring reminiscent of dynamic soaring but with periods of flapping flight as demonstrated in Fig 5.20. This behaviour was similarly predicted when the boundary layer is narrowed but the inclusion of powered cycles could be more realistic, over coming the issues they faced

[4]Not the mechanical power.

with energy conservation in their simplified model [170]. Rather than gaining altitude with surplus kinetic energy at each cycle the simulation (and gull) simply soared into the wind until the airspeed reduced due to drag, then quickly turned downwind while initiating powered flight in order to receive a significant speed boost from the tailwind. This covers significantly distance quickly while reducing the time spent flapping.

The second gradient soaring strategy involves a vertical undulation comparable to dolphin soaring as described by [74] and shown in Fig 5.21. In dolphin soaring spatial and temporal gusts are exploiting by using vertical shear. Consider an upward gust, the gust will have an increasing gradient before a peak and then the gradient will reverse. In this case the gull should climb through the increasing updraught and dive through the decreasing updraught in order to harvest a positive air relative power. Conversely in a downward gust the opposite is true, where the gull dives initially, then climbs into the decreasing downdraught.

In both cases, soaring occurs in positive power manoeuvres as described by Lawrance [8] and requires the ability to sense the wind field. With the advances in wind gradient sensing it could soon be possible to implementing gradient soaring strategies in complex urban flow fields could provide significant gains.

5.4.5 Review of methods

The methods in this Chapter have some limitations, firstly, due to the size of the modelled area, the lower accuracy QUIC-URB model was used to generate the wind field environments. Further to this, the model used a 10 x 10 x 5 meter grid resolution. This was interpolated to give a finer resolution in the vertical direction but at a cost in accuracy. The method of spatial node mapping provided a means for initiating a globally optimised search, where other literature increased the number of nodes only at large gradient changes, this method used uniform spacing and implemented an additional heading dimension. This provided two main benefits, firstly, it allowed power-assisted gradient soaring behaviour and secondly, it provided the opportunity to circle and visit every available space. The spatial grid size was generated based on the physical constraints of a gull-sized platform such that no move presented unrealistic manoeuvrers. The step-wise energetic state changes do simplify the dynamics somewhat but the performance comparisons between the simulation and gulls' trajectories should verify gradient soaring in complex flow is energetically efficient and that a wind-sensing platform with

a short-range receding horizon planner could stand to gain signifiant energy savings.

5.5 Conclusions

- The simulations outperformed the gulls in terms of the directness of the flights which effected the energy savings.
- Using global optimisation, A* and ideal combination, could increase soaring percentage by as much as 20% but at a huge cost in terms of processing time.
- A local optimiser, GDFS, could make significant energy savings compared to flying the shortest path and these savings increase up to 48% with the increasing disparity between powered and gliding flight.
- The local optimiser performs most similarly to the gulls in terms of the soaring percentage, energy savings and distances flown, with a BMR ratio of 3.5, interestingly, this value taken from the literature in two different studies.
- Increasing wind speed results in an increase amount of harvested energy but at the potential cost of increased power requirements.
- It appears that the urban gulls in this study exploit the wind gradients during flight in a method resembling shallow-arc dynamic soaring but use a combination of flapping and soaring flight modes to increase the kinetic energy transferred.
- The global optimisation method could be adapted for pre-planning SUAV routes where simulations for a set of prevailing wind conditions and commutes were run in advance such as in airway network design.
- The local optimisation method could be integrated into in-flight mission planning where the SUAV trajectory is required to update on-the-fly

CHAPTER 6

SUMMARY AND CONCLUSIONS

This thesis aimed to discover the flight strategies that commuting gulls utilise in the urban environment with the purpose of applying these strategies in a path planner for an SUAV operating in the same urban environments. Studying the flight strategies of birds is nothing new, but, this was the first time that technology has allowed the investigation of free-flying birds through such complex wind fields and it led to three key discoveries. Firstly, that gulls implement a position based velocity control scheme in orographic soaring which is likely to reduce control costs. Secondly, that gulls are able to soar extensively in the urban environment and this is likely facilitated by closely paired minimum power and best glide velocities. Thirdly, that gulls implement gradient soaring strategies in complex flow to reduce energetic costs of flight. All these strategies could be implemented in SUAV technology to improve flight performance. Furthermore, integrating a velocity optimisation loop and cost function directly inspired by these urban gulls in to existing path planners was found to reduce flight costs in windy conditions by as much as half compared to traditional methods and led to energy harvesting through gradient soaring techniques.

In Chapter 3, it was determined that gulls take advantage of man-made infrastructure varying their flight paths to reduce energy costs and commute more efficiently. The gulls were found soar in orographic updraughts generated by the anthropogenic cliff of terrace buildings, offsetting their sink rate to maintain, and even gain, altitude. The gulls had opportunity to minimise their flight times by flying in regions with a greater

updraught strength, instead they maintain a limited velocity range and varied their position within the quasi-circular updraught generated as a method of reducing control costs by mitigating the effects of gusts. This was a previously unrealised and useful flight strategy that could be implemented in control schemes for UAVs in gusty, orographic conditions.

Due to the success of the first experiment, the experimental complexity was increased and a city-wide expansion initiated. The subsequent Chapter described the tagging of 11 urban nesting gulls and the analysis of their soaring strategies during commuting flights. The results demonstrated that the gulls soared extensively through a combination of different soaring and gliding strategies. The gulls combined thermalling and gliding the most often, but were also able to perform orographic soaring on overcast days demonstrating the abundance of environmental energy available in a range of conditions. In addition, the gulls implemented different velocity optimisation techniques depending on the soaring strategy utilised. When thermalling, the gulls reduced air speed to just above the minimum sink, as would be expected in order to gain the greatest altitude, but, when gliding between thermals the gulls did not optimise for flight time in line with Speed-to-Fly but maintained an airspeed just above the best glide velocity. While performing orographic soaring the gulls flew slower than expected if adjusting to horizontal winds alone, which could indicate that they reduced air speed to take advantage of the updraughts in line with CoT theory. Most importantly, the flight speeds of the gulls and frequency at which they switched between flapping, mixed, orographic soaring and gliding flight indicate that the gulls could be switching flight modes to significantly cut energy costs; flapping at minimum power velocity requires the lowest mechanical power and the performance curves indicate that it would be possible to quickly take advantage of updraughts present in the environment due to the close proximity of the best glide and minimum power velocities. This has particular relevance to SUAV technology where being able to take advantage of soaring opportunities could result in significant energy savings, it was estimated that the gulls were able to reduce their flight costs by 31% and, with a dual flight mode, this could also be possible in urban SUAVs.

The final stage of this thesis implemented a global and local energy optimising path planner within 27 QUIC-URB wind models generated with the wind conditions of selected urban gull commutes. The path planner included the velocity optimisation strategy outlined in Chapter 4 and formulates a cost function based on the power ratio of different flight modes. The path planner also implemented dynamics equations which allowed both static and gradient soaring types. A local optimisation strategy, with a

greedy distance to goal heuristic to accelerate solve time was found to be less effective than a global optimum but still produced valuable energy savings. Other research in this area where wave-based algorithms have been used have opted for conservative heuristic models, however, this has limited investigations to simple, often 2D models, unrepresentative of the real-world and less applicable for SUAV application. Using greedy distance heuristics can been implemented to improve solve times, particularly useful for real-world application. This research demonstrates that significant energy savings can still be achieved with a greedy heuristic method with the additional benefit of drastically reduced computation time. Finally, gradient soaring techniques were discovered in the simulation and gull trajectories, where this strategy was found to be effective for harvesting environmental energy, especially at high wind speeds. The flight mode power ratio selected based on respiratory experiments in gulls was found to accurately predict the percentage of soaring flight and when this value was increased to align with the higher power demands in SUAVs it was found that energy saving plateaued at approximately 50% of the cost of a fully-powered, direct flight.

Each Chapter has used a unique methods to gain insight into the flight strategies of soaring birds in order to understand how energy savings can be made in an SUAV flying in a complex urban environment. In this process, three main strategies were uncovered; a position-based gust-mitigating velocity control scheme used in orographic soaring, a velocity optimisation method to that facilitates soaring with dual-flight modes, and two gradient soaring techniques - one which takes advantage of vertical variations and one which uses a power-assisted shallow-arc method to take advantage of cross winds. Each of these strategies could be implemented in SUAV technology to improve stability and reduce energy costs enabling greater range and endurance during urban mission.

The first strategy has recently been explored further [11], a flight dynamics and control model for a powered SUAV was tested in simulation flying in the same orographic conditions as the birds in Chapter 3. Additionally, a Dryden gust turbulence model was added to the wind field in order to more closely represent real-world conditions. Mirroring the gulls' behaviour, it was found that the optimum position during orographic soaring in high winds was directly over the leading edge of the building as this provided the best compromise of reduced throttle and control effort. This model relied on the SUAV being directed to maintain trajectory on the crest of the lift tunnel, this could be problematic in real-world applications due to an unknown wind field. However, as the optimum position occurs directly over the leading edge of the building it could be possible to implement an

optic-flow based control scheme. There is potential that an optic-flow system could not only provide a means of identifying the location of the updraught crest but also provide additional feedback in trajectory following [171] and gust stabilisation [172].

Chapter 4 highlighted the suitability of gulls to the urban environment. The LBB and HG are facultative soaring birds, this facilitates energy savings through soaring as well as the ability to perform agile and powerful manoeuvres such as those required when reacting to gusts, avoiding obstacles and when foraging on-the-wing, as well as during ground based take-off and landing. All of these are traits that could be desirable in urban SUAVs so it could be worth considering gull wing morphology when designing urban ready platforms. Not all urban environments are the same, in the UK the buildings are relatively low in height and there tends be green spaces integrated within the city. Additionally, the weather is highly variable, with warm weather in the summer producing thermals but overcast and windy weather tends to be the norm for most of the year. Therefore, the most suitable platforms would be primarily optimised for wind based energy harvesting but also with the ability to perform thermalling. However, if an engineer was designing SUAV platforms for a hotter climate they may want to optimise for thermal-based soaring. A good strategy would be to observe the popular bird species living in that location, for example, in much of Florida it is common to see Vultures living in urban areas and they can be seen thermalling for much of the year. Therefore, when designing a platform to be used in a city such as Orlando, it could be more beneficial to implement wing morphology optimised primarily for thermal soaring.

City substrates tend to have material properties which lend themselves to thermal propagation such that in the right weather conditions the urban environment can have an abundance of thermal sources, a combination of thermal columns and bubbles, both of which can be used for soaring. Chapter 4 found that during the summer breeding season the gulls implemented extensive use of thermal to cut energy costs. Despite not being as morphologically suited to thermal based soaring as other birds, the gulls were still able to perform commuting flights with as much as 100% soaring. Clearly, thermals can provide a suitable source of energy for soaring in urban environments but a problem remaining is the ability to predict the locations of thermals. Recent work has seen the development of a fully autonomous thermal soaring UAV [173, 174] in which a dynamic map of thermal was updated on-the-fly and used to achieve long endurance flights lasting over an hour with almost no propulsion. The flight test took place at a location which was known to experience thermals based on the number of soaring birds in the area meaning that the UAV was almost guaranteed to find a thermal source. This could be a different

matter when flying in a city unguided. It is expected that birds uses visual cues to find thermals such as cloud features or other birds thermalling, so perhaps computer vision will be applied to this task in the future. A potential alternative could be to integrate some level of thermal map within a UAV route network, sensors could be placed in areas where thermals are likely to propagate, such as car parks, such that the state of thermal hotspots could be known in advance. Furthermore, certain locations could be designed with thermal propagation in mind, for example, a UAV delivery company could coat the roof of warehouse buildings with a bespoke material in order to make thermal development more likely.

In Chapter 4, it was discovered that the gulls optimised for velocity in both flapping and soaring flight modes and that utilising both flight behaviours together could lead to greater energy savings. By flying at minimum power velocity in flapping flight the birds were able to quickly slow down or speed up at very little extra cost and this is likely to facilitate an increase in energy harvesting on windy days. In Chapter 5 this was further confirmed with evidence of power assisted gradient soaring. In this strategy, the platform soared into the wind but used powered flight downwind. This was an effect means of reducing flight costs but requires dual-flight modes. Recent hardware developments mean propellers are now capable of self-folding [175] which can reduce drag, and even regenerative braking [176, 177]. Regenerative soaring has the potential to be implemented in long periods of gliding, in consistent energy harvesting such as in static soaring, or during the soaring headwind sections of flight in the gradient based soaring technique. While energy gain from regenerative braking systems are minor, it could be sufficient in supplying all non-motor based power requirements (communications, sensors, etc.) which could result in zero cost periods of soaring flight.

In Chapter 5 an A* algorithm with an ideal heuristic was compared to a greedy, short-horizon algorithm. Both algorithms have shortcomings, the A*-ideal path planner struggles with scalability, requiring large computation times and memory. On the other hand, the DFS algorithm with a greedy heuristic returns sub-optimal solutions but performed well in computation solve times and low memory use. The A*-ideal planner produced flights with an average of 20% more soaring than the more local GDFS planner, however, the reduce computation time meant that the GDFS was a more realistic simulation method. For this reason the GDFS was used to explore the effects of adjusting power cost ratios and found that energy costs in fixed location flights could be as much as halved when costs between powered and soaring flight modes matched that of a SUAV. For this research, it was not possible to explore the power cost ratios with the global

planner due to the increase in solve times but future work could consider whether energy savings could be increased by adopting a different path planner, for example, integrating a receding horizon, adding random walk such as with RRT algorithms, or adding multi-objective optimisation. Furthermore, the velocity optimisation and gradient soaring strategies require an accurate method of wind sensing, both instantaneous conditions and predictive gradients, sensors such as these have recently become available and have demonstrated potential in both gust stabilisation and gradient soaring applications [76, 152, 178] so the obvious next stage of research is to characterise sensors such as these and implement them in an upgraded path planner with a truly naive wind field. Additionally, it would be interesting to discover how much imperfect sensing and variable wind fields reduce performance. Introducing these factors would effect both the shortest path flights as well as the path planner trajectories as both cases implemented wind-aware velocity optimisation, however, it is not known to what extent sensor uncertainty and turbulence may factor. Additional upgrades to the path planner could include a full dynamics and control model for a gull sized SUAV, as the point mass model has limited accuracy. The power and glide performance curves will also effect the results due to their role in determining the optimum velocity which has an impact on the ability to perform gradient soaring.

There were two gradient soaring techniques demonstrated in Chapter 5; a power-assisted shallow-arc soaring strategy which utilised strategic changes of orientations within a cross-wind, and a dolphin soaring strategy that used pockets of updraughts. However, there could be more wind-gradient based energy sources available within the urban environment [8]. For example, wind shear is available in more urban locations such as on the lee-ward side of buildings, or at the corner of a building where wind shadowing can occur. Other gradients could also be useful, as an example, the wind funnelling effect of urban canyons could be used to increase inertial speed. Future research could investigate other sources of wind gradients to see if these could also facilitate gradient soaring strategies. While birds can offer inspiration for flight techniques they don't necessarily operate under the same performance constraints. For example, gulls use a limited range of their possible airspeed so would not perform sling shot manoeuvres which could combine the shear layer at the corner of a building with fast funnelled wind in the urban canyon, however, this could be beneficial for an SUAV immediately following take-off.

Cities of the future will no doubt have SUAVs occupying the airspace. SUAV technology is rapidly advancing and small platforms have already started demonstrating worth

in both commercial and public service domains. Occupation of the airspace will require careful planning as the number of aerial vehicles, which current consists mainly of manned aircraft, looks to expand a hundred, if not a thousand, fold to include UAVs with various levels of autonomy. The Single European Sky Air Traffic Management Research (SESAR) group have recently published an updated to their proposal for the integration of UAS into a traffic management system and it includes pre-defined routes, similar to the road and air traffic systems currently in place [179]. UAS airspace integration would unify airspace management but could limit the soaring potential of SUAVs which require dynamic planning flexible with variable wind conditions. It would be advisable for wind conditions of urban airspaces to be considered in the design of these routes. For example, the consideration of any prevailing wind direction and average wind speed could be used find the cost effective routes. Rows of high-rise buildings could be built such that they generate lift and also shelter the rest of the urban area from strong winds or even facilitate wind-based renewable energy with the installation of wind turbines. An additional health and environmental benefit of successfully integrating SUAV transport would be the reduction of road traffic and consequential air pollution, a great problem of our time. As UAVs become more integrated in urban life, potentially providing communication networks, performing dull maintenance jobs, delivering commercial or emergency medical supplies, it could become a priority manipulate the airspace to facilitate soaring SUAVs. However, when designing the cities of the future it will also be important for engineers to consider the nature already habiting the airspace. Birds have and still do, teach us so much with regards to flight, from the formative years not much longer than a century ago, right through to the modern day and the development of autonomous soaring vehicles.

APPENDIX A

APPENDIX A: GULL BIOMETRICS

Record of the gull biometrics collected at the time of capture and tagging.

Table A.1: Gull biometrics: case 2

TagID -	**Sex** -	**Year** -	**Head** (mm)	**Bill** (mm)	**Nostril** (mm)	**Base** (mm)	**Gonys** (mm)	**Tarsus** (mm)	**Span** (m)	**Mass** (Kg)	**Wing** (m^2)	**AR** -	**MAC** (m)	**Front** (m^2)
5307	F	2016	106.45	46.55	20.90	17.35	16.25	59.65	1.192	0.658	0.177	8.018	0.149	0.0062
5308	F	2016	109.70	45.65	21.45	18.10	16.60	61.20	1.055	0.790	0.157	7.099	0.149	0.0070
5309	F	2016	113.00	49.10	23.80	18.40	16.50	NA	1.078	0.760	0.140	8.285	0.130	0.0068
5310	F	2016	108.80	49.35	21.50	19.50	16.65	61.45	1.233	0.655	0.179	8.501	0.145	0.0061
5311	F	2016	112.70	48.80	24.00	18.35	16.40	62.45	1.240	0.758	0.196	7.843	0.158	0.0068
5476	F	2017	109.50	NA	NA	16.80	NA	NA	1.228	0.710	0.190	7.960	0.154	0.0065
5478	M	2017	115.80	NA	NA	17.50	NA	NA	1.092	0.765	0.170	7.018	0.156	0.0068
5479	F	2017	109.40	NA	NA	16.85	NA	NA	1.041	0.720	0.143	7.603	0.137	0.0065
5481	F	2017	109.35	NA	NA	15.40	NA	NA	1.119	0.710	0.165	7.589	0.147	0.0065
5482	M	2017	119.00	NA	NA	18.15	NA	NA	1.179	0.870	0.191	7.265	0.162	0.0074
5484	F	2017	110.25	NA	NA	16.45	NA	NA	1.122	0.810	0.150	8.382	0.134	0.0071
5485	F	2017	107.15	NA	NA	12.00	NA	NA	1.171	0.690	0.159	8.623	0.136	0.0064
5555	**A**	**2017**	**110.93**	**47.89**	**22.33**	**17.07**	**16.48**	**61.19**	**1.146**	**0.741**	**0.168**	**7.849**	**0.146**	**0.0067**

APPENDIX B

APPENDIX B: URBAN GULL DATABASE

The Urban Gull database was created in order to manage the large number of amalgamated datasets. At the highest tier, the bird data was split into three main data tables relating to the biometrics, nest status and tag calibration, these tables are linked using the metal ring number. Each tag has an identifier this was used to link the sensor data to the tag. Following this, each GPS fix recorded by the tag has been given a unique identifying number which links behavioural, geographical and weather data tables. One further table was created to keep additional data including breeding phase data collected through observation, trip and flight identification numbers and known locations.

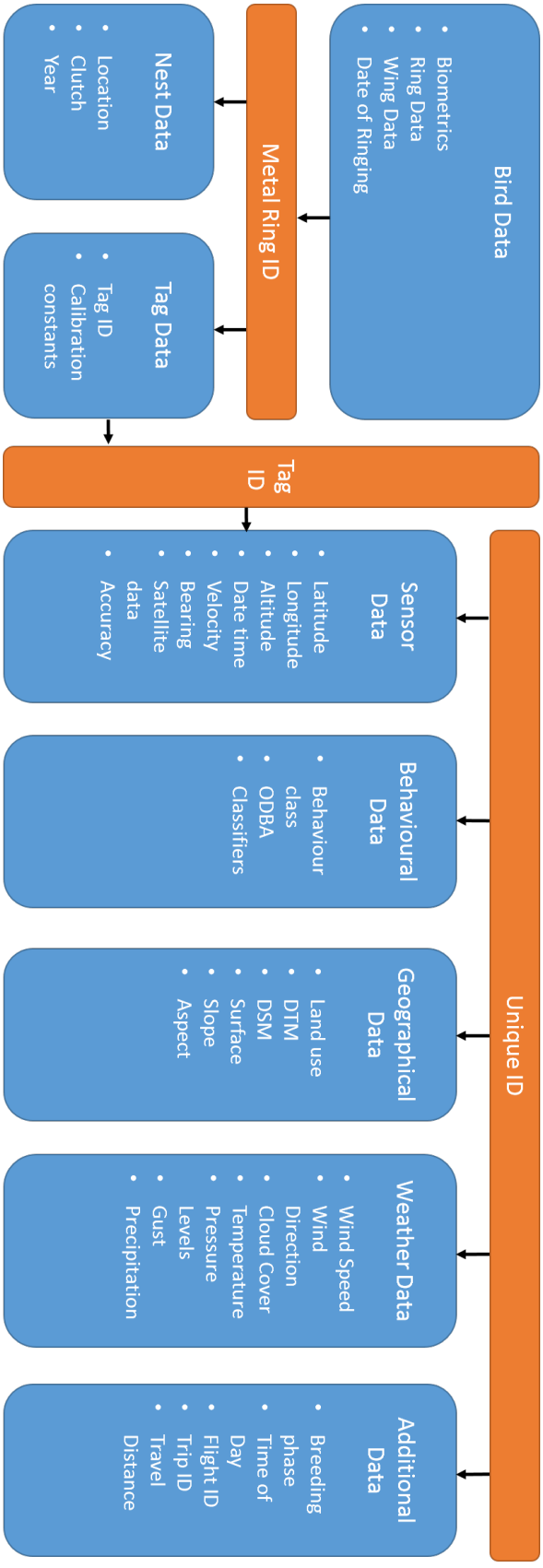

Figure B.1: The urban gull database structure showing the table names with categorise of data in blue and the linking identifiers in orange.

APPENDIX C

Appendix C: Soaring Strategy Validation

The sensitivity test for the soaring strategy validation was performed by varying the threshold values for the flight strategy classification decision tree.

The results from the altitude and circling thresholds in figures C.2 and C.3 are slightly misleading. It appears percentages of flight strategies classified as Orographic and Thermal soaring are feeding into each other but on manual inspection it was found that these are both feeding into the Other classification. This category contains high-altitude, straight flight, and low-altitude, flight with high directional variance. The first is likely an example of gulls flying through detached thermal bubbles. The second, represents circling behaviour on updraughts likely to be generated by wind flow.

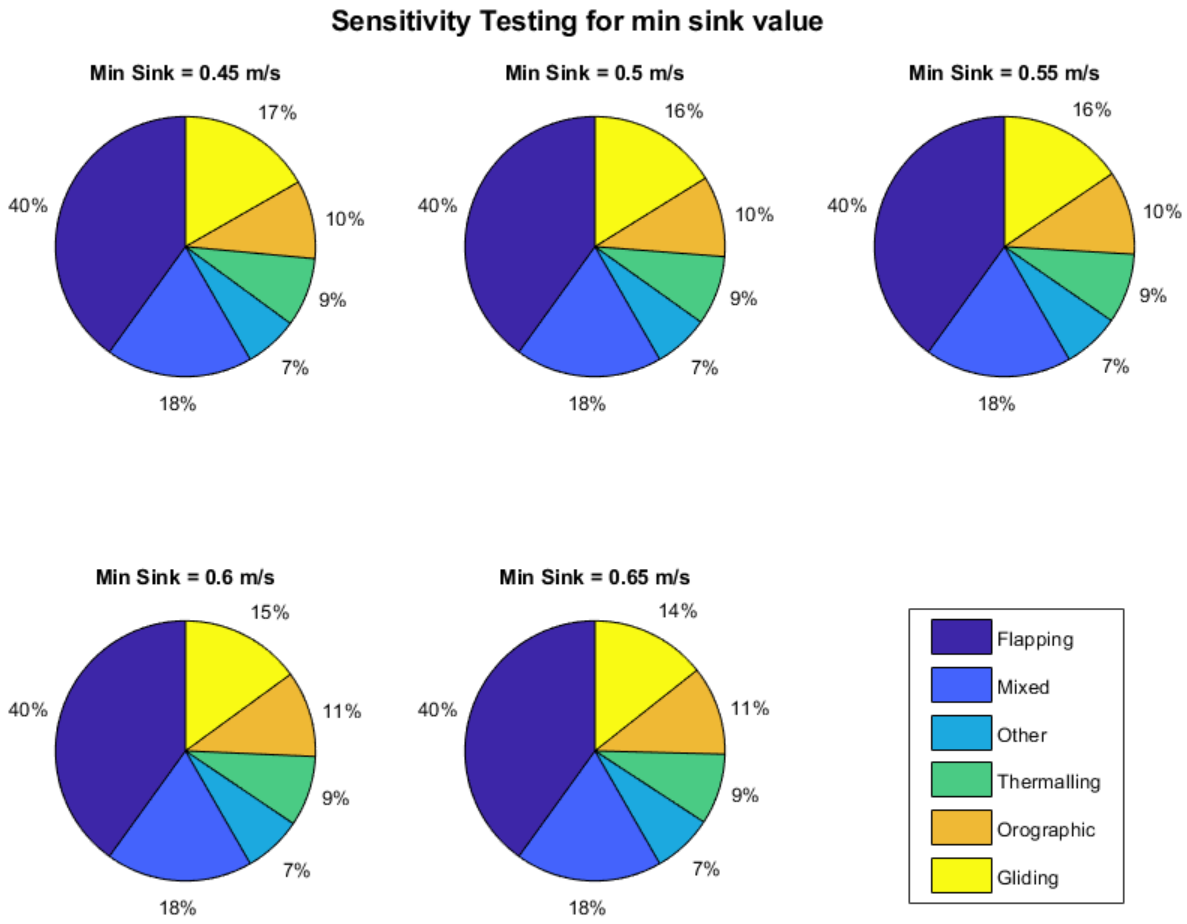

Figure C.1: Sensitivity testing for the minimum sink value shows that the variation in results is minor. Therefore a value of 0.55 m/s was chosen as this is closest to the average minimum sink value of the average LBB model of 0.56 m/s.

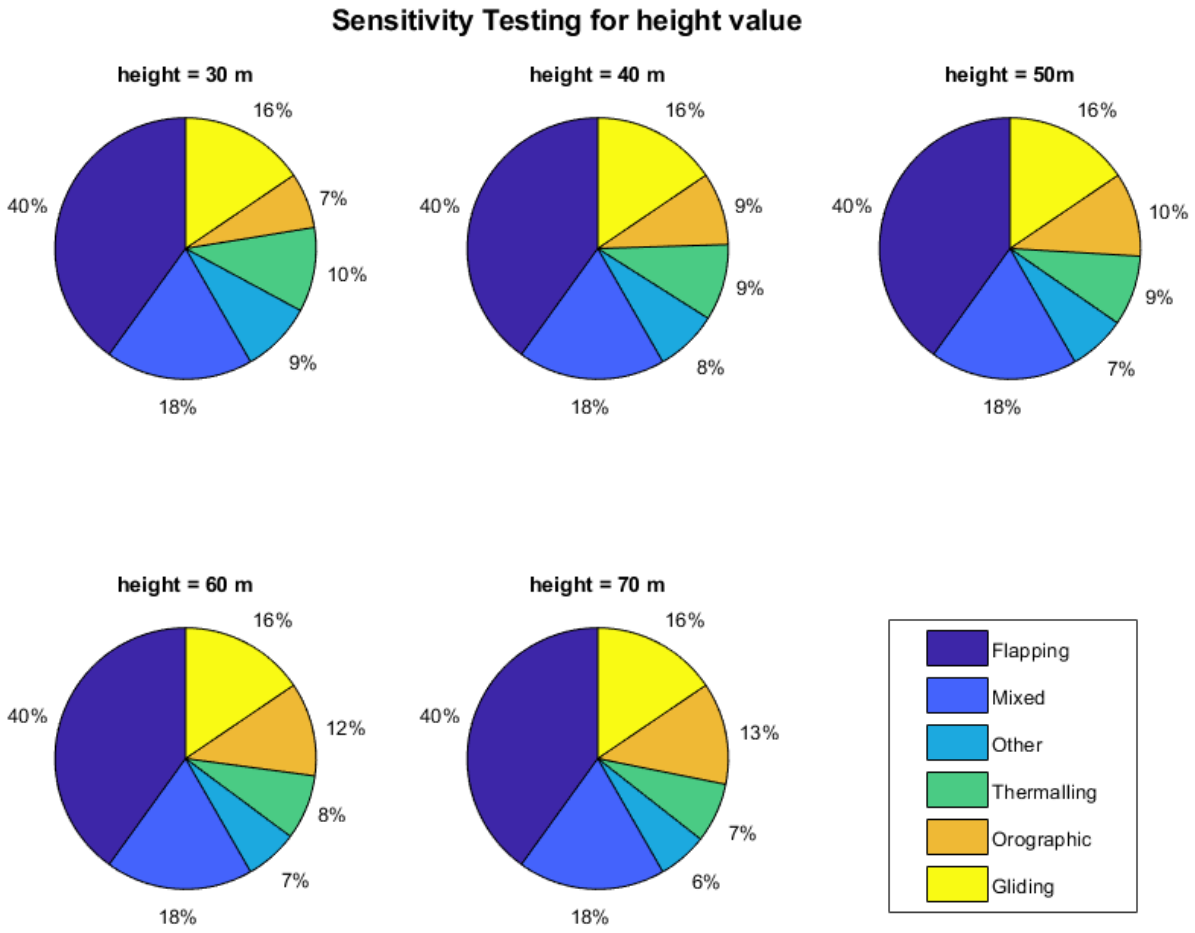

Figure C.2: Sensitivity testing for the height above the surface threshold value used to determine if a gull could be in orographic soaring mode. The values vary by a few percent, as gulls fly an average of 30 meters above the surface but are also able to soar on terrain and very large buildings a higher value was chosen.

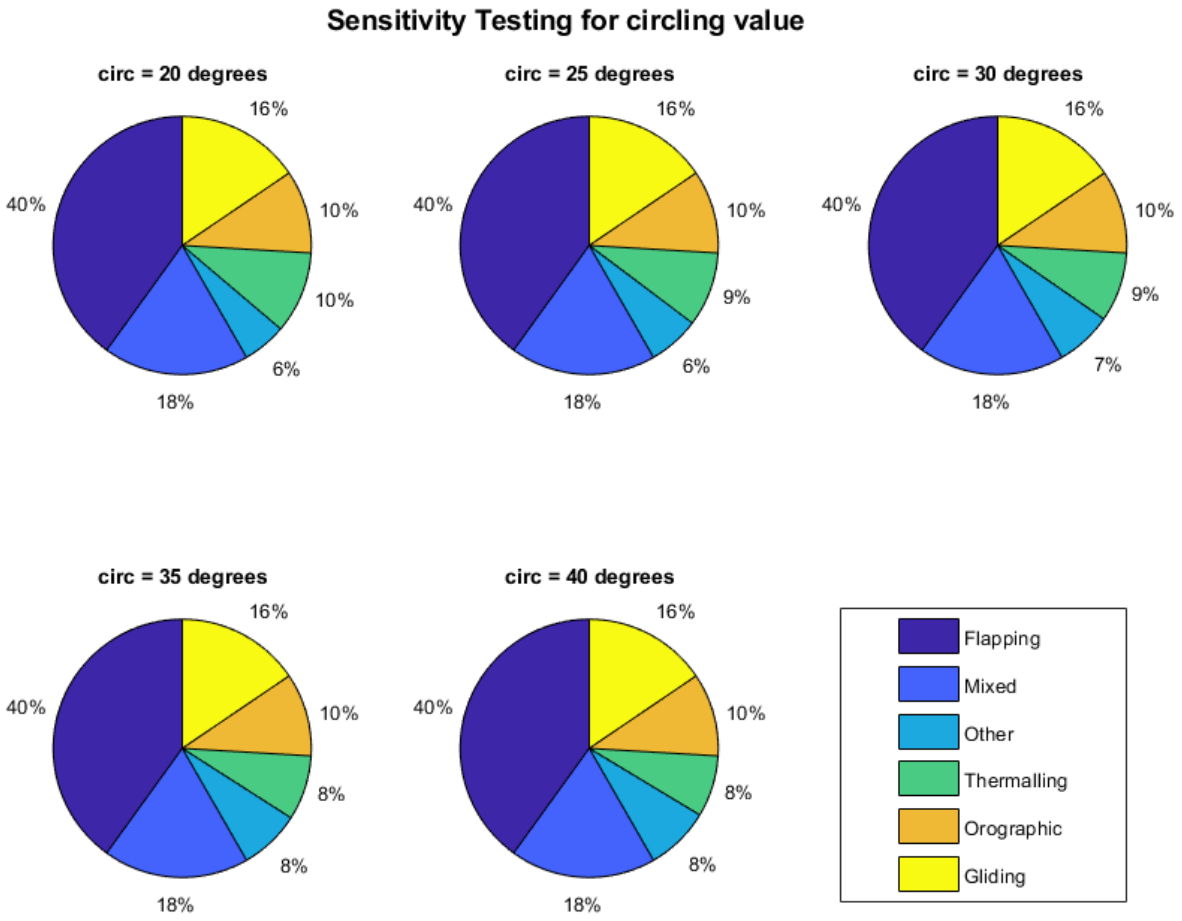

Figure C.3: Sensitivity testing for the directional variation threshold value used to determine if a gull is using circling flight such as when thermalling. There are slight variations between Thermalling and Other flight strategies, these all occur at high altitude when the thermal columns appeared to have a large radii. As such, a relatively low directional variance of 30 degrees was chosen for the threshold value as it included all wide column thermalling examples in a randomly selected observation set.

APPENDIX D

APPENDIX D: COMMUTING FLIGHTS

Additional flight path examples with increasing BMR ratios GBFS simulations compared to gull commuting flights.

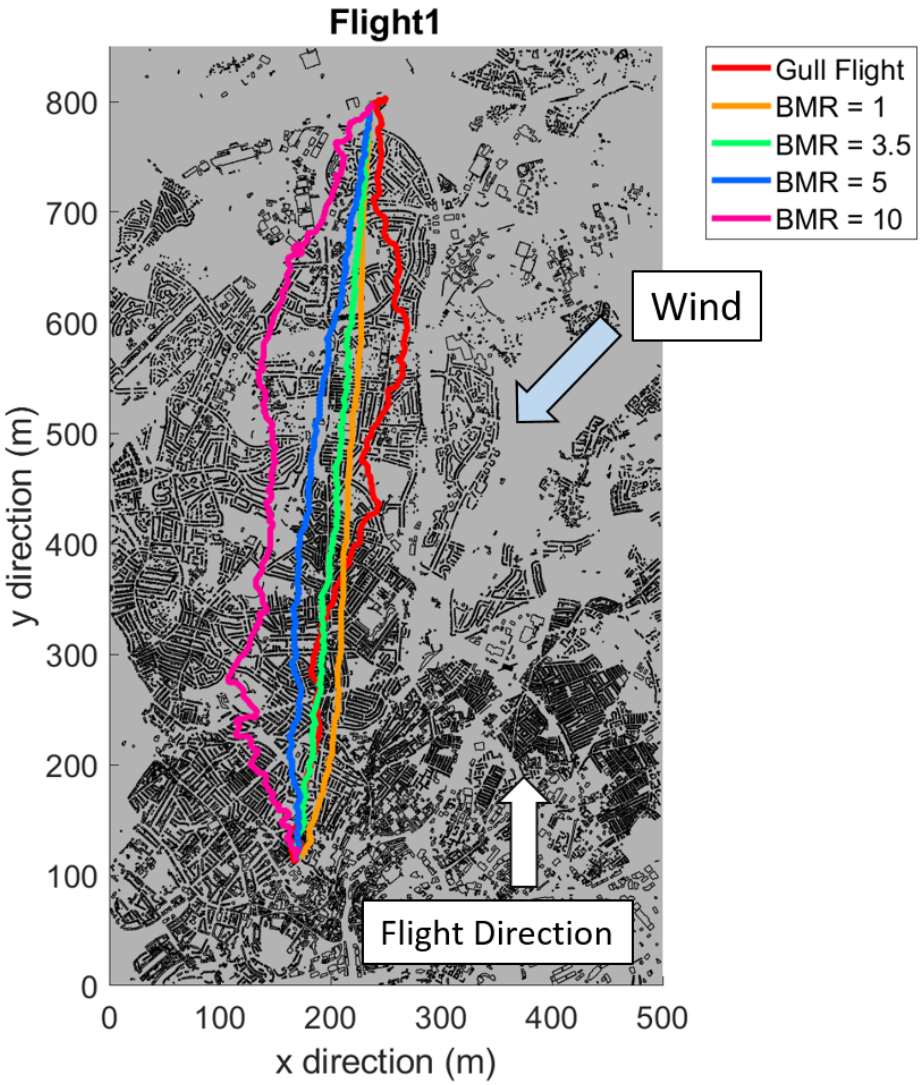

Figure D.1: The simulation examples for BMR ratios 1 (orange), 3.5 (green), 5 (blue) and 10 (pink) accompanied by the corresponding gull flight (red). Flight direction and wind marked with arrows. Wind speed = 2.75 ms^{-1}, Wind Direction = 50.0° from North.

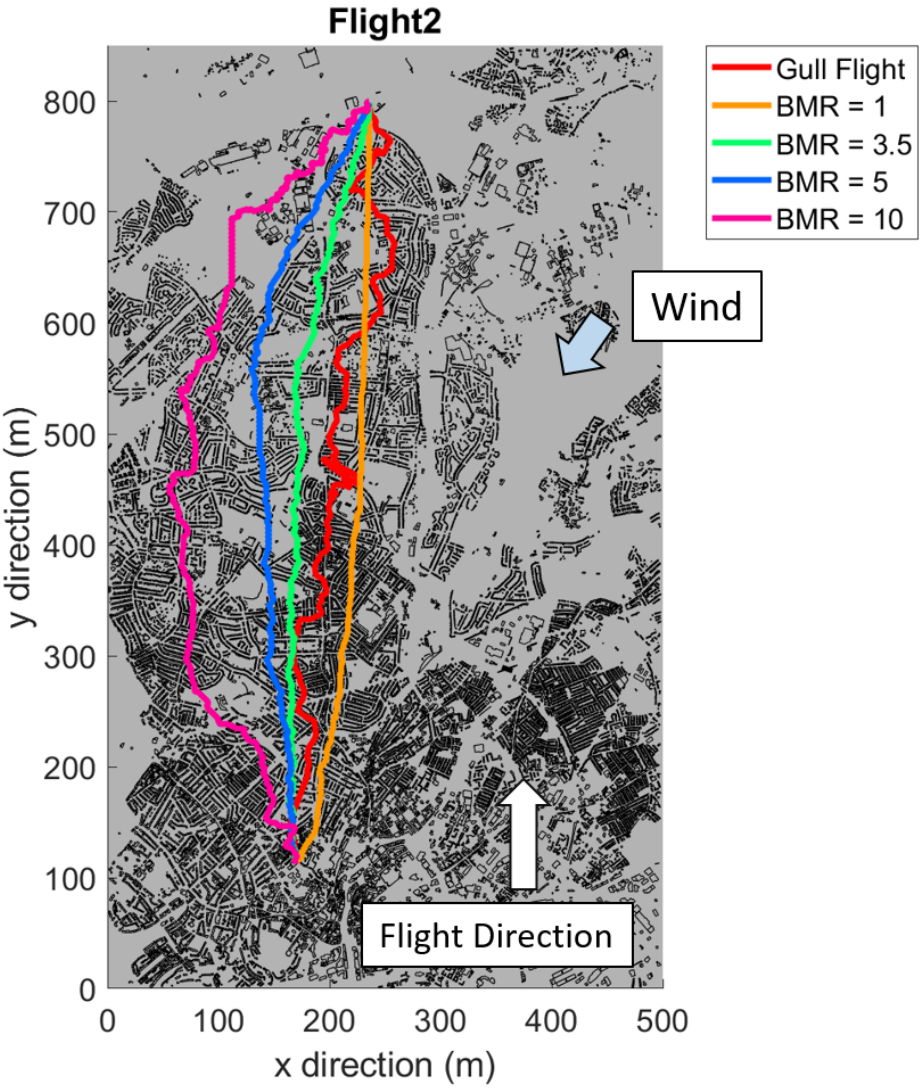

Figure D.2: The simulation examples for BMR ratios 1 (orange), 3.5 (green), 5 (blue) and 10 (pink) accompanied by the corresponding gull flight (red). Flight direction and wind marked with arrows. Wind speed = 6.16 ms^{-1}, Wind Direction = 56.5° from North.

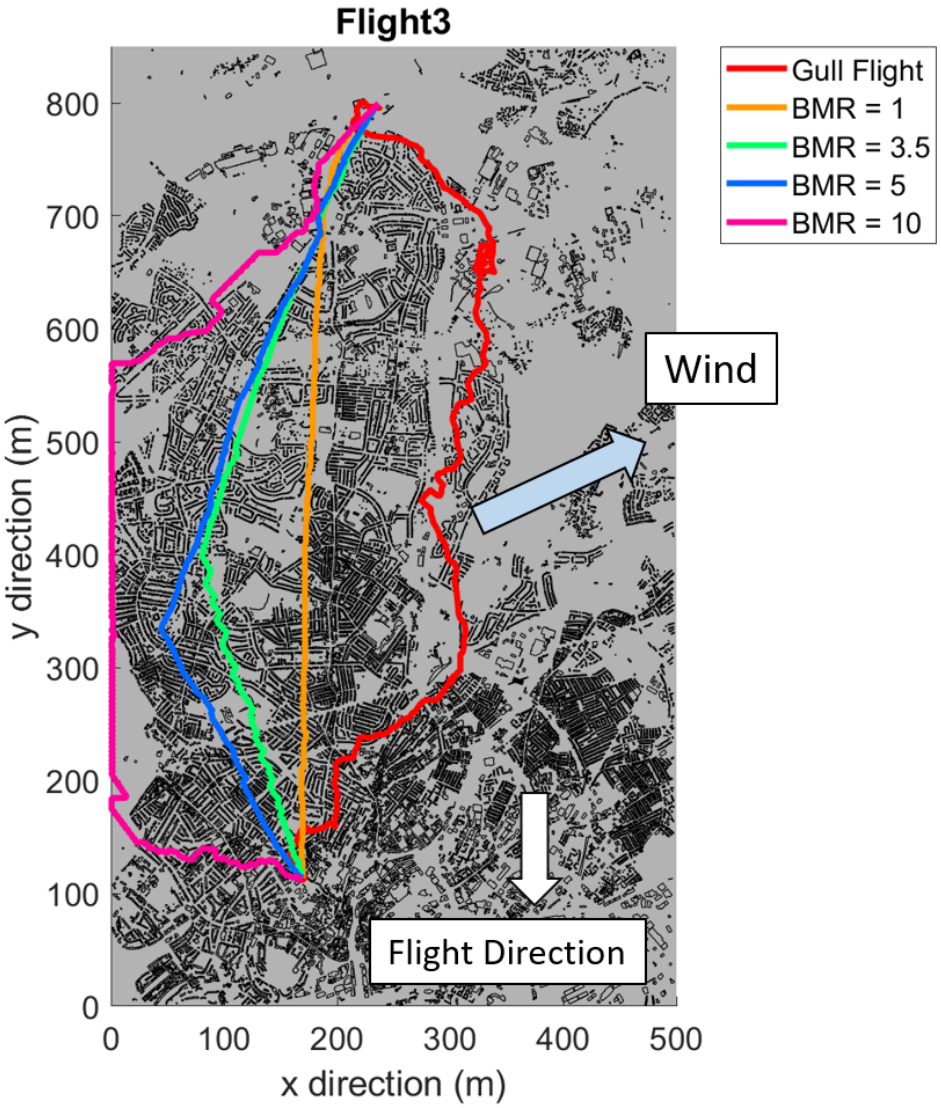

Figure D.3: The simulation examples for BMR ratios 1 (orange), 3.5 (green), 5 (blue) and 10 (pink) accompanied by the corresponding gull flight (red). Flight direction and wind direction marked with arrows. Wind speed = 8.13 ms^{-1}, Wind Direction = 258.4° from North.

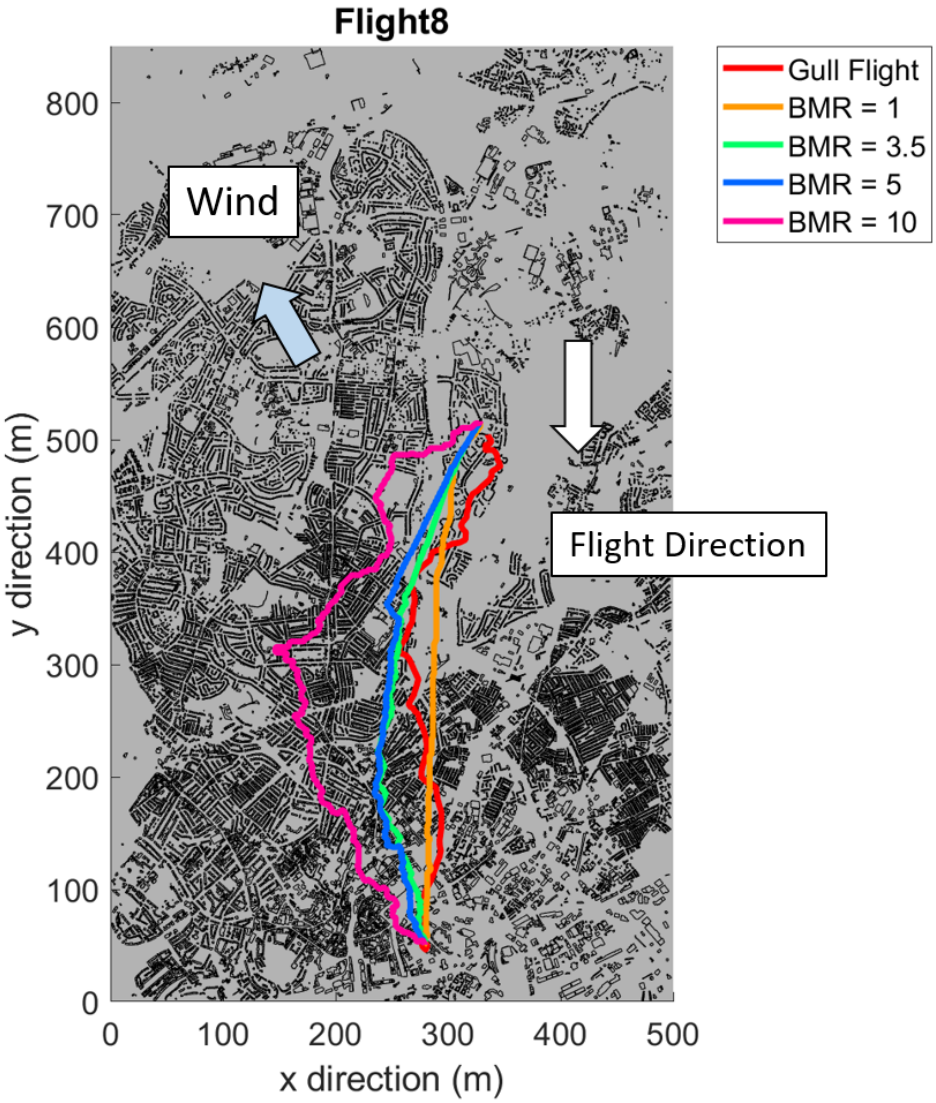

Figure D.4: The simulation examples for BMR ratios 1 (orange), 3.5 (green), 5 (blue) and 10 (pink) accompanied by the corresponding gull flight (red). Flight direction and wind direction marked with arrows. Wind speed = 4.15 ms^{-1}, Wind Direction = 150.0° from North.

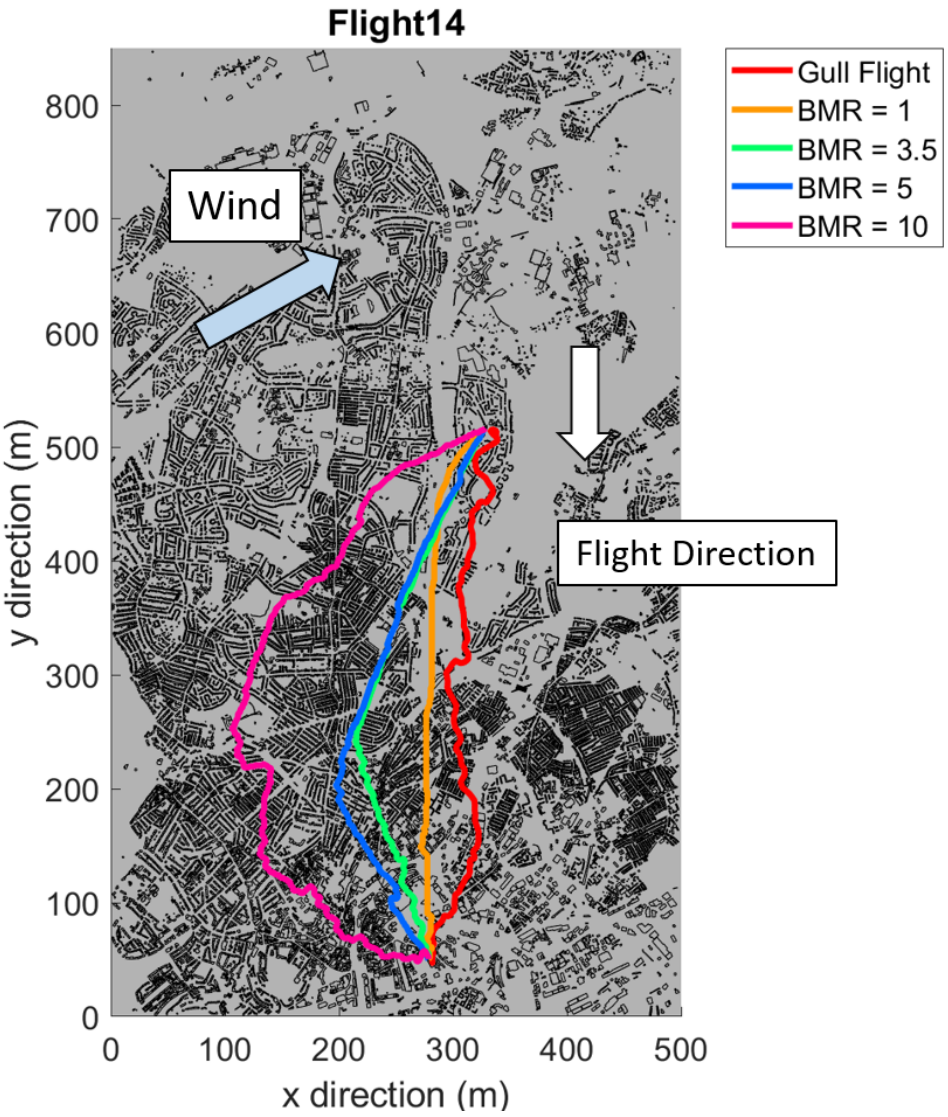

Figure D.5: The simulation examples for BMR ratios 1 (orange), 3.5 (green), 5 (blue) and 10 (pink) accompanied by the corresponding gull flight (red). Flight direction and wind direction marked with arrows. Wind speed = 6.97 ms^{-1}, Wind Direction = 254.0° from North.

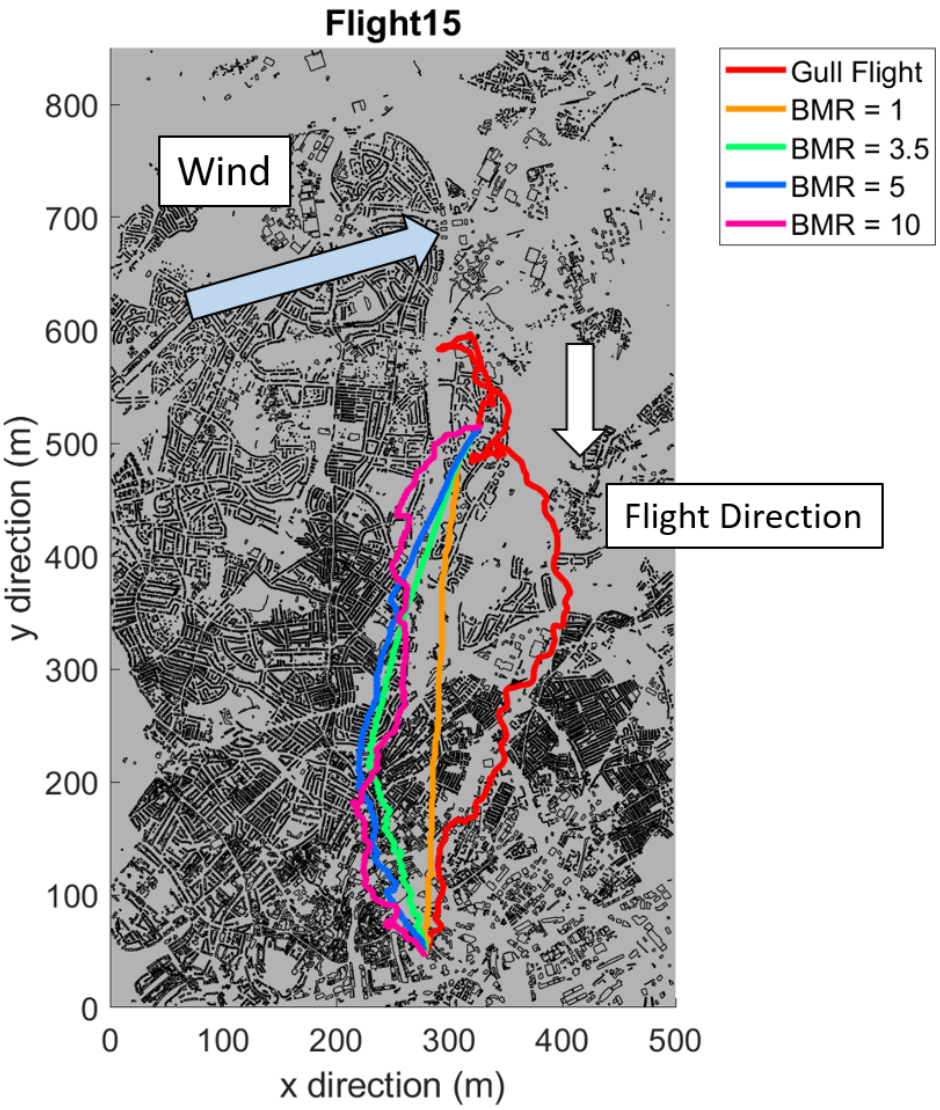

Figure D.6: The simulation examples for BMR ratios 1 (orange), 3.5 (green), 5 (blue) and 10 (pink) accompanied by the corresponding gull flight (red). Flight direction and wind direction marked with arrows. Wind speed = 11.4 ms^{-1}, Wind Direction = 267.1° from North.

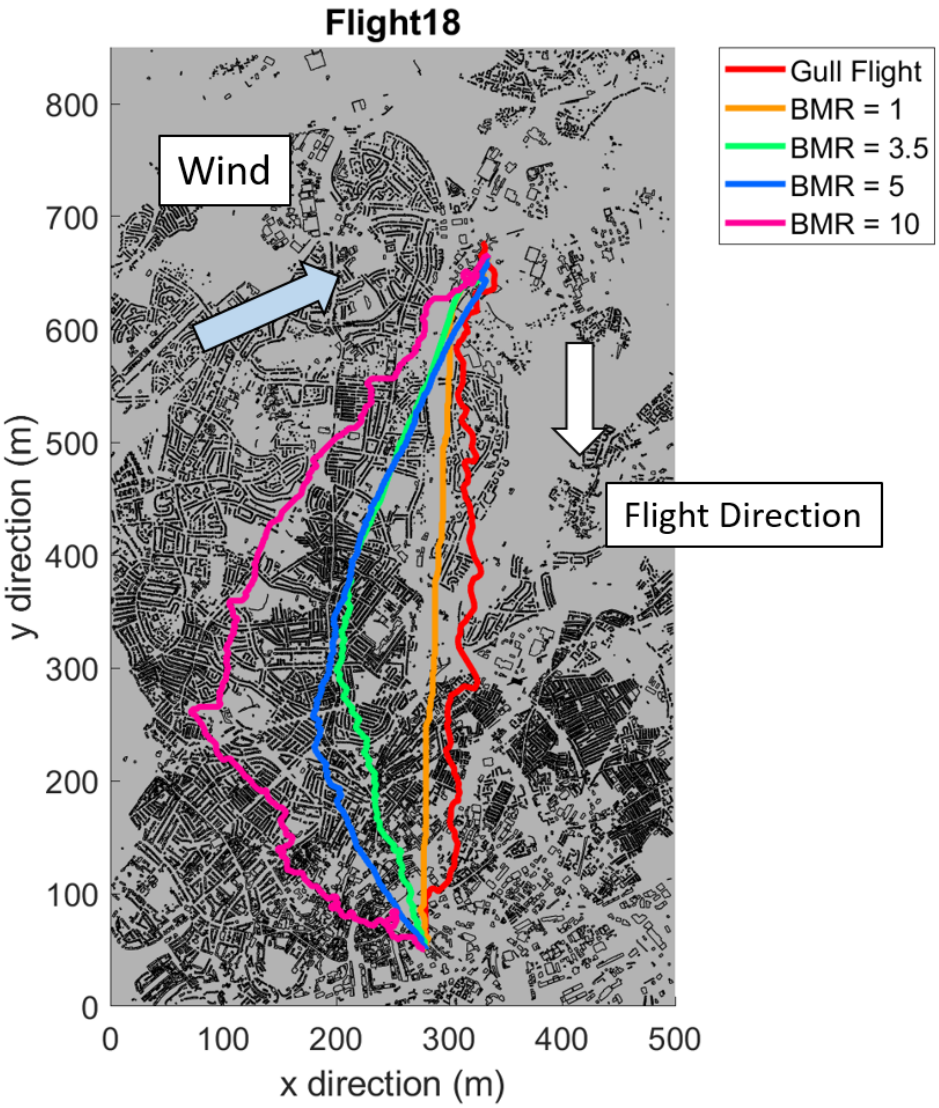

Figure D.7: The simulation examples for BMR ratios 1 (orange), 3.5 (green), 5 (blue) and 10 (pink) accompanied by the corresponding gull flight (red). Flight direction and wind direction marked with arrows. Wind speed = 6.85 ms^{-1}, Wind Direction = 259.0° from North.

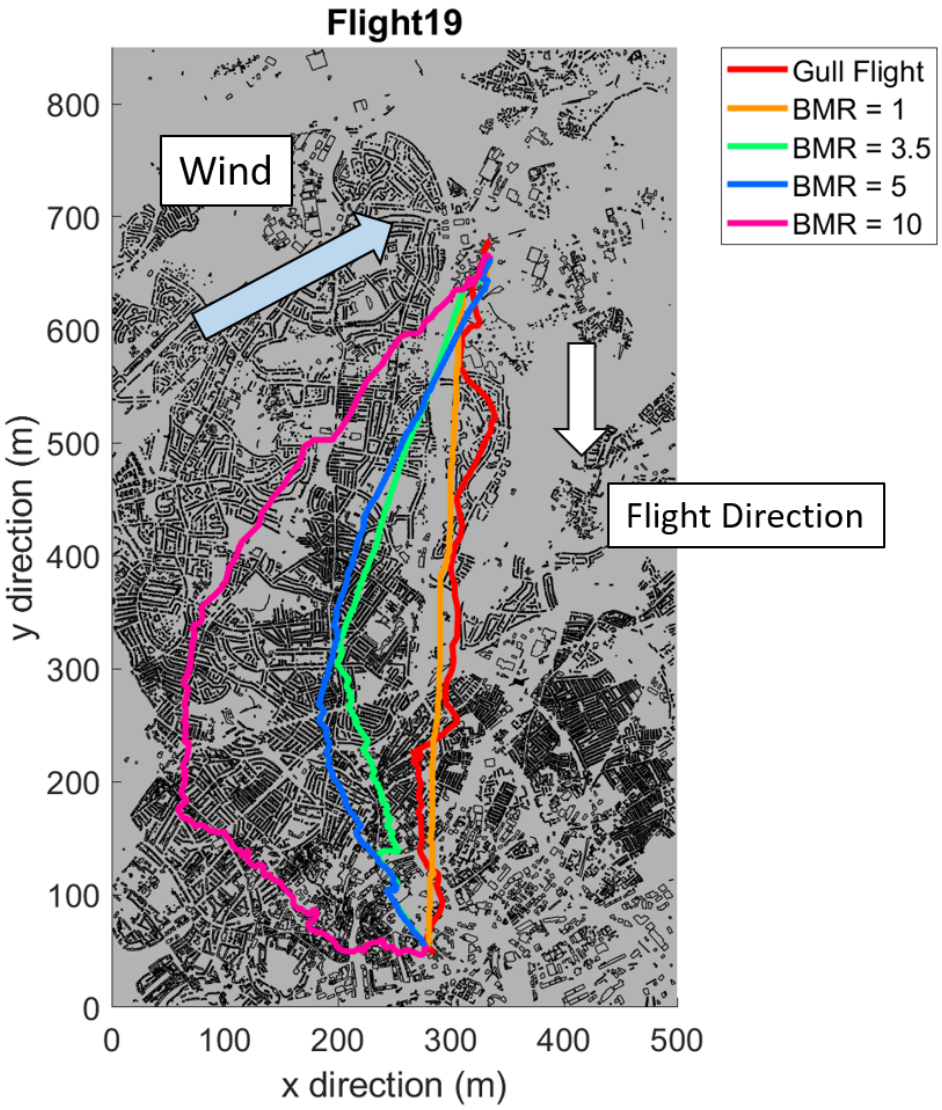

Figure D.8: The simulation examples for BMR ratios 1 (orange), 3.5 (green), 5 (blue) and 10 (pink) accompanied by the corresponding gull flight (red). Flight direction and wind direction marked with arrows. Wind speed = 9.5 ms^{-1}, Wind Direction = 254.9° from North.

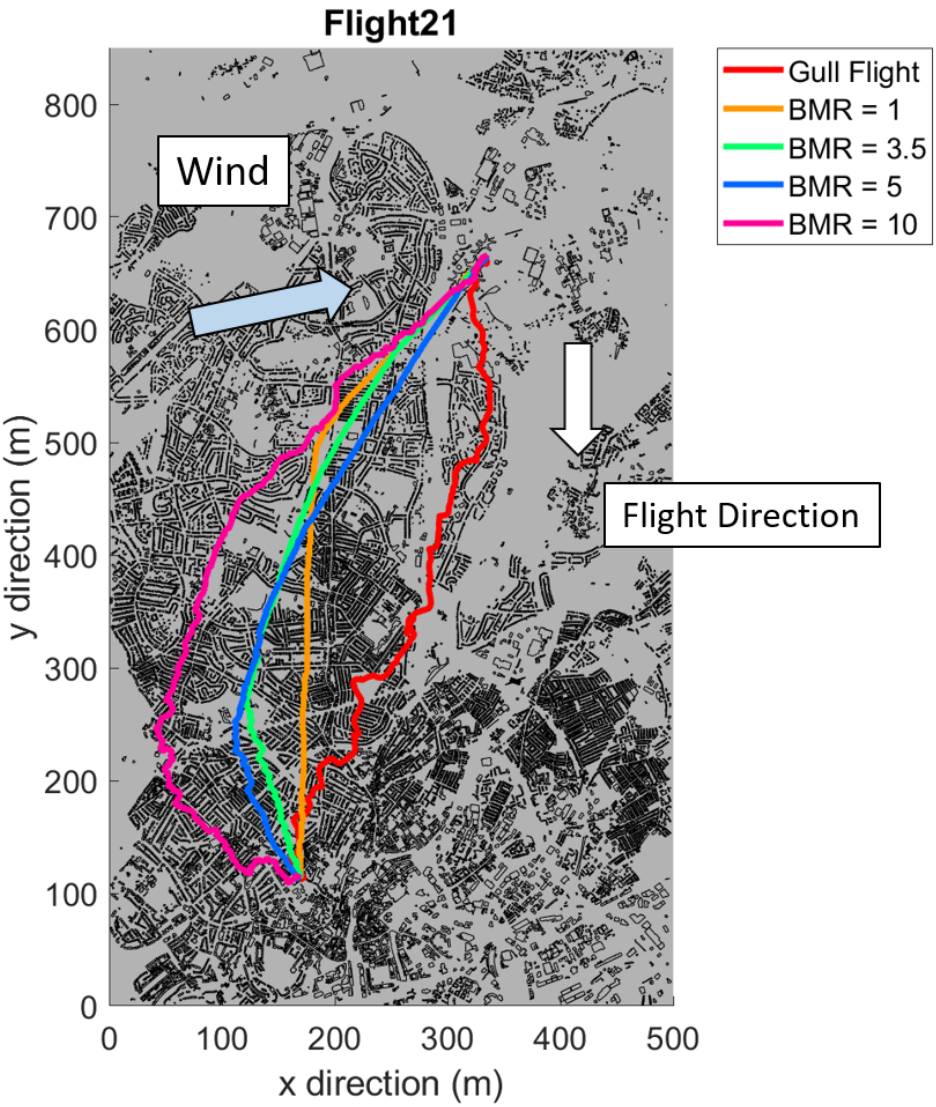

Figure D.9: The simulation examples for BMR ratios 1 (orange), 3.5 (green), 5 (blue) and 10 (pink) accompanied by the corresponding gull flight (red). Flight direction and wind direction marked with arrows. Wind speed = 7.2 ms^{-1}, Wind Direction = 271.2° from North.

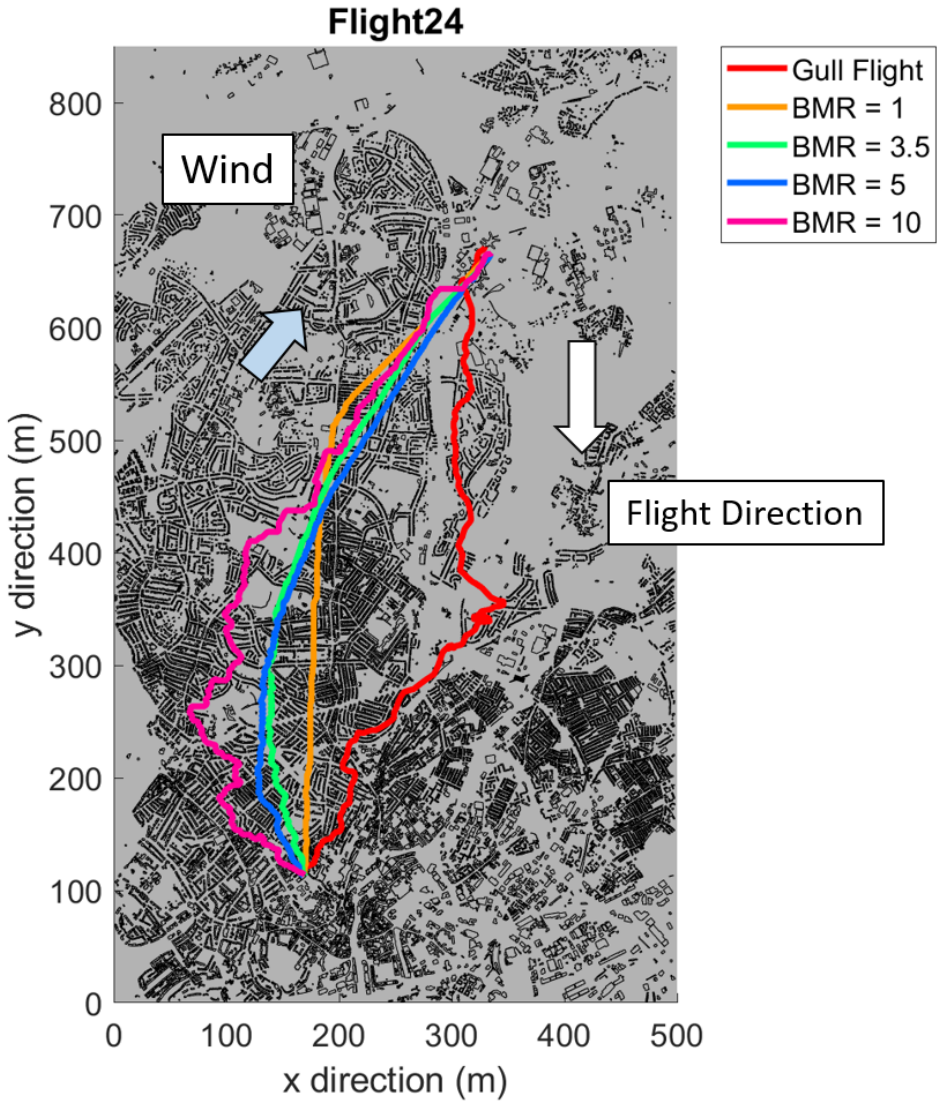

Figure D.10: The simulation examples for BMR ratios 1 (orange), 3.5 (green), 5 (blue) and 10 (pink) accompanied by the corresponding gull flight (red). Flight direction and wind direction marked with arrows. Wind speed = 3.7 ms^{-1}, Wind Direction = 232.3° from North.

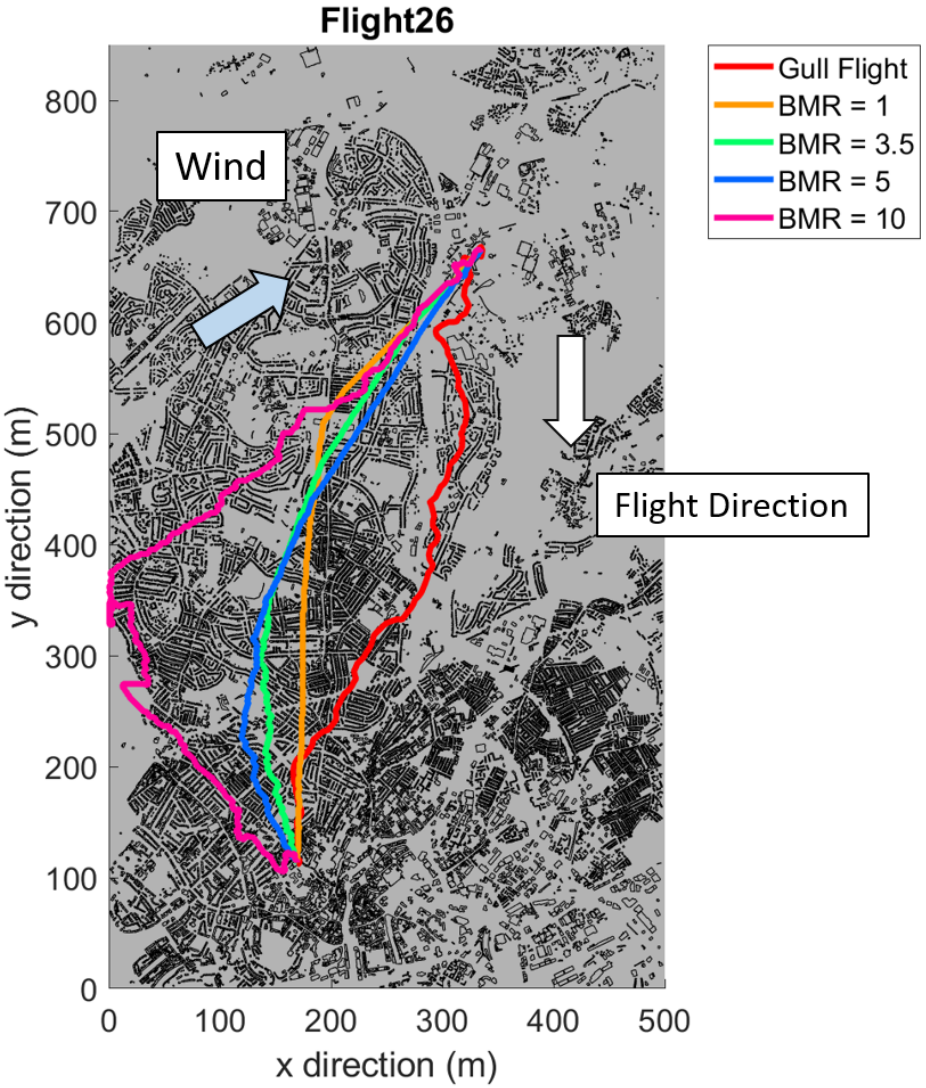

Figure D.11: The simulation examples for BMR ratios 1 (orange), 3.5 (green), 5 (blue) and 10 (pink) accompanied by the corresponding gull flight (red). Flight direction and wind direction marked with arrows. Wind speed = 251.3 ms^{-1}, Wind Direction = 254.9° from North.

APPENDIX E

APPENDIX E: GRADIENT SOARING

Additional gradient soaring examples found in simulation and gull trajectories.

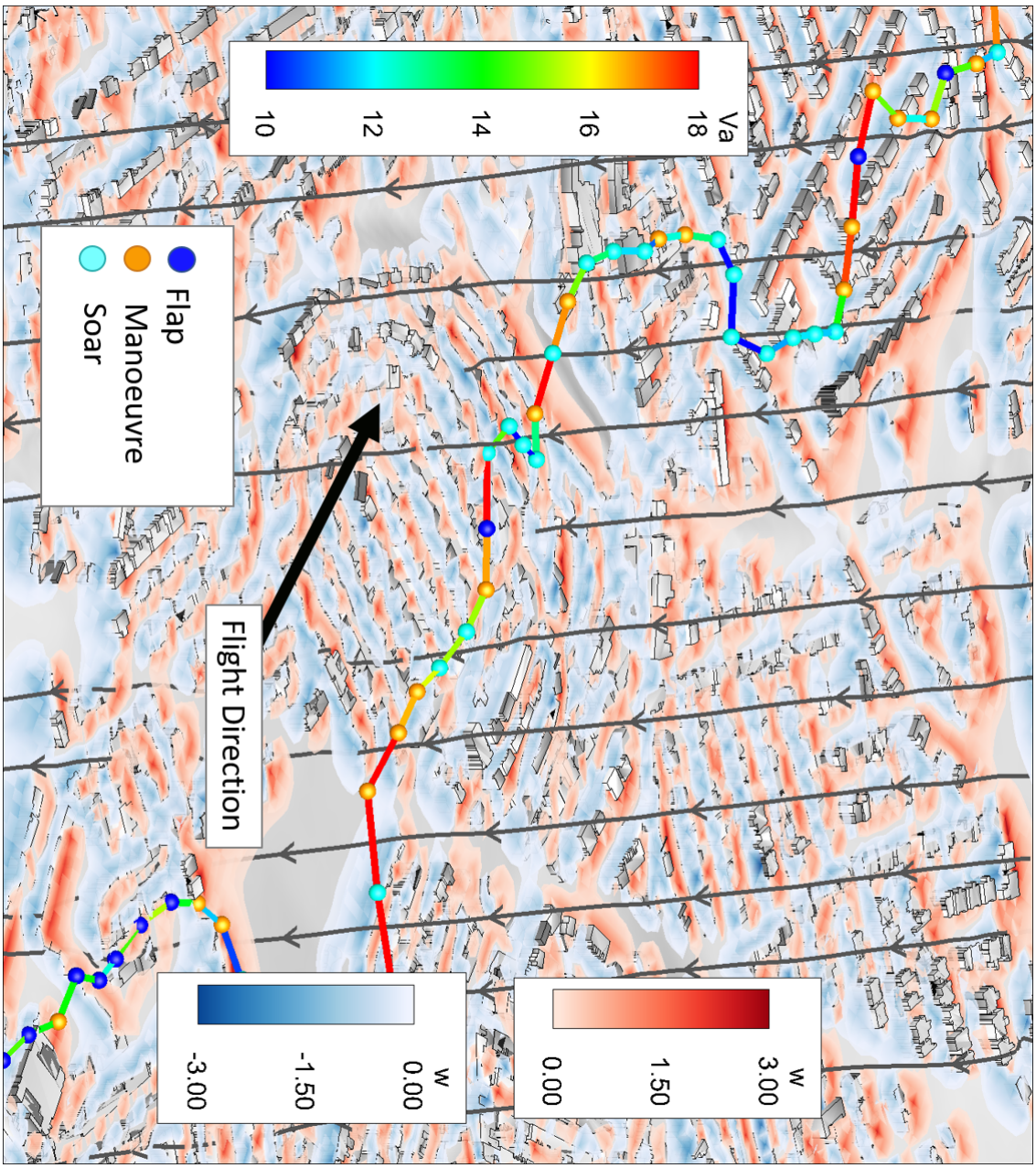

Figure E.1: Gradient soaring behaviour in a gull a variation of flight direction and airspeed allow for a high percentage of soaring flight while traversing a strong horizontal wind gradient. The wind direction is shown by the flow vectors (grey) and the vertical wind, w, demonstrates the up- and down-draught

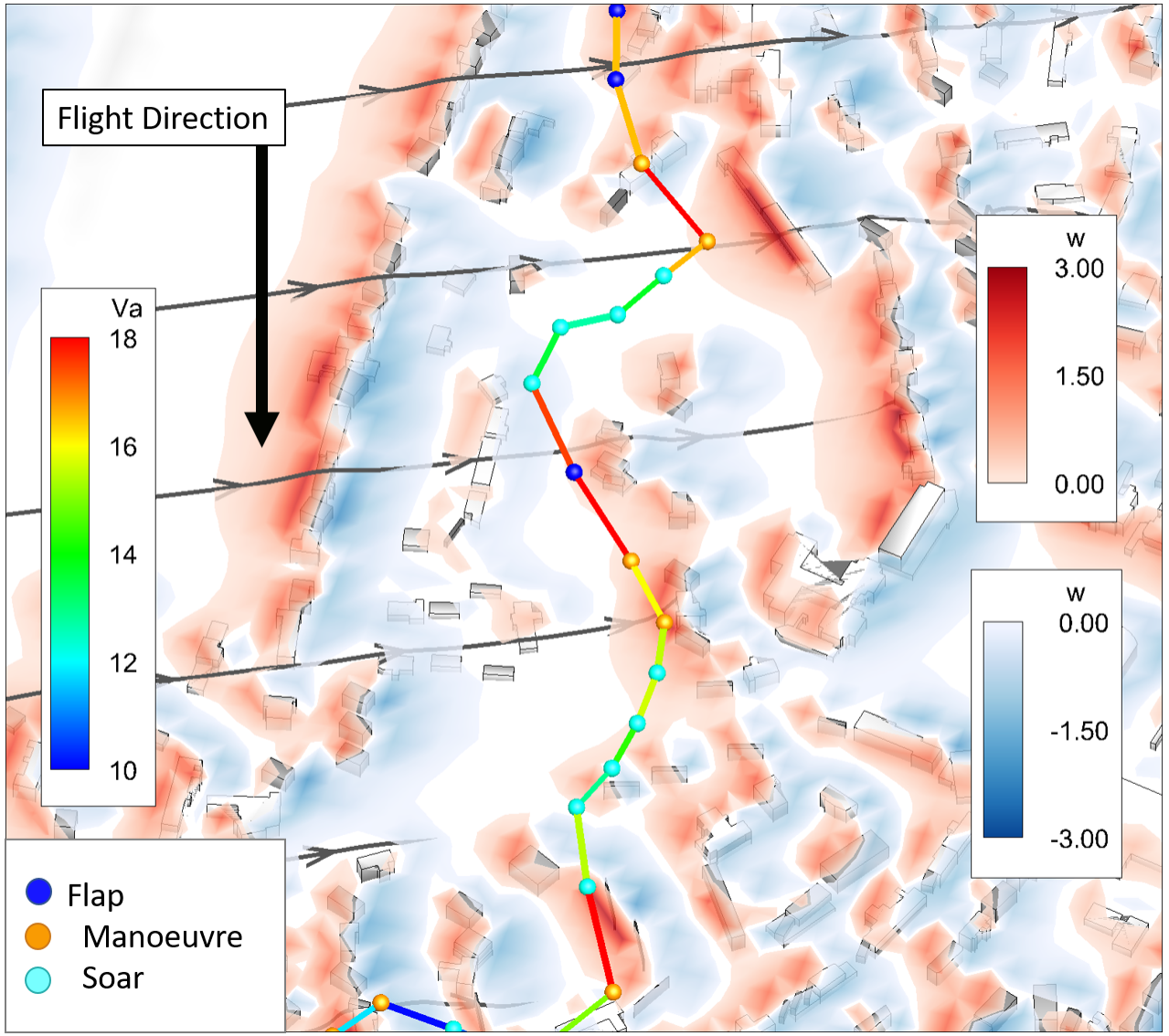

Figure E.2: Gradient soaring behaviour in a gull a variation of flight direction and airspeed allow for a high percentage of soaring flight while traversing a strong horizontal wind gradient. The wind direction is shown by the flow vectors (grey) and the vertical wind, w, demonstrates the up- and down-draught

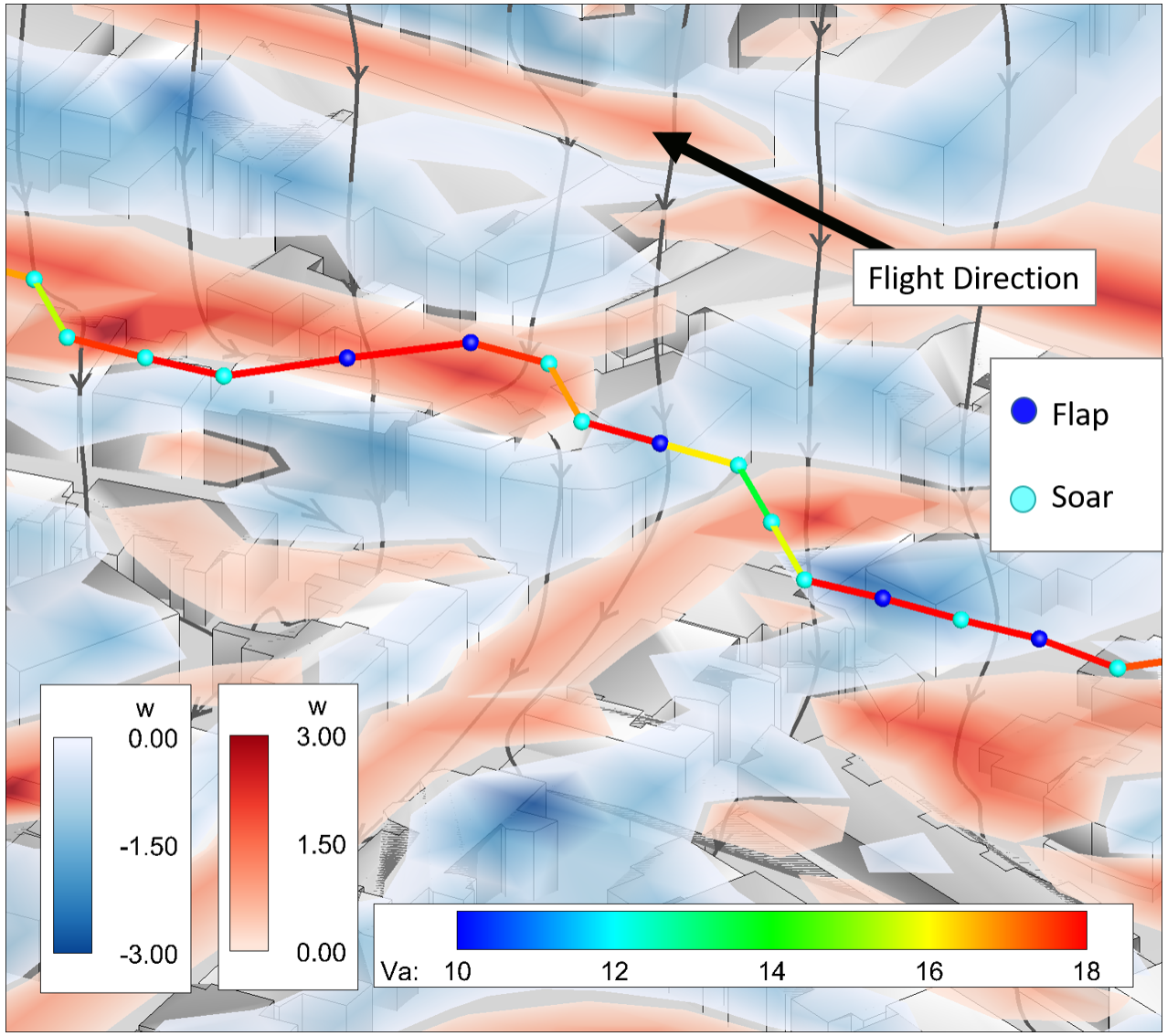

Figure E.3: Dolphin soaring being implemented by the path planner. The plots show a similar technique used in both cases where soaring occurs in the updraught before diving in the down draught, as the down draught finishes there is added lift reinitiating climb. The wind direction is shown by the flow vectors (grey) and the vertical wind, w, demonstrates the up- and down-draughts.

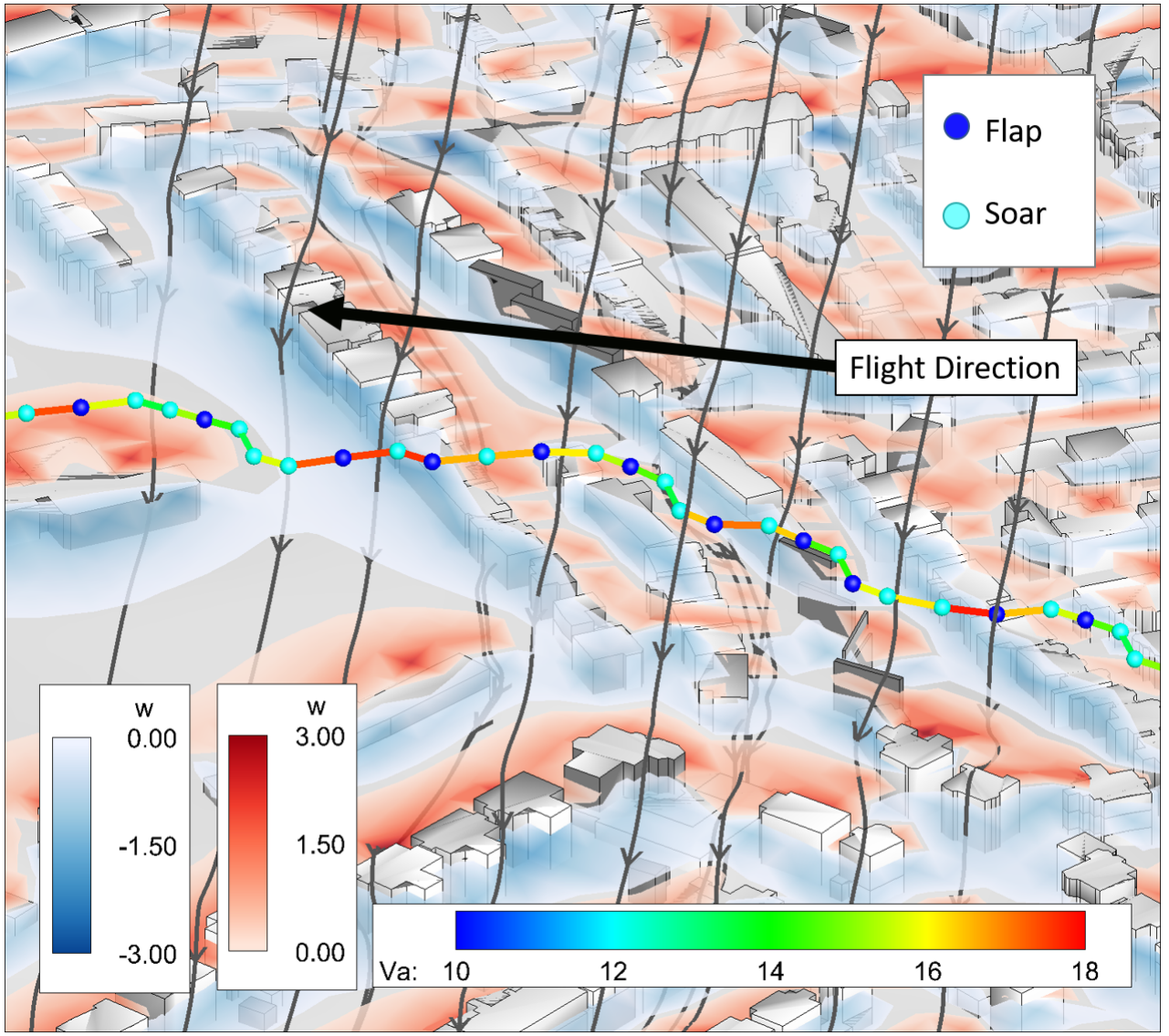

Figure E.4: Dolphin soaring being implemented by the path planner. The plots show a similar technique used in both cases where soaring occurs in the updraught before diving in the down draught, as the down draught finishes there is added lift reinitiating climb. The wind direction is shown by the flow vectors (grey) and the vertical wind, w, demonstrates the up- and down-draughts.

BIBLIOGRAPHY

[1] Eric Bonabeau, Marco Dorigo, and Guy Theraulaz.
Swarm intelligence: from natural to artificial systems.
Number 1. Oxford university press, 1999.

[2] M Dijkstra, JJ Van Baar, RJ Wiegerink, TSJ Lammerink, JH De Boer, and GJM Krijnen.
Artificial sensory hairs based on the flow sensitive receptor hairs of crickets.
Journal of micromechanics and microengineering, 15(7):S132, 2005.

[3] Hedenstrom Anders, L Christoffer Johansson, and Geoffrey R Spedding.
Bird or bat comparing airframe design and flight performance.
Bioinspiration and biomimetics, 4(1):015001, 2009.

[4] Xinyan Deng, Luca Schenato, Wei Chung Wu, and S Shankar Sastry.
Flapping flight for biomimetic robotic insects part i system modeling.
Robotics, IEEE Transactions on, 22(4):776–788, 2006.

[5] Yoseph Bar-Cohen.
Biomimetic using nature to inspire human innovation.
Bioinspiration and Biomimetics, 1(1):P1, 2006.

[6] Zsuzsa Ákos, Máté Nagy, Severin Leven, and Tamás Vicsek.
Thermal soaring flight of birds and unmanned aerial vehicles.
Bioinspiration & biomimetics, 5(4):045003, 2010.

[7] Anjan Chakrabarty and Jack W Langelaan.
Energy maps for long-range path planning for small-and micro-uavs.
In *Guidance, Navigation and Control Conference*, volume 2009, page 6113, 2009.

[8] Nicholas RJ Lawrance.
Autonomous soaring flight for unmanned aerial vehicles.

PhD thesis, University of Sydney, 2011.

[9] Emily LC Shepard, Rory P Wilson, W Gareth Rees, Edward Grundy, Sergio A Lambertucci, and Simon B Vosper.
Energy landscapes shape animal movement ecology.
The American Naturalist, 182(3):298–312, 2013.

[10] Emily LC Shepard, Cara Williamson, and Shane P Windsor.
Fine-scale flight strategies of gulls in urban airflows indicate risk and reward in city living.
Philosophical Transactions of the Royal Society B: Biological Sciences, 371(1704): 20150394, 2016.

[11] A Guerra-Langan, S Araujo-Estrada, and S Windsor.
Uav control costs mirror bird behaviour when soaring close to buildings.
In *11th International Micro Air Vehicle Competition and Conference, Spain, 2019*, 2019.

[12] Jay Spenser.
The Airplane.
Collins, 2008.

[13] John D Anderson Jr.
A history of aerodynamics: and its impact on flying machines, volume 8.
Cambridge University Press, 1997.

[14] Fred Howard.
Wilbur and Orville: A Biography of the Wright Brothers.
Courier Corporation, 2013.

[15] George Cayley.
On aerial navigation.
William Nicholson, 1810.

[16] Colin J Pennycuick.
Modelling the flying bird, volume 5.
Elsevier, 2008.

[17] Colin J Pennycuick.
A wind-tunnel study of gliding flight in the pigeon columba livia.

Journal of experimental Biology, 49(3):509–526, 1968.

[18] Jack E Cermak.
Wind-tunnel development and trends in applications to civil engineering.
Journal of wind engineering and industrial aerodynamics, 91(3):355–370, 2003.

[19] Edward M Kraft.
After 40 years why hasn't the computer replaced the wind tunnel?
Technical report, ARNOLD ENGINEERING DEVELOPMENT CENTER ARNOLD AFS TN, 2010.

[20] Cao Shuyang, Akira Nishi, Kimitaka Hirano, Shigehira Ozono, Hiromori Miyagi, Hiromori Kikugawa, Yuji Matsuda, and Yasuo Wakasugi.
An actively controlled wind tunnel and its application to the reproduction of the atmospheric boundary layer.
Boundary-layer meteorology, 101(1):61–76, 2001.

[21] Bhagirath Addepalli, MJ Brown, ER Pardyjak, and I Senocak.
Evaluation of the quic-urb wind model using wind-tunnel data for step-up street canyons.
In *American Meteorological Society Seventh symposium on urban environment, San Diego, CA*, 2007.

[22] Michael J Brown, Akshay Gowardhan, Matt Nelson, Mike Williams, and Eric R Pardyjak.
Evaluation of the quic wind and dispersion models using the joint urban 2003 field experiment dataset.
In *AMS 8th Symp. Urban Env*, 2009.

[23] Balwinder Singh, Bradley S Hansen, Michael J Brown, and Eric R Pardyjak.
Evaluation of the quic-urb fast response urban wind model for a cubical building array and wide building street canyon.
Environmental fluid mechanics, 8(4):281–312, 2008.

[24] Laurence R Newcome.
Unmanned aviation: a brief history of unmanned aerial vehicles.
American Institute of Aeronautics and Astronautics, 2004.

[25] Guowei Cai, Jorge Dias, and Lakmal Seneviratne.

A survey of small-scale unmanned aerial vehicles: Recent advances and future development trends.
Unmanned Systems, 2(02):175–199, 2014.

[26] Anouck R Girard, Adam S Howell, and J Karl Hedrick.
Border patrol and surveillance missions using multiple unmanned air vehicles.
In *2004 43rd IEEE Conference on Decision and Control (CDC)(IEEE Cat. No. 04CH37601)*, volume 1, pages 620–625. IEEE, 2004.

[27] Teodor Tomic, Korbinian Schmid, Philipp Lutz, Andreas Domel, Michael Kassecker, Elmar Mair, Iris Lynne Grixa, Felix Ruess, Michael Suppa, and Darius Burschka.
Toward a fully autonomous uav: Research platform for indoor and outdoor urban search and rescue.
IEEE robotics & automation magazine, 19(3):46–56, 2012.

[28] Cornelius A Thiels, Johnathon M Aho, Scott P Zietlow, and Donald H Jenkins.
Use of unmanned aerial vehicles for medical product transport.
Air medical journal, 34(2):104–108, 2015.

[29] Chase C Murray and Amanda G Chu.
The flying sidekick traveling salesman problem: Optimization of drone-assisted parcel delivery.
Transportation Research Part C: Emerging Technologies, 54:86–109, 2015.

[30] Eli S Bridge, Kasper Thorup, Melissa S Bowlin, Phillip B Chilson, Robert H Diehl, René W Fléron, Phillip Hartl, Roland Kays, Jeffrey F Kelly, W Douglas Robinson, et al.
Technology on the move: recent and forthcoming innovations for tracking migratory birds.
BioScience, 61(9):689–698, 2011.

[31] K Von Hünerbein, H-J Hamann, E Rüter, and W Wiltschko.
A gps-based system for recording the flight paths of birds.
Naturwissenschaften, 87(6):278–279, 2000.

[32] Willem Bouten, Edwin W Baaij, Judy Shamoun-Baranes, and Kees CJ Camphuysen.
A flexible gps tracking system for studying bird behaviour at multiple scales.

Journal of Ornithology, 154(2):571–580, 2013.

[33] Ulla M Norberg.
Evolution of flight.
In *Vertebrate Flight*, pages 257–266. Springer, 1990.

[34] Jack W Langelaan, Nicholas Alley, and James Neidhoefer.
Wind field estimation for small unmanned aerial vehicles.
Journal of Guidance, Control, and Dynamics, 34(4):1016–1030, 2011.

[35] Judy Shamoun-Baranes, Willem Bouten, E Emiel van Loon, Christiaan Meijer, and CJ Camphuysen.
Flap or soar? how a flight generalist responds to its aerial environment.
Phil. Trans. R. Soc. B, 371(1704):20150395, 2016.

[36] Brian Stone Jr and Michael O Rodgers.
Urban form and thermal efficiency: how the design of cities influences the urban heat island effect.
American Planning Association. Journal of the American Planning Association, 67 (2):186, 2001.

[37] Michael J Allen and Victor Lin.
Guidance and control of an autonomous soaring uav.
NASA Technical Memorandum, 214611, 2007.

[38] Larry M Silverberg, Dahan Xu, et al.
Dubins waypoint navigation of small-class unmanned aerial vehicles.
Open Journal of Optimization, 8(02):59, 2019.

[39] Daniel J Edwards and Larry M Silverberg.
Autonomous soaring: The montague cross-country challenge.
Journal of Aircraft, 47(5):1763–1769, 2010.

[40] Judy Shamoun-Baranes, Olivier Liechti, Yoram Yom-Tov, and Yossi Leshem.
Using a convection model to predict altitudes of white stork migration over central israel.
Boundary-Layer Meteorology, 107(3):673–681, 2003.

[41] Colin J Pennycuick.

Thermal soaring compared in three dissimilar tropical bird species, fregata magnificens, pelecanus occidentals and coragyps atratus.
Journal of Experimental Biology, 102(1):307–325, 1983.

[42] Zsuzsa Ákos, Máté Nagy, Severin Leven, and Tamás Vicsek.
Comparing bird and human soaring strategies.
Proceedings of the National Academy of Sciences, 105(11):4139–4143, 2008.

[43] Paul B MacCready.
Optimum airspeed selector.
Soaring (January–February), 10(11), 1958.

[44] DH Lenschow and PL Stephens.
The role of thermals in the convective boundary layer.
Boundary-Layer Meteorology, 19(4):509–532, 1980.

[45] Iain Guilliard, Richard Rogahn, Jim Piavis, and Andrey Kolobov.
Autonomous thermalling as a partially observable markov decision process (extended version).
arXiv preprint arXiv:1805.09875, 2018.

[46] AS Monin and AMf Obukhov.
Basic laws of turbulent mixing in the surface layer of the atmosphere.
Contrib. Geophys. Inst. Acad. Sci. USSR, 151:163–187, 1954.

[47] John Roy Garratt.
The atmospheric boundary layer.
Earth-Science Reviews, 37(1-2):89–134, 1994.

[48] Todd E Katzner, Philip J Turk, Adam E Duerr, Tricia A Miller, Michael J Lanzone, Jeff L Cooper, David Brandes, Junior A Tremblay, and Jérôme Lemaître.
Use of multiple modes of flight subsidy by a soaring terrestrial bird, the golden eagle aquila chrysaetos, when on migration.
Journal of the Royal Society Interface, 12(112):20150530, 2015.

[49] Elspeth Sage, Willem Bouten, Bart Hoekstra, Kees CJ Camphuysen, and Judy Shamoun-Baranes.
Orographic lift shapes flight routes of gulls in virtually flat landscapes.
Scientific reports, 9(1):9659, 2019.

[50] JJ Videler, D Weihs, and S Daan.
Intermittent gliding in the hunting flight of the kestrel, falco tinnunculus l.
Journal of experimental Biology, 102(1):1–12, 1983.

[51] PHOEBE Barnard.
Windhovering patterns of three african raptors in montane conditions.
Ardea, 74(2):151–158, 1986.

[52] Graham K Taylor, Kate V Reynolds, and Adrian LR Thomas.
Soaring energetics and glide performance in a moving atmosphere.
Philosophical Transactions of the Royal Society B: Biological Sciences, 371(1704): 20150398, 2016.

[53] Edmund Bromley Jr.
Aviation weather forecasts in tomorrow's flight service system.
Bulletin of the American Meteorological Society, 56(3):372–375, 1975.

[54] Richard A Wolters.
The art and technique of soaring.
McGraw-Hill Companies, 1971.

[55] Ann Welch, Frank Irving, and Lorne Welch.
New soaring pilot.
Murray, 1977.

[56] Reuter.
Hawaii: New world record for two-place glider set.
www.itnsource.com, July 2017.

[57] Jack Langelaan.
Long distance/duration trajectory optimization for small uavs.
In *AIAA Guidance, Navigation and Control Conference and Exhibit*, page 6737, 2007.

[58] Anjan Chakrabarty and Jack W Langelaan.
Energy-based long-range path planning for soaring-capable unmanned aerial vehicles.
Journal of Guidance, Control, and Dynamics, 34(4):1002–1015, 2011.

[59] Wesam H Al-Sabban, Luis F Gonzalez, and Ryan N Smith.
Wind-energy based path planning for unmanned aerial vehicles using markov decision processes.
In *Robotics and Automation (ICRA), 2013 IEEE International Conference on*, pages 784–789. IEEE, 2013.

[60] C White, EW Lim, S Watkins, A Mohamed, and M Thompson.
A feasibility study of micro air vehicles soaring tall buildings.
Journal of Wind Engineering and Industrial Aerodynamics, 103:41–49, 2012.

[61] Alex Fisher, Matthew Marino, Reece Clothier, Simon Watkins, Liam Peters, and Jennifer L Palmer.
Emulating avian orographic soaring with a small autonomous glider.
Bioinspiration & biomimetics, 11(1):016002, 2015.

[62] John Ware and Nicholas Roy.
An analysis of wind field estimation and exploitation for quadrotor flight in the urban canopy layer.
In *2016 IEEE International Conference on Robotics and Automation (ICRA)*, pages 1507–1514. IEEE, 2016.

[63] Lord Rayleigh.
The soaring of birds.
Nature, 27:534–535, 1883.

[64] Philip L Richardson.
Leonardo da vinci's discovery of the dynamic soaring by birds in wind shear.
Notes and Records: the Royal Society journal of the history of science, 73(3):285–301, 2019.

[65] G Sachs and P Bussotti.
Application of optimal control theory to dynamic soaring of seabirds.
In *Variational analysis and applications*, pages 975–994. Springer, 2005.

[66] Colin J Pennycuick.
Gust soaring as a basis for the flight of petrels and albatrosses (procellariiformes).
Avian Science, 2(1):1–12, 2002.

[67] Gottfried P Sachs.

Optimal acceleration procedure from launch to maximum speed in high-speed dynamic soaring.
In *AIAA Scitech 2020 Forum*, page 0024, 2020.

[68] G Sachs, J Traugott, AP Nesterova, and F Bonadonna.
Experimental verification of dynamic soaring in albatrosses.
Journal of Experimental Biology, 216(22):4222–4232, 2013.

[69] Markus Deittert, Arthur Richards, Chris Toomer, and Anthony Pipe.
Dynamic soaring flight in turbulence.
In *AIAA Guidance, Navigation, and Control Conference*, page 6012, 2009.

[70] Wenceslao E Shaw-Cortez and Eric Frew.
Efficient trajectory development for small unmanned aircraft dynamic soaring applications.
Journal of Guidance, Control, and Dynamics, 38(3):519–523, 2015.

[71] Yiyuan J Zhao.
Optimal patterns of glider dynamic soaring.
Optimal control applications and methods, 25(2):67–89, 2004.

[72] Taras Kiceniuk.
Dynamic soaring and sailplane energetics.
Technical Soaring, 25(4):221–227, 2001.

[73] Taras Kiceniuk.
Calculations on soaring sink.
Technical Soaring, 25(4):228–230, 2001.

[74] E Dickmanns.
Optimal dolphin-style soaring.
OSTIV Publications, 16, 1981.

[75] Jack W Langelaan.
Gust energy extraction for mini and micro uninhabited aerial vehicles.
Journal of guidance, control, and dynamics, 32(2):464–473, 2009.

[76] Nikola Gavrilovic, A Mohamed, Matthew Marino, Simon Watkins, Jean-Marc Moschetta, and Emmanuel Bénard.
Avian-inspired energy-harvesting from atmospheric phenomena for small uavs.

Bioinspiration & biomimetics, 14(1):016006, 2018.

[77] Abdulghani Mohamed, Mujahid Abdulrahim, Simon Watkins, and Reece Clothier.
Development and flight testing of a turbulence mitigation system for micro air vehicles.
Journal of Field Robotics, 33(5):639–660, 2016.

[78] Clara García-Ripollés, Pascual López-López, and Vicente Urios.
First description of migration and wintering of adult egyptian vultures neophron percnopterus tracked by gps satellite telemetry.
Bird Study, 57(2):261–265, 2010.

[79] Eric WM Stienen, Peter Desmet, Bart Aelterman, Wouter Courtens, Simon Feys, Nicolas Vanermen, Hilbran Verstraete, Marc Van de Walle, Klaas Deneudt, Francisco Hernandez, et al.
Gps tracking data of lesser black-backed gulls and herring gulls breeding at the southern north sea coast.
ZooKeys, (555):115, 2016.

[80] Colin J Pennycuick.
Gliding flight of the white-backed vulture gyps africanus.
Journal of Experimental Biology, 55(1):13–38, 1971.

[81] Johan Mooij, Axel Paulsch, and Wolfgang Scholze.
Reintroduction of the lesser white-fronted goose anser erythropus in fennoscandia with the help of microlight aircraft.
Waterbirds around the world, pages 633–634, 2006.

[82] Colin James Pennycuick.
The ornithodolite: an instrument for collecting large samples of bird speed measurements.
Philosophical Transactions of the Royal Society of London. B, Biological Sciences, 300(1098):61–73, 1982.

[83] Jelle Treep, Gil Bohrer, Judy Shamoun-Baranes, Olivier Duriez, Renato Prata de Moraes Frasson, and Willem Bouten.
Using high resolution gps tracking data of bird flight for meteorological observations.
Bulletin of the American Meteorological Society, (2015), 2015.

[84] HJ Williams, ELC Shepard, O Duriez, and SA Lambertucci.
Can accelerometry be used to distinguish between flight types in soaring birds?
Animal Biotelemetry, 3(1):1, 2015.

[85] Kathryn Knight.
Shags take advantage of headwind to take off.
Journal of Experimental Biology, 219(3):296–296, 2016.

[86] Yukihisa Kogure, Katsufumi Sato, Yutaka Watanuki, Sarah Wanless, and Francis Daunt.
European shags optimize their flight behavior according to wind conditions.
Journal of Experimental Biology, 219(3):311–318, 2016.

[87] James D McLaren, Judy Shamoun-Baranes, CJ Camphuysen, and Willem Bouten.
Directed flight and optimal airspeeds: homeward-bound gulls react flexibly to wind yet fly slower than predicted.
Journal of Avian Biology, 47(4):476–490, 2016.

[88] LG Halsey, ELC Shepard, F Quintana, A Gomez Laich, JA Green, and RP Wilson.
The relationship between oxygen consumption and body acceleration in a range of species.
Comparative Biochemistry and Physiology Part A: Molecular & Integrative Physiology, 152(2):197–202, 2009.

[89] Matthew W Orr, Steven J Rasmussen, Etan D Karni, and William B Blake.
Framework for developing and evaluating mav control algorithms in a realistic urban setting.
In *Proceedings of the 2005, American Control Conference, 2005.*, pages 4096–4101. IEEE, 2005.

[90] Bradley Stoor, Stanley Pruett, Mathrew Duquette, Robert Subr, and Tim MtCastle.
Urban simulation environment.
In *AIAA Modeling and Simulation Technologies Conference and Exhibit*, page 6262, 2006.

[91] Thomas Alerstam and Å Lindström.
Optimal bird migration: the relative importance of time, energy, and safety.
In *Bird migration*, pages 331–351. Springer, 1990.

[92] Susanne Åkesson and Anders Hedenström.
Wind selectivity of migratory flight departures in birds.
Behavioral Ecology and Sociobiology, 47(3):140–144, 2000.

[93] Thomas Alerstam, Anders Hedenström, and Susanne Åkesson.
Long-distance migration: evolution and determinants.
Oikos, 103(2):247–260, 2003.

[94] Raymond HG Klaassen, Bruno J Ens, Judy Shamoun-Baranes, Klaus-Michael Exo, and Franz Bairlein.
Migration strategy of a flight generalist, the lesser black-backed gull larus fuscus.
Behavioral Ecology, 23(1):58–68, 2011.

[95] Thomas Alerstam.
Optimal bird migration revisited.
Journal of Ornithology, 152(1):5–23, 2011.

[96] Envionmental Agency.
Lidar composite dem, October 2019.
URL `https://data.gov.uk/dataset/lidar-composite-dtm-2m`.

[97] DigiMaps.
Ordnance survey data uk, 2015.

[98] Eric R Pardyjak and Michael Brown.
Quic-urb v1. 1 theory and user guide.
Los Alamos National Laboratory, Los Alamos, NM, 2003.

[99] National Tide and Sea Level Facility.
Chart datum and ordnance datum, 2015.

[100] Esri.
Geoxchange, 2015.

[101] Tide Times.
Mumbles tide times, 2015.

[102] John Mellor.
The Art of Pilotage.
Sheridan House Incorporated, 1990.

[103] Matthew Nelson and Michael Brown.
QUIC-URB v6. 01 The QUIC Start Guide, 2013.

[104] Akshay A Gowardhan, Eric R Pardyjak, Inanc Senocak, and Michael J Brown.
A cfd-based wind solver for an urban fast response transport and dispersion model.
Environmental fluid mechanics, 11(5):439–464, 2011.

[105] WMO.
Wmo guide to meteorological instruments and methods of observation.
1996.

[106] Chuck Taylor.
Geographic/utm coordinate converter, 2015.

[107] John David Anderson Jr.
Fundamentals of aerodynamics.
Tata McGraw-Hill Education, 2010.

[108] CJ Pennycuick, Susanne Åkesson, and Anders Hedenström.
Air speeds of migrating birds observed by ornithodolite and compared with predictions from flight theory.
Journal of the Royal Society Interface, 10(86):20130419, 2013.

[109] Nicholas RJ Lawrance and Salah Sukkarieh.
Wind energy based path planning for a small gliding unmanned aerial vehicle.
In *AIAA Guidance, Navigation, and Control Conference*, page 6112, 2009.

[110] Anouk Spelt, Cara Williamson, Judy Shamoun-Baranes, Emily Shepard, Peter Rock, and Shane Windsor.
Habitat use of urban-nesting lesser black-backed gulls during the breeding season.
Scientific reports, 9(1):1–11, 2019.

[111] *Bird-inspired Velocity Optimization for UAVs in the Urban Environment*, 2020.

[112] Simon Watkins, Juliette Milbank, Benjamin J Loxton, and William H Melbourne.
Atmospheric winds and their implications for microair vehicles.
AIAA journal, 44(11):2591–2600, 2006.

[113] S Watkins, M Thompson, B Loxton, and M Abdulrahim.
On low altitude flight through the atmospheric boundary layer.
International Journal of Micro Air Vehicles, 2(2):55–68, 2010.

[114] Simon Watkins, Alex Fisher, Abdulghani Mohamed, Matthew Marino, Mark Thompson, Reece Clothier, and Sridhar Ravi.
The turbulent flight environment close to the ground and its effects on fixed and flapping wings at low reynolds number.
In *5th European Conference for Aeronautics and Space Sciences, Munich, Germany, 1–5 July 2014*, 2013.

[115] Murat Bronz, Jean Marc Moschetta, Pascal Brisset, and Michel Gorraz.
Towards a long endurance mav.
International Journal of Micro Air Vehicles, 1(4):241–254, 2009.

[116] Caleb White, Simon Watkins, Ee Lim, and Kevin Massey.
The soaring potential of a micro air vehicle in an urban environment.
International Journal of Micro Air Vehicles, 4(1):1–14, 2012.

[117] KP Dial, AA Biewener, BW Tobalske, and DR Warrick.
Mechanical power output of bird flight.
Nature, 390(6655):67, 1997.

[118] Tyson L Hedrick, Bret W Tobalske, and Andrew A Biewener.
How cockatiels (nymphicus hollandicus) modulate pectoralis power output across flight speeds.
Journal of Experimental Biology, 206(8):1363–1378, 2003.

[119] Vance A Tucker and G Christian Parrott.
Aerodynamics of gliding flight in a falcon and other birds.
Journal of Experimental Biology, 52(2):345–367, 1970.

[120] CJ Pennycuick, Carlton E Heine, Sean J Kirkpatrick, and MARK R FULLER.
The profile drag of a hawk's wing, measured by wake sampling in a wind tunnel.
Journal of Experimental Biology, 165(1):1–19, 1992.

[121] D Lentink, UK Müller, EJ Stamhuis, R De Kat, W Van Gestel, LLM Veldhuis, Per Henningsson, Anders Hedenström, John J Videler, and Johan L Van Leeuwen.
How swifts control their glide performance with morphing wings.
Nature, 446(7139):1082, 2007.

[122] MIKAEL Rosen and A Hedenstrom.
Gliding flight in a jackdaw: a wind tunnel study.
Journal of Experimental Biology, 204(6):1153–1166, 2001.

[123] Colin J Pennycuick.
Bird flight performance.
Oxford University Press, 1989.

[124] E De Margerie, JB Mouret, S Doncieux, and JA Meyer.
Artificial evolution of the morphology and kinematics in a flapping-wing mini-uav.
Bioinspiration & biomimetics, 2(4):65, 2007.

[125] Tyson L Hedrick, Cécile Pichot, and Emmanuel De Margerie.
Gliding for a free lunch: biomechanics of foraging flight in common swifts (apus apus).
Journal of Experimental Biology, 221(22):jeb186270, 2018.

[126] C Ji Pennycuick.
Field observations of thermals and thermal streets, and the theory of cross-country soaring flight.
Journal of Avian Biology, pages 33–43, 1998.

[127] MetOffice.
Unified model, November 2017.
URL `https://www.metoffice.gov.uk/research/modelling-systems/unified-model`.

[128] U.S. Navy NGA GEBCO Data SIO, NOAA.
Google earth image, October 2019.

[129] Jack Langelaan.
Biologically inspired flight techniques for small and micro unmanned aerial vehicles.
In *AIAA guidance, navigation and control conference and exhibit*, page 6511, 2008.

[130] Vincent Bonnin, Emmanuel Bénard, J-M Moschetta, and CA Toomer.
Energy-harvesting mechanisms for uav flight by dynamic soaring.
International Journal of Micro Air Vehicles, 7(3):213–229, 2015.

[131] Snorri Gudmundsson, Vladimir V Golubev, Sergey Drakunov, and Charles Reinholtz.
Bio-inspired opportunistic approaches in energy-conserving/harnessing flight-path modeling for uas.
In *AIAA Modeling and Simulation Technologies Conference*, page 3676, 2016.

[132] Duo-Neng Liu, Zhong-Xi Hou, Zheng Guo, Xi-Xiang Yang, and Xian-Zhong Gao.
Bio-inspired energy-harvesting mechanisms and patterns of dynamic soaring.
Bioinspiration & biomimetics, 12(1):016014, 2017.

[133] Haider Taha.
Urban climates and heat islands: albedo, evapotranspiration, and anthropogenic heat.
Energy and buildings, 25(2):99–103, 1997.

[134] Martin Eshelby.
Aircraft performance: Theory and practice.
American Institute of Aeronautics and Astronautics, Inc., 2000.

[135] CJ Pennycuick.
The soaring flight of vultures.
Scientific American, 229(6):102–109, 1973.

[136] Derek Piggott.
Understanding gliding: the principles of soaring flight.
Barnes & Noble, 1977.

[137] Dmitriy Makovkin and Jack W Langelaan.
Optimal persistent surveillance using coordinated soaring.
In *AIAA Guidance, Navigation, and Control Conference*, page 0261, 2014.

[138] Federal Aviation Regulations.
Part 23 airworthiness standards: Normal, utility, acrobatic and commuter category airplanes, 1991.

[139] Sergio A Araujo-Estrada, Francis Salama, Colin M Greatwood, Kieran T Wood, Thomas S Richardson, and Shane P Windsor.
Bio-inspired distributed strain and airflow sensing for small unmanned air vehicle flight control.
In *AIAA Guidance, Navigation, and Control Conference*, page 1487, 2017.

[140] Francois Callou and Gilles Foinet.
Method for controlling a multi-rotor rotary-wing drone, with cross wind and accelerometer bias estimation and compensation, Nov 2016.
US Patent 9,488,978.

[141] Farhan Mohammed, Ahmed Idries, Nader Mohamed, Jameela Al-Jaroodi, and Imad Jawhar.
Uavs for smart cities: Opportunities and challenges.
In *2014 International Conference on Unmanned Aircraft Systems (ICUAS)*, pages 267–273. IEEE, 2014.

[142] Hamid Menouar, Ismail Guvenc, Kemal Akkaya, A Selcuk Uluagac, Abdullah Kadri, and Adem Tuncer.
Uav-enabled intelligent transportation systems for the smart city: Applications and challenges.
IEEE Communications Magazine, 55(3):22–28, 2017.

[143] Stuart J Russell and Peter Norvig.
Artificial intelligence: a modern approach.
Malaysia; Pearson Education Limited,, 2016.

[144] Voemir Kunchev, Lakhmi Jain, Vladimir Ivancevic, and Anthony Finn.
Path planning and obstacle avoidance for autonomous mobile robots: A review.
In *International Conference on Knowledge-Based and Intelligent Information and Engineering Systems*, pages 537–544. Springer, 2006.

[145] Robert Tarjan.
Depth-first search and linear graph algorithms.
SIAM journal on computing, 1(2):146–160, 1972.

[146] Shimon Even.
Graph algorithms.
Cambridge University Press, 2011.

[147] Thomas H Cormen, Charles E Leiserson, Ronald L Rivest, and Clifford Stein.
Greedy algorithms.
Introduction to algorithms, 1:329–355, 2001.

[148] RV Baudinette and K Schmidt-Nielsen.
Energy cost of gliding flight in herring gulls.
Nature, 248(5443):83–84, 1974.

[149] VANCE A Tucker.
Metabolism during flight in the laughing gull, larus atricilla.
American Journal of Physiology-Legacy Content, 222(2):237–245, 1972.

[150] Pablo Muñoz, María D R-Moreno, and David F Barrero.
Unified framework for path-planning and task-planning for autonomous robots.
Robotics and Autonomous Systems, 82:1–14, 2016.

[151] Sven Koenig and Maxim Likhachev.
Fast replanning for navigation in unknown terrain.
IEEE Transactions on Robotics, 21(3):354–363, 2005.

[152] Nikola Gavrilović, Murat Bronz, and Jean-Marc Moschetta.
Bioinspired energy harvesting from atmospheric phenomena for small unmanned aerial vehicles.
Journal of Guidance, Control, and Dynamics, pages 1–15, 2020.

[153] Anna Gagliardo, Paolo Ioalé, and Verner P Bingman.
Homing in pigeons: the role of the hippocampal formation in the representation of landmarks used for navigation.
Journal of Neuroscience, 19(1):311–315, 1999.

[154] Roswitha Wiltschko and Wolfgang Wiltschko.
Avian navigation: from historical to modern concepts.
2003.

[155] Julien R Serres, Thomas J Evans, Susanne Åkesson, Olivier Duriez, Judy Shamoun-Baranes, Franck Ruffier, and Anders Hedenström.
Optic flow cues help explain altitude control over sea in freely flying gulls.
Journal of the Royal Society Interface, 16(159):20190486, 2019.

[156] Anna Gagliardo, Joël Bried, Paolo Lambardi, Paolo Luschi, Martin Wikelski, and Francesco Bonadonna.
Oceanic navigation in cory's shearwaters: evidence for a crucial role of olfactory cues for homing after displacement.
Journal of Experimental Biology, 216(15):2798–2805, 2013.

[157] Enrica Pollonara, Paolo Luschi, Tim Guilford, Martin Wikelski, Francesco Bonadonna, and Anna Gagliardo.
Olfaction and topography, but not magnetic cues, control navigation in a pelagic seabird: displacements with shearwaters in the mediterranean sea.
Scientific reports, 5(1):1–10, 2015.

[158] Gaia Dell'Ariccia and Francesco Bonadonna.
Back home at night or out until morning? nycthemeral variations in homing of anosmic cory's shearwaters in a diurnal colony.
Journal of Experimental Biology, 216(8):1430–1433, 2013.

[159] Gabrielle Nevitt.
Foraging by seabirds on an olfactory landscape.
American Scientist, 87(1):46, 1999.

[160] Gabrielle A Nevitt, Marcel Losekoot, and Henri Weimerskirch.
Evidence for olfactory search in wandering albatross, diomedea exulans.
Proceedings of the National Academy of Sciences, 105(12):4576–4581, 2008.

[161] Niko Tinbergen.
The herring gull's world: a study of the social behaviour of birds.
1953.

[162] Alejandro Sotillo, Jochen Depestele, Wouter Courtens, Magda Vincx, and Eric WM Stienen.
Consumption of discards by herring gulls larus argentatus and lesser black-backed gulls larus fuscus off the belgian coast in the breeding season.
Ardea, 102(2):195–206, 2014.

[163] Olivier Duriez, Akiko Kato, Clara Tromp, Giacomo Dell'Omo, Alexei L Vyssotski, François Sarrazin, and Yan Ropert-Coudert.
How cheap is soaring flight in raptors? a preliminary investigation in freely-flying vultures.
PLoS One, 9(1), 2014.

[164] Tyson L Hedrick, James R Usherwood, and Andrew A Biewener.
Wing inertia and whole-body acceleration: an analysis of instantaneous aerodynamic force production in cockatiels (nymphicus hollandicus) flying across a range of speeds.
Journal of Experimental Biology, 207(10):1689–1702, 2004.

[165] Hans Dieter Luke.
The origins of the sampling theorem.
IEEE Communications Magazine, 37(4):106–108, 1999.

[166] Ben Schellenberg, Thomas S Richardson, Robert J Clarke, Matt Watson, Jim Freer, Alex McConville, and Gustavo Chigna.
Bvlos operations of fixed-wing uavs for the collection of volcanic ash above fuego volcano, guatemala.
In *AIAA Scitech 2020 Forum*, page 2204, 2020.

[167] Ben Schellenberg, Tom Richardson, Matt Watson, Colin Greatwood, Robert Clarke, Rick Thomas, Kieran Wood, Jim Freer, Helen Thomas, Emma Liu, et al.
Remote sensing and identification of volcanic plumes using fixed-wing uavs over volcán de fuego, guatemala.
Journal of Field Robotics, 36(7):1192–1211, 2019.

[168] Vitor H Paiva, Tim Guilford, Jessica Meade, Pedro Geraldes, Jaime A Ramos, and Stefan Garthe.
Flight dynamics of coryŠs shearwater foraging in a coastal environment.
Zoology, 113(1):47–56, 2010.

[169] RJ Spivey, S Stansfield, and CM Bishop.
Analysing the intermittent flapping flight of a manx shearwater, puffinus puffinus, and its sporadic use of a wave-meandering wing-sailing flight strategy.
Progress in oceanography, 125:62–73, 2014.

[170] Gabriel D Bousquet, Michael S Triantafyllou, and Jean-Jacques E Slotine.
Optimal dynamic soaring consists of successive shallow arcs.
Journal of The Royal Society Interface, 14(135):20170496, 2017.

[171] Stefan Hrabar, Gaurav S Sukhatme, Peter Corke, Kane Usher, and Jonathan Roberts.
Combined optic-flow and stereo-based navigation of urban canyons for a uav.
In *2005 IEEE/RSJ International Conference on Intelligent Robots and Systems*, pages 3309–3316. IEEE, 2005.

[172] Aymeric Denuelle, Saul Thurrowgood, Reuben Strydom, Farid Kendoul, and Mandyam V Srinivasan.
Biologically-inspired visual stabilization of a rotorcraft uav in unknown outdoor environments.
In *2015 International Conference on Unmanned Aircraft Systems (ICUAS)*, pages 1084–1093. IEEE, 2015.

[173] Nathan T Depenbusch, John J Bird, and Jack W Langelaan.
The autosoar autonomous soaring aircraft, part 1: Autonomy algorithms.
Journal of Field Robotics, 35(6):868–889, 2018.

[174] Nathan T Depenbusch, John J Bird, and Jack W Langelaan.
The autosoar autonomous soaring aircraft part 2: Hardware implementation and flight results.
Journal of Field Robotics, 35(4):435–458, 2018.

[175] Ryan Goldstein.
Self-folding propeller, Jan 2020.
US Patent 10,543,915.

[176] Jay Michael Todd Matlock.
Evaluation of hybrid-electric propulsion systems for unmanned aerial vehicles.
PhD thesis, 2019.

[177] Minu Theresa Mathew.
An energy efficient renewable power supply system with power regeneration equipped in a uav.

[178] Abdulghani Mohamed, Kevin Massey, Simon Watkins, and Reece Clothier.
The attitude control of fixed-wing mavs in turbulent environments.
Progress in Aerospace Sciences, 66:37–48, 2014.

[179] SESAR.
European atm master plan: Roadmap for the safe integration of drones into all classes of airspace.
Technical report, Single European Sky Air Traffic Management Research Group, 2018.
URL `https://www.sesarju.eu`.